Identification and characterisation of epigenetic mechanisms in osteoblast differentiation of human mesenchymal stem cells

Anneke Kramm

St Catherine's College

Nuffield Department of Orthopaedics, Rheumatology
and Musculoskeletal Sciences
University of Oxford

Thesis submitted for the degree of Doctor of Philosophy

Hilary Term 2014

Identification and characterisation of epigenetic mechanisms in osteoblast differentiation of human mesenchymal stem cells

Anneke Kramm

St Catherine's College

Submitted for the degree of Doctor of Philosophy, Hilary 2014

Abstract

A major therapeutic challenge in musculoskeletal regenerative medicine is how to effectively replenish bone tissue lost due to pathological conditions such as fracture, osteoporosis, or rheumatoid arthritis. Mesenchymal stem cells are currently investigated for applications in bone-tissue engineering and human bone marrow-derived mesenchymal stem cells (hMSCs) could be a promising source for generation of tissue-engineered bone. However, the therapeutic potential of MSCs has not been fully exploited due to a lack of knowledge regarding the identity, nature, and differentiation of hMSCs. Epigenetic mechanisms regulating the chromatin structure as well as specific gene transcription are crucial in determination of stem cell differentiation. With the aim to systematically identify epigenetic factors that modulate MSC differentiation, the work in this thesis encompasses an approach to identify epigenetic mechanisms underlying, initiating, and promoting osteoblast differentiation, and the investigation of individual epigenetic modulators. Various osteogenic inducers were validated for differentiation of MSCs and an assay allowing assessment of differentiation outcome was developed. This assay was subsequently employed in knockdown experiments with lentiviral short hairpin RNAs and inhibitor screens with small molecules targeting putative druggable epigenetic modulator classes. This approach identified around 100 epigenetic modulator candidates involved in osteoblast differentiation, of these candidates approximately 2/3 downregulated and 1/3 upregulated alkaline phosphatase (ALP) activity. Serving as a proof-of-concept, orthogonal validation experiments employing locked nucleic acid (LNA) knockdown were performed to validate a subset of candidates. Two identified target genes were selected for further investigation. Bromodomain-containing protein 4 (BRD4) was identified as one component of epigenetic regulation; its inhibition led to a decrease in ALP expression, downregulation of key osteoblast transcription factors Runx2 and Osterix, as well as impaired bone matrix formation. Knockdown of lysine (K)-specific demethylase 1A (KDM1A/LSD1) upregulated ALP activity and treatment with a small molecule inhibitor targeting KDM1A led to an increase in ALP, RUNX2, and bone sialoprotein expression. Intriguingly, in a transgenic mouse model overexpressing Kdm1a a decrease in bone volume and bone mineral density was observed, thus supporting the hypothesis that KDM1A is a central regulator of osteoblast differentiation.

Acknowledgements

There are many people without whom the completion of this thesis would not have been possible. I am deeply grateful to have been given the opportunity to study at Oxford and would like to express my sincere gratitude to my supervisors Professor Udo Oppermann and Dr James Dunford. Thank you both so much for your support, guidance, trust, encouragement, and critique.

I would also like to thank Dr. Afsie Sabokbar for all her support throughout the years - from my PhD application to the thesis submission! Thank you so much for everything!

With regard to the mouse work presented in this study, I would like to thank Professor Roland Schuele for providing the Kdm1a mouse model, David McGarry and James Dunford for all their support with the experiments, and Andrew Freidin for helping me with the CT scans. I also would like to express my sincere gratitude to Dr James Edwards who has provided excellent support and advice, and always had a couple of minutes for a quick chat about mice.

I would like to express my sincere gratitude to Dr Stefan Kubicek at the CeMM in Vienna who has provided excellent support and advice with the shRNA and compound screens. My time in Vienna was invaluable and not only laid the basis for this thesis' work but was also filled with great people and wonderful experiences. In particular, I would like to thank Ernestine Leitner for all her help with robots and all the fun we had climbing in and around the platform, Freya Klepsch for her help with the protein interaction analysis, Tess Lu for great company in many late nights' work, and especially Marco Licciardello for everything else and for his friendship. You guys are brilliant!

A huge Thank You goes to the Oppermann group at the Botnar Research Centre for making my time in the lab (and office, shhh!) such an enjoyable and rewarding experience. Thank you all so much for all your help and support and for sharing your technical, scientific, and life knowledge with me - Laurynas for his help with bioinformatics and ChIP

experiments, Ed for heatmaps and structures, Kelly and Na for help with the mice, Peter for advice on compounds, Clarence for everything microscopy-related, Debs for her help with pretty much everything, Fernando for microarray studies, and Graham for answering many qPCR-related questions.

At the Botnar Research Centre, I have been privileged to work with wonderful people, thank you all very much for making me go to work happily every morning and for being my friends.

During the last four years, I made many good friends whom I would like to thank for making my time in Oxford so special. My dearest virus buddy, Aliaa, thank you for keeping up with me, for all the lovely trips, the coffee and tea breaks, for your green thumb, and simply for being a great friend. My friends in college, especially Christina, Christoph, and Robert, I would like to thank for making me feel at home, for many fun nights and not to forget our most sincere and big discussions about everything and nothing at Mario's (I'm still waiting for the apartment complex in Albania!)! My Friday pub gang, especially James, John, Chitra, and Sarah, you all made a working week worthwhile!
Not only do we look alike, we also share the same thoughts – my dear Kelly, thank you so much for being my desk-mate, my lab-buddy, my popcorn-friend, my little sister, and simply you!

What would life be without friends, and what would Oxford be without you.

I am deeply grateful to have my "Mädels" at home, thank you so much for not letting go of me and being my friends.

My dearest Jochen, who walked into my life half-way through my DPhil and simply didn't leave – thank you so much for standing by my side, for supporting me, and for all the joy and fun life is with you.

Finally, I would like to thank my wonderful parents and my brother for their unconditional love and support. You have been a constant source of support and encouragement and I could not have made it through this without you.

Contents

1 Introduction **1**

1.1 Tissue engineering 1

1.2 Stem cells 2

1.2.1 Types of stem cells 3

1.2.2 Mesenchymal stem cells 5

1.3 Bone function and development 10

1.3.1 Musculoskeletal pathologies 15

1.3.2 Osteogenic signalling pathways 16

1.4 Epigenetics 25

1.4.1 Methylation 28

1.4.2 Acetylation 31

1.4.3 Bromodomains 32

1.4.4 Epigenetic mechanisms in osteogenic differentiation 33

1.5 Summary 36

1.6 Aims of this thesis 37

2 Investigation of different osteogenic inducers and development of osteoblast differentiation assay **39**

2.1 Introduction 39

2.2 *In vitro* osteoblast differentiation methods 39

2.3 Chapter outline 43

2.4 Materials and Methods 44

2.4.1 Cell culture 44

2.4.2 Cell viability assay 45

2.4.3 Alkaline phosphatase assay 45

2.4.4 RNA extraction and cDNA synthesis 46

2.4.5 Microarray study 46

2.4.6 Cell fixation 46

2.4.7 Alizarin Red S staining 47

2.5 Dexamethasone-induced gene expression profile of human mesenchymal stem cell-derived osteoblasts 48

2.6 Development of a generic assay for assessment of osteoblast differentiation . 54

2.7 Validation of different osteoblast induction methods 58

2.7.1 Osteoblast gene expression analysis by quantitative polymerase chain reaction 58

2.7.2 Matrix mineralisation assessed by Alizarin Red S 59

2.8 Conclusion and discussion 60

3 Identification of epigenetic modulators in osteoblast differentiation 63

3.1 Introduction 63

3.1.1 Tools for interference with epigenetic modulators 64

3.2 Materials and Methods 68

3.2.1 Alkaline phosphatase assay optimisation for high-throughput screening 68

3.3 ShRNA knockdown of epigenetic modulators 69

3.3.1 TRC shRNA library 69

3.3.2 Lentiviral delivery optimisation – viral titration and cell selection . . 70

3.3.3 Brief overview of assay protocol 74

3.3.4 Data analysis of MSC differentiation assay 74

3.3.5 Screen validation and selection criteria for shRNA hits 75

3.3.6 Results – Analysis of hits derived from shRNA screen 78

3.3.7 Network analysis of hits identified in shRNA screen 87

3.3.8 Target gene interactions 94

3.3.9 Target gene selection for shRNA screen and selection of follow up targets 97

3.3.10 Selected hits from shRNA screen 98

3.3.11 Validation of shRNA targets by locked nucleic acids knockdown . . . 106

3.4 Small molecule inhibitor screen 111

3.4.1 Results – Hits derived from small molecule inhibitor screen 113

3.4.2 Dose-response assays for selected small molecule inhibitor hits 115

3.4.3 Selected hits from small molecule inhibitor screen 121

3.5 Final selection of two follow-up targets – BRD4 and KDM1A 122

3.6 Conclusion and discussion 123

4 The role of bromodomain containing protein 4 (BRD4) in osteoblast differentiation 127

4.1 Background . . . 127

4.2 Recapitulation of earlier results and aim of this study . . . 130

4.3 Materials and Methods . . . 132

4.3.1 Cell culture . . . 132

4.3.2 Long-term differentiation under (+)-JQ1 treatment . . . 132

4.3.3 RNA extraction and cDNA synthesis . . . 132

4.3.4 Alizarin Red S staining . . . 133

4.3.5 Oil Red O staining . . . 133

4.4 Results . . . 133

4.4.1 The effect of (+)-JQ1 on cell proliferation . . . 133

4.4.2 The effect of (+)-JQ1 on osteoblastic gene expression . . . 136

4.4.3 Hierarchical clustering of genes expressed under (+)-JQ1 treatment 138

4.4.4 (+)-JQ1 inhibits bone matrix mineralisation . . . 145

4.4.5 Oil Red O staining to determine adipogenic differentiation potential 149

4.4.6 (+)-JQ1 treatment of primary bone marrow-derived patient cells . . 150

4.5 Conclusion and discussion . . . 152

5 The effect of lysine-specific demethylase 1A (KDM1A) on human mesenchymal stem cell differentiation and murine bone development 160

5.1 Background . . . 160

5.2 Aim of this study . . . 163

5.3 Materials and Methods . . . 164

5.3.1 Mouse tissue preparation . . . 164

5.3.2 Bone marrow flush . . . 165

5.3.3 MicroCT analysis of mouse long bones . . . 166

5.3.4 Isolation and culture of cells from mouse cortical bone . . . 167

5.3.5 RNA extraction and cDNA synthesis . . . 168

5.4 Results . . . 168

5.4.1 Treatment of human mesenchymal stem cells with a small molecule inhibitor targeting KDM1A leads to an increase in osteoblast gene expression . . . 168

5.4.2 The transgenic mouse model of *Kdm1a* . . . 171

5.4.3 Transgenic mice overexpressing Kdm1a show a significant decrease in trabecular bone volume and bone mineral density . . . 172

5.5 Conclusion and discussion . . . 178

6 Discussion and future perspectives 182

References 193

A Appendix **222**

A.1 Reagents and media compositions 222

A.2 Primer sequences for qPCR 223

A.3 Dexamethasone-induced gene expression - microarray data 224

A.4 Alkaline phosphatase assay validation 226

A.5 Setup short hairpin RNA screen 228

A.5.1 PLACEBO Platform 228

A.5.2 Vector maps for viral plasmids 230

A.5.3 Assay optimisation with regard to PLACEBO facility 231

A.6 shRNA targets 236

A.6.1 Gene list 236

A.6.2 Short list shRNA target genes 241

A.7 Protein network analysis 244

A.8 Assay method small molecule inhibitor screen 250

A.9 Dose-response experiments of hits derived from small molecule inhibitor screen 251

A.9.1 DOT1L 251

A.9.2 SAHA 252

A.9.3 Valproic acid 252

A.9.4 (-)-JQ1 253

A.10 (+)-JQ1 treatment - microarray data 253

List of Figures

1.1 Different potencies of stem cells 3

1.2 The multipotency of MSCs 6

1.3 Stages of osteogenic differentiation 8

1.4 Schematic overview of bone structure 11

1.5 Osteogenesis - intramembranous and endochondral ossification 12

1.6 Bone remodelling 13

1.7 Osteogenic signalling pathways I - BMP, TGF-β, and PTH signalling 19

1.8 Osteogenic signalling pathways II - Calcitonin, Hedgehog, WNT, and JAK/STAT signalling 22

1.9 Osteogenic signalling pathways III - FGF, Notch, and NELL-1 signalling . . 24

1.10 Organisation of DNA 26

1.11 Methylation of lysines 28

2.1 Heatmap of gene expression under dexamethasone treatment 48

2.2 Principal component analysis of dexamethasone-induced differentiation . . . 50

2.3 Time course of alkaline phosphatase expression in osteoblast differentiation under different inducers 57

2.4 Gene expression analysis of osteoblast genes under different inductions . . . 59

2.5 Mineralisation potential of different osteogenic inducers 60

3.1 Workflow of this thesis 64

3.2 Lentiviral delivery of shRNA and the mechanism of RNA interference in mammalian cells 66

3.3 shRNA and small molecule inhibitors principle 67

3.4 Optimisation of viral transfection 72

3.5 Optimisation of viral transfection - GFP control virus. 73

3.6 ShRNA screen on MSCs differentiating into osteoblasts - illustration of hit distribution and selection 77

3.7 Venn-diagram of shRNA hits in inducing conditions 83

3.8 Effects of hairpins targeting *UBE2A* on cell viability and alkaline phosphatase activity 84

3.9 Knockdown of *UBE2A* with hairpin 4 and hairpin 5 85

3.10 Network 1 “Gene Expression, Infectious Disease, Embryonic Development ” 91

3.11 Network 2 “Cell Cycle, DNA Replication, Recombination, and Repair, Cellular Assembly and Organisation” 92

3.12 Network 3 “Cell-To-Cell Signalling and Interaction, Inflammatory Response, Infectious Disease” 93

3.13 Network 4 “Cellular Compromise, Cell-To-Cell Signalling and Interaction, Cancer” 94

3.14 Protein-protein interactions of hit genes 96

3.15 *BRD4* knockdown by hairpin 1 and hairpin 5 99

3.16 *KDM1A* knockdown by hairpins 2, 3 and 4 101

3.17 *JMJD8* knockdown by hairpin 3 and hairpin 4 103

3.18 *MORF4L1*knockdown by hairpin 3 and hairpin 4 104

3.19 *PHIP* knockdown by hairpin 3 105

3.20 Locked nucleic acid knockdown of epigenetic target genes 108

3.21 LNA knockdown of epigenetic target genes and its effect on alkaline phosphatase activity 109

3.22 Compound screen on MSCs under dexamethasone-induced differentiation . 113

3.23 Dose response curves under (+)-JQ1 treatment. 116

3.24 Dose response curve under RVX-208 treatment 117

3.25 Dose response curve under bromosporine treatment 118

3.26 Dose response curves under K00135 treatment 119

3.27 Dose response curves under 5-Iodotubercidin treatment 120

3.28 Dose response curves under CXD-101 treatment. 121

4.1 Structural analysis of BRD4 and (+)-JQ1 complexes 128

4.2 Structure based phylogenetic tree of the human bromodomain family 128

4.3 Effect of BET compounds on cell viability and alkaline phosphatase expression of differentiating MSCs 131

4.4 Chemical structure of the active enantiomer (+)-JQ1 and the inactive stereoisomer (-)-JQ1 131

4.5 Effect of (+)-JQ1 treatment on cell proliferation 135

4.6 Changes in osteoblast gene expression under (+)-JQ1 treatment. 137

4.7 Hierarchical clustering of genes regulated under dexamethasone and (+)-JQ1 treatment 138

4.8 Network “Lipid Metabolism, Small Molecule Biochemistry, Developmental Disorder” 145

4.9 Canonical pathways affected by BET protein inhibition 146

4.10 Alizarin Red S staining of MSCs under dexamethasone and (+)-JQ1 treatment 147

4.11 Alizarin Red S quantification of MSCs under dexamethasone and (+)-JQ1 treatment 148

4.12 Oil Red O stainings of MSCs under dexamethasone and (+)-JQ1 treatment 149

4.13 (+)-JQ1 treatment of primary cells 151

5.1 KDM1A functions in regulation of gene expression 161

5.2 Domain organisation and crystal structure of KDM1A 162

5.3 Mouse tissue preparation 165

5.4 MicroCT scan of mouse bones - different measurement areas 167

5.5 Dose response curve using the GSK690 inhibitor 169

5.6 Structure of the GSK690 inhibitor 169

5.7 Osteoblast gene expression under KDM1A inhibitor treatment 170

5.8 BV and BV/TV in different mouse age cohorts 173

5.9 BV and BV/TV values as measured for transgenic and wild type mice . . . 174

5.10 Three-dimensional rendered images from MicroCT scans 175

5.11 Bone mineral density measurement of young and middle-aged mice 176

5.12 Comparison of BMD and alkaline phosphatase activity in young cohort . . 177

A.1 Validation of alkaline phosphatase and cell viability assay 226

A.2 Validation of alkaline phosphatase substrate stability 227

A.3 Platform setup at PLACEBO Vienna 228

A.4 Vector map pLKO TRC001 230

A.5 Vector map pLKO TRC005 230

A.6 Setup for virus distribution 232

A.7 JANUS setup for lentivirus transduction 233

A.8 JANUS setup for alkaline phosphatase assay 235

A.9 Dose response curves under DOT1L-inhibitor treatment. 251

A.10 Dose response curves under SAHA treatment. 252

A.11 Dose response curves under valproic acid treatment. 252

A.12 Dose response curves under (-)-JQ1 treatment. 253

List of Tables

1.1 Epigenetic modifications and related "writers", "readers", and "erasers" . . . 27

2.1 List of media . . . 45

2.2 Dexamethasone-induced gene expression . . . 51

2.3 Bone functions annotations of genes expressed under dexamethasone treatment . . . 53

2.4 Upstream regulators of osteoblast gene expression under dexamethasone treatment . . . 54

3.1 Example of short hairpin sequences targeting *KDM1A* . . . 70

3.2 shRNA hits derived by selection process . . . 80

3.3 List of manually selected shRNA hits . . . 81

3.4 Number of shRNA hits per condition and direction of their effect . . . 81

3.5 List of hit genes and their epigenetic domains - part I . . . 86

3.6 List of hit genes and their epigenetic domains - part II . . . 87

3.7 Network analysis of of hits identified in shRNA screen . . . 88

3.8 ShRNA hit genes in protein complexes . . . 97

3.9 Selected hits from shRNA screen . . . 98

3.10 Medium conditions for compound screen . . . 111

3.11 List of small molecule inhibitors . . . 112

3.12 List of small molecule inhibitor hits . . . 114

4.1 50 highest regulated genes under dexamethasone treatment . . . 140

4.2 50 highest regulated genes under Dex + (+)JQ1 treatment 142

4.3 Fold changes in gene expression of bone-related genes under (+)-JQ1 treatment. 143

4.4 The three top gene networks under Dex + (+)-JQ1 treatment 144

4.5 Genes in the canonical pathway "PPARa/RXRa Activation" 145

4.6 (+)-JQ1 selectivity within BET protein target family 154

5.1 List of transgenic mice and related wild types 172

A.1 Media compositions used in this thesis 223

A.2 Primer sequences 223

A.3 Dexamethasone-induced gene expression - microarray data I 224

A.4 Dexamethasone-induced gene expression - microarray data II 225

A.5 List of equipment present in the PLACEBO platform 229

A.6 ShRNA gene target list as provided by PLACEBO - part I 236

A.7 ShRNA gene target list as provided by PLACEBO - part II 237

A.8 ShRNA gene target list as provided by PLACEBO - part III 238

A.9 ShRNA gene target list as provided by PLACEBO - part IV 239

A.10 ShRNA gene target list as provided by PLACEBO - part V 240

A.11 ShRNA target genes - knockdown results *BRD4* and *KDM1A* 241

A.12 ShRNA target genes - knockdown results *JMJD8* and *MORF4L1* 242

A.13 ShRNA target genes - knockdown results *PHIP* and *UBE2A* 243

A.14 Protein complexes - Part I 245

A.15 Protein complexes - Part II 246

A.16 Protein complexes - Part III 247

A.17 Protein complexes - Part IV 248

A.18 Protein complexes - Part V 249

List of abbreviations

ALP	Alkaline phosphatase (liver, bone, kidney)
ARS	Alizarin Red S
AS	Ankylosing spondylitis
BMD	Bone mineral density
BMP	Bone morphogenetic protein
BRD	Bromodomain
BV	Bone volume
ChIP	Chromatin immunoprecipitation
Col1	Collagen 1
DMEM	Dulbecco's modified Eagle's medium
DNMT	DNA methyltransferase
ECM	Extracellular matrix
EtOH	Ethanol
FAD	Flavin adenine dinucleotide
FGF	Fibroblast growth factor
FOP	Fibrodysplasia ossificans progressiva
GAG	Glycosaminoglycans
GC	Glucocorticoid

GPCR	G-Protein coupled receptor
GR	Glucocorticoid receptor
GRE	Glucocorticoid response element
HAT	Histone acetyltransferase
HDAC	Histone deacetylase
IPA	Ingenuity® Knowledge Base/Ingenuity Pathway Analysis
JAK/STAT	Janus kinase/Signal transducer and activator of transcription
KDM	Histone demethylase, lysine (K)-specific
MMP	Matrix metalloprotease
MOI	Multiplicity of infection
MSC	Mesenchymal stem cells (hMSCs, human mesenchymal stem cells)
MPC	Mesenchymal progenitor cell
NAD+	Nicotinamide adenine dinucleotide
NMC	NUT (nuclear protein in testis) midline carcinoma
NFATc1	Nuclear factor of activated T cells, cytoplasmic, calcineurin-dependent 1
NF-κβ	Nuclear factor kappa-β
OA	Osteoarthritis
OI	Osteogenesis imperfecta
OC	Osteocalcin

ON	Osteonection
OPG	Osteoprotegerin
OPN	Osteopontin
OSM	Oncostatin M
Osx	Osterix
PBS	Phosphate buffered saline
PCA	Principal component analysis
PFA	Paraformaldehyde
PHD	Plant Homeo Domain
P-TEFb	Positive transcription elongation factor complex
PTH	Parathyroid hormone
PTM	Post-translational modification
qPCR	Quantitative polymerase chain reaction
RA	Rheumatoid arthritis
RANK	Receptor activator of nuclear factor kappa-β
RANKL	Receptor activator of nuclear factor kappa-β ligand
RFU	Relative fluorescence unit
RUNX2	Runt-related transcription factor 2 (also CBFA1)
SAHA	Suberoylanilide hydroxamic acid

SGC	Structural Genomics Consortium
shRNA	Short hairpin RNA
siRNA	Small interfering RNA
TGF-β	Transforming growth factor-beta
TNF-α	Tumour necrosis factor-α
TRAP	Tartrate resistant acid phosphatase
TSA	Trichostatin A
TV	Tissue volume
VDR	Vitamin D receptor
VDRE	Vitamin D response element

1 Introduction

1.1 Tissue engineering

The generation of bone tissue for transplantation purposes is in high demand in clinical settings such as orthopaedic surgery. With an ageing population and a general shortage of donor tissue, the stem cell field holds a promising future in biological repair with a broad spectrum of potential clinical applications. The requirement for regeneration and replacement of skeletal tissues is enormous, ranging from skeletal defects arising from developmental abnormalities, to inflammatory bone diseases, tumours and degenerative diseases such as osteoarthritis and osteoporosis. However, this demand can barely be satisfied. At present, autologous bone grafting is generally considered as being the "gold standard" for the replacement of osseous tissues [1]. As bone tissue is "simply" transplanted from one part of the body to another in the same individual it is unlikely to cause immune rejection and in addition already contains elements that are critical for promoting bone formation, for example the bone scaffold structure and growth factors. However, autologous bone tissue from healthy bones is of limited availability, and a surgical intervention always involves the risk of post-operative pain and complications at the donor site, such as potential injuries to surrounding arteries, nerves, and tissues, and a general risk of infection [2–4]. In contrast, allogenic or xenogenic transplantations, which use transplants sourced from a genetically non-identical member of the same species as the recipient, or from another species, bear a risk of immunological rejection and transmission of diseases. To fill this gap in tissue availability, scientists and surgeons developed synthetic grafts with

similar properties to bone. These are often made of hydroxyapatite, the bone mineral, or other biocompatible substances, and are formed into a scaffold that would allow bone growth [5]. This osteoconductive method has been improved over the last years by adding growth factors that induce the differentiation of osteoprogenitor cells into osteoblasts, the bone forming cells. To take this one step further and promote osteogenesis within the graft, the application of stem cells has gained increased significance stimulating research over the last decades [6]. With the progress of combining scaffolds, progenitor cells, and growth factors, tissue engineering has the potential to overcome the aforementioned limitations by creating functional tissues that have the capacity for growth and self-repair [7–9]. In the next section, the different types of stem cells available for tissue engineering will be presented and their advantages as well as accompanying risks will be discussed.

1.2 Stem cells

Stem cells have the potential to develop into many different cell types during early life and growth. They can be distinguished from other cells by two major characteristics: First, they are unspecialised with an unlimited self-renewing capacity through cell division (mitosis), and second, under specific physiological or experimental conditions they can differentiate into tissue-specific cell types. Referred to as "potency", stem cells are characterised by their capacity to differentiate into other cell types [10]. The cell with the greatest potency is the totipotent zygote with the ability to divide and produce every differentiated cell type of an organism. During development, when cell fate is determined, the potency of a cell is gradually reduced and eventually only the potential to generate a few or one cell type will remain (figure 1.1).

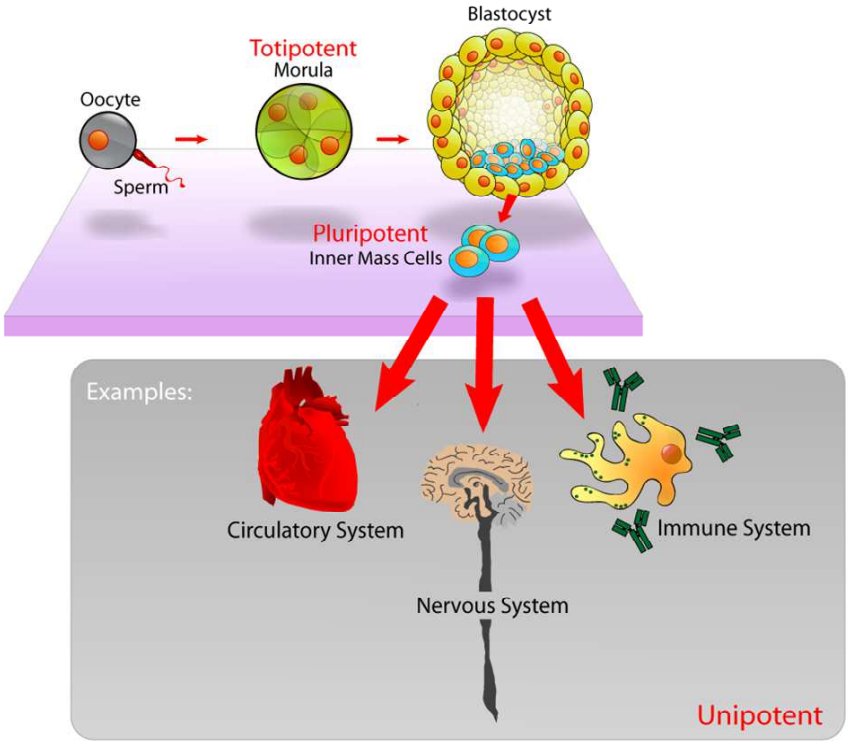

Figure 1.1: Different potencies of stem cells. The zygote is totipotent, the cell with the greatest differentiation potential and can divide to produce all the differentiated cells in an organism. With differentiation and lineage decisions made, cells lose their potency. Adapted from [11].

Almost a decade ago, scientists discovered that this is not a one-way street and that mature somatic cells can be converted into stem cells, the so-called induced pluripotent stem cells (iPSCs) [12].

1.2.1 Types of stem cells

Apart from the iPSC method, stem cells are derived from two main sources: embryonic stem (ES) cells are obtained from the inner cell mass of blastocysts, and adult stem cells can be found in various tissues of the body. The main difference between these two types of stem cells is their ability to differentiate into other cell types; ES cells can become every cell type of the body, whereas adult stem cells are already limited in their differentiation capability depending on their tissue of origin. It is postulated that the primary role of

undifferentiated adult stem cells is the repair and maintenance of the tissue in which they are found. Adult stem cells have been identified in many organs and tissues including bone marrow, blood, brain, skin, lung, heart, liver, gut, testes, glands, and skeletal muscle [13–16]. Mesenchymal and hematopoietic stem cells were shown to circulate in the body and if required can for example remain in an infected tissue and quickly produce cells needed to fight the infection or suppress the immune response [17, 18]. The application of embryonic stem cells with their origin in the inner cell mass of blastocysts formed through *in vitro* fertilisation has always been afflicted with ethical concerns about the destruction of human embryos. Their usage is still controversial and researchers strive to find alternatives [19,20]. Consequently, the use of adult stem or progenitor cells in both clinical applications and medical development has been further developed in recent years. Adult bone marrow-derived stromal cells with their ability to differentiate into mesenchymal cell types, e.g. osteoblasts, chondrocytes, adipocytes, tenoblasts, and stromal cells, have been the focus of intensive efforts aiming at their translation to new therapeutic approaches. With regard to osteoregenerative purposes and production of new functional bone, or as tools for studying both normal and pathological osteogenesis and osteogenic diseases, these cells are of great interest. In addition to naturally occurring stem cells, it was recently discovered that adult somatic cells, such as fibroblasts or blood cells, can be reprogrammed into cells with stem cell-like functions, so-called induced pluripotent stem (iPS) cells. Yamanaka et al. identified four transcription factors, namely OCT4, SOX2, KLF4, and C-MYC, as being sufficient to reprogram somatic cells to express genes and factors important for maintaining the defining properties of embryonic stem (ES) cells. These transcription factors are known to be important for the self-renewal of undifferentiated embryonic stem cells and for a wide range of cellular processes, including development, proliferation, differentiation, and cell

growth. The generation of mouse iPS cells was first reported in 2006, followed by the generation of human iPS cells in 2007 [12, 21]. Although reprogrammed cells were shown to meet the defining criteria for pluripotent stem cells and display common ES cell markers, it still remains to be elucidated if iPS and ES cells differ in significant ways. Both ES and iPS cells can form teratomas, cell masses that contain cells from all three germ layers, and produce chimeric offspring. Global gene expression profiles and epigenetic states of iPS cells have been shown to be highly similar to ES cells, but it still remains unknown if ES-cell-like characteristics are re-established throughout the genome [22–24]. The concern that the reprogramming might not lead to fully comparable cells and that the cells possess an epigenetic memory has still not been ruled out [25–27].

1.2.2 Mesenchymal stem cells

Mesenchymal stem cells (MSCs) are adult stem cells of stromal origin and can be obtained from different parts of the body, including bone marrow, adipose tissue, dental tissue, and blood. MSCs express a set of surface markers, including CD105, CD90, CD44, CD166, CD29, CD73, and also CD106, and are negative for CD14, CD34, and CD45 [28]. However, no specific markers currently exist that can reliably discriminate between MSCs and fibroblasts [29].

MSCs are multipotent stem cells and corresponding to their origin have the potential to differentiate into mesenchymal cell types, e.g. osteoblasts, chondrocytes, adipocytes, tenoblasts, and stromal cells, as well as the myogenic lineage, and therefore play an important role in tissue repair and regeneration processes of the adult organism (figure 1.2). In the early 1970's, Friedenstein and colleagues were the first to report the presence of cells that could be isolated from the adult bone marrow stroma. These cells could proliferate

and form colonies *ex vivo* as adherent cells, exhbited fibroblast-like morphology, and gave rise to multiple tissues found within the skeleton - bone, cartilage, adipocytes, fibroblasts, and myelosupportive stroma [30].

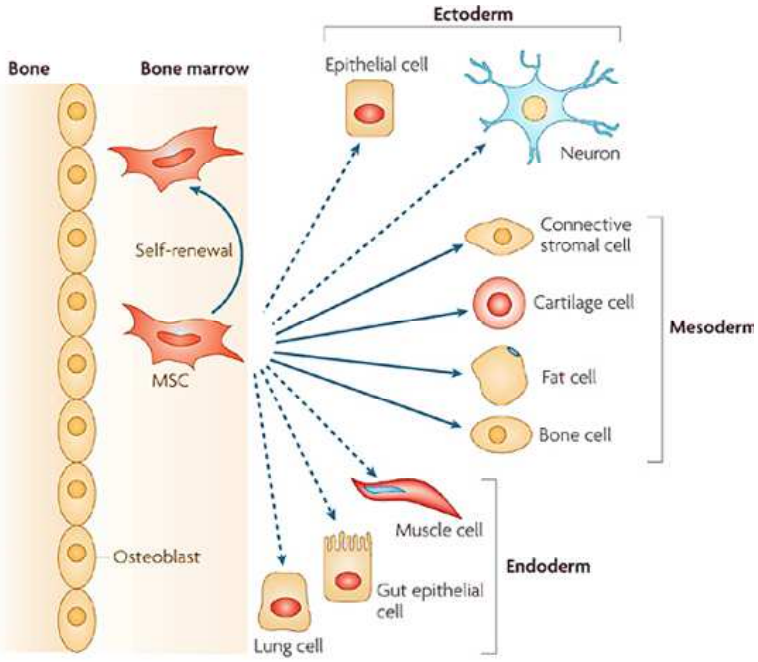

Figure 1.2: The multipotency of MSCs. MSCs have the ability to self-renew and to differentiate towards the mesodermal lineage. Transdifferentiation into cells of other lineage *in vivo* is still controversial (dashed arrows). Adapted from [31].

Compared to this "skeletal stem cell" found in the bone marrow stroma, the "mesenchymal stem cell" as termed by Caplan [32], can be found almost everywhere in the body and is thought to be endowed with a much broader multipotency (figure 1.2) [33–35]. Although the broader definition has become more popular and attained universal use, with regard to our interest in bone development, the original understanding of skeletal stem cells is underlying the work in this thesis. MSCs are known for their anti-inflammatory properties and immune modulatory capabilities. They regulate immune responses through interact-

ing with and suppressing the activation of T-cells, B-cells, dendritic cells, as well as natural killer cells, and by inhibiting the release of pro-inflammatory cytokines [31, 36]. Although MSCs isolated from the previously mentioned different sources share a considerable degree of overlap in their expression profile, they are known to have distinct variations in the pattern and level of gene expression. For instance, adipose tissue-derived multipotent stromal cells show a higher level of secretion of cytokines involved in immunomodulatory effects than bone marrow-derived multipotent stromal cells [37]. In osteoarthritis (OA), MSCs contribute to maintenance of healthy tissues by acting as reservoirs of repair-competent cells, influencing host-cell behaviour by activating a paracrine response and by reducing inflammation [38]. To date, there are around 400 registered clinical trials (www.clinicaltrials.gov) using MSCs to treat various conditions, including bone defects, wound healing, inflammatory diseases such as OA, rheumatoid arthritis (RA), and multiple sclerosis, as well as diabetes. Some of these early trials are already completed and 31 are even in Phase III or IV (as in March 2014), supporting the therapeutic potency of MSCs. Nevertheless, there are drawbacks: surgical bone marrow aspirations only yield limited numbers of MSCs (approximately one stem cell in 30,000 cells) and with donor age the proliferation rate of adult MSCs decreases, thus their ability to expand and differentiate is limited [39, 40].

The potential of MSCs as source for cell-based regenerative technologies is limited by our understanding of their development, knowledge about factors and pathways influencing cell fate decisions towards a specific cell type, as well as epigenetic modifications occurring during their differentiation. In order for MSCs to commit to the osteoblast lineage, a combined action of signal transduction pathways induced by bone-promoting cytokines is required. In *in vitro* differentiation studies, MSCs have been shown to respond to various

osteogenic induction factors, including the extracellular matrix-promoting agent ascorbic acid, beta-glycerophosphate, a phosphate source promoting bone matrix mineralisation, and the synthetic glucocorticoid agonist dexamethasone [41–43]. Other factors, such as members of the bone morphogenetic protein family (BMPs), and the calcium-regulating 1,25-dihydroxyvitamin D_3 are also known to play an important role in *in vitro* osteoblast differentiation [44–47]. Lately, the cytokine oncostatin M has been shown to promote mesenchymal stem cell differentiation [48, 49]. All these factors will be presented in more detail in chapter 2. During the differentiation process towards the osteogenic lineage, MSCs pass through different stages of development.

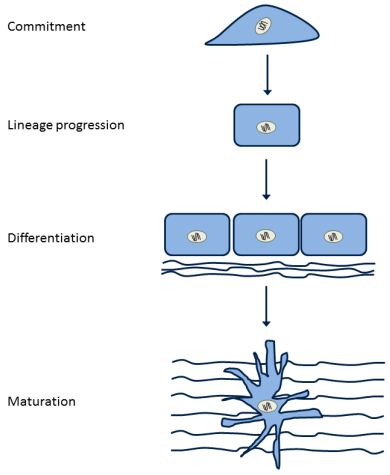

Figure 1.3: Stages of osteogenic differentiation. Mesenchymal stem cells commit to the osteoblastic lineage, in which early stages they are characterised by expressing the transcription factors RUNX2 and Osterix (OSX). This ultimately leads to the development of osteoblasts and subsequent full maturation, in which a subset of osteoblasts can become osteocytes upon being entombed in the bone matrix. Adapted from [50].

Following initiation, the first part of differentiation is characterised by the commitment phase, where cells leave their stem cell-like state; this is directly followed by the lineage progression phase, where early markers of the chosen lineage are expressed. During osteogenic differentiation, this entails the expression of early marker transcription factors RUNX2 and Osterix (OSX) [51, 52]. This stage is succeeded by the full differentiation and ultimately the maturation phase, in which osteoblasts are fully differentiated and captured within mineralised tissue where they become osteocytes (figure 1.3) [53].

The differentiation of stem cells into the osteogenic lineage for subsequent use in bone tissue engineering and bone reconstruction offers a chance to overcome various problems in regenerative medicine. In developed countries, an increased incidence of osteodegenerative diseases, such as osteoporosis and osteoarthritis, represents a public health issue afflicting a high proportion of the elderly population. Together with systemic disorders like osteogenesis imperfecta (OI) and fibrous dysplasia this generates a major need for healthy bone tissue which is exacerbated by a general shortage of donor cells, tissues and organs. The generation of bone cells through differentiation of MSCs could possibly not only help age-related diseases, but could also provide useful applications in bone reconstruction after traumatic bone injuries and treatment of skeletal deficiencies. Furthermore, predetermined bone forming cells could be used for transplantation to repair and strengthen porous, weak, and fragile bone matrix in systemic bone disorders. However, to meet these demands and opportunities, well-defined and efficient protocols for tissue generation are needed and have to fulfil clinical safety standards ensuring the generation of high-quality homogeneous cell populations. In order to generate these protocols, we need a clear understanding of the basic biology and the differentiation process from stem cells into osteoblasts and despite the important advances made in the past, there is still considerable ambiguity regarding these processes. These uncertainties have a major impact on the envisioned therapeutic application of MSCs and can only be overcome by a thorough assessment of genetic and epigenetic mechanisms underlying the differentiation into bone-forming cells. Before discussing known mechanisms involved in osteogenesis, and leading over to how this thesis will contribute to a better understanding, a brief overview of bone function, development, and remodelling is given.

1.3 Bone function and development

Bone and cartilage are the two tissue components constituting the endoskeleton of vertebrates. Although of rigid structure, bone is a dynamic organ that is constantly remodelled to adapt to the forces placed upon it.

The human skeleton serves six major functions [54]:

- Support: Bone supports tissues and muscles by providing a rigid shape.
- Protection: The rigidity of the bones protects inner organs from damage, for example the rib cage and the skull.
- Movement: Bones enable body movements by acting as levers and points of attachment for muscles, and together with the joints the three provide the principal mechanics for movement.
- Production of blood cells: The skeleton is the site for haematopoiesis, the development of blood cells that takes place in the bone marrow.
- Storage of minerals and energy: Bones serve as a reservoir for calcium and phosphate. The bone marrow is also involved in iron metabolism and the yellow bone marrow acts as a storage reserve for fatty acids.
- Part of the endocrine system regulating energy metabolism: For example, bone cells release osteocalcin, which regulates insulin production and insulin sensitivity in the body and thereby contributes to the regulation of blood glucose levels and fat deposition [55, 56].

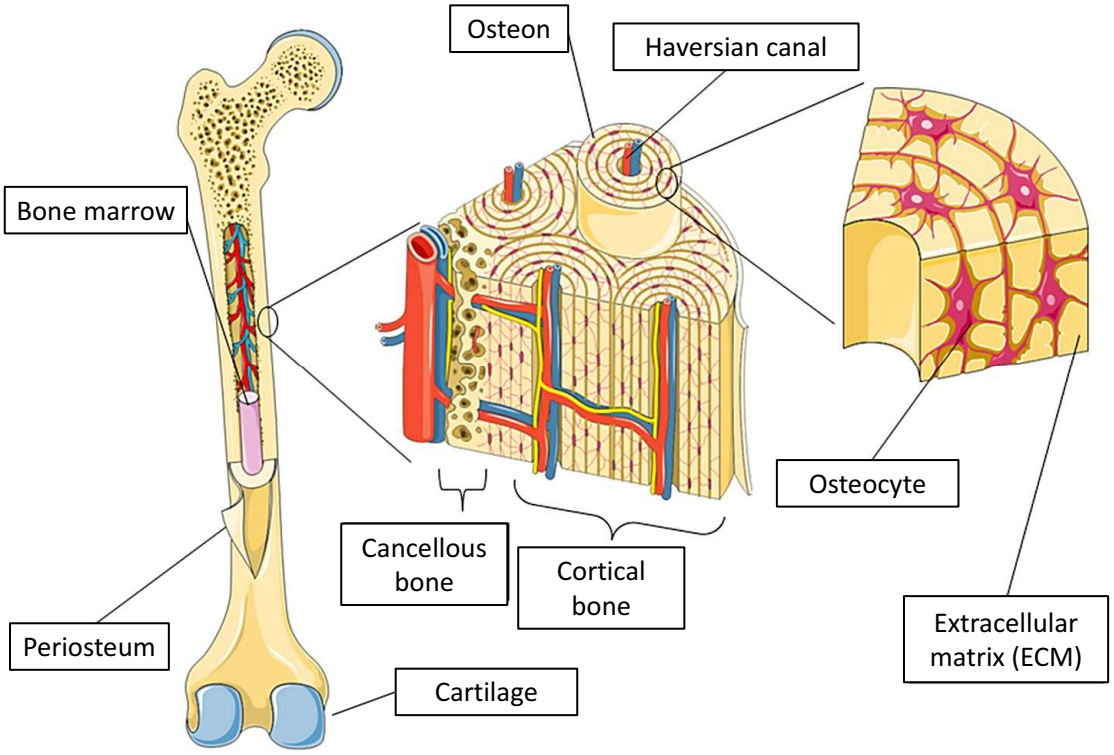

Figure 1.4: Schematic overview of bone, depicting gross overview, and cellular distribution. The periosteum is a membrane covering the outer surface of bones. Osteocytes are cells derived from osteoblasts that become trapped in the extracellular matrix (ECM). The osteon or haversian system is the functional unit of compact bone, containing the nerves and blood supplies. Adapted from [57].

There are five types of bones found in the human body: long, short, flat, irregular, and sesamoid bones [58]. Most of the long bones are found in the limbs and are characterised by a shaft, the diaphysis that is much longer than it is wide, a high proportion of compact bone, and lesser amounts of bone marrow. Short bones in wrists and ankles have only a thin layer of compact bone, as do flat bones like the skull and sternum. Finally, there are irregularly shaped bones including vertebrae and the pelvis that do not fit in any of the above categories, and sesamoid bones, which are embedded in tendon. Bone tissue is a type of dense connective tissue composed of compact (cortical) bone and spongy cancellous (trabecular) bone (figure 1.4) [59]. The bone organ consists of a mineralised matrix

composed primarily of inorganic hydroxyapatite ($Ca_5(PO_4)_3(OH)$), organic collagen, and growth factors. Within the matrix, a specialised bone cell type can be found, the osteocyte. These cells are derived from osteoblasts that become "trapped" in the matrix. There are two ways in which bone tissue formation (osteogenesis) occurs: intramembranous ossification is the direct laying down of bone into the primitive connective tissue, while endochondral ossification forms bone by replacing a cartilaginous precursor that evolved earlier during (embryonic) development (figure 1.5).

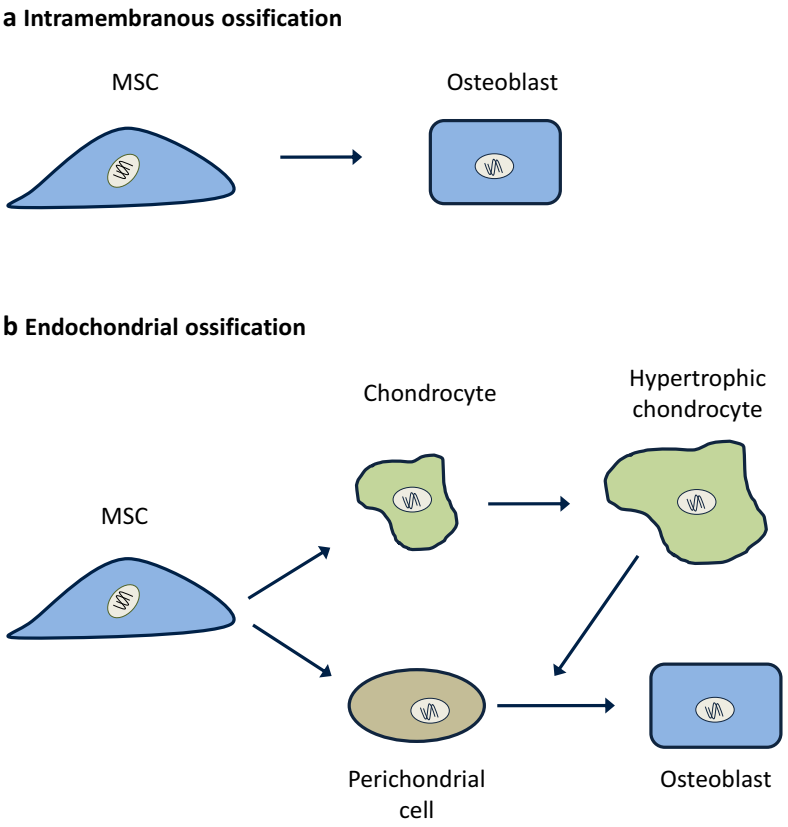

Figure 1.5: Osteogenesis can occur in two different ways: During intramembranous ossification (a), mesenchymal stem cells differentiate directly into osteoblasts. By contrast, during endochondral ossification (b), mesenchymal stem cells condense and differentiate into perichondrial cells and chondrocytes first before becoming osteoblasts. Adapted from [60].

Bone is constantly being remodelled in a dynamic process in which mature bone tissue is replaced by new tissue. Bone remodelling not only occurs during early growth or following

injuries, but also in response to repetitive micro-damage from normal physical activity, and regulates calcium and phosphate levels in the body. In the first year of life almost 100% of the skeleton is replaced, whereas in adults remodelling only occurs for about 10% of total bone. During bone remodelling, the integrity of the skeleton is maintained through the balanced activities of its constituent cell types. Osteoblasts are the cells responsible for the synthesis and mineralisation of bone; osteoclasts, large multinucleated cells, are responsible for the dissolution and resorption of bone, and osteocytes act as mechanosensors and exert endocrine functions (figure 1.6) [61].

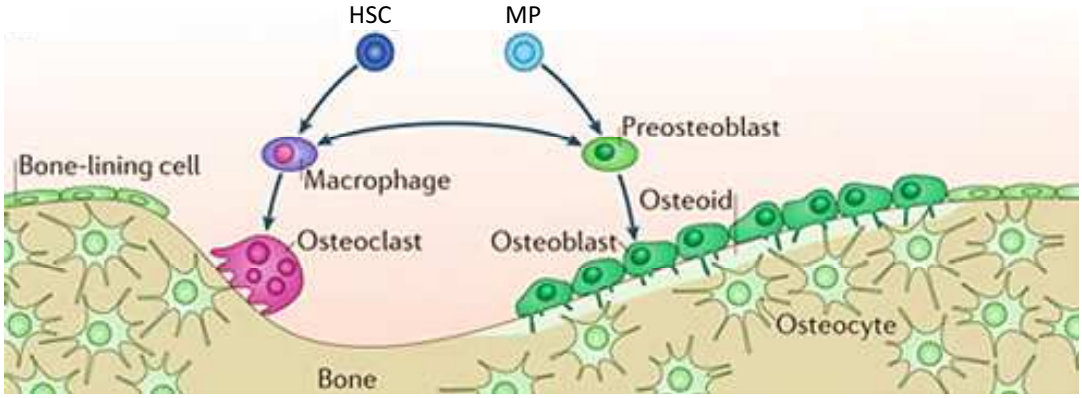

Figure 1.6: Bone remodelling is a fine balance act between osteoclasts (which are responsible for bone resorption) and osteoblasts (which are responsible for bone formation). Osteoclasts arise from haematopoietic stem cells, whereas osteoblasts arise from mesenchymal stem cells. HSC, haematopoietic stem cells; MP, mesenchymal progenitors. Adapted from [60].

While osteoblasts and osteocytes are derived from mesenchymal precursors, osteoclasts are of haematopoietic origin. These cells are tightly coupled and their balanced interplay is essential for maintaining a stable bone mass. Indeed, an imbalance leading to reduced osteoblast activity and/or increased osteoclast function results in bone loss and osteoporosis. Osteoclast differentiation is controlled by the receptor activator of nuclear factor kappa-β (RANK)/receptor activator of nuclear factor kappa-β ligand (RANKL) pathway that relies on cell-cell interaction between osteoblasts and osteoclast precursors. Upon

RANKL binding, amongst others NF-κβ (nuclear factor-κβ) and NFATc1 (nuclear factor of activated t cells, cytoplasmic, calcineurin-dependent 1) are activated, inducing a set of genes leading to cell fusion and expression of proteolytic enzymes necessary for osteoclast function, such as tartrate resistant acid phosphatase (TRAP), Cathepsin K, and matrix metalloproteases (MMPs). Once activated and differentiated, osteoclasts adhere to the site of resorption and form a "lacuna" through sealing of the underlined bone matrix by a cytoskeletal rearrangement and the subsequent formation of an actin ring [62]. By forming a specialised cell membrane, the "ruffled border", osteoclasts increase their secretion and resorption surface. Dissolved bone material is taken up via transcytosis and released into the extracellular compartment [63]. In a balanced system, bone resorption is followed by synthesis of new bone by osteoblasts, a process that takes substantially longer than the resorption. Bone resorption is regulated by osteoblasts and controlled through the RANKL/RANK/osteoprotegerin (OPG) system. OPG is an osteoblast-secreted decoy receptor that protects the skeleton from excessive bone resorption by binding to RANKL and preventing it from binding to its receptor on osteoclasts, RANK. Osteocytes, although metabolically less active, are also involved in the regulation of bone turnover, the control of mineral metabolism, and the response to loading through various mechanosensory mechanisms [53]. In addition, osteoclasts are regulated by several hormones, including parathyroid hormone (PTH) and calcitonin, signalling mechanisms that will be discussed in the following subsection 1.3.2 describing osteogenic signalling pathways.

1.3.1 Musculoskeletal pathologies

There are many classified skeletal pathologies with one of the most common being osteoporosis, a disease characterised by a reduction in bone mass and bone mineral density (BMD). Osteoporosis is most common in women after menopause when oestrogen levels decline. The lack of oestrogen leads to an imbalance between bone formation and resorption, resulting in inadequate formation of new bone [64]. Another skeletal disorder leading to a decrease in bone mass and strength, but with a very different underlying mechanism, is Osteogenesis Imperfecta (OI). A deficiency in type 1 collagen, the main component of connective tissue, which is caused by the substitution of an amino acid in the collagen triple helix structure leads to weaker and brittle bone. The incidence of OI is estimated to be one per 20,000 live births and presently there is no cure [65]. Rheumatoid arthritis (RA) is an autoimmune disease that results in a chronic, systemic inflammatory disorder that affects primarily (synovial) joints, leading to the destruction of articular cartilage, ankylosis (fusion) of the joints and wear of bones [66]. Ankylosing spondylitis (AS) is another chronic inflammatory disease that mainly affects joints in the spine and in the pelvis, causing eventual fusion of the spine [67]. For both, pathogenesis is not yet fully understood, and as a result, disease management and treatment are often unsatisfactory. Osteoarthritis (OA) is a disease leading to a loss in bone strength as a secondary effect. OA can be caused by a variety of reasons, including hereditary, developmental, metabolic, and mechanical deficits, as well as injury. It is initiated by a degenerative process that eventually causes loss of cartilage and a corresponding lack of protection of bone surfaces leading to bone damage [68]. According to the National Health Service (NHS), it is the most common type of arthritis found in the UK, with around one million patients per annum seeing their general practitioner (GP), leading to more than 140,000 hip and knee

replacement surgeries. Skeletal disorders are not only caused by a loss of bone but a disease pattern can also be obtained due to excessive bone growth. In Fibrodysplasia ossificans progressiva (FOP), a symptom sometimes referred to as "Stone Man Syndrome", a mutation of the body's repair mechanism causes fibrous tissue, including muscle, tendon, and ligaments, to be ossified spontaneously or when damaged. The genetic cause of FOP was discovered within the *ACVR1* gene (activin A receptor, type 1), which encodes a type I bone morphogenetic protein (BMP) transmembrane receptor [69]. A number of point mutations in this gene were reported to lead to its constitutive activation, which in turn induces alkaline phosphatase activity, upregulates BMP-4 and downregulates BMP antagonists [70].

1.3.2 Osteogenic signalling pathways

The formation and development of bone tissue is a strictly controlled process, in which various extrinsic factors, including hormones and growth factors, activate osteoblast and osteoclast specific signalling proteins and transcription factors required for osteogenic differentiation [71]. This process is tightly regulated by cytokines, small proteins (approximately 5-20kDa) which are important in cell signalling that regulate the expression of cell-lineage specific transcription factors. In osteoblast differentiation, bone morphogenetic proteins (BMPs), transforming growth factor (TGF)-β, parathyroid hormone (PTH), calcitonin, members of the hedgehog morphogens, Wnt, JAK/STAT (Janus kinase/signal transducer and activator of transcription), fibroblast growth factor (FGF), Notch, and NEL-like protein 1 signalling proteins are involved in the initiation of signal transduction cascades leading to osteoblast lineage commitment (figure 1.7 to figure 1.9) [60,72,73]. The key event in osteoblast differentiation is the activation of the transcription factor RUNX2

(also known as Cbfa1), which is targeted by all of the above signalling pathways [51,74,75]. After activation, RUNX2 interacts with transcriptional activators, repressors and other co-regulatory proteins such as the transcription factor Osterix (OSX) and regulates the expression of numerous osteoblast genes including alkaline phosphatase (*ALPL*), collagen 1 (*COL1*), osteopontin (*OPN*), osteonectin (*SPARC*), osteocalcin (*BGLAP*), and bone sialoprotein (*IBSP*) [52]. Mice with a homozygous knockout for *Runx2* (*Runx2*$^{-}$/$^{-}$) show an absence of differentiated osteoblasts as well as mineralisation and die shortly after birth [76].

Bone morphogenetic protein (BMP) signalling plays a key role in skeletal development, bone remodelling and maintenance of bone homeostasis, and controls osteoblast-specific genes through binding of SMAD proteins (SMAD1, -5, and -8), the intracellular mediators of BMP signalling. The SMAD proteins are homologs of the Caenorhabditis elegans protein SMA and the Drosophila protein MAD (mothers against decapentaplegic). The family members BMP-2, -4, and -7 are known to stimulate expression of osteoblast markers in osteoprogenitors, cells that are committed to osteoblast differentiation (figure 1.7) [77–79].

Members of the **transforming growth factor beta** (TGF-β) superfamily are proteins that play an important role in signalling pathways involved in various cellular processes including cell growth and development, as well as differentiation and are amongst the most abundant cytokines found in the bone matrix. Like BMPs, these proteins interact with a conserved family of cell surface serine/threonine-specific protein kinase receptors (composed of type I and II subtypes), and generate intracellular signals using SMAD2 and -3, which act as transcription factors to regulate target gene expression (figure 1.7) [80].

Signalling through the **parathyroid hormone** (PTH) shows both anabolic and catabolic

effects on bone. PTH increases the activity of the cytochrome P450 superfamily member 1-α-hydroxylase, which converts 25-hydroxycholecalciferol to 1,25-dihydroxyvitamin D_3, the active form of vitamin D, thereby enhancing osteogenesis. 1,25-dihydroxyvitamin D_3 increases the availability of calcium and phosphate for incorporation into bone and stimulates the production of osteocalcin and osteopontin in osteoblasts [81–83]. With a more direct effect, PTH can also bind to osteoblasts, stimulating them to increase their expression of RANKL and inhibiting their expression of OPG. The lack of competitive OPG facilitates the binding of RANKL to RANK and stimulates osteoclast precursors to fuse, forming multinucleated new osteoclasts and thereby increasing bone resorption. A similar effect was shown for 1,25-dihydroxyvitamin D_3, which binds to its receptor (vitamin D receptor, VDR) on osteoblasts, induces RANKL expression and downregulates OPG (figure 1.7) [84].

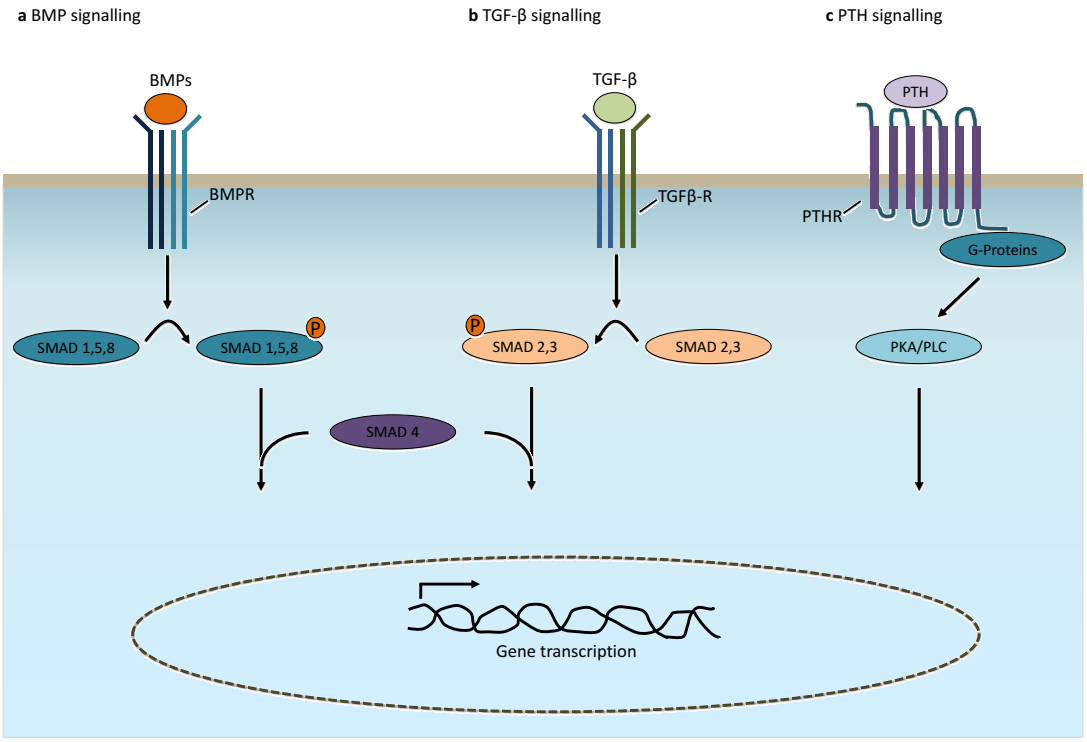

Figure 1.7: Osteogenic signalling pathways I. a | Bone morphogenetic protein (BMP) signalling stimulates osteoblast differentiation and function. Binding of BMP-2 or BMP-4 to their receptors results in phosphorylation of SMAD1, -5 or -8. These then form a complex with their partner, SMAD4, and enter the nucleus to regulate gene expression. b | TGF-β signalling. TGF-β superfamily ligands bind to a type II receptor, which recruits and phosphorylates a type I receptor and then phosphorylates SMAD2, or -3 which can then bind SMAD4, and accumulate in the nucleus where they act as transcription factors and participate in the regulation of target gene expression. c| Parathyroid hormone (PTH) stimulates osteogenic cell proliferation. The PTH receptor is a G-protein-coupled receptors (GPCR) which associates with at least two signal transduction systems, the cAMP-dependent protein kinase (PKA) pathway and the phospholipase C (PLC). Both systems take part in regulation of a number of target proteins involved in bone and cartilage development. Adapted from [85, 86].

Calcitonin, also known as thyrocalcitonin, is a hormone that in humans is produced by the parafollicular cells (C-cells) of the thyroid gland, which counteracts the effects of PTH. Calcitonin generally participates in calcium (Ca^{2+}) and phosphate metabolism, both important components of extracellular matrix and essential for ossification. Calcitonin reduces blood calcium levels and thereby influences bone formation and remodelling, but also protects against calcium loss from the skeleton during periods of calcium mobilisation, such as lactation [87]. The hormone exercises its effects in two different ways, on the one hand by inhibiting osteoclast activity in bone, thereby preventing calcium release [88], and on the other hand by inhibiting calcium absorption by the intestine and kidney (figure 1.8) [89–91].

Hedgehog and Wnt signalling pathways control bone formation and development through regulation of *RUNX2* expression and both function to drive differentiation of osteochondrogenic progenitor cells towards the osteoblast lineage [92–94]. Wnt proteins are glycoproteins related to the Drosophila melanogaster protein Wingless, a segment polarity gene involved in the formation of the body axis during embryonic development. Hedgehog signalling also takes its name from a segment polarity gene found in Drosophila, and the involved ligands are key regulators during vertebrate embryonic development [95–97]. Both pathways were shown to integrate signals, e.g. the effect of BMP-2 on mineralisation was reported to be partly mediated by the induction of a Wnt autocrine/paracrine loop (canonical Wnt/β-catenin signalling), which appears to be responsible for alkaline phosphatase induction (figure 1.8) [73]. Similarly, Hedgehog-induced osteoblastogenesis requires BMP signalling and together they elicit a synergistic expression of alkaline phosphatase activity [98].

A role for **JAK/STAT** signalling as negative regulator of BMP-induced osteogenic dif-

ferentiation was proposed by Levy et al. [99]. In hMSCs, phosphorylation of STAT3 tyrosine was mediated by JAK2 as response to BMP-2 and -4. Conversely, another publication showed that under dexamethasone and BMP-2 treatment, the knockout of *STAT3* by siRNA (small interfering RNA) suppresses the synergistic effects of the two inducers, suggesting that STAT3 is required for osteogenic differentiation (figure 1.8) [100].

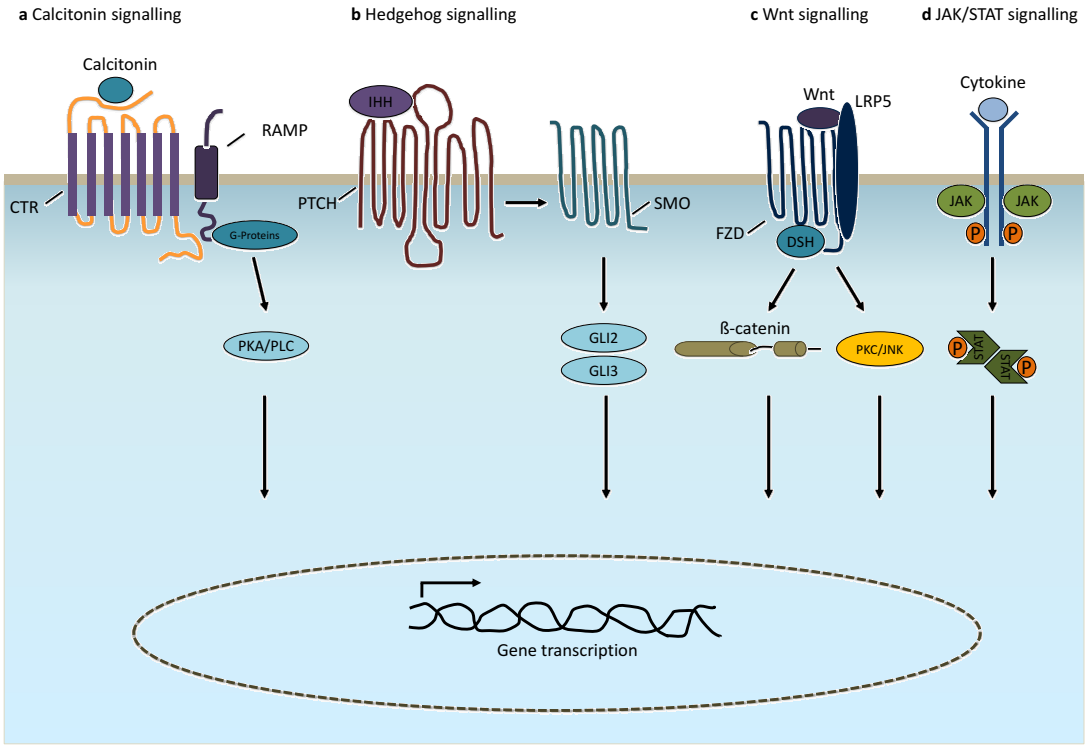

Figure 1.8: Osteogenic signalling pathways II. a| The activities of calcitonin (CT) are mediated by high affinity calcitonin receptors (CTRs). The G- protein-coupled receptor associates with at least two signal transduction systems, the cAMP-dependent protein kinase (PKA) pathway and the phospholipase C (PLC). Activation of the PLC also causes the release of Ca^{2+} from intracellular stores. Receptor activity modifying proteins (RAMPs) are single-transmembrane domain proteins that provide a mechanism for the diversification and regulation of receptor function. b| Hedgehog signalling through Indian hedgehog (IHH) is required for osteoblast differentiation through endochondral ossification. IHH binding to the receptor Patched (PTCH) activates signalling through Smoothened (SMO), thereby activating the GLI2/3 complex and promoting gene expression. c|WNT signalling promotes osteoblast differentiation. During β-catenin-dependent WNT signalling, β-catenin is stabilised following binding of WNT to its receptors Frizzled (FZD) and lipoprotein receptor-related protein 5 (LRP5), and activation of dishevelled (DSH), leading to the transcription of β-catenin target genes. β-catenin-independent signalling forms a similar transmembrane complex and activates secondary messengers such as protein kinase C (PKC) or c-Jun N-terminal kinases (JNKs). d|JAK/STAT signalling. JAKs are activated by cytokine binding to the cell-surface cytokine receptors and dimerisation of two receptor molecules. Through dimerisation the two JAKs come into close proximity, where they can phosphorylate each other, and upon binding also STATs. Once phosphorylated, two STATs form a dimer, an active transcription factor that enters the nucleus and regulates the transcription of various genes that regulate cell proliferation and differentiation. Adapted from [85, 86].

Fibroblast growth factors (FGFs) are known to play important roles in skeletal development and postnatal osteogenesis by activating FGF receptors (FGFRs) and downstream signalling pathways that control cells of the osteoblast, adipocyte, and chondrocyte lineage (figure 1.9) [101, 102].

Another highly conserved signalling system, the **Notch** pathway, has been reported to play a major role in the commitment of mesenchymal cells to the osteoblastic lineage (figure 1.9). Hilton et al. suggested that Notch signalling in bone marrow acts to maintain a pool of mesenchymal progenitors by suppressing osteoblast differentiation [103].

The role of **NELL-1** signalling in osteogenesis was first discovered in premature bone formation in human sporadic coronal craniosynostosis [104]. NELL-1 is expressed during both intramembranous and endochondral bone formation and in several *in vivo* studies, such as calvarial defect and spinal fusion models, it was demonstrated that NELL-1 signalling shows a comparable bone regeneration capacity to BMP-2. Furthermore, NELL-1 was reported to be directly regulated by RUNX2 [105–107]. Recent *in vitro* and *in vivo* data showed that NELL-1 can also promote osteogenesis by exerting an anti-adipogenic effect and repressing adipocyte differentiation and gene expression possibly via a Hedgehog-dependent mechanism (figure 1.9) [108].

In summary, the intricate cell signalling processes allow induction of osteoblast differentiation via a variety of pathways, which are however very closely related and characterised by a high degree of cross-talk. Precise organisation of this orderly process is essential for an organised cascade of events to be initiated. The switch from mesenchymal stem cell homeostasis to specific gene transcription required for differentiation is orchestrated by epigenetic mechanisms that are highly dynamic in regulating the chromatin structure. In recent years, significant progress has been made in deciphering the epigenetic mechanisms underlying differentiation in general and a review on the findings is given in the next section.

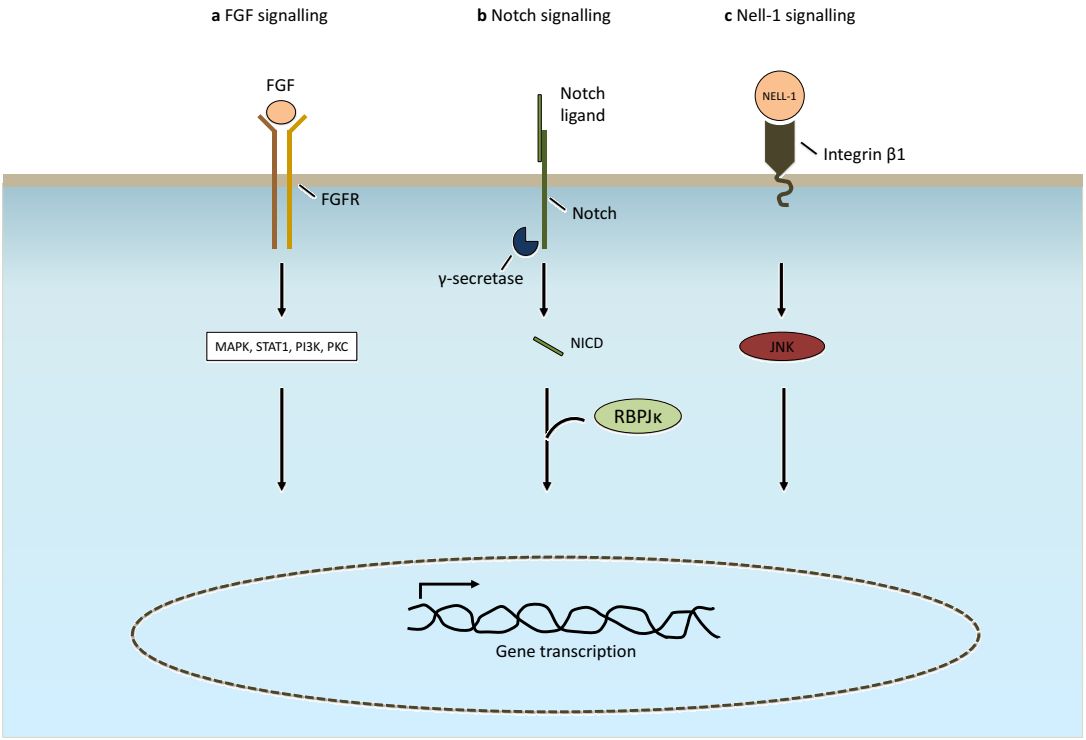

Figure 1.9: Osteogenic signalling pathways III. a| Fibroblast growth factor (FGF) signalling has diverse roles in osteoblast lineage cells. FGFs function by binding to cell surface tyrosine kinase FGF receptors (FGFR), leading to the activation of multiple signalling modules (MAPK, mitogen-activated protein kinase; STAT1, signal transducer and activator of transcription 1; PI3K, phosphoinositide 3-kinase, PKC). FGF signalling regulates pre-osteoblast proliferation and osteoblast differentiation, as well as the function of mature osteoblasts. However, the precise stages at which FGFs regulate proliferation and differentiation, and the intracellular signalling cascades responsible for each function, remain to be elucidated. b | Notch signalling inhibits osteoblast differentiation. Following binding to their ligands, Notch receptors are proteolytically cleaved by the γ-secretase complex, leading to release of the Notch intracellular domain (NICD) from the plasma membrane. NICD interacts with RBPJκ and together they activate downstream target genes, ultimately leading to inhibition of osteoblast differentiation. c | NELL-1 signalling. NELL-1 is a secreted osteoinductive protein that binds to the cell surface receptor integrin β1. Multiple intracellular signalling pathways have been shown to increase after NELL-1 stimulation and although the exact mechanism is still unknown, NELL-1 treatment results in increased *RUNX2* transcription and induction of osteogenic programming. Adapted from [85, 86].

1.4 Epigenetics

The term "epigenetics" was coined in 1942 by Conrad Hal Waddington (1905-1975), a British developmental biologist, who described how gene regulation modulates development and phenotypes. Waddington proposed the concept of an "epigenetic landscape" to represent the process of cellular fate determination during development [109]. Visualising the irreversible cell fate determinations as marbles travelling down a valley with ridges representing the "choices" the cells have to made, Waddington used this conceptual model as a metaphor for biological development, at that time not even knowing about genes and their role in heredity and development. Today, with additional knowledge about genes, heredity, and cell fate determination, epigenetics is defined as "the study of heritable changes in gene activity that are not caused by changes in the DNA sequence" [110, 111]. Epigenetic regulation of gene expression is known to occur due to alterations in chromatin proteins that do not change the DNA sequence, but alter the chromatin architecture and the accessibility of genes, resulting in changes to gene expressions that are preserved during cell division. These chromatin proteins (i.e. histones) pack and order the DNA into nucleosomes, which are fundamental structural repetitive units, formed by 146 base pairs wrapped around a histone protein core. The protein core is an octamer composed of two copies of each histone subunit H2A, H2B, H3 and H4, linked by histone H1, which "sits" on the structure and binds to the linker DNA between the nucleosomes, stabilising the structure and keeping the DNA in place [112, 113]. Each of the core subunits is characterised by an architectural motif near their C-terminus, termed the "histone fold" that allows the assembly into a nucleosome [114]. In addition, the subunits have a more flexible N-terminal tail that protrudes from the nucleosome and can be subjected to a variety of post-translational modifications (PTMs) as outlined below (figure 1.10).

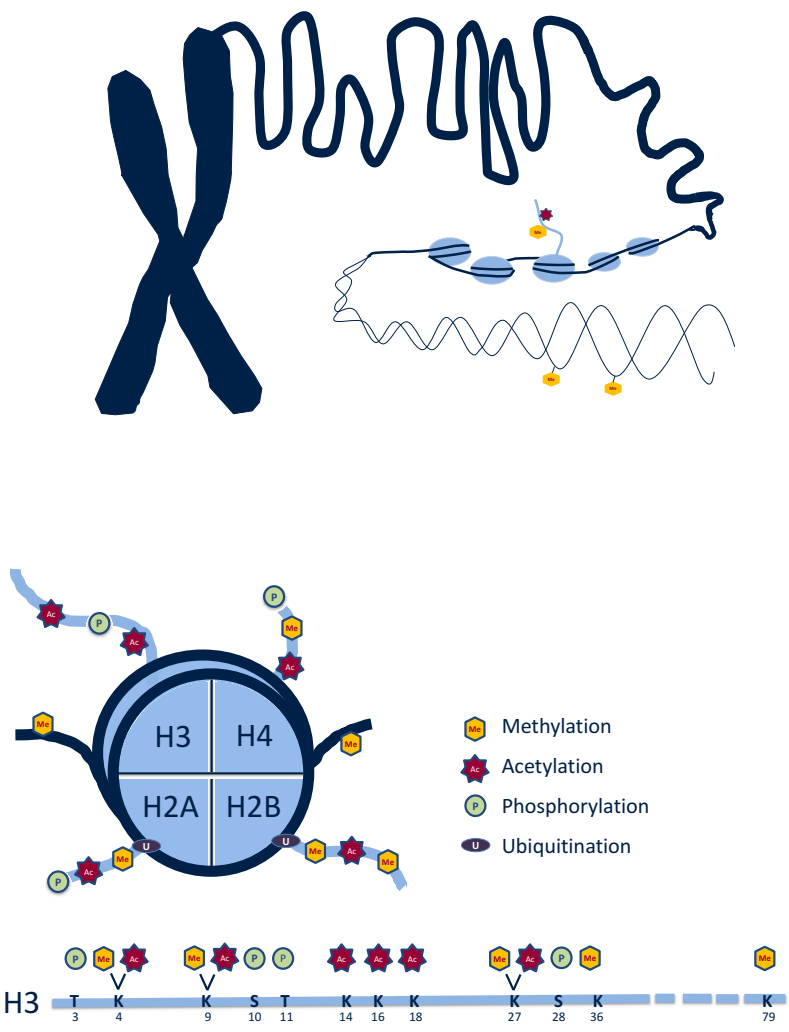

Figure 1.10: Organisation of DNA in an eukaryotic cell. DNA is packaged with proteins (histones) into nucleosomes to form chromatin fibres that make up the chromosomes. By this organisation, DNA is packaged into a smaller volume, strengthened to prevent damage and allows controlled mitosis (replication) and transcription. Posttranslational modifications of histone proteins, including methylation, acetylation, phosphorylation, and ubiquitination, alter their interaction with the DNA and thereby allow gene regulation. The tail of histone 3 is shown as an example for different modifications. Adapted from [115].

Epigenetic modifications switch genes on or off during growth and development, which makes epigenetics fundamental to cellular differentiation and stem cell linage commitment. The main epigenetic mechanisms of gene regulation are DNA methylation and histone modifications, including methylation and acetylation of lysine residues, phosphory-

lation of serine and threonine residues, or other less common PTMs including sumoylation and ubiquitination of lysine residues [116]. The establishment, maintenance or erasure, and recognition of these histone modifications are implemented by so called “writers”, “erasers”, and “readers”. These are molecules that attach (’write’) and erase modifications to DNA or histones, or that bind to (’read’) a specific epigenetically modified site (table 1.1) [117]. In this work, with regard to the following chapters, the “writers” and “erasers” for methylation and acetylation as well as the “reader” class bromodomains will be further discussed.

Epigenetic Mechanism	**"Writer" Enzymes**	**"Reader" Domains**	**"Eraser" Enzymes**	**Function**	**Ref.**
DNA Methylation	DNA methyltransferases	Methyl-CpG binding domains	Active DNA demethylation (enzymes unknown), passive DNA demethylation (passive process)	Genomic stability	[118]
Histone Methylation	Protein methyltransferases (PMTs)	Mainly chromodomains; tudor domains; PHD fingers; bromodomains	Histone demethylases	transcriptional repression or activation; DNA repair; stress response; ageing	[119]
Histone Acetylation	Histone acetyltransferases	Tandem bromodomains; tandem PHD fingers	Histone deacetylases	transcriptional activation, associated with euchromatin	[120]
Histone Arginine Methylation	Protein arginine methyltransferases (PRMTs)	Tudor domains (recognise symmetrically dimethylated arginines)	Histone demethylases; peptidyl arginine deiminases (PADIs) (putative)	transcriptional regulation	[121]
Histone Ubiquitination	Ubiquitin E2 conjugases, ubiquitin E3 ligases	Unknown	Ubiquitin-specific proteases	transcriptional activation, crosstalk with other chromatin modifications	[122]
Histone Phosphorylation	Kinases (e.g. proteine kinase C, Haspin, Aurora B)	Chromoshadow domains (phosphoTyrosine); 14-3-3 proteins (phosphoSerine); BRCT proteins	Protein tyrosine phosphatases; protein serine/threonine phosphatases	Response to DNA damage; DNA repair, transcription and chromatin compaction (mitosis) and relaxation	[123]

Table 1.1: Epigenetic modifications and related "writers", "readers", and "erasers". Known functions and references are given for each mechanism.

1.4.1 Methylation

Methylation contributes to epigenetic inheritance by either DNA methylation or protein methylation, i.e. the methylation of lysine or arginine residues on histones [124]. Protein methylation is carried out by histone methyltransferases, adding methyl groups to either arginine or lysine residues. Arginine can be methylated once (monomethylated arginine) or twice (dimethylated arginine), whereas lysine can be monomethylated, dimethylated, and trimethylated by protein methyltransferases (figure 1.11).

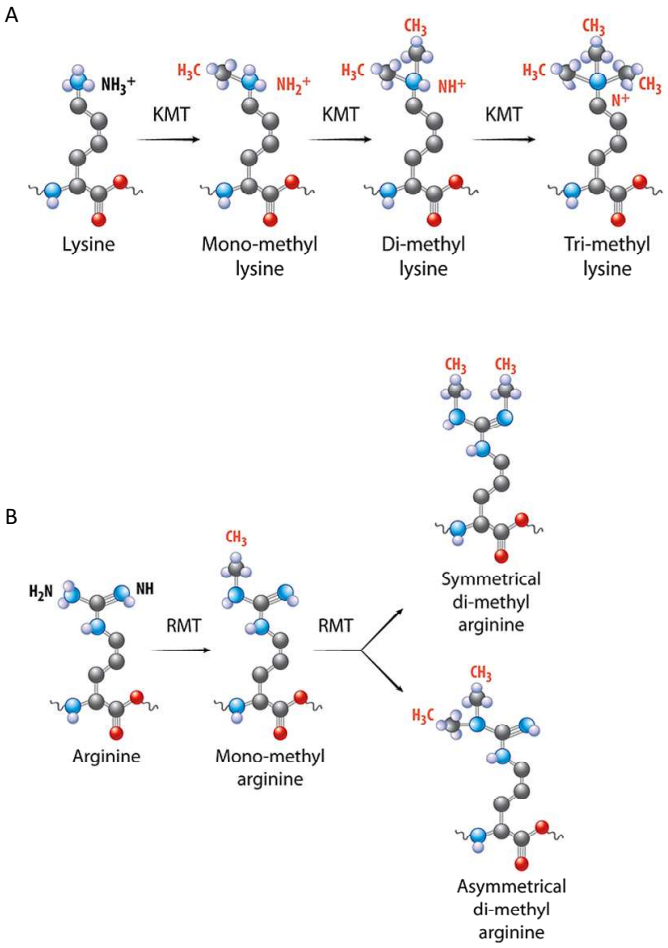

Figure 1.11: Methylation of lysines (A) and arginines (B). Lysine can be monomethylated, dimethylated, and trimethylated by lysine methyltransferases, whereas arginine can be methylated once (monomethylated arginine) or twice (dimethylated arginine). Adapted from [125].

The consequences of PTMs on histones are alterations of biochemical properties, resulting in global chromatin changes and epigenetically repressed or activated gene expression. They also elicit more versatile effects by recruiting specialised "reader"-domains that recognise specific modifications and facilitate downstream chromatin-modulating events. In DNA methylation a methyl group is added to the 5' position of the cytosine pyrimidine ring and typically occurs at CpG dinucleotides. Unmethylated CpGs are often grouped in clusters, called CpG islands, which are typically located around the promoters of housekeeping genes and other frequently expressed genes essential for cell functions. As DNA methylation is re-established during cell division, it provides genomic stability and constitutes a form of "memory" for the cell. Only recently methylation was also discovered as a modification method for RNA, with N6-methyladenosine (m6A) identified as the most abundant internal modification of messenger RNA in eukaryotes. Although its mammalian function remains unknown, both mRNAs and long non-coding RNAs (lncRNAs) were shown to harbour m6A modification [126]. Furthermore, the discovery of mammalian RNA demethylases suggests a dynamic regulation of these modifications [127]. In mammals, methylation is carried out by DNA methyltransferases (DNMTs), providing the basis for maintenance of methylation marks and for *de novo* methylation. DNA methyltransferase 1 (DNMT1) is responsible for the preservation of methyl marks during each cellular DNA replication cycle, preventing passive demethylation, while the methyltransferases DNMT3a and DNMT3b catalyse *de novo* methylation [128]. The effects of DNA methylation are potentiated by the recruitment of DNA binding proteins, among them methyl-CpG-binding proteins which repress transcription from methylated gene promoters. These proteins act as structural proteins, which then again recruit a variety of chromatin remodelling and modifying factors, such as histone deacetylase (HDAC) com-

plexes, leading to chromatin compaction and in consequence to transcriptional repression [129]. For many years, histone methylation was thought to be a permanent and irreversible modification, and that the methylated histone tail would only be removed by histone exchange. This was supported by studies showing that the half-life of histone methyl marks was approximately equal to that of histones themselves [130]. However, since 2004, when in a ground-breaking study Shi et al. demonstrated that the amine oxidase KDM1A/LSD1 (Lysine (K)-Specific Demethylase 1A) could demethylate lysine 4 on histone H3 in an FAD (flavin adenine dinucleotide)-dependent reaction [131, 132], additional histone demethylases have been found. Highlighting the importance of KDM1A for normal development, the targeted homozygous deletion of murine Kdm1a has been shown to result in early embryonic lethality, later discussed in chapter 5 [133]. Two other research groups reported the discovery of the first histone arginine demethylase peptidyl arginine deiminase 4 (PAD4) that functions as a histone deiminase, with the ability to convert monomethyl arginine to citrulline [134, 135]. In 2006, the first JmjC domain-containing protein was demonstrated to be a histone demethylase [136]. JHDM1 (JmjC domain-containing histone demethylase 1) was the first demethylase shown to specifically demethylate H3K36. The Jumonji C (JmjC) domain utilises Iron(II) and 2-oxoglutarate as cofactors and catalyses lysine demethylation of histones through an oxidative reaction. The name Jumonji (Japanese for "cruciform") was originally derived from a mouse mutation that affected neural tube development and produced a cross-like structure on the neural plate [137]. Up to date, there are six different subfamilies of Jumonji-type histone lysine demethylases (KDMs) with a variety of domains serving essential functions in regulating the epigenetic landscape of the chromatin environment. The identification of histone demethylases challenged the concept of histone methylation as stable and ir-

reversible marks, and suggested that histone methylation is much more dynamic than it was thought for a long time.

1.4.2 Acetylation

Acetylation of lysine residues on the N-terminal tail is one of the most frequently occurring post-translational modifications of histone proteins. Histone tails are positively charged due to occurrence of lysine and arginine amino acids, which together with the negatively charged DNA leads to a tight packaging of chromatin. It is thought that acetylation by histone acetyltransferases (HATs) neutralises the positive charge by changing amines to amides and thereby decreasing the ability of histones to bind to DNA. This causes an opening of the chromatin architecture, allowing for regulatory elements to bind and transcription to occur. On the contrary, removal of the acetyl group by histone deacetylases (HDACs) increases the positive charge and condenses the DNA structure, thereby preventing transcription. Histone acetyltransferases acetylate lysine residues on histone proteins by transferring an acetyl group from acetyl CoA to form ε-N-acetyl-lysine. HATs were traditionally divided into two classes based on their subcellular localisation, found either in the nucleus (class A) or in the cytoplasm (class B), but are now generally divided into the two major classes, the MYST and the GNAT families. The GNAT family is characterised by the presence of a bromodomain and acetylates lysines on histone H2B, whereas the MYST family exhibit zinc fingers and chromodomains modifying H2A. Both GNAT and MYST family have been shown to acetylate lysines on histones H3 and H4 [138]. Histone deacetylases are classified into four classes depending on sequence homology and domain organisation [139]. Class I HDACs are mostly localised within the nucleus, whereas class II HDACs shuttle between the nucleus and the cytoplasm. Knockout analysis of differ-

ent class I and class II HDAC proteins indicates that class I HDACs play a role in cell survival and proliferation, whereas class II HDACs may have tissue-specific roles. Class I and II are considered "classical" HDACs whose activities are inhibited by Trichostatin A (TSA) [140], whereas class III is a family of nicotinamide adenine dinucleotide (NAD^+)-dependent proteins not affected by TSA. These are also known as members of the Sirtuin family of proteins [141, 142]. The only member of class IV is HDAC11, which was first described in 2002 and displays characteristics of both class I and class II HDACs [143]. In the past decade, HDAC inhibitors were “discovered” as new agents in cancer therapy [144]. This was based on several cancer promoting mutations and chromosomal translocations resulting in repression of transcription through abnormal recruitment and activation of HDACs, thus, developing potent inhibitors against these classes could be essential in targeting cancer [145]. Trials have shown an anti-proliferative effect on cancer in cell culture, animal models and in humans with both haematological and solid tumours, however, the exact mechanism by which this effect is exerted is still unknown [146]. Recently, HDAC inhibitors have also been considered for therapy in autoimmunity and transplantation, given that selective inhibitors are developed [147]. From the time acetylation was discovered, research has emerged to show that lysine acetylation not only changes the organisation of chromatin but also generates binding sites for specific protein-protein interaction domains, such as the acetyl-lysine-binding bromodomain, which will be discussed in the next section.

1.4.3 Bromodomains

Bromodomains (BRDs) are found in several chromatin-associated proteins, e.g. histone acetyltransferases, and constitute evolutionarily conserved protein-protein interac-

tion modules that recognise ε-N-lysine acetylation motifs. Their name is derived from the Indian word 'Brahma' (meaning "fate") for the first bromodomain-containing protein to be identified in Drosophila melanogaster [148]. The bromodomain comprises a 110 amino acids wide region that is most often present only once per protein, but can also occur multiple times. In the BET subfamily of bromoproteins, with the four members BRD2, BRD3, BRD4, and the testis-specific isoform BRDT, two N-terminal BRDs are present [149,150]. To date, there are 61 unique human bromodomains that can be clustered into eight distinct families based on structural similarity, because despite large sequence variations, all bromodomains share a three-dimensional structure important for substrate specificity [151]. This conserved fold comprises a left-handed bundle of four alpha helices (αA, αB, αC, αZ) linked by diverse loop regions (ZA and BC loops) [152]. In co-crystal structures with peptide ligands it could be shown that the acetylated lysine residue is recognised by a central hydrophobic cavity within the bromodomain module and is anchored by a hydrogen bond with an asparagine residue present in most bromodomains (see chapter 4 for more information) [153]. BRDs have an important role in the targeting of chromatin-modifying enzymes to specific sites and in the recruitment of proteins to macromolecular complexes, and thereby regulate the transcription of e.g. growth-promoting genes or cell cycle regulators. For instance, BRD4 and BRD2 are key mediators of transcriptional elongation by recruiting the positive transcription elongation factor complex (P-TEFb) [154, 155]. BRD4 will be discussed in more detail later in this thesis (chapter 4).

1.4.4 Epigenetic mechanisms in osteogenic differentiation

As outlined previously, in recent years there has been a growing interest in applying mesenchymal stem cells to tissue engineering and increased efforts have been made to elucidate

the molecular mechanisms of their directed differentiation. The exact molecular mechanisms governing the differentiation of bone marrow derived stem cells into osteoblasts remain largely unknown and detailed systematic investigations of underlying epigenetic mechanisms are missing. To summarise, recent publications have proposed roles of mainly HDACs, methyltransferases and demethylases in osteogenic differentiation. Maroni et al. showed that pan-HDAC chemical inhibition by using Trichostatin A, or knockdown of HDAC1 and -3 in adipose tissue-derived mesenchymal stem cells, leads to an early activation of RUNX2 and ALPL, while concomitantly decreasing PPAR-γ and its target genes required for adipogenic differentiation [156]. In BMP-9-mediated osteogenic differentiation of mouse mesenchymal stem cells, TSA also potentiates the activity of early marker alkaline phosphatase as well as late markers osteopontin (OP), osteocalcin (BGLAP), and furthermore promotes matrix mineralisation [157]. A previous study had already shown that HDAC3 interacts with the amino terminus of key transcription factor RUNX2 and could thereby suppress RUNX2-mediated activation of the osteocalcin promoter. Suppression of *Hdac3* in MC3T3 pre-osteoblasts by RNA interference consequently accelerated the expression of Runx2 target genes, osteocalcin, osteopontin, and bone sialoprotein. However, Runx2 levels were not significantly altered [158]. In contrast, *Hdac3* conditional knockout mice, although of normal size and weight, showed a progressive loss of trabecular and cortical bone mass with age. Mineralisation of cortical bone was reduced and the mice suffered frequent fractures, and indicating that the reduction in bone mass was caused by defects in osteoblast formation and activity these mice also showed a lower bone resorption [159]. However, HDACs, and also HDAC3, were shown to also influence osteoclast differentiation. Suppression of HDAC3 expression was reported to inhibit their differentiation, whereas osteoclasts suppressed for HDAC7 expression had accelerated differentiation

when compared to control cells [160]. Another pan-HDAC inhibitor, suberoylanilide hydroxamic acid (SAHA) suppressed osteogenic colony formation and decreased gene expression of immature osteoblasts when applied to murine bone marrow-derived adherent cells *in vitro*. Interestingly, mature osteoblasts appeared to be resistant with an increased activity, suggesting that the response of osteoblasts to SAHA is dependent on their differentiation state [161]. Epigenetic modifications involving demethylases were reported to constitute a crucial part in mesenchymal stem cell differentiation. Both histone demethylases KDM4B and KDM6B have been observed to play critical roles in osteogenic commitment of MSCs by removing H3K9me3 and H3K27me3 chromatin marks [162]. Depletion of *KDM4B* or *KDM6B* significantly reduced osteogenic differentiation and increased adipogenic differentiation. Interestingly, increased levels of H3K27me3- and H3K9me3-positive bone marrow-derived MSCs were found in ovariectomised and ageing mice in which adipogenesis was highly active. The interaction of NO66, a Jumonji family histone demethylase, with the transcription factor Osterix was reported to inhibit OSX-mediated promoter activation, with NO66 demethylating H3K4me and H3K36me [163]. Two other enzymes involved in histone modifications, the histone-lysine N-methyltransferase enhancer of zeste homology 2 (EZH2) and lysine demethylase 6A (KDM6A), displayed different transcript levels during MSC differentiation [164, 165]. Enforced expression of EZH2, which trimethylates H3K27 (H3K27me3) promoted adipogenic differentiation *in vitro* and inhibited osteogenic differentiation potential *in vitro* and *in vivo*. In contrast, enforced expression of KDM6A, which removes the repressive H3K27me3 mark on chromatin, inhibited adipogenesis *in vitro* and promoted osteogenic differentiation *in vitro* and *in vivo*. Conversely, inhibition of EZH2 activity and knockdown of *EZH2* gene expression resulted in decreased adipogenesis and increased osteogenesis, and similarly for KDM6A/*KDM6A*, in increased adipogenesis and

decreased osteogenesis. On the other hand, a contradictory effect on bone metabolism of yet another histone methyltransferase, SETDB1, was observed in knockout animals and *SETDB1*-null mesenchymal stem cells. Its deletion severely impairs osteoblast differentiation and trabecular bone formation, however has no effect on osteoclastogenesis [166]. Lastly, DNA methyltransferase inhibitor 5-azacytidine was shown to significantly facilitate osteogenic differentiation when MSCs were pre-treated with the compound for 24 hours prior to osteogenic induction. Treatment was accompanied by hypomethylation of genomic DNA and increased osteogenic gene expression [167, 168]. However, although epigenetic modifications are key elements in mesenchymal stem cell biology and development, still relatively little is understood about potential key factors responsible for pattern changes during osteoblast differentiation.

1.5 Summary

A major therapeutic challenge is how to replace bone once it is lost under various pathological conditions, as mammals have a limited capacity to repair bone defects caused by common bone diseases such as osteoporosis, rheumatoid arthritis or osteoarthritis. To meet this high demand for healthy bone cells and tissue, stem cells are currently investigated for application in bone-tissue engineering and human bone marrow-derived mesenchymal stem cells (hMSCs) could be a promising source for tissue-engineered bone. However, their potential is limited by a lack of knowledge regarding the regulation of transition from hMSCs to osteoblasts, the bone forming cells. A better understanding of the epigenetic mechanisms underlying, initiating, and promoting differentiation could help shedding light on this process.

1.6 Aims of this thesis

The therapeutic potential of human mesenchymal stem cells in tissue engineering is not fully utilised yet due to a lack of knowledge regarding the identity, nature, and development of MSCs. With the aim to systematically analyse the epigenetic side of MSC development, the work in this thesis shall encompass a broad approach to identify epigenetic mechanisms involved in osteoblast differentiation as well as specific investigation of identified individual targets.

The first aim is to test different induction mechanisms of osteoblast differentiation in order to allow a comprehensive analysis of the bone phenotype under different conditions.

Second, an assay to assess osteoblast differentiation will be developed and validated for repeatable performance in high-throughput experiments.

Subsequently, two approaches to identify epigenetic modifiers, knockdown by short hairpin RNAs and protein inhibition by small molecules will be pursued, leading to a list of target genes potentially involved in osteoblast differentiation.

Finally, the function of two target genes regarded as strong candidates for involvement in epigenetic regulation of osteoblast differentiation will be studied in cell culture and a mouse model.

Therefore, the structure of this thesis is as follows:

Chapter 1 gives an introduction to the relevant fields involved in the work of this thesis.

In **Chapter 2** the various *in vitro* differentiation methods are presented and applied to human mesenchymal stem cells. An assay for measuring alkaline phosphatase activity as a means of osteoblast differentiation is developed and tested for different osteogenic inducers.

The work in **Chapter 3** utilises the aforementioned assay in short hairpin RNA and small molecule inhibitor screens. The methods used to identify epigenetic modifiers involved in osteoblast differentiation are described, the hit selection process is presented, and the chapter concludes with a list of target genes.

Chapter 4 is showing work performed on bromodomain-containing protein 4 (BRD4), one of the two main follow-up targets. Its effect on osteoblast differentiation is assessed by microarray analysis, and various biochemical and cell-based assays.

Chapter 5 is dealing with the role of the second follow-up target, lysine-specific demethylase 1 (KDM1A) in osteoblast differentiation. Utilising a small molecule inhibitor and a transgenic mouse model, its effect on bone formation is investigated.

Chapter 6 summarises the previously presented data, discusses its relevance and gives an overview of future perspectives.

Every chapter has a short chapter-specific introduction stating the aim and finishes with a conclusion. Relevant methods are specified in each chapter and a flow chart of this thesis' work is shown at the beginning of chapter 3.

2 Investigation of different osteogenic inducers and development of osteoblast differentiation assay

2.1 Introduction

To address the first aim of my thesis, the validation of different osteoblast induction mechanisms, differentiation assays with various inducing factors were performed. Beginning with a literature review on *in vitro* differentiation methods, an assessment was made about the osteoblast differentiation potential of human mesenchymal stem cells. This resulted in the development of a generic assay that is subsequently employed to test different induction methods. Three induction methods were chosen, validated and applied to screen short hairpin RNA-mediated knockdown and small molecule inhibition described later in chapter 3.

2.2 *In vitro* osteoblast differentiation methods

One of the most remarkable characteristics of mesenchymal stem cells (MSCs) is their ability to differentiate into osteoblasts *in vivo* and *in vitro*, providing an important model system for bone biology and regulation of bone formation [31]. *In vitro* differentiation can be achieved by culturing in the appropriate induction medium containing the basic growth supplements beta-glycerophosphate and ascorbic acid 2-phosphate, and additional inducive factors such as dexamethasone, BMPs, 1,25-dihydroxyvitamin D_3, or cytokines. Although all these factors were demonstrated to induce osteoblast differentiation (see below), they remain controversial, as the different treatments were shown to have varied effects on differentiation and produce osteoblastic cells with different phenotypic characteristics. In human osteoblast cells differentiated from bone marrow, Jorgensen et al. found

that alkaline phosphatase activity was increased by dexamethasone, but not by BMP-2 treatment [169]. In addition, expression of the late cellular differentiation marker osteocalcin was low in cultures treated with dexamethasone or BMP-2, but in combination with 1,25-dihydroxyvitamin D_3, BMP-2 displayed an increased osteocalcin production while the combination with dexamethasone completely suppressed it. The osteoblast transcription factor RUNX2 was shown to be differently regulated by various osteoblast differentiating reagents. Treatment with dexamethasone, BMP-2, or TGF-β, led to an increase of *RUNX2* expression with BMP-2 showing an earlier enhancement. Induction by means of 1,25-dihydroxyvitamin D_3 led to an initial inhibitory effect followed by a lower, but still stimulating effect after 48 hours, indicating that the rapid stimulatory effect on osteocalcin expression by 1,25-dihydroxyvitamin D_3 is independent of RUNX2 [78].

The synthetic glucocorticoid (GC) agonist **dexamethasone** is one of the best studied *in vitro* inducers for osteoblast differentiation; however, there has been controversy about its effects as it has been shown to have contrasting dual functions in bone metabolism. On the one hand, it is a prerequisite supplement for effective *in vitro* osteoblast differentiation, and on the other hand it is known to be a catabolic factor inducing bone loss or osteoporosis under prolonged drug treatment [170,171]. In addition, dexamethasone was reported to induce adipogenesis as well as osteogenesis in multipotent stromal cells from human adipose tissue [172]. However, in *in vitro* differentiation models of bone marrow osteogenic stromal cells, dexamethasone induced morphological changes, increased alkaline phosphatase expression and was essential for matrix mineralisation [173]. It was therefore suggested that the different effects of dexamethasone on differentiation might be dependent on the stage of development and that human osteoblast differentiation needs to be triggered by GCs in a specific time-window during the early stages of development [174]. Cellular

responses to glucocorticoids are dependent on the binding of GCs to the intracellular glucocorticoid receptor (GR), which in turn translocates to the nucleus and modulates gene expression. Interactions with DNA are mediated by either targeting specific glucocorticoid response elements (GRE) or nGRE (negative GRE) [175]. Depending on the nature of the GRE, the overall process of GR binding can result in activation or repression of genes containing GR-binding sites. The GR has also been shown to interact with chromatin remodelling complexes such as the cAMP-response element-binding (CREB)-protein and the SWI/SNF (SWItch/Sucrose NonFermentable) complex [176]. Dexamethasone was shown to increase the effects of vitamin D and its receptor in a GR-dependent manner. In squamous cell carcinoma, the anti-tumour effects of 1,25-dihydroxyvitamin D_3 were increased in combination with dexamethasone [177].

1,25-dihydroxyvitamin D_3 plays a role in the regulation of early stages of osteoblast differentiation, but similar to dexamethasone, it was reported to also exert effects on adipogenesis. In primary rat calvaria cells, it stimulated differentiation into adipocytes [178]; however, overall 1,25-dihydroxyvitamin D_3 is thought to favour the differentiation into the osteoblast instead of the adipogenic lineage [179]. It stimulates alkaline phosphatase transcription, expression and activity during both proliferation and differentiation [180], induces the production of osteocalcin [181], stimulates synthesis of collagen type 1, and regulates osteopontin expression [182]. Conversely, 1,25-dihydroxyvitamin D_3 was shown not to have an effect on the expression of another extracellular matrix protein, bone sialoprotein (IBSP), in human bone marrow stromal cells. However, when added in addition to dexamethasone-treated cultures, high levels of IBSP could be observed [182]. The vitamin D receptor (VDR) plays a central role in the effects of 1,25-dihydroxyvitamin D_3 on bone metabolism. VDR knockout mice display hypocalcemia and osteomalacia, a condition

characterised by a softening of the bone caused by defective bone mineralisation [183]. In addition, 1,25-dihydroxyvitamin D_3-mediated osteoclast formation was abolished in the VDR knockout mice, indicating that the VDR on osteoblasts is essential for osteoclast differentiation [84]. Once the nuclear VDR is activated, it recognises vitamin D response elements (VDRE) in the promoter sequence of vitamin D-regulated genes [184].

Bone morphogenetic proteins (BMPs) are known for their ability to initiate, promote, and maintain chondrogenesis and osteogenesis [185, 186]. Particularly BMP-2 and -6 are thought to be inducers of osteoblast differentiation [187]. Many of the cellular functions and signalling pathways of BMP-2 are not fully understood, but seem to involve multiple cross-talks involving SMAD, Wnt, and MAPK signalling pathways [186, 188, 189]. As all other inducers, BMP-2 exhibits varied effects on osteoblast differentiation, and continuous treatment with BMP-2 alone was also reported to result in a less efficient enhancement of *in vitro* matrix mineralisation [190].

Finally, mesenchymal stem cells and osteoblasts not only respond to growth and differentiation factors, but have also been shown to be responsive to a number of locally acting **cytokines**. In addition to the active regulatory role of MSCs in response to inflammation, infection, and wound healing (as briefly discussed in the introduction), MSCs are also receptive to and regulated by cytokines. A number of interleukins, mainly interleukin 1 and 6, tumour necrosis factor-α (TNF-α), as well as oncostatin M (OSM, a member of the interleukin 6 subfamily), were shown to induce osteoblast differentiation [191, 192]. In two reports, activated monocytes/macrophages were shown to induce osteoblastogenesis of MSCs through OSM secretion [48, 193]. However, the osteoblast promoting effect of OSM was only shown in early, but not late, bone marrow mesenchymal stem cells; in mature osteoblasts, OSM inhibited osteoblast gene expression and bone mineralisation [194]. The

different responses caused by various inducers presented can be attributed to a variety of causes, for instance the difference in species (e.g. human, mouse, rat), different culture conditions, and different stages of differentiation. In addition, the tissue the cells are originating from can exhibit diverse levels and compositions of growth factors, hormones, and cytokines, all together leading to different responses. In order to dissect the varied effects on osteoblast differentiation, this thesis aims to identify epigenetic modifications that underlie these differences and to potentially discover unique chromatin modification pathways caused by different induction methods.

2.3 Chapter outline

With the aim to identify unique mechanisms underlying differentiation induced by different factors, a selection of diverse differentiation conditions was made. Initially, the general ability of the employed human MSCs to differentiate into osteoblasts was tested using the well-studied inducer dexamethasone. Subsequently, various inducers at different concentrations were applied to MSCs with differentiation assessed using an assay measuring the early bone marker alkaline phosphatase. Finally, three induction methods were chosen and their differentiation induction potential was confirmed by quantitative polymerase chain reaction (qPCR) analysis of osteoblast gene expression. All conditions were tested on the same passage of one human mesenchymal stem cell line in order to minimise any cell origin-related effects.

2.4 Materials and Methods

2.4.1 Cell culture

Human MSCs from a 21 years old female donor were cultured in MesenPRO-RS™ medium (MSC, Life Technologies) for expansion. To induce osteogenesis, cells were cultured until confluency was reached and stem cell medium (MSC) was replaced with basic osteogenic medium (OD). For the initial experiment using dexamethasone, the osteogenic medium (+DEX) was composed of DMEM/F12 supplemented with 15% fetal bovine serum (FBS), 1% penicillin/streptomycin (P/S), 1% non-essential amino acids (NEAA), 2mM glutamine, 50µg/ml ascorbic acid, 10mM beta-glycerophosphate, and 10nM dexamethasone. In addition, a control medium (CM) was employed, composed of DMEM/F12 supplemented with 15% FBS, 1% P/S, 1% NEAA, and 2mM glutamine, representing a basal medium with neither growth factors for stem cell maintenance nor inducive supplements facilitating osteoblast differentiation. In subsequent experiments with varying inducers, media composed of DMEM/F12 supplemented with 10% FBS, 1% P/S, 1% NEAA, 2mM glutamine, 50µg/ml ascorbic acid, 10mM beta-glycerophosphate (basic osteogenic medium, OD) containing either 10 or 100nM dexamethasone (+DEX), 1nM 1,25-dihydroxyvitamin D_3 (+VitD3), 100ng/ml BMP-2 (+BMP), or 10 to 100ng/ml oncostatin M (+OSM) were applied. For the final confirmation of the differentiation potential of the three inducers, the concentrations used were 10nM for dexamethasone, 1nM for 1,25-dihydroxyvitamin D_3, and 10ng/ml for oncostatin M (table 2.1). A comprehensive list of all medium compositions and supplement concentrations used in this thesis can be found in appendix A.1.

Name	Composition
MSC	MesenPro-RS™ + 1% P/S
CM	DMEM F/12 + 15% FBS + 1% P/S + 1% NEAA + 2mM glutamine
OD	DMEM F/12 + 15% FBS + 1% P/S + 1% NEAA + 2mM glutamine + 50µg/ml ascorbic acid + 10mM beta-glycerophosphate
+DEX	DMEM F/12 + 15% FBS + 1% P/S + 1% NEAA + 2mM glutamine + 50µg/ml ascorbic acid + 10mM beta-glycerophosphate + 10-100nM dexamethasone
+VitD3	DMEM F/12 + 15% FBS + 1% P/S + 1% NEAA + 2mM glutamine + 50µg/ml ascorbic acid + 10mM beta-glycerophosphate + 1nM 1,25-dihydroxyvitamin D_3
+OSM	DMEM F/12 + 15% FBS + 1% P/S + 1% NEAA + 2mM glutamine + 50µg/ml ascorbic acid + 10mM beta-glycerophosphate + 10-100ng/ml OSM
+BMP	DMEM F/12 + 15% FBS + 1% P/S + 1% NEAA + 2mM glutamine + 50µg/ml ascorbic acid + 10mM beta-glycerophosphate + 100ng/ml BMP2

Table 2.1: List of media used during assay development and their detailed composition

2.4.2 Cell viability assay

Cells were incubated with Presto Blue® (Life Technologies) for 30mins at 37°C. Fluorescence was measured using a fluorescence plate reader (FLUOStar OPTIMA, BMG Labtechnologies; excitation 544nm, emission 590nm, gain 1255). For more detail on the Presto Blue® mechanism, see subsection 2.6.

2.4.3 Alkaline phosphatase assay

The assay can be performed either directly on lysed cells in 96 or 384 well plates or with purified protein lysates. If done directly in plates, cells were washed twice in PBS and lysed using CelLytic M™ (Sigma-Aldrich; addition of 2% mammalian protein inhibitor cocktail, Sigma-Aldrich). After 15mins incubation, the plate was sealed and shaken on a plate shaker at around 10 Hertz for 30s. The substrate for alkaline phosphatase, 4-Methylumbelliferyl phosphate (4-MUP; Sigma-Aldrich) was added directly onto the cells. If performed with purified protein lysates, cell lysates were spun down and the supernatant was collected. Total protein concentration was determined using BCA assay (Pierce, Rockford, IL) and an aliquot was used in the alkaline phosphatase assay. The activity

of alkaline phosphatase will form the soluble fluorescent substance 4-Methylumbelliferone (4-MU) which was detected using a fluorescence plate reader (FLUOStar OPTIMA, BMG Labtechnologies; top-read; excitation 360nm, emission 460nm, gain 800). Alkaline phosphatase activity was measured at 0, 30, and 60mins after substrate addition.

2.4.4 RNA extraction and cDNA synthesis

Cells were cultured in previously mentioned media compositions and harvested on the following days post-induction: day 1, 3, 5, 7, 14, 21, 28. Cells were washed twice in PBS and RNA was extracted using the Qiagen RNAeasy Mini Kit. cDNA was synthesised from up to 0.5µg of RNA by reverse transcription in a total volume of 20µl using random primers. Expression of genes was tested using cDNA specific primers, targeting housekeeping genes Actin B, GAPDH, and 18S, osteoblast genes Runx2, Osterix, bone sialoprotein, collagen 1A1, osteocalcin, osteonectin, and alkaline phosphatase. PCR was performed for 40 cycles of denaturation (95°C for 20s), annealing (95°C for 1s), and extension (60°C for 1min). The primer sequences can be found in appendix A.2.

2.4.5 Microarray study

Microarray analysis was performed using the Illumina bead array HT12.V4 and samples were normalised using RMA (Robust Multi-array Average) [188]. Values are indicative for fold-change normalised to undifferentiated MSCs on day 1.

2.4.6 Cell fixation

Cells were washed twice in PBS and fixed in either 4% paraformaldehyde (PFA) or 70% Ethanol (EtOH) for 20-30mins at room temperature. Fixative was removed and cells were

washed again three times in PBS and stored at 4°C in PBS.

2.4.7 Alizarin Red S staining

Alizarin Red S staining (ARS) was used to identify calcium in the extracellular matrix. Cells were washed twice in PBS and fixed in 70% EtOH for 20-30mins. Fixative was removed and cells were stained with 1.5% ARS solution (pH 4.1-4.2) for 15mins at room temperature before being washed three times in double distilled H_2O (ddH_2O). Calcium deposits were observed under microscope (bright-field) and plates were scanned using an Epson scanner (Epson Perfection 3200 Photo). The incorporated dye was extracted with 10% (v/v) acetic acid, shaken on a plate shaker for 1 hour, and absorbance was measured at 405nm.

2.5 Dexamethasone-induced gene expression profile of human mesenchymal stem cell-derived osteoblasts

Dexamethasone-induced differentiation was employed as a "prototype" differentiation protocol. To assess changes in gene expression induced by dexamethasone treatment, microarray studies were performed. Genes showing a change in gene expression at least at two time points of differentiation (any two days of day 7, 14, and 21), with no change in the control medium, were considered as stably up- or downregulated genes caused by dexamethasone, yielding a total of 176 stably regulated genes. As seen in figure 2.1, the majority of these (110) were genes upregulated under dexamethasone treatment, while 66 genes were downregulated. To confirm and also illustrate the change dexamethasone is causing in mesenchymal stem cells, a principal component analysis (PCA) was performed. A PCA identifies the essential variable in a dataset, in this case the condition under

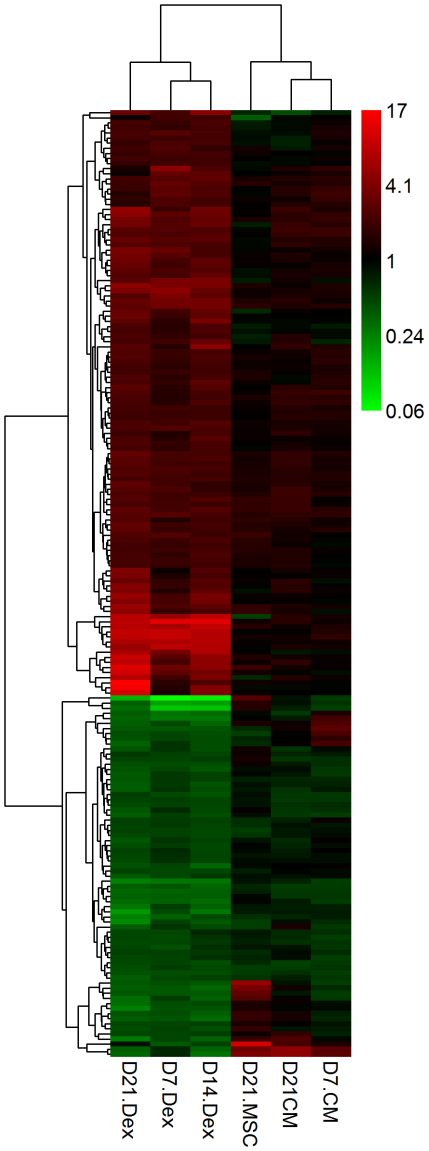

Figure 2.1: Hierarchical clustering of stably regulated genes of a microarray study of MSCs undergoing dexamethasone-induced differentiation. Changes in gene expression are indicated in red (increase) or green (decrease). Time points shown are indicative for cells in MSC medium after 21 days (MSC), in control medium (CM) after 14 and 21 days, and in complete osteogenic differentiation medium containing dexamethasone (+DEX) after 7, 14, and 21 days.

which the largest possible variance could be observed. The result can be seen in figure 2.2. The first principal component (1 = x-axis) has the largest possible variance and each succeeding component (2 = y-axis) has the highest uncorrelated variance. Differentiation induction by dexamethasone accounted for the largest possible variance, i.e. for as much variability in the data as possible. The most significant change could already be observed within the first seven days of differentiation; subsequently only minor changes were seen. Cells remaining in mesenchymal stem cell medium showed an expression profile unrelated to the dexamethasone profile and were therefore found on the y-axis, indicating the second principal component. Application of the control medium (CM) led to a minor change in the direction of dexamethasone-induced changes, but to a lower extent, suggesting that the control medium allowed cells to differentiate, but did not direct differentiation towards osteogenesis.

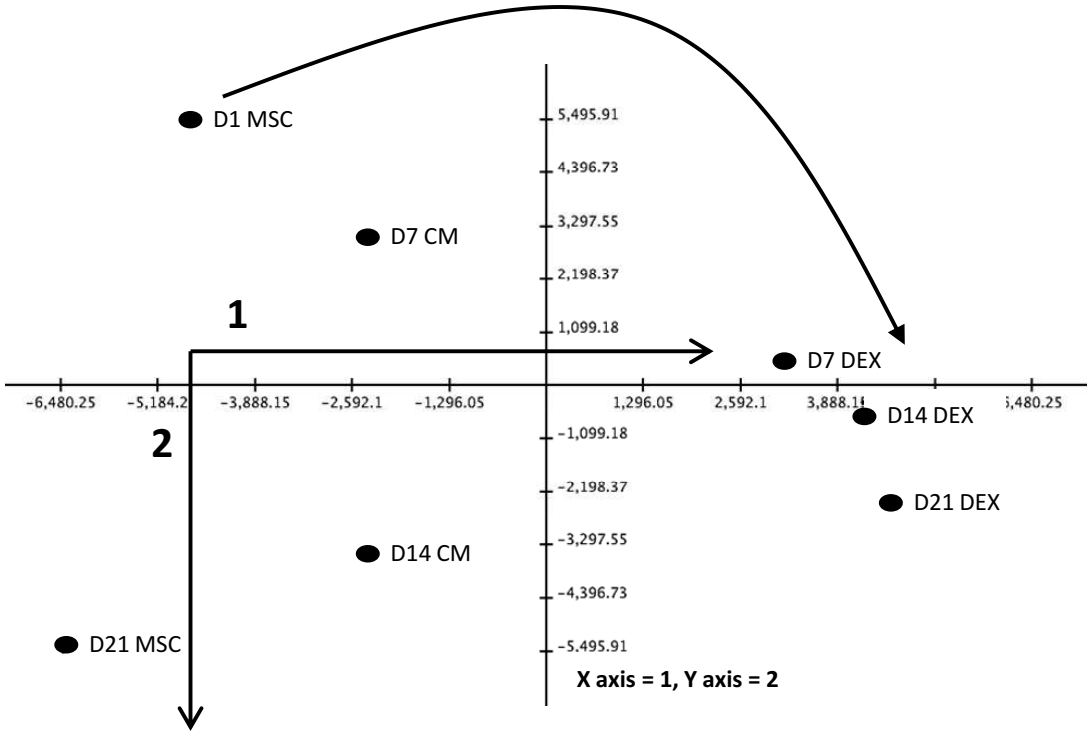

Figure 2.2: Principal component analysis of dexamethasone-induced differentiation. The first principal component (1) is shown on the x-axis and the second component on the y-axis (2). The straight arrows indicate the direction of change, the curved arrow shows the biggest difference from D1 MSC to D7 DEX. Day 1 (D1) to day 21 (D21) of culture are shown. MSC, mesenchymal stem cell medium; CM, control medium; DEX, osteogenic differentiation medium containing dexamethasone.

The list of all regulated genes can be found in appendix A.3, here only the highest upregulated ones, generating a dexamethasone-induced profile, will be discussed. In table 2.2, the 12 highest upregulated genes on day 21 with their fold changes compared to the MSCs on day 1 are presented and their relation (based on publications) to osteoblast development and bone is indicated.

Gene symbol	Entrez Gene Name	Fold Change	Type(s)	Associated with "bone"
APOD	apolipoprotein D	16.3	lipid transporter	✓
CADM3	cell adhesion molecule 3	15.3	other	
SUSD2	sushi domain containing 2	12.1	other	✓
DARC	Duffy blood group, chemokine receptor	11.3	G-protein coupled receptor	✓
OLFML2A	olfactomedin-like 2A	10.1	other	
OMD	osteomodulin	9.2	other	✓
FAM167A	family with sequence similarity 167, member A	8.6	other	
LEPR	leptin receptor	8.4	transmembrane receptor	✓
BMP6	bone morphogenetic protein 6	7.9	growth factor	✓
CRISPLD2	cysteine-rich secretory protein LCCL domain containing 2	7.7	other	
WFDC1	WAP four-disulfide core domain 1	7.6	other	
FBLN1	fibulin 1	7.4	other	

Table 2.2: Dexamethasone-induced gene expression. The highest upregulated genes under dexamethasone treatment on day 21 are shown and their fold change, type, and association with bone are indicated.

Apolipoprotein D (APOD) is a member of the lipocalin superfamily of lipid transport proteins and has been reported to be highly upregulated upon osteoblast differentiation [195,196]. Its expression was shown to be specifically up-regulated by p73 and p63, but not by p53 [197]. Interestingly, a paper from Sasaki et al. reported that the p73 isoform TAp73 induces osteoblast differentiation in the human osteosarcoma cell line Saos-2 via APOD transactivation, as assessed by alkaline phosphatase activity and that APOD knockdown abrogates the p73-mediated alkaline phosphatase induction [197]. ApoD was also reported to physically interact with the Leptin receptor, a gene that is also found upregulated in this dataset (table 2.2) [198].

Cell adhesion molecule 3 (CADM3) is a member of the nectin-like family of cellular adhesion molecules involved in cell adhesion and extracellular matrix formation, both important processes for bone matrix formation [199].

The role of the **duffy blood group atypical chemokine receptor** (DARC), a G-protein coupled receptor, in osteoblast formation is unknown, however, it was reported to negatively regulate bone mineral density (BMD) by increasing osteoclast formation [200].

Osteomodulin (OMD), also called osteoadherin, is a cell-binding keratan sulfate proteoglycan of the extracellular matrix (ECM) and was shown to be regulated by transcription factor RUNX2, as well as by the cytokines TGF-β and BMP-2 [201,202]. It was suggested

that OMD is an osteoblast maturation marker induced by osteoclast activity [203].

Sushi domain containing 2 (SUSD2) was only recently discovered as a specific marker for the isolation of bone marrow-derived MSCs capable to differentiate into osteoblasts, adipocytes, and chondrocytes [204].

The **leptin receptor** (LEPR) functions as a receptor for the adipose tissue-specific hormone leptin. The addition of leptin to human marrow stromal cells was reported to enhance their osteoblast differentiation potential and inhibit the differentiation into adipocytes [205]. The receptor is expressed by both bone marrow-derived stromal cells as well as osteoblasts, with leptin regulating mesenchymal progenitor cell (MPC) differentiation and osteoblast function [206].

Bone morphogenetic protein 6 (BMP-6) is a member of the TGF-β superfamily of proteins. The role of TGF-β signalling in osteoblast differentiation was already described in the introduction, and also BMP-6 is able to induce all osteogenic markers in mesenchymal stem cells [187].

Alkaline phosphatase was also upregulated under dexamethasone treatment and can be seen in table 2.3.

For a functional analysis the 176 genes were associated with biological functions and/or diseases in the Ingenuity® Knowledge Base (IPA, Ingenuity Pathway Analysis) [207]. Functions related to bone biology and the genes involved are shown in table 2.3; these include stimulation, differentiation, and mineralisation of osteoblasts, as well as morphology of bone and bone remodelling. It has to be noted that genes included in the functional analysis are genes with various effects on bone and can be both promoting and inhibiting differentiation.

Functions annotation	Genes
Differentiation of osteoblasts	*ABL1, BMP6, IGFBP5, IL11, PRKD1, STC1, TOB1, TWIST1*
Mineralisation of osteoblasts	*ALPL, BMP6, PTGS2*
Stimulation of osteoblasts	*BMP6, PLAU*
Differentiation of bone marrow cells	*BMP6, CDKN2B, IL11, LRRC17, NFKBIA, TSC22D3*
Mineralisation of bone marrow cells	*PRKD1, PTGS2*
Morphology of bone	*ALPL, BMP6, CLEC3B, DACT1, DARC, FBN2, GPER, MMP2, SOX9, TWIST1, ZBTB16*
Mineralisation of bone	*ALPL, BMP6, CLEC3B, POSTN, PTGS2, SOX9, TWIST1*
Remodelling of bone	*CST3, FBN2, IGFBP5, IL11, PTGS2, TOB1*

Table 2.3: Bone functions annotations of genes regulated under dexamethasone treatment as analysed by IPA.

IPA also suggested potential upstream transcriptional regulators that can explain the observed gene expression changes. The analysis identified the regulators that were most significantly associated to the data set. Fisher's exact test was used to calculate a p-value determining the probability that the association between the genes in the dataset and the regulator is explained by chance alone. The most significant upstream regulators, transforming growth factor-β1 (TGF-β1), the steroid ligand progesterone, dexamethasone, and interleukin-1β (IL-1β), and their target molecules in the dataset are displayed in table 2.4. The role of TGF-β signalling and dexamethasone in osteoblast differentiation was already described in the introduction of this thesis (see subsection 1.3.2 and 2.2), as well as the function of IL-1 was presented in this chapter. Progesterone is known for its bone-promoting effects and used in therapies promoting bone formation and bone mineral density [208, 209]. Interestingly, another feature of the IPA analysis that predicts whether the transcriptional regulators are likely to be activated or inhibited, categorised dexamethasone as activated regulator, supporting that the gene expression profile seen is caused by dexamethasone.

Upstream Regulator	Molecule Type	Predicted Activation State	p-value of overlap	Target molecules in dataset
TGFB1	growth factor		9.77E-15	*ABL1, ANPEP, ATXN1, BMP6, CCND3, CD14, CDH2, CDKN2B, COL8A1, CORIN, CST3, DARC, ESM1, FBLN1, FTH1, GCNT1, HAS2, HSPB2, HTRA1, IGFBP5, IGFBP6, IL11, KRT19, MMP2, NET1, NFKBIA, PLAU, PLAUR, POSTN, PSPH, PTGER2, PTGS2, S100A10, SERPINH1, SIRPA, SOX9, SPHK1, TGIF1, TNC, TSC22D3, TWIST1, TYMP, ZFP36, ZFP36L2*
Progesterone	chemical - endogenous mammalian		1.64E-14	*AEBP1, AKR1C4, ALPL, APOD, BCAT1, CCND3, CDH2, CDKN2B, CFD, CST3, FTH1, IGFBP5, IRS2, LEPR, LEPROT, MMP2, MUC1, NET1, NFKBIA, PBX3, POSTN, PPAP2B, PTGER2, PTGS2, SPHK1, TYMP*
Dexamethasone	chemical drug	Activated	3.11E-14	*AEBP1, AKR1C4, APOD, CCND3, CDKN2B, CFD, CRISPLD2, CST3, DUSP5, FBLN1, FBN2, FKBP5, FTH1, IFITM1, IFITM3, IGFBP5, IGFBP6, IL11, IRS2, KCNK6, LPAR1, MME, MMP2, MUC1, NET1, NFKBIA, OMD, OXTR, P4HA2, PCDH19, PLAU, POSTN, PTGS2, RASD1, RPS6KA2, S100A10, SAA1, SOX9, SPHK1, TNC, TSC22D3, ZBTB16, ZFP36, ZFP36L2*
IL1B	cytokine		6.71E-11	*A4GALT, ALPL, CD14, CSRNP1, DUSP5, FKBP5, HAS2, IGFBP5, IL11, IRS2, KRT19, MARCKSL1, MMP2, MUC1, NFKBIA, OXTR, PLAU, PTGS2, S100A10, SAA1, SERPINH1, SOX9, TOB1, TSC22D3, TWIST1, TYMP, ZFP36*

Table 2.4: Upstream regulators and their target molecules of osteoblast differentiation as calculated by IPA. P-values were calculated using Fisher's exact test.

2.6 Development of a generic assay for assessment of osteoblast differentiation

The approach employed in this study, aiming at the identification of epigenetic modulators involved in osteoblast differentiation, required the development of an assay for the assessment of differentiation. With the aim to utilise both short hairpin RNA knockdowns and small molecule inhibition, the assay was intended to be a short and reliable process allowing comprehensive screenings. Alkaline phosphatase (ALP) was chosen as marker

characterising osteoblast differentiation. Although known to be present in many cell types, it is considered a valid osteoblast signature and also has the advantage of being an early marker, having its peak at day seven of differentiation. The activity of alkaline phosphatase was measured by using the substrate 4-methylumbelliferyl phosphate (4-MUP). Its dephosphorylation yields the fluorescent and stable product 4-methylumbelliferone (4-MU), which can be detected using a fluorescence plate reader [210]. For the purpose of this thesis it was essential that any kind of treatment, either with shRNA or compounds, was not affecting cell viability. Therefore, a measurement of the cells' metabolic activity as surrogate for cell viability was added to the assay, which could be undertaken prior to alkaline phosphatase activity measurements without affecting the downstream application. This way, the same cells could be tested for both cell viability and alkaline phosphatase activity. The active ingredient of the assay used (Presto Blue®, Life Technologies), is resazurin, a non-toxic and non-fluorescent cell permeable compound. Upon entering cells it is reduced to resorufin, yielding a red fluorescence signal that can be measured using a fluorescence plate reader. The validity of both assays was tested by applying the substrates to different cell densities, thereby ensuring the accuracy of the test regarding a linear relation of signal to cell number, and by testing the fluorescence stability of the product over time (see appendix A.4). The assay was tested as a time course on human mesenchymal stem cells undergoing osteoblast differentiation under different inducing conditions. Different concentrations and combinations of supplements were applied and the change in alkaline phosphatase activity caused by the inducers was compared to the basic osteogenic medium (OD). In addition, the initial change in expression caused by this basic osteogenic medium was also compared to cells remaining in mesenchymal stem cell medium (MSC), confirming that the basic osteogenic medium is osteopromotive. A list of

all media compositions used can be found in appendix A.1. Figure 2.3 shows the activity of alkaline phosphatase on day 5 - 8 of differentiation. For day 5 and 8, the baseline activity for cells in MSC medium is also shown, confirming the increased induction of alkaline phosphatase by applying osteogenic media. The single inducers applied, dexamethasone, 1,25-dihydroxyvitamin D_3, and oncostatin M, led to a significant increase in alkaline phosphatase activity on all four days of assessment (figure 2.3). Combinations of inducers, e.g. dexamethasone and 1,25-dihydroxyvitamin D_3, led to a further increase in activity, but with regard to dissecting the inducer-specific effects on osteoblast differentiation, these conditions were not further considered. However, these results confirmed previously published results, supporting the robustness of this assay. Higher concentrations of single inducers caused reduction in cell viability and did not necessarily lead to an increase in ALP activity as shown for dexamethasone (concentrations applied: 10nM and 100nM). For oncostatin M, a higher concentration led to an increase in ALP activity, however with regard to cell viability (cell death-like cell cluster formation could be observed, data not shown) the lower concentration was chosen for further experiments. Treatment with BMP-2 did not show a significant increase in alkaline phosphatase activity and attenuated the effect of 1,25-dihydroxyvitamin D_3. The time point chosen to be optimal for the assay was day 7, represented by assay results for "7 days" as shown in figure 2.3, capturing the peak in alkaline phosphatase expression for most of the conditions. Based on their effect on alkaline phosphatase expression and cell viability, the three inducers chosen were dexamethasone (10nM; in figures abbreviated to Dex), 1,25-dihydroxyvitamin D_3 (1nM; in figures abbreviated to vitamin D3), and oncostatin M (10ng/ml; in figures abbreviated to OSM).

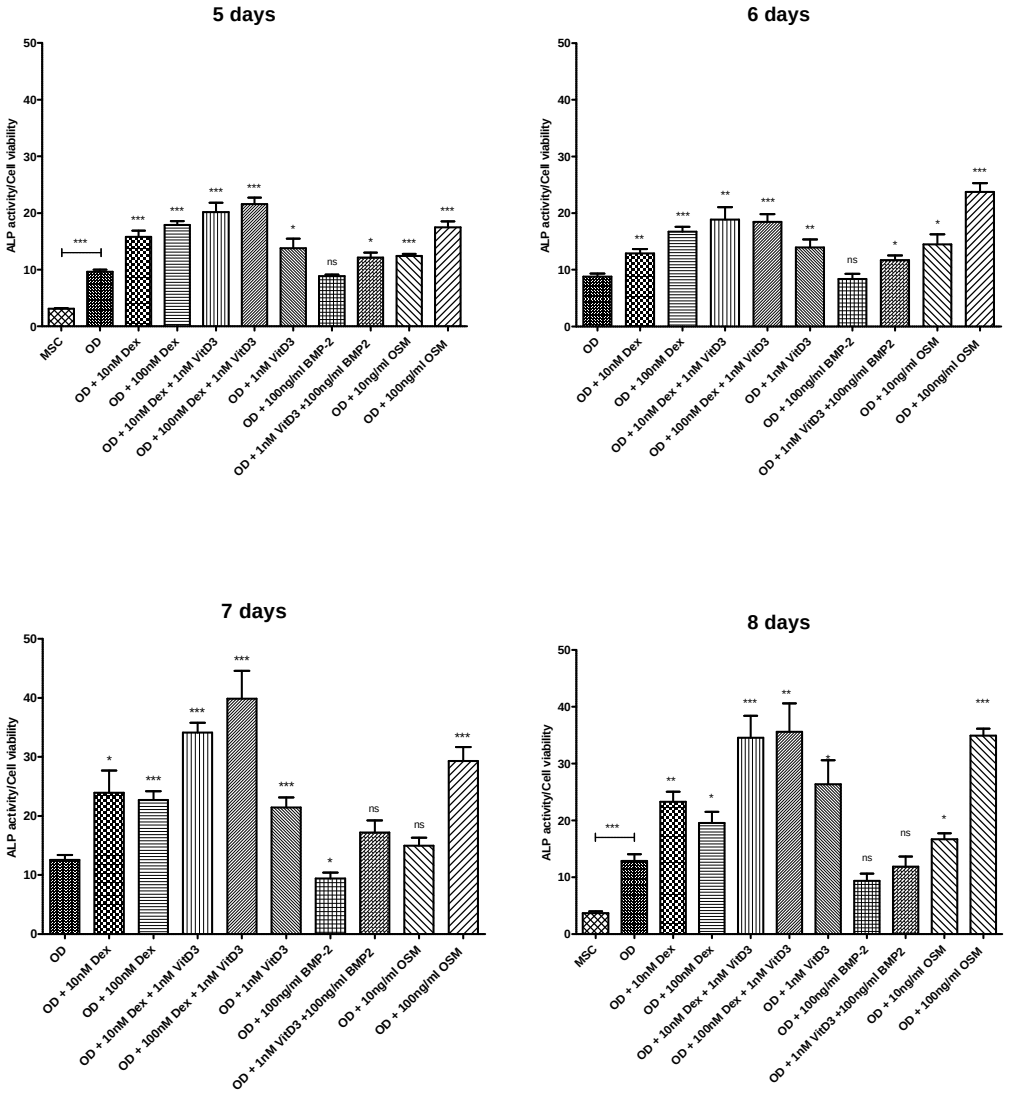

Figure 2.3: Time course of ALP peak activities under different osteoblast differentiation inducing conditions. Alkaline phosphatase activity and cell viability of differentiating human mesenchymal stem cells were assessed from 5 to 8 days of differentiation. Different media conditions are indicated on the x-axis and the alkaline phosphatase activity normalised to cell viability is shown on the y-axis. More information about media compositions can be found in appendix A.1. P-values were calculated with unpaired t-tests comparing to OD unless otherwise indicated (*** < 0.001, **<0.01, *<0.05). N = 6

2.7 Validation of different osteoblast induction methods

2.7.1 Osteoblast gene expression analysis by quantitative polymerase chain reaction

Different osteogenic induction methods were reported to have varied effects on differentiation and produce osteoblastic cells with different phenotypic characteristics. To gain a better understanding of this difference before applying the differentiation protocols to further experiments, the effects of 1,25-dihydroxyvitamin D_3 and cytokine oncostatin M were assessed. For completeness, and to confirm the initial microarray analysis, dexamethasone was also included in the analysis. Human MSCs were treated for 21 days with medium containing supplements as described in subsection 2.4.1. RNA was collected and gene expression profiles of selected marker genes were assessed by quantitative polymerase chain reaction (qPCR). In addition, the potential of the inducers to promote matrix mineralisation was assessed by ARS staining, allowing the detection of calcium deposits in the matrix. The identity of the differentiated mesenchymal stem cells was confirmed by the detection of, among others, alkaline phosphatase and osteocalcin (*BGLAP*), which are classical osteoblast-specific marker genes (figure 2.4). Treatment with dexamethasone and 1,25-dihydroxyvitamin D_3 led to an increase in alkaline phosphatase expression of approximately 100-fold for +DEX and 30-fold for +VitD3, while oncostatin M led to an increase of around 3.5-fold. Osteocalcin (*BGLAP*) expression was slightly increased under dexamethasone and oncostatin M treatment (1.6-fold for +DEX, 1.3-fold for +OSM) and highly increased for 1,25-dihydroxyvitamin D_3 (16.4-fold).

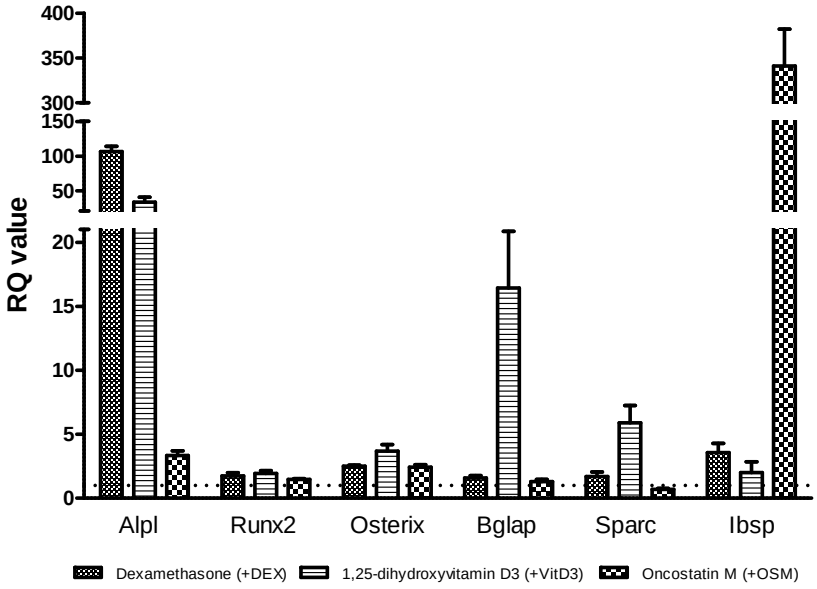

Figure 2.4: Gene expression analysis of osteoblast genes. The three different inducers, as indicated below the graph were analysed for expression of alkaline phosphatase (*ALPL*), *RUNX2*, *OSX*, osteocalcin (*BGLAP*), osteonectin (*SPARC*), and bone sialoprotein (*IBSP*). Changes as measured on day 7 of differentiation are shown as fold change compared to the MSC control.

Other genes assessed were transcription factors *OSX* (2.4 - 3.7-fold induction) and *RUNX2* (1.5-fold - 2-fold induction), as well as matrix components bone sialoprotein (*IBSP*) and osteonectin (*SPARC*). As described earlier, 1,25-dihydroxyvitamin D_3 led to the highest increase in osteocalcin expression compared to dexamethasone and oncostatin M.

2.7.2 Matrix mineralisation assessed by Alizarin Red S

In order to complete the confirmation of an osteoblast phenotype, the mineralisation of the cell matrix was analysed. Alizarin Red S was used to detect calcium depositions in the matrix, followed by acetic acid extraction and quantification. All three inducers, dexamethasone, 1,25-dihydroxyvitamin D_3, and oncostatin M, led to matrix mineralisation as measured by ARS (figure 2.5). Compared to the non-treated control, all inducers caused a significant increase, confirming their differentiation induction potential, with oncostatin

M showing the highest level of calcium deposition.

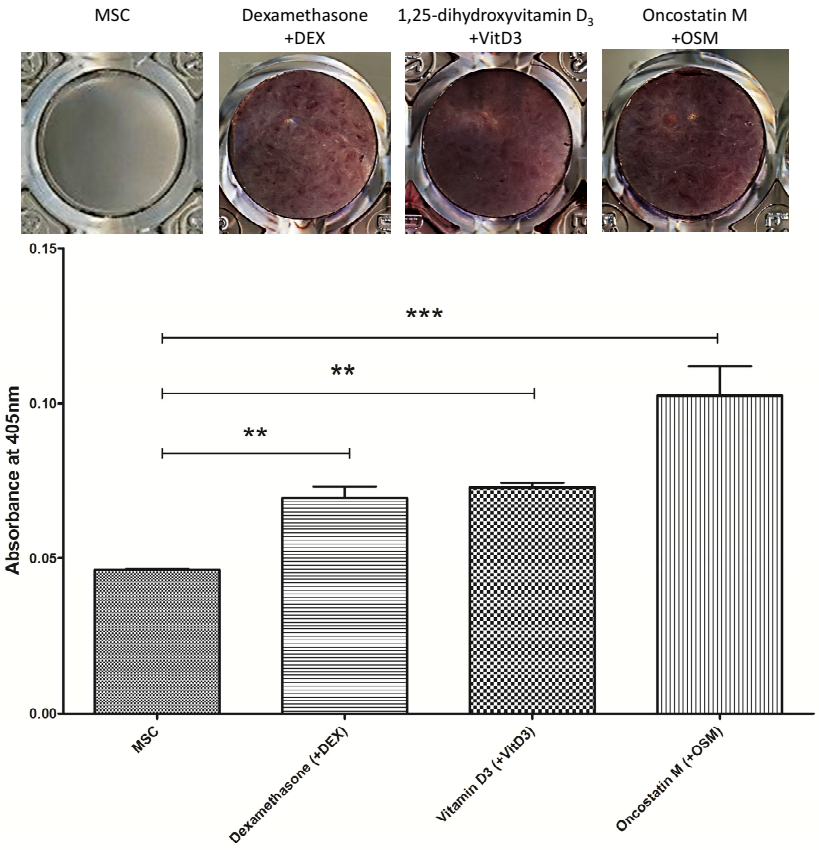

Figure 2.5: Mineralisation potential of inducers. Alizarin Red S staining was used for the detection of calcium. Calcium deposition as seen on day 21 was quantified using acid extraction and compared to the MSC control. P-values were calculated using One-way ANOVA (Bonferroni post-test - *** < 0.001, **<0.01, *<0.05). n=3

2.8 Conclusion and discussion

Different factors inducing osteoblast differentiation display varied effects and produce osteoblastic cells with different phenotypic characteristics. In this chapter, the differentiation potential of the employed human mesenchymal stem cells was confirmed using three different inducers, namely dexamethasone, 1,25-dihydroxyvitamin D_3, and oncostatin M. Dexamethasone will be used as the main model for differentiation in future experiments and its expression profile was also assessed by microarray analysis. Various concentrations and combinations of different inducers were tested in the development of a generic assay

to be used for knockdown and inhibition experiments and three conditions and a timeline for the experiments were chosen. With regard to the literature, it became obvious that there is not just one way leading to induction of osteoblast differentiation, and indeed the three different inducers tested showed differences in gene expression. The gene expression profiles as assessed by microarray gave a complex picture of osteoblast differentiation. Genes that were previously unknown for being involved in the process were discovered in our dataset, for instance Sushi domain-containing 2 (*SUSD2*), a gene that was only recently identified as an MSC-specific marker [204]. Specific osteoblast marker genes, such as *RUNX2*, *OSX*, *ALP*, and *BGLAP* were confirmed by microarray and qPCR, as well as through activity measurements for alkaline phosphatase. Although all three inducers chosen showed an osteoblast phenotype, it should be mentioned that many of the known protocols for differentiation are based on pre-osteoblast cells, thus might potentially not be sufficient for mesenchymal stem cells in order to differentiate to the same level. For instance, control experiments with human osteoblast cell lines (hOb, kindly provided by Dr. Philippa Hulley in the same department) showed higher mineralisation levels under dexamethasone treatment as assessed by ARS (data not shown), whereas the human mesenchymal stem cells used here, although surely mineralising, only showed a fraction of the calcium deposits of hOb. Mesenchymal stem cells might require more time for full differentiation and mineralisation, which is why in this work they were differentiated for up to four weeks.

The development of an osteoblast differentiation assay was pursued under two leading points – it had to be time-efficient and reliable. Alkaline phosphatase was chosen as early osteoblast differentiation marker, and with all inducers having their peak in ALP activity around the same time, i.e. 7 days into differentiation, the time frame for the assay was set.

The cell viability assay, measuring metabolic activity, could however only be an estimate of the cell number. To account for the possibility that for instance a small number of cells exhibit high levels of alkaline phosphatase activity, as it could theoretically be caused by a knockdown, in subsequent experiments the cell viability and alkaline phosphatase activity were first considered separately before normalisation in order to assure correct assessment. The optimisation of this assay for the purpose of screening short hairpin RNAs and small molecules will be presented in the next chapter. BMPs, the best known family of proteins involved in the development of bone and cartilage, were initially assessed in this work, but in our hands BMP-2 proved to be unable to sufficiently induce alkaline phosphatase expression. 100ng/µl BMP-2 were shown to be inhibitory to ALP activity, with only a slight increase when 1,25-dihydroxyvitamin D_3 was added. With regard to our aim to identify differences in epigenetics specific for each inducer, these combinations were not further considered.

3 Identification of epigenetic modulators in osteoblast differentiation

3.1 Introduction

The major aim of this thesis is to identify epigenetic modifiers involved in osteoblast differentiation. For this purpose, both knockdown experiments with short hairpin RNAs (shRNAs) and inhibition experiments with small molecule inhibitors were carried out. Starting with a broad approach targeting a significant subset of known epigenetic modifiers, the aim was to identify a number of hits for future follow up. The two different approaches with shRNA and small molecule inhibitors allowed for comprehensive screening, also amenable to high-throughput, with particular assessment opportunities for some targets where both shRNA and compound were available. In addition, these two different mechanisms of interference made it possible to assess the difference of structural and functional (= catalytic) roles some of these modifiers might play. As outlined in chapter 1, the field of the study of epigenetic mechanisms involved in mesenchymal stem cell differentiation has grown in recent years, but especially with regard to their therapeutic potential there is still a lot to be investigated and understood. This thesis will provide the first systematic approach identifying epigenetic mechanisms underlying osteoblast differentiation. In this chapter, the tools used for interference, shRNAs and compounds will be first introduced, followed by a short description of the optimisation of the generic assay with regard to the screenings. Subsequently, detailed methods and results for shRNA and compound screen will be discussed, concluding with a target hit list. From this hit list two target genes are followed up in more detail, work that will be discussed in the following chapters (for flow chart see figure 3.1).

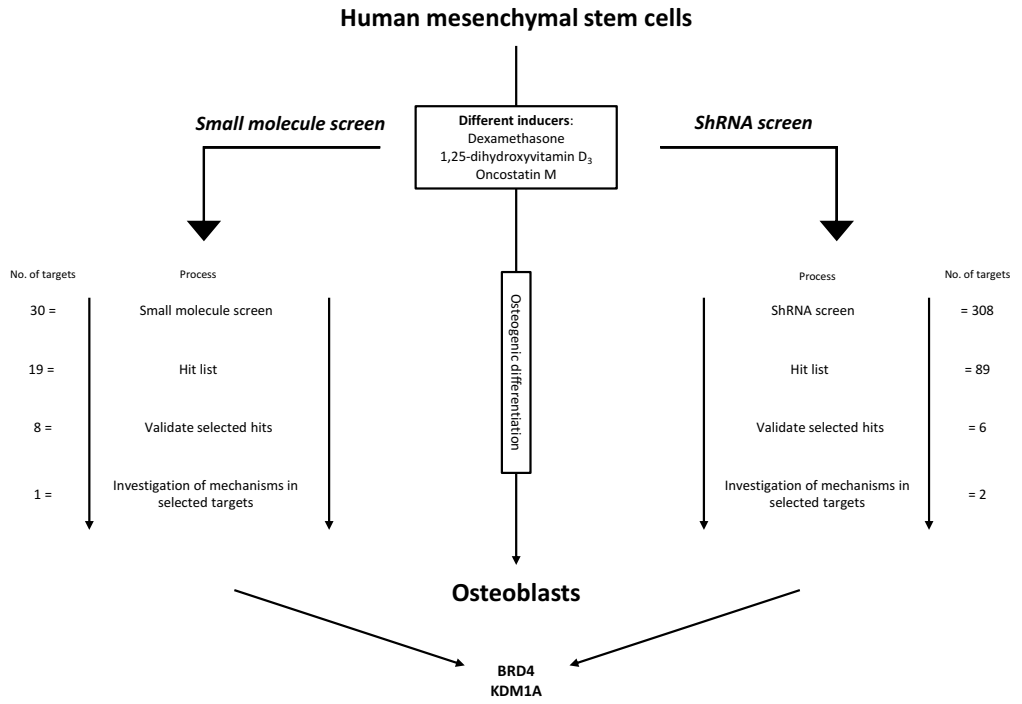

Figure 3.1: Workflow of this thesis. The differentiation of human mesenchymal stem cells into osteoblasts was discussed in chapter 2, in chapter 3 both the shRNA and small molecule inhibitor screen will be presented. Chapter 4 and 5 will present two follow-up targets, BRD4 and KDM1A.

3.1.1 Tools for interference with epigenetic modulators

3.1.1.1 Short hairpin RNAs

RNA interference (RNAi) is a cellular process providing a mechanism for mRNA degradation and thereby allowing regulation and direction of gene expression [211]. An important cellular defence mechanism against parasitic genes, such as viruses and transposons, it is found in many eukaryotes including humans [212]. In recent years, RNAi has emerged and been developed as a powerful tool to study gene function. Application of small interfering RNAs (siRNAs) that can be either provided as siRNA or short hairpin RNA (shRNA), allows for a specific knockdown of target mRNAs in a cell. ShRNAs are introduced into cells by means of lentivirus transduction, bringing the advantage of permanent

integration into the cell's genome, thereby allowing for a stable knockdown [213]. In our system, shRNA expression is driven by a U6 promoter to ensure their stable expression. The U6 promoter is a Polymerase III promoter type, a system shown to be optimal for producing shRNAs as the promoter contains all essential elements upstream of the expressed RNA allowing precise initiation and termination of transcription. Once expressed, the long RNA primary transcript derived from the integrated gene will be cleaved by DROSHA, an RNase III endonuclease, to produce a characteristic stem-loop structure (hairpin).

The pre-shRNA is then transported out of the nucleus (figure 3.2). In the cytoplasm, both shRNA and siRNA, as well as microRNAs (miRNAs, small non-coding RNAs), follow the same mechanism of target mRNA destruction. The RNAi pathway is initiated by DICER, an enzyme that cleaves the exogenous double-stranded RNA into short fragments of approximately 20-25bp. The double-stranded siRNA, consisting of a passenger strand and a guide strand, is then unwound into two single-stranded RNAs. Following this, the guide strand is incorporated into the RNA-induced silencing complex (RISC), while the passenger strand is degraded. The guide strand is used as a template for recognition of the complementary target mRNA, with which the siRNA forms a double-stranded RNA. Subsequently, the target mRNA will be cleaved by the active components of the RISC, endonucleases called argonaute proteins. Through this degradation, the translation of the mRNA and accordingly the expression of the gene are prevented [215]. Compared to siRNA, shRNA is constantly synthesised in host cells, leading to more durable gene silencing.

In this work, a library of short hairpins generated by the Broad Institute (Cambridge, MA, USA), targeting a significant subset of epigenetic modulators (308 target genes; the complete list can be found in appendix A.6.1), covering different modifications on chro-

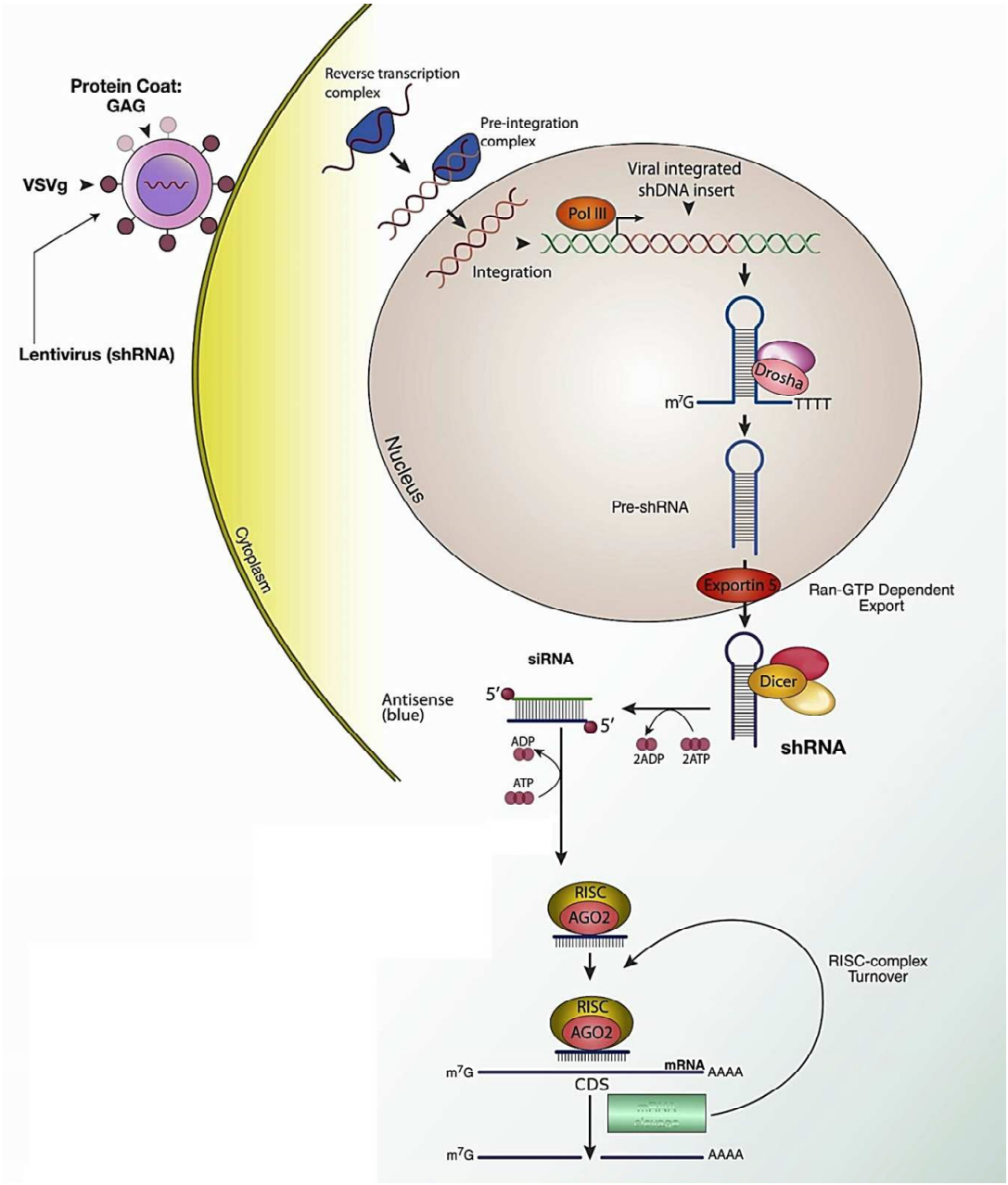

Figure 3.2: Lentiviral delivery of shRNA and the mechanism of RNA interference in mammalian cells. Adapted from [214].

matin, was applied to hMSCs undergoing osteogenic differentiation under various induction methods. Each epigenetic gene of interest was targeted separately by up to five hairpin structures in order to improve gene coverage and increase knockdown efficacy.

3.1.1.2 Small molecule inhibitors

A focussed library of small molecules targeting different epigenetic classes was employed to interfere with epigenetic modifying enzymes.

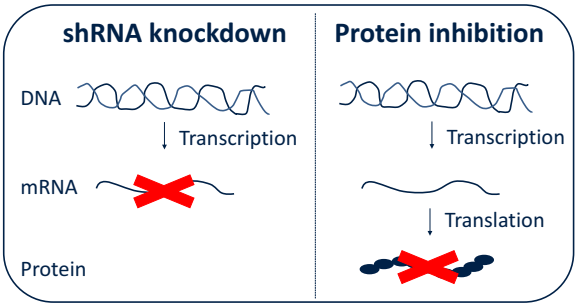

Figure 3.3: shRNA and small molecule inhibitors principle. Knockdown by shRNA leads to an inhibition on transcriptional level whereas small molecule inhibition only targets the translated protein and inhibits its functional, but possibly not structural role.

Availability of potent and cell-permeable compounds is of particular advantage, not only because they facilitate long-term cell treatment at low doses, but compared to RNAi they also allow the elucidation of the difference between the functional and structural roles of a protein (figure 3.3). Some of the inhibitors used in this work were targeting the same genes as some of the shRNAs, with the small molecules inhibiting the active sites of the proteins or protein-protein interactions (e.g. in bromodomains). This is of interest, since it is expected that some of the target proteins function as scaffolds or structural proteins, while others have a catalytic function, or both, as demonstrated e.g. for certain histone demethylases such as JMJD3 [216]. The library of small molecules was compiled by a public-private partnership between the Structural Genomics Consortium (SGC), Oxford, and nine pharmaceutical companies. Hits derived from these small molecule inhibitor screens were followed up in more detailed dose-response experiments

and osteoblast differentiation assays.

3.2 Materials and Methods

The tools used for interference with epigenetic modulators were already presented in the previous subsections and will be explained in more detail with regard to the employed shRNA and compound libraries in the next sections. For a better coherence and understanding of the particular screening steps, more detailed materials and methods will be presented within each section for both shRNA and small molecule inhibitor screen. The optimisation of the alkaline phosphatase assay will be briefly explained in the next section, and more information with regard to equipment and methods can be found in appendix A.5.

3.2.1 Alkaline phosphatase assay optimisation for high-throughput screening

The assay employed to assess osteoblast differentiation, as described in chapter 2, was optimised for high-throughput screenings. In order to save time and consumables and allow a large number of short hairpin RNAs and small molecule inhibitors to be assessed, the assay initially developed for a 96 well plate format was miniaturised to 384 well plates. The cell number was adapted with regard to cell confluency, differentiation time, and alkaline phosphatase activity measurement. It was found that approximately 1000 human mesenchymal stem cells could be seeded into one well (0.056cm^2 growth area) which resulted in sufficient density and stable confluency for the intended assay duration of 10 days.

3.3 ShRNA knockdown of epigenetic modulators

The shRNA screen was undertaken at the PLACEBO (Chemical Screening and Platform Austria for Chemical Biology) laboratory at the Research Center for Molecular Medicine of the Austrian Academy of Sciences (Ce-M-M-) in Vienna, Austria.

3.3.1 TRC shRNA library

The public-private RNAi Consortium (TRC, The RNAi Consortium) at the Broad Institute (Cambridge, USA), a joint venture between MIT and Harvard (USA), has developed libraries of shRNAs against human and murine targets over the past decade [217]. These libraries are now commercially available from Sigma-Aldrich and Thermo-Fisher under the names MISSION shRNA and TRC Lentiviral shRNA, respectively. However, for this thesis' work a library obtained directly from the Broad Institute was available at PLACEBO in Vienna. The shRNAs were delivered via a lentiviral system (see paragraph 3.1.1.1), permitting a permanent integration into the genome and stable transcription; in addition it offers a selection possibility to obtain a defined population showing homogenous knockdown. The epigenetic target genes were selected based on known epigenetic modifications, their related proteins/enzymatic modifiers and potential druggability. These covered the range from the aforementioned writers, such as methyltransferases and acetylases, readers, such as PHD domains and bromodomains, and erasers, such as demethylases and deacetylases. The list of shRNA target genes addressed in this thesis is shown in appendix A.6.1. The shRNA was cloned into the AgeI and EcoRI restriction sites of the pLKO vectors, with each target sequence not more than approximately 2kb in length to keep the total plasmid size below 9kb (for vector maps see appendix A.5.2). The puromycin selection cassette (PAC) was under the control of a human phosphoglycerate kinase (hPGK)

promoter which provided a high level of constitutive gene expression. Relevant lentiviral controls carrying the pLKO vector with a puromycin resistance cassette as well as inserts for GFP, RFP, lacZ, or no insert at all were used as negative comparators. Positive controls causing cell death were obtained by either no addition of virus or by a virus carrying an insert toxic to the cells (pgw). This "positive/negative" labelling was derived from screens against e.g. cancer cells, where cell death would be a positive result. In our case, it was desirable for the cells to survive, which will be reflected in the hit selection criteria discussed later on. Each epigenetic gene of interest was targeted by up to five different short hairpin sequences in order to improve gene coverage and knockdown efficacy (for an example see table 3.1).

Gene symbol	Vector	Clone name	Clone ID	Target sequence	% Remaining	Hairpin no
KDM1A	pLKO.1	NM_015013.1-1812s1c1	TRCN0000046068	GCCTAGACATTAAACTGAATA	5	4
KDM1A	pLKO.1	NM_015013.1-2168s1c1	TRCN0000046069	GCTCCAATACTGTTGGCACTA	30	1
KDM1A	pLKO.1	NM_015013.1-775s1c1	TRCN0000046070	CCAACAATTAGAAGCACCTTA	34	3
KDM1A	pLKO.1	NM_015013.1-1232s1c1	TRCN0000046071	GCTACATCTTACCTTAGTCAT	4	2
KDM1A	pLKO.1	NM_015013.1-1896s1c1	TRCN0000046072	CCACGAGTCAAACCTTTATTT	5	5

Table 3.1: Example of short hairpin sequences targeting *KDM1A*. The % remaining indicates the level of percent remaining gene expression as assessed by TRC in various cell lines. Each hairpin was giving a number (1-5) in order to facilitate the denotation.

3.3.2 Lentiviral delivery optimisation – viral titration and cell selection

In order to determine the best conditions for viral transduction, a titration experiment using different levels of multiplicity of infection (MOI) of pooled virus and different puromycin concentrations was performed. In virology, the MOI describes the ratio of infectious agents (virus) to infection targets (in this case MSCs), i.e. the number of virus particles to the number of cells. The MOI had to be high enough in order to infect the majority of the cells, producing a sufficiently large population of cells with the desired knockdown. In addition, the required puromycin concentration had to be determined beforehand. It had to be high enough to eliminate cells that were not transfected, but

low enough not to put too much additional selection stress on the successfully transfected cells. For this test, cells were seeded and allowed to attach for one night before virus at different MOIs was added. The tests revealed that the optimal seeding density in order to obtain around 1000 successfully transfected cells was in fact 1250 cells, as around 1/5 of cells would not survive viral transduction and selection. The derived MOI was 10 and the concentration of puromycin 5µg/ml. Furthermore, the titration showed the need for an additional transfection reagent. A common carrier is polybrene (hexadimethrine bromide), a cationic polymer used to increase the efficiency of transfection when transducing cells with viruses. It acts by neutralising the charge repulsion between the virions and sialic acid moieties on the cell surface [218]. As the graphs in figure 3.4 show, polybrene was essential to facilitate viral entry and transduction. Even with low puromycin concentrations virtually no cells survived without polybrene pre-treatment (on average 10-30% survival rate at 1-2µg/ml puromycin). Conversely, with polybrene the survival rate of cells even at medium range MOIs was highly improved. The chosen parameters of 10 for the MOI and 5µg/ml puromycin showed a clear window between successfully transfected cells of MOIs between 5 and 20, and lower MOIs, avoiding a higher and potentially toxic puromycin concentration. Transduction efficiency was also tested employing a GFP control virus and the MSCs were proven to be easily transduced (figure 3.5). In addition, the duration for the viral transduction was optimised (data not shown). It yielded an optimal transduction time of 36 hours, allowing sufficient time for the virus to integrate into the genome, followed by a 24 hours selection period with puromycin, providing sufficient time for the antibiotic to eliminate non-transduced cells.

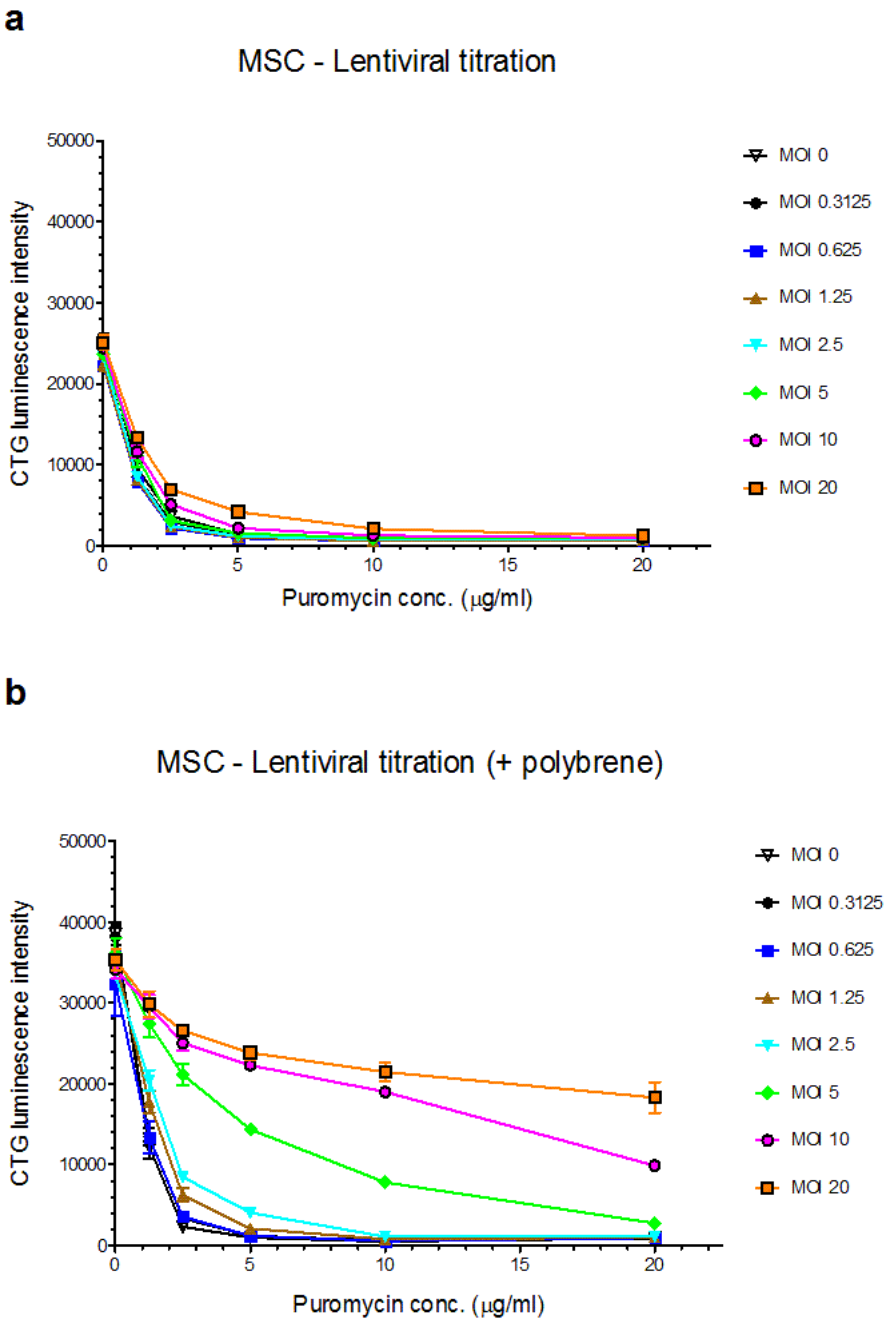

Figure 3.4: Optimisation of MOI and puromycin concentrations and testing of transfection agent. Different MOIs from 0-20 were tested together with puromycin concentrations of 0-20µg/ml. As a readout, the CellTiter-Glo® luminescent cell viability assay (CTG) was used, determining the number of viable cells based on quantitation of intracellular ATP, an indicator of metabolically active cells. Plot A shows titration without addition of polybrene, plot B is with addition of polybrene.

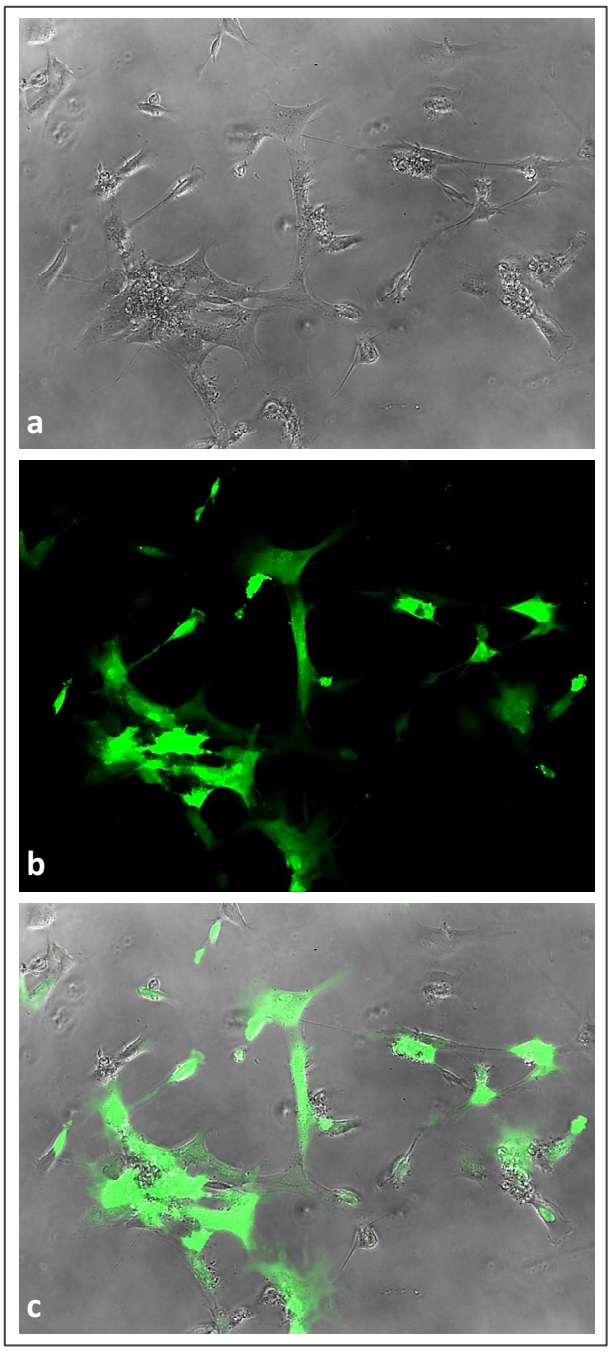

Figure 3.5: Optimisation of viral transfection - GFP control virus. A GFP control virus was applied to the cells in order to assess the transduction efficiency of lentiviral particles in hMSCs. Phase contrast image can be seen in figure a, figure b shows the GFP fluorescence, and figure c an overlay (10x objective).

3.3.3 Brief overview of assay protocol

As outline in the validation experiments above, human mesenchymal stem cells were seeded into 384 well plates at a density of 1250 cells per well. Approximately 24 hours after seeding, cells were treated with polybrene and transduced with virus at an MOI of 10. After 36 hours, cells were selected using puromycin at a concentration of 5µg/ml. The selection process was ended after 24 hours and medium was changed to the respective differentiation medium (for media list and compositions see appendix A.1). Medium was changed again on day 3 and 5 of differentiation. On day 7 of differentiation, cell viability and alkaline phosphatase activity were measured as described below and in more detail in appendix A.5.3. The cell viability reagent Presto Blue® was added to each well and plates were incubated at 37°C for 30 minutes. The cell viability was read (exc 535 - em580, gain 1, 1%) before cells were washed three times with PBS. Subsequently, the cell lysis buffer was added and plates were incubated at room temperature for 15 minutes, followed by a 30sec shake at 10 Hertz. Lastly, the ALP assay substrate 4-MUP was added and the plate was immediately transferred to the fluorescence plate reader and read at Exc 340 – Em 520 (gain 1, 0%) to obtain a T_0 for the ALP activity. The plate was read again at 30 minutes (T_{30}) and 60 minutes (T_{60}) after substrate addition.

3.3.4 Data analysis of MSC differentiation assay

The obtained data (all reads from the Envision plate reader measuring cell viability and alkaline phosphatase activity) was fed into a programme called Pipeline Pilot [219]. This software allowed the consolidation of all reads and all required information about e.g. virus distribution, plate conditions, and plate orders. Once all data was matched (e.g. which virus was in which well under which condition) it was uploaded into a software called

Spotfire (TIBCO Software) that was used for visualisation when setting the selection criteria.

3.3.5 Screen validation and selection criteria for shRNA hits

In order to analyse the results of the screen, the control samples had to be assessed for performance. The "positive" controls were the ones having an effect, for instance vectors carrying the toxic component pgw, or samples where no virus was added at all and therefore all cells died. "Negative" controls were samples in which the viral particle contained e.g. RFP, GFP, lacZ, or no gene at all in the place of the shRNA. The average of all negative controls per plate set was set as 100% as these cells were considered as being "normal" without a specific gene being knocked down. A clear window between positive and negative controls could be observed. Subsequently, all other hairpin structures were compared to their respective controls, i.e. to the controls in the same plate under same culture medium condition. For assessing the alkaline phosphatase activity, the difference of the ALP value at 60 minutes after substrate addition (T_{60}) compared to T_0 was calculated and used for further calculations. Hits were selected based on fulfilling a range of stringent criteria - at least two short hairpin sequences per gene had to be effective in down- or upregulating alkaline phosphatase, and they had to show the same effect for both replicates. Above all, cell viability had to be at least 50% of the cell viability of the control cells, while alkaline phosphatase activity at 60mins had to be below 80% (for a downregulating hit) or above 100% (for an upregulating hit) of the control values (percentage of control, POC). In addition, to allow a simple judgement of hits falling into the "high ALP" or "low ALP" range, the calculation of a ratio was introduced. In order to identify genes with a very high and very low ALP activity, respectively, while ensuring good cell viability, a ratio

of alkaline phosphatase activity (ALP) to cell viability to be met by each hairpin was applied. For upregulating hits, it was set to 2, while for downregulating hits it was set to 0.5. Initially, the ratio for upregulating hits was set to 1.5 (see criterion **1** below) but it turned out to potentially not be stringent enough and to result in a high number of hits (>100). Therefore it was set more stringent (see criterion **2** on the next page), to ensure that only very consistent and strong hits would fall under these criteria.

Explanation of parameters in criteria:

- Cell Viability = value for cell viability measurement expressed as fluorescence unit
- ALP_{60} = value for alkaline phosphatase activity at 60mins (T_{60}) after substrate addition normalised to T_0 and expressed as fluorescence unit
- POC = percentage of control, i.e. values were compared and normalised to set of controls as explained above: (Signal of gene - Mean signal of positive controls) / (Mean signal of negative controls - Mean signal of positive controls) $\times 100$ = POC
- Ratio = POC ALP_{60}/POC Cell Viability

The criteria for hit selection shown below were set as above discussed, and criterion 2 was chosen with regard to a more stringent selection.

1 POC Cell Viability $\geq$ 50% AND [(POC ALP60 $<$ 80% AND Ratio $<$ 0.5) OR [(POC ALP60 $>$ 100% AND Ratio $>$ 1.5)]

2 POC Cell Viability $\geq$ 50% AND [(POC ALP60 $<$ 80 % AND Ratio $<$ 0.5) OR [(POC ALP60 $>$ 100% AND Ratio $>$ 2)]

Hit hairpins identified through these criteria were classified as up- or downregulating, $\uparrow$ (red) and $\downarrow$ (green) and the selection is illustrated in figure 3.6. Hairpins that fell under

the 50% threshold of cell viability were not considered even if the ratio was met (asterisks). In the graph below, the distribution of hits can be seen. This graph is only for illustration purposes, as the actual data set is too large to display. The original data consists of >300 genes tested for up to 5 different hairpins in duplicate in 5 different medium conditions, with 4 different readouts (cell viability; alkaline phosphatase activity at 0, 30, and 60mins), which summed up to >70,000 data points.

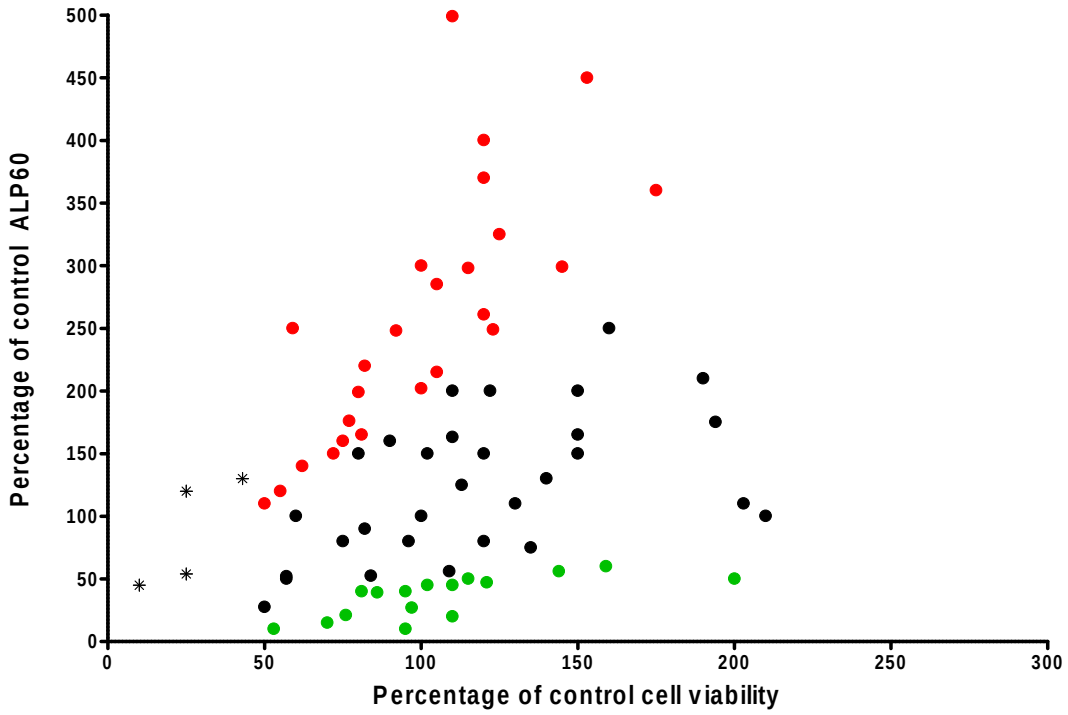

Figure 3.6: ShRNA screen on MSCs differentiating into osteoblasts - illustration of hit distribution and selection. Red dots indicate a gene (i.e. hairpin) upregulating ALP activity, green dots are indicative for a gene (i.e. hairpin) downregulating ALP activity (measured at 60mins). Asterisks show genes not fulfilling the 50% cell viability threshold. Black dots are genes not matching the selection criteria.

All red dots represent hits fulfilling the criterion "POC ALP_{60} > 100% AND Ratio > 2". For example, for a hairpin with a POC ALP_{60} of 325 and a POC cell viability of 125, the ratio is 2.6, thus the hairpin was considered an upregulating hit. Likewise, for a hairpin with a POC ALP_{60} of 45 and a POC cell viability of 110, the ratio calculates as 0.4, thus

the hairpin was considered a downregulating hit and displayed by a green dot (POC ALP_{60} $< 80\%$ AND Ratio < 0.5). Black dots represent hairpins not fulfilling the criteria and were not further considered in this case. However, some genes were later selected manually for further analysis, as discussed in the following sections. As seen in figure 3.6, cell viability values higher than the values of the control samples could be obtained. This is due to the nature of the Presto Blue® assay, measuring metabolic activity rather than cell viability. Thus, cells potentially metabolically stimulated due to a knockdown can exhibit a higher metabolic activity and consequently a higher cell viability measurement. However, with the aim to avoid skewness in the data, unnaturally high levels of cell viability were carefully considered and if doubted, the associated samples were dismissed.

3.3.6 Results – Analysis of hits derived from shRNA screen

The hit selection yielded a total number of 74 hit genes. Approximately two thirds of these (48 genes) were downregulating alkaline phosphatase activity and 26 genes were upregulating the activity (table 3.2). In addition, a number of genes were "manually" added to the hit list (table 3.3). For instance, if hairpins against a gene did not fulfil all selection criteria to be called a hit gene, but still showed interesting changes with regard to alkaline phosphatase activity, they were considered for manual addition. These additional hits were selected based on the extent of alkaline phosphatase activity (decreasing or increasing), hairpin efficiencies (if known), similar trend in hairpins (e.g. number of hairpins with an effect - two hairpins having a similar effect rather than one in all conditions), consistency in duplicates, or based on comparable results from compound screens. From this approach, another 15 hits were identified, 10 of which were downregulating and 5 upregulating alkaline phosphatase activity. Hits identified through the stringent criteria can

be found in table 3.2 and the additional genes in table 3.3. A summary of all hits identified under different differentiation conditions is shown in table 3.4. 75 of the hits were found in the three main inducing conditions (dexamethasone, 1,25-dihydroxyvitamin D_3, and oncostatin M, as selected in chapter 2), with dexamethasone presenting the majority of hits. Hits could theoretically also be "shared" hits between the conditions, with *UBE2A* being the only one shared between all main conditions (figure 3.7). As indicated in table 3.2 and table 3.3, other genes showed a similar trend, but did not fulfil all criteria to be "officially" counted as a hit in all conditions. These were *KDM1A*, *JMJD8*, *MORF4L1*, and *PHIP* as seen in the first table, and *HDAC2*, *MYST4*, *SUV420H2*, and *TDRD6* in the second table. However, *UBE2A*, *KDM1A*, *JMJD8*, and *MORF4L1* were considered the strongest hits between those, as they had two hairpins causing the same effect throughout all conditions.

Table 3.4 shows the number of hit genes per condition. For example, under dexamethasone treatment (+DEX), 52 targets were identified as hits, with 44 of them downregulating alkaline phosphatase activity, and 8 hits upregulating alkaline phosphatase activity. Genes that only fulfilled the hit selection criteria in one condition were considered "unique" hits for this condition. In the case of dexamethasone, 35 out of the 44 targets downregulating ALP activity were unique for one of the conditions, as well as 3 of the upregulating targets. Overall, 66 hits were unique for a condition, with dexamethasone representing the condition with the most unique hits (=38).

Gene symbol	CM	OD	+DEX	+VitD3	+OSM	Comments
AKAP1			↓			
ALG13			↓			
ARID1A			↓			
ARID4A			↓			Similar effect in other conditions
ASF1A			↓			
ASH1L			↓			
ATAD2			↓			
AURKA			↓			
AURKB			↓			
BAZ1A			↓			
BAZ2B			↓			
BPTF			↓			
BRD3					↑	Similar effect in other conditions
BRD7			↓			
BRD8			↓			
BRDT			↓			
BRWD1			↓			
C14ORF169			↓			
C2ORF60					↑	Similar effect in other conditions
CECR2			↓			
CHD2			↓			
CHD6			↓			Similar effect in other conditions
CHD8			↓			
CHD9				↑		Similar effect in other conditions
CHRAC1			↓			
CXXC1		↑	↓	↑		
DIDO1			↓			
DPF1		↓				
EHMT1	↓					
ELP3	↓	↓				
EP300		↓				
EZH1			↓			Similar effect in other conditions
EZH2	↓					
FBXL19	↓					
HDAC7	↓					
HDAC8				↑		
HIF1AN	↓					
HIRA				↑		
ING2				↑		
JHDM1D		↑		↑		
JMJD6	↓					
JMJD8	↑	↑	↑	↑		Hairpin 3 and 4 in all conditions
KAT2A				↑		Similar effect in other conditions
KAT2B			↑			
KAT5		↓	↓			
KDM1A		↑		↑		Hairpin 2, 3, and 4 in all conditions
KDM1B			↓			Similar effect in other conditions
KDM3B		↓				
MBD5				↑		
MECOM		↓	↓			
MINA				↑		Similar for hairpin 1 in other conditions
MLL4		↑				
MORF4L1		↑	↑			Hairpin 3 and 4 in all conditions
MTA1		↑		↑		
MTA2				↑		Similar effect in other conditions
MYST2				↑		
PHF11				↑		Similar effect in other conditions
PHF3				↑		Similar effect in other conditions
PHIP			↑			Hairpin 3 in all conditions
PRDM8			↓			Similar effect in other conditions
SET			↓	↓		
SETD1A	↓					
SETDB1			↓			
SIN3B			↓			Similar effect in other conditions
SIRT7				↓		Similar effect in other conditions
SMARCB1			↓	↓		
SMC2			↓			Similar effect in other conditions
SMYD1		↓	↓	↓		
SP100	↓					
TRAF7				↑		
TRIM24	↑	↑	↑	↑		
TRIM33	↓		↓			Similar effect in other conditions
UBE2A	↑	↑	↑	↑	↑	
ZMYND8				↑		Similar effect in other conditions

Table 3.2: shRNA hits derived by selection process. Table is showing the respective condition in which the hits were found, with ↑ and ↓ indicating an up- or downregulation of alkaline phosphatase activity. Coloured cells in the inducing conditions (e.g. purple for dexamethasone) are indicative for a hit that is unique for that condition. If a target had a hairpin showing a similar effect over all conditions, the respective row was coloured in red. Additional comments are made if a trend could be observed. Medium conditions and abbreviations: CM, control medium; OD, basic osteogenic medium lacking the main inducer; +DEX, complete osteogenic medium containing dexamethasone; +VitD3, complete osteogenic medium containing 1,25-dihydroxyvitamin D_3; +OSM, complete osteogenic medium containing oncostatin M.

Gene symbol	CM	OD	+DEX	+VitD3	+OSM	Comments
BAZ1B			↓			Hairpins 1-4 in Dex
BRD2			↓			Hairpins 1, 2, and 4 in Dex
BRD4			↓			Hairpins 1 and 5 in Dex (and slightly in VitD3 and OSM)
BRPF3			↓			Hairpins 1, 2, 3, and 5 in Dex
CAPRIN2				↑	↑	Hairpins 2 and 5 in OSM; hairpin 5 in VitD3
CDYL2			↓			All hairpins in Dex
DNMT3B	↓	↓				Hairpins 3-5 in CM and OD
HDAC2			↑			Hairpin 3 in all conditions
MYST4				↑	↑	Hairpin 4 in all conditions
PRDM1			↓			All hairpins in Dex, generally low in all conditions
PRMT2			↓			Hairpin 2 in all conditions
PRMT7			↓		↓	All hairpins in Dex and OSM
SMC4				↓	↓	Hairpins 2, 4, and 5 in VitD3 and in OSM
SUV420H2				↑	↑	Hairpin 5 in all conditions
TDRD6			↑	↑		Hairpin 2 in all conditions

Table 3.3: List of manually selected shRNA hits. Hits were selected based on hairpin efficiencies, similar trend in hairpins (count of hairpins - rather two hairpins having a similar effect than one in all conditions), consistency in duplicates, etc. The reason for choosing the gene as a hit is explained in the comment. Table is showing the respective condition in which the hits were found, with ↑ and ↓ indicating an up- or downregulation of alkaline phosphatase activity. Coloured cells in the inducing conditions (e.g. purple for dexamethasone) are indicative for a hit that is unique for that condition. If a target had a hairpin showing a similar effect over all conditions, the respective row was coloured in red. Additional comments are made if a trend could be observed. Medium conditions: control medium, CM; basic osteogenic medium lacking the main inducer, OD; complete osteogenic medium containing dexamethasone, +DEX; complete osteogenic medium containing 1,25-dihydroxyvitamin D_3, +VitD3; complete osteogenic medium containing OSM, +OSM

CM		OD		+DEX		+VitD3		+OSM	
14 hits		17 hits		52 hits		29 hits		8 hits	
up	down	up	down	up	down	up	down	up	down
3	11	9	8	8	44	24	5	6	2
of them unique		of them unique		of them unique		of them unique		of them unique	
up	down	up	down	up	down	up	down	up	down
-	8	1	3	3	35	13	1	2	-

Table 3.4: Number of shRNA hits per condition and direction of their effect (up- or downregulating alkaline phosphatase activity). Number of shared and unique hits is indicated. Information about conditions (= media compositions) can be found in appendix A.1.

The control medium culture condition (CM) without any osteogenic supplement, was employed as a background control, with the lowest alkaline phosphatase activity compared to all other conditions. Considering the low baseline level of ALP activity, only a small change in activity was required to lead to a further reduction, potentially yielding the 11 downregulating hits. Interestingly, the condition with incomplete differentiation medium containing ascorbic acid and beta-glycerophosphate but no main inducer (OD),

showed a number of targets upregulating alkaline phosphatase activity. With regard to the already present supplements facilitating osteoblast differentiation, the targets found in this condition were of particular interest, as they imply that one single modification, i.e. knockdown of a target gene, could be sufficient to induce differentiation. The increase in ALP activity following the knockdown of these targets also implies that these genes under normal conditions might suppress alkaline phosphatase expression and potentially osteoblast differentiation. Under inducing conditions, there was an interesting difference to be observed between the three different inducers. Both 1,25-dihydroxyvitamin D_3 and oncostatin M, although with smaller number of hits in comparison, showed more hits upregulating alkaline phosphatase activity, while dexamethasone treatment showed more hits downregulating ALP activity. As dexamethasone is the most potent inducer of alkaline phosphatase (as seen in chapter 2), it is likely that a smaller increase in activity would not be sufficient to lead to a significant change in comparison to the control. In slightly less inducive conditions like +VitD3 and +OSM, the scope for reaching a significant difference compared to the control might be larger. The Venn diagram in figure 3.7 shows the distribution of hits in the three different induction conditions. All conditions share one hit, *UBE2A*, and another 12 genes are shared by at least two conditions. Overall, the majority of hits obtained were represented by targets leading to a downregulation of alkaline phosphatase activity. This is mainly due to the way the selection criteria were set, with the ratio calculation excluding a number of potential hits upregulating ALP activity. As it could be seen in figure 3.6, although in many cases upregulating ALP activity, targets displayed in black were not considered as hits. With the aim to be stringent and only allow "strong" hits to enter the hit list, this decision had to be made, accepting the possible miss of potential targets. Also, as only one particular time point was chosen for

assessment, any changes in ALP activity occurring beforehand or afterwards were to be missed. As described in chapter 2, the time point was chosen based on the peak in ALP observed during a time course of 8 days. If the knockdown of a particular gene led to a delay or even an advance in ALP activity, it was only partially, if at all, detected in this assay. However, as previously discussed, all targets were assessed manually afterwards and in some cases added to the hit list.

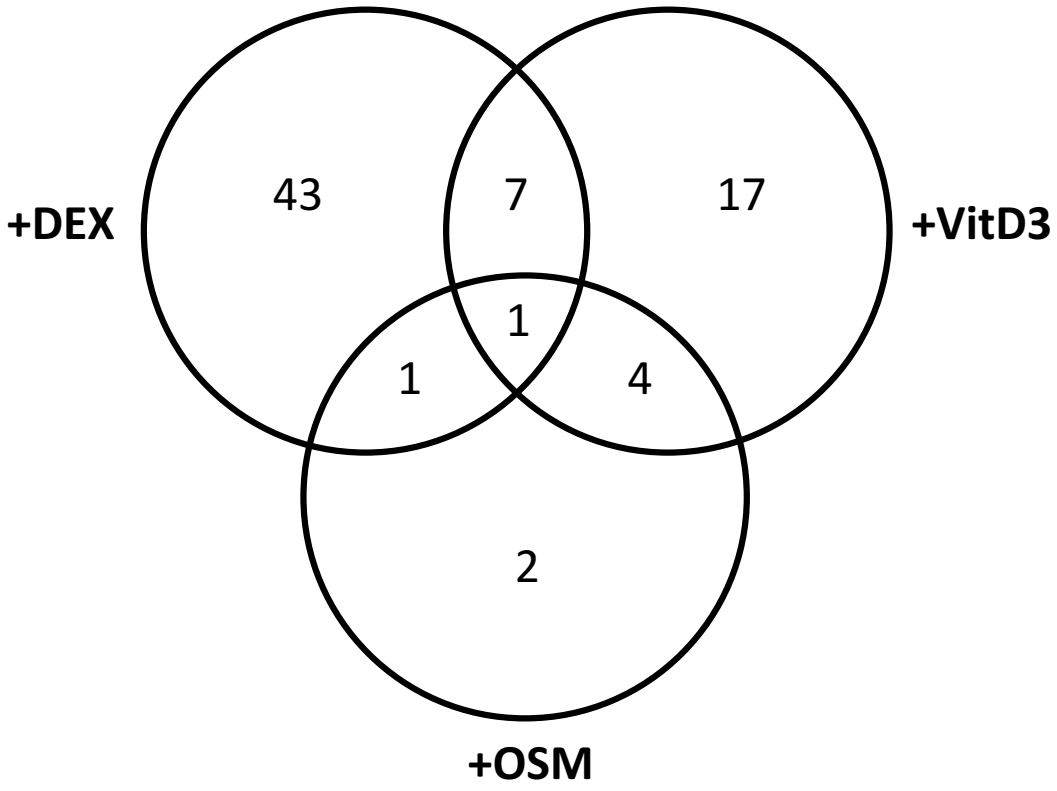

Figure 3.7: Venn diagram of 75 hits identified in three different screening conditions (dexamethasone, 1,25-dihydroxyvitamin D_3 and oncostatin M).

As an example for all 308 target genes and 89 derived hits, *UBE2A* is shown here in detail with its knockdown effect on cell viability and alkaline phosphatase activity for all hairpins in all conditions (figure 3.8). Knockdown of *UBE2A* resulted in upregulation of alkaline phosphatase activity in all conditions and even in the absence of external

osteogenic induction, as observed in the control medium (CM), which lacks induction components such as ascorbic acid, beta-glycerophosphate, and the main inducer. For two different hairpins, hairpin 4 and 5, the effects are shown in more detail (figure 3.9). Both hairpins had an increasing effect on alkaline phosphatase activity in all conditions, very consistently for hairpin 4. Although originating from two different plates and processed and measured in two different sets, duplicate samples were very consistent in both cell viability and alkaline phosphatase activity.

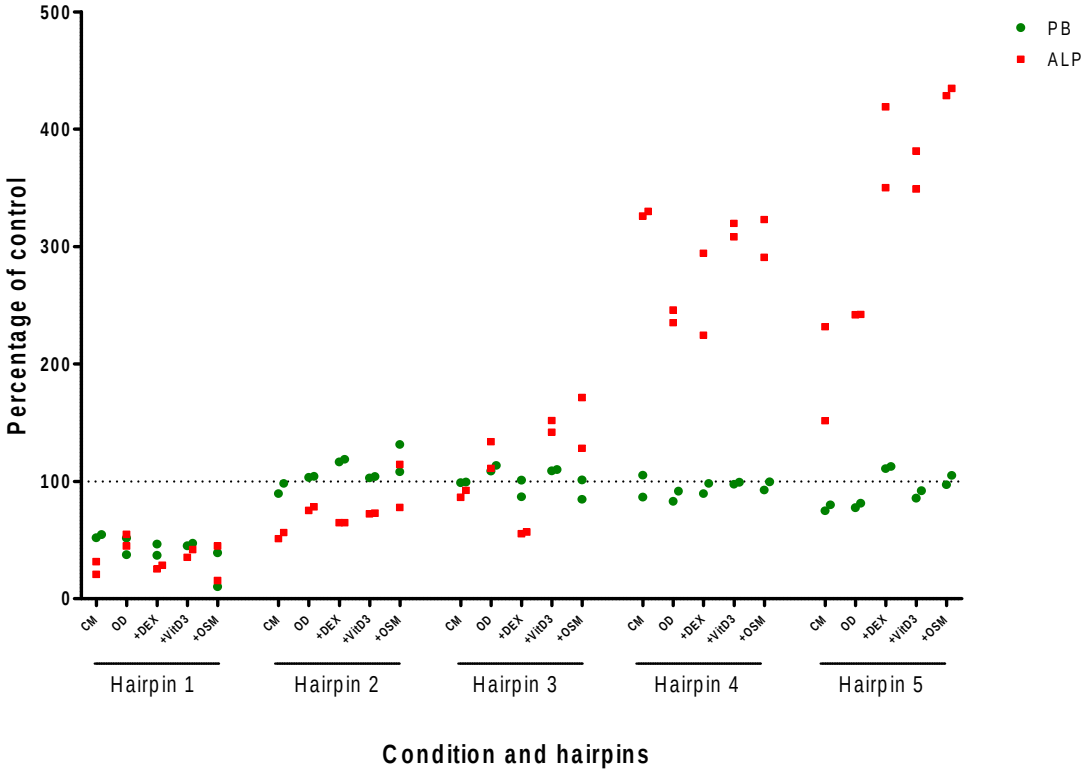

Figure 3.8: Effects of hairpins targeting *UBE2A* on cell viability and alkaline phosphatase activity. Hairpins 1 to 5 are shown on the x-axis in the five different conditions applied. The y-axis shows the percentage of control, with the dotted line indicating 100%. Green dots show Presto Blue® measurements (= cell viability) and red dots show alkaline phosphatase activity.

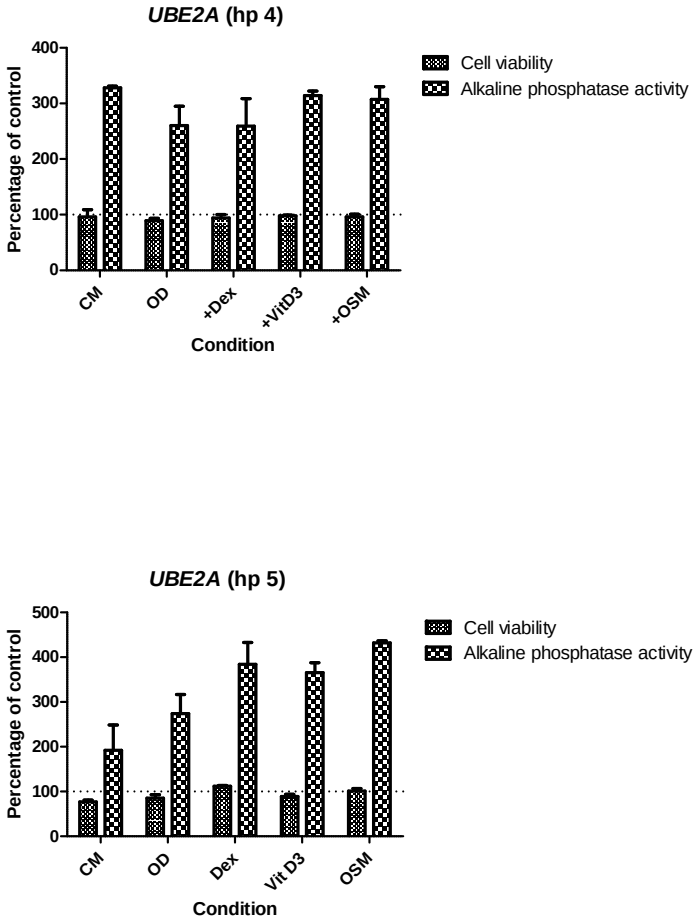

Figure 3.9: Knockdown of *UBE2A* with hairpin 4 and hairpin 5. Different induction conditions are on the x-axis and the y-axis shows the cell viability and alkaline phosphatase activity as percentage of control. The dotted line indicates the 100% level of the control. Information about conditions (= media compositions) can be found in appendix A.1.

Other hit genes derived from the shRNA screen are shown in more detail and with more information in subsection 3.3.10, where the general hit selection will be presented. In tables 3.5 and 3.6, each of the hit genes was categorised with regard to its epigenetic domain. Domains highlighted were chromodomains (methylated histone binding), tudor domains (methylated arginine binding), PHD domains ((Plant Homeo Domain; methylated lysine binding), bromodomains (acetylated lysine binding), MBD domains (Methyl-CpG-binding), HDMs (histone demethylases), HMTases (histone methyltransferases), PRMTs (protein arginine N- methyltransferases), HATs (histone acetyltransferases), HDACs (his-

tone deacetylases), and DNMTs (DNA methyltransferases).

Gene symbol	Chromo	Tudor	PHD	Bromo	MBD	HDM	HMTase	PRMT	HAT	HDAC	DNMT	Other
AKAP1		Tudor										
ALG13		Tudor										
ARID1A												DNA binding
ARID4A	Chromo	Tudor										
ASF1A												Histone chaperone
ASH1L			PHD	Bromo			KMT					
ATAD2				Bromo								
AURKA												Kinase
AURKB												Kinase
BAZ1A			PHD	Bromo								
BAZ1B			PHD	Bromo								
BAZ2B			PHD	Bromo								
BPTF			PHD	Bromo								
BRD2				Bromo								
BRD3				Bromo								
BRD4				Bromo								
BRD7				Bromo								
BRD8				Bromo								
BRDT				Bromo								
BRPF3			PHD	Bromo								
BRWD1				Bromo								
C14ORF169						HDM						
C2ORF60						HDM						
CAPRIN2												RNA binding
CDYL2	Chromo											
CECR2				Bromo								
CHD2	Chromo											
CHD6	Chromo											
CHD8	Chromo											
CHD9	Chromo											
CHRAC1												Histone fold
CXXC1			PHD									
DIDO1			PHD									
DNMT3B											DNMT	
DPF1			PHD									
EHMT1							KMT					
ELP3									HAT			
EP300				Bromo								
EZH1							KMT					
EZH2							KMT					
FBXL19			PHD									
HDAC2										HDAC		
HDAC7										HDAC		
HDAC8										HDAC		
HIF1AN						HDM						
HIRA												Histone chaperone
ING2			PHD									
JHDM1D			PHD			HDM						
JMJD6						HDM						
JMJD8						HDM						
KAT2A				Bromo					HAT			
KAT2B				Bromo					HAT			
KAT5	Chromo											
KDM1A						HDM						
KDM1B						HDM						
KDM3B						HDM						
MBD5					MBD							
MECOM							KMT					
MINA						HDM						
MLL4			PHD				KMT					
MORF4L1	Chromo											

Table 3.5: List of hit genes and their epigenetic domains (if known) - part I. A total of all genes displaying a particular domain is shown at the bottom of each column. Domains considered were: Chromo, chromodomains; Tudor, tudor domains; PHD, PHD domains; Bromo, bromodomains, MBD, MBD domains; HDM , histone demethylase (including monoamine oxidases and Jumonji type-oxygenases); HMT, histone methyltransferase; PRMT, protein arginine N- methyltransferases; HAT, histone acetyltransferases; HDAC, histone deacetylase; DNMT, DNA methyltransferase. For more detail, see text.

Gene Symbol	Chromo	Tudor	PHD	Bromo	MBD	HDM	HMTase	PRMT	HAT	HDAC	DNMT	Other
MTA1												DNA binding
MTA2												DNA binding
MYST2									HAT			
MYST4			PHD									
PHF11			PHD									
PHF3			PHD									
PHIP				Bromo								
PRDM1							KMT					
PRDM8							KMT					
PRMT2								PRMT				
PRMT7								PRMT				
SET												Unknown
SETD1A							KMT					
SETDB1		Tudor										
SIN3B												Unknown
SIRT7										HDAC		
SMARCB1												Unknown
SMC2												Unknown
SMC4												Unknown
SMYD1							KMT					
SP100				Bromo								
SUV420H2							KMT					
TDRD6		Tudor										
TRAF7												TRAF/zinc finger
TRIM24			PHD	Bromo								
TRIM33			PHD									
UBE2A												UBQ conjugating
ZMYND8			PHD									
TOTAL	**8**	**5**	**19**	**21**	**1**	**10**	**11**	**2**	**4**	**4**	**1**	

Table 3.6: List of hit genes and their epigenetic domains - part II. A total of all genes displaying a particular domain is shown at the bottom of each column. Domains considered were: Chromo, chromodomains; Tudor, tudor domains; PHD, PHD domains; Bromo, bromodomains, MBD, MBD domains; HDM , histone demethylase (including monoamine oxidases and Jumonji type-oxygenases); HMT, histone methyltransferase; PRMT, protein arginine N- methyltransferases; HAT, histone acetyltransferases; HDAC, histone deacetylase; DNMT, DNA methyltransferase. For more detail, see text.

The majority of domains present in the identified hits were PHD and bromodomains, with 19 and 21 proteins containing these domains identified, respectively. Both domain types are so-called "reader" domains, with bromodomains recognising acetylated lysines and PHD domains recognising methylated lysines. They often occur together, as it can be seen for seven of the shRNA targets, displayed in tables 3.5 and 3.6.

3.3.7 Network analysis of hits identified in shRNA screen

Epigenetic modifications require interactions between different modifiers, and modulators are often found in chromatin regulatory complexes. In order to identify networks in which the obtained targets are involved, hits were analysed using the Ingenuity® Knowledge Base (IPA, Ingenuity Pathway Analysis). For network generation, all 89 gene identifiers and

their ranking values (up- or downregulation, ↑/↓) were uploaded into the IPA application. Each gene identifier was mapped to its corresponding object in the database and overlaid onto a global molecular network developed from information contained in the Ingenuity® Knowledge Base. Networks of potentially interacting proteins were identified and placed into node-edge diagrams comprised of focus molecules (shRNA identified genes) and other interacting molecules. Networks of network eligible molecules were then algorithmically generated based on their connectivity. With regard to the targets found in this screen showing different effects on alkaline phosphatase activity, some of them downregulating and others upregulating alkaline phosphatase activity, network analysis could facilitate understanding of dependencies and interplay between these target genes. The four largest networks are displayed in table 3.7.

Network ID	**Associated network functions**	**Score**	**No of targets**
1	Gene Expression, Infectious Disease, Embryonic Development	58	25
2	Cell Cycle, DNA Replication, Recombination, and Repair, Cellular Assembly and Organisation	57	25
3	Cell-To-Cell Signalling and Interaction, Inflammatory Response, Infectious Disease	32	16
4	Cellular Compromise, Cell-To-Cell Signalling and Interaction, Cancer	11	7

Table 3.7: Network analysis of of hits identified in shRNA screen. The four largest networks and associated functions as calculated by IPA are shown. The score is derived from a p-value and indicates the likelihood of the focus genes in a network being found together due to random chance. The p-value was calculated using Fisher's exact test and displayed as the exponent: p-score = -log10 (p-value).

To rank the networks and determine their significance, a score was computed according to the fit of that network to the set of target genes (= focus genes) uploaded. The score is derived from a p-value and indicates the likelihood of the focus genes in a network being found together due to random chance. The p-value was calculated using Fisher's exact test and displayed as the exponent: p-score = -log10 (p-value). With 25 targets present,

respectively, specifically network 1 and network 2 showed the tight connectivity of the epigenetic modulators, of which many function in protein complexes and are dependent on recruitment of complex partners, while others occupy similar binding sites on histones. The top four networks, based on Fisher's exact test, were associated with "Gene Expression, Infectious Disease, Embryonic Development", "Cell Cycle, DNA Replication, Recombination, and Repair, Cellular Assembly and Organisation", "Cell-To-Cell Signalling and Interaction, Inflammatory Response, Infectious Disease", and "Cellular Compromise, Cell-To-Cell Signalling and Interaction, Cancer". The functions assigned to these networks can be widespread, for instance functions assigned to the first network include expression and transcription of DNA and RNA, as well as formation, modification, and remodelling of chromatin, confirming the involvement of the target genes in epigenetic modifications. The networks are shown in detail on the following pages (figure 3.10 to figure 3.13). Various functional information for the target genes was taken into account by the software and is displayed by the symbol in the legend. Several interactions between target genes could be observed, both direct and indirect. For example, network 2 displayed a significant number of indirect interactions; indirect interactions are defined as a change in gene expression of one gene when another gene is targeted. One example for an interaction displayed as indirect is the relationship between BRD4 and KAT2A (genes can be found in network 2 in figure 3.11). Based on published microarray analysis showing that the inhibition of human BRD4 protein by the inhibitor (+)-JQ1 decreases the expression of human *KAT2A* mRNA in multiple myeloma cell lines, the IPA software displays this relationship as indirect [220]. An example for a direct interaction is the binding of KDM1A to PRDM1 (BLIMP1), where binding to each other at the same target sites was observed in plasma cell differentiation (genes can be found in network 1 in figure 3.10) [221]. No particular

key nodes could be found in each network, however, in network 1 the focus appeared to be around histone 3 and the transcriptional co-activator EP300. Network 2 showed histone 4 and histone deacetylase 2 (HDAC2) as main interactors, while network 3 centred around ubiquitin C (UBC). Nuclear factor of kappa light polypeptide gene enhancer in b-cells (NFκB), vascular endothelial growth factor (VEGF), as well as MAP kinase/ERK family members (ERK) appeared to be in the centre of interactions of network 4. NFκB, VEGF, and ERK have previously been shown to be involved in osteoblast differentiation and ossification [222–224]. Within the networks, more interactions between target genes having a contrary effect on alkaline phosphatase activity could be seen than between genes having a similar effect (i.e. same direction of change). In addition, genes which knockdown inhibited alkaline phosphatase activity showed more interactions than genes having an upregulating effect. For genes with an upregulating effect, it is only interactions between homologous proteins such as MTA1 and MTA2 [225], or proteins of the same family, e.g. KAT2A and KAT2B (see network 2 in figure 3.11).

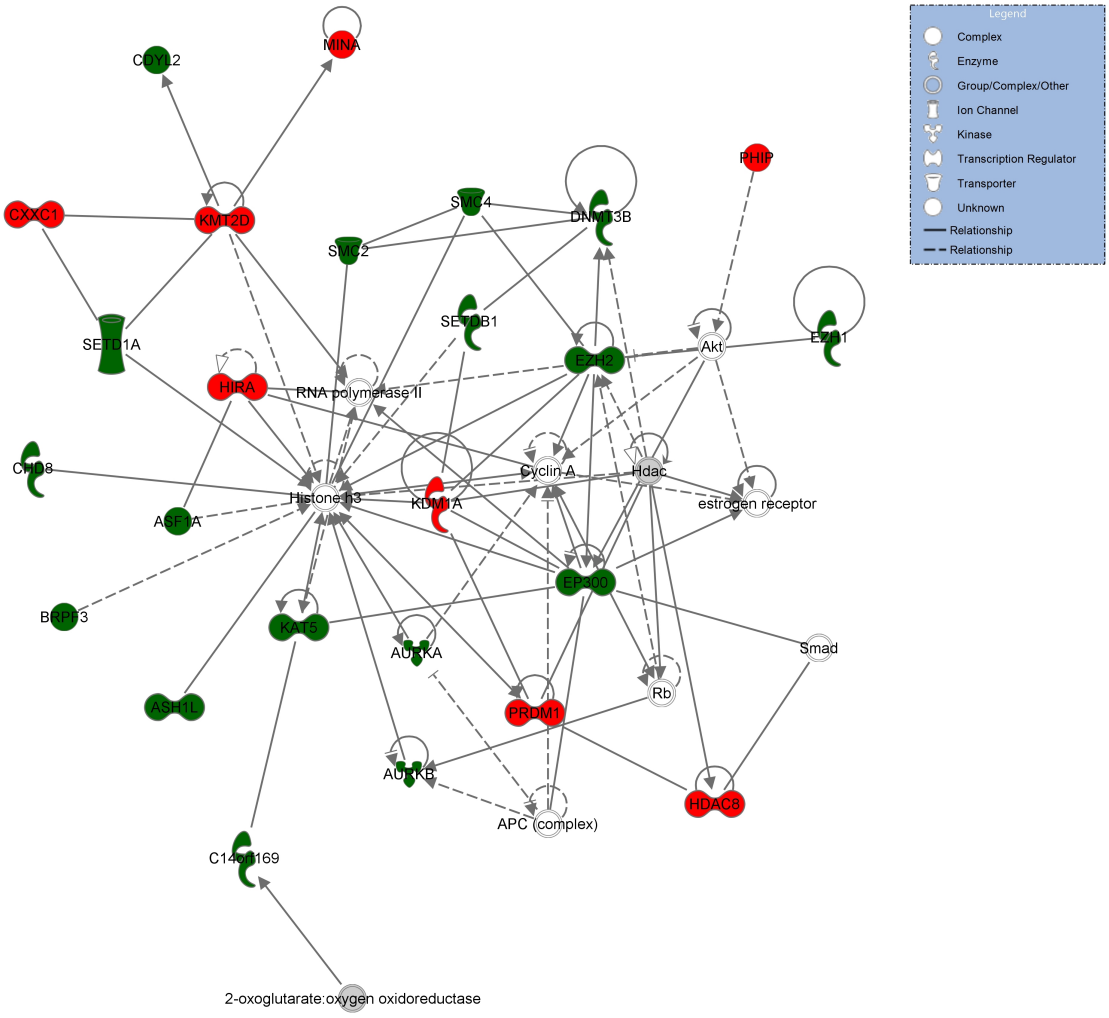

Figure 3.10: Network 1 “Gene Expression, Infectious Disease, Embryonic Development”, containing 25 hit genes as calculated by IPA. Targets leading to an upregulation of alkaline phosphatase activity when being knocked down are shown in red; targets leading to a downregulation are shown in green. Components in grey are additional genes by which hit genes are connected. A direct relationship is indicated by a solid line, whereas an indirect relationship is indicated by a dashed line.

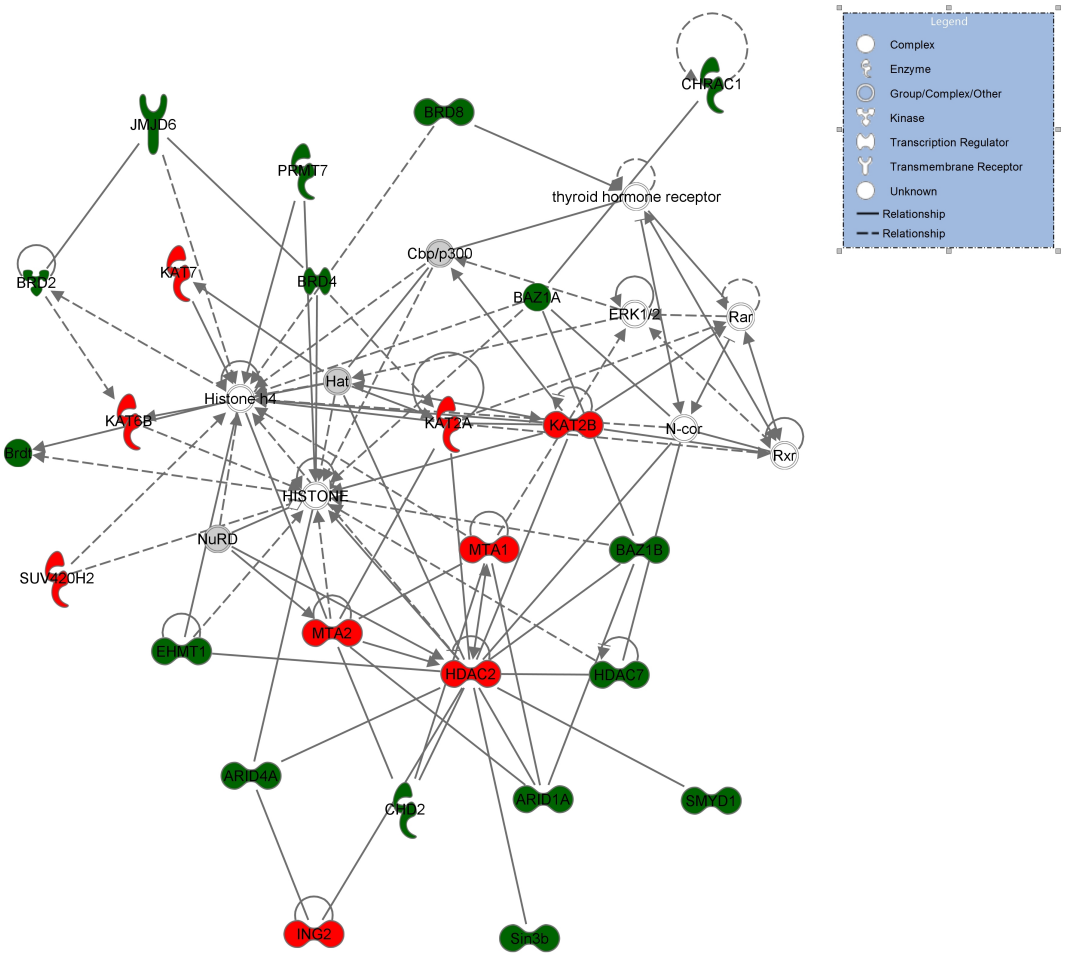

Figure 3.11: Network 2 “Cell Cycle, DNA Replication, Recombination, and Repair, Cellular Assembly and Organisation”, containing 25 hit genes as calculated by IPA. Targets leading to an upregulation of alkaline phosphatase activity when being knocked down are shown in red; targets leading to a downregulation are shown in green. Components in grey are additional genes by which hit genes are connected. A direct relationship is indicated by a solid line, whereas an indirect relationship is indicated by a dashed line.

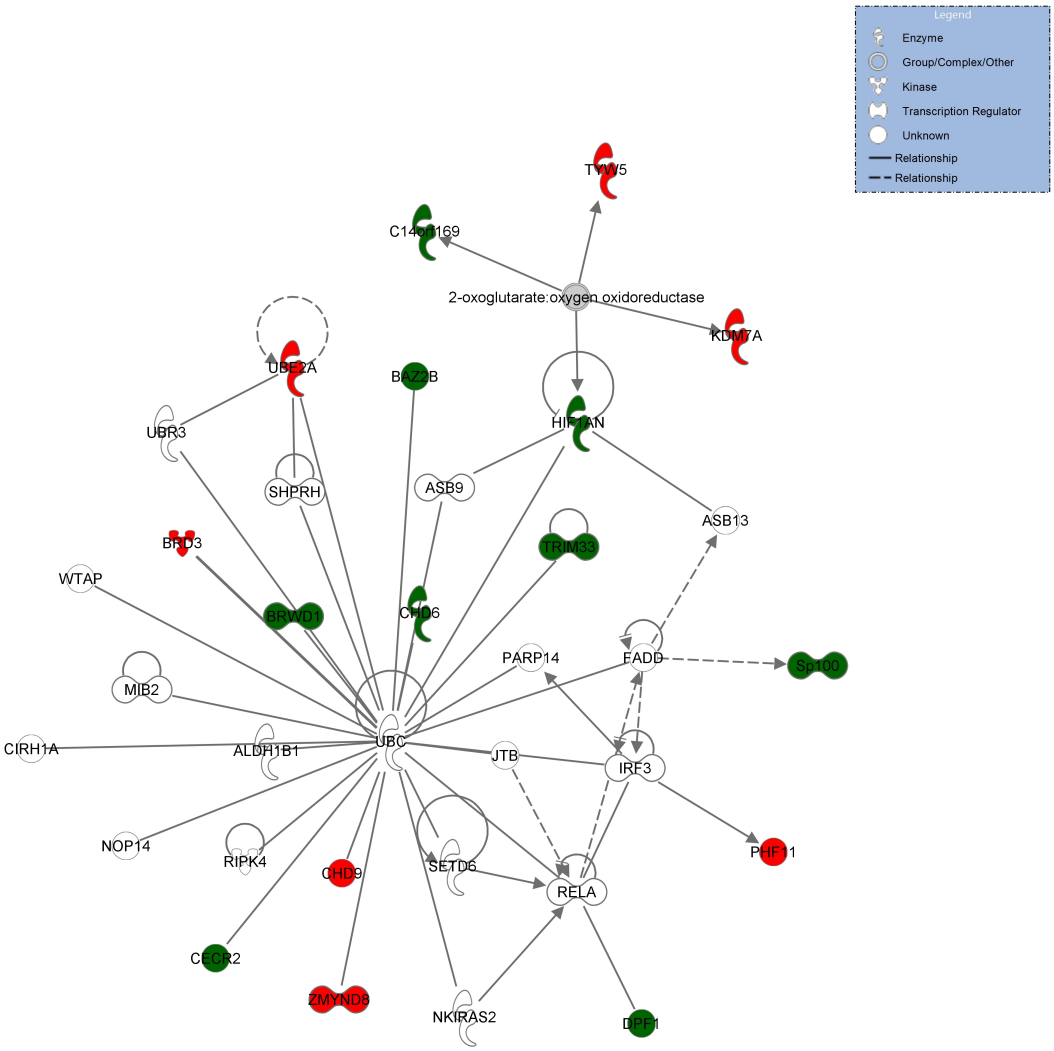

Figure 3.12: Network 3 "Cell-To-Cell Signalling and Interaction, Inflammatory Response, Infectious Disease", containing 16 hit genes as calculated by IPA. Targets leading to an upregulation of alkaline phosphatase activity when being knocked down are shown in red; targets leading to a downregulation are shown in green. Components in grey are additional genes by which hit genes are connected. A direct relationship is indicated by a solid line, whereas an indirect relationship is indicated by a dashed line.

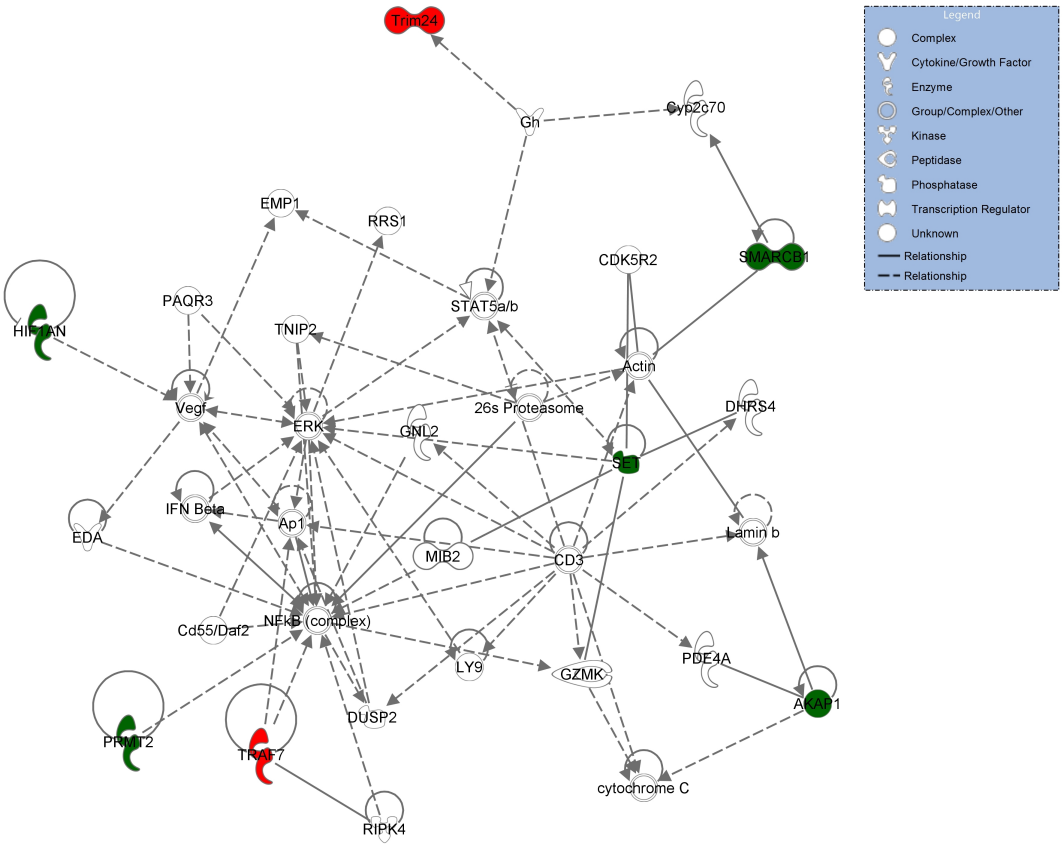

Figure 3.13: Network 4 "Cellular Compromise, Cell-To-Cell Signalling and Interaction, Cancer", containing 7 hit genes as calculated by IPA. Targets leading to an upregulation of alkaline phosphatase activity when being knocked down are shown in red; targets leading to a downregulation are shown in green. Components in grey are additional genes by which hit genes are connected. A direct relationship is indicated by a solid line, whereas an indirect relationship is indicated by a dashed line.

3.3.8 Target gene interactions

In addition to the network analysis, all hits were analysed for potential interaction partners using the protein-protein interaction (PPI) database at the Ce-M-M- in Vienna. Figure 3.14 gives an overview of this analysis, with the most significant interaction partners of the identified targets displayed. Tumor protein P53 has been shown to interact with a large number of epigenetic modifiers and recruits them to modify transcription. One of the genes with most hit interactions is the estrogen receptor 1 (*ESR1*), a finding supporting the IPA results (*ESR1* can be found in the largest network, network 1). A confirmation, highlight-

ing the utility of this analysis, is the fact that histones H3, H4, and H2A/B were identified as network components, demonstrating the involvement of targets in modifying and interacting with chromatin. In a second step the hits and interaction partners were mapped to known complexes, in this manner it was possible to determine which protein complexes were represented by the obtained targets. The five complexes with the largest number of hits involved are shown in table 3.8. The largest complex (= 15 hits and interactors; complex coverage of approximately 80%) is the LARC complex (LCR-associated remodelling complex), associated with functions such as DNA conformation modification (and organisation of chromosome structure), transcriptional control, modification by acetylation and deacetylation, as well as DNA binding [226], which was also reported to be involved in the prevention of transcriptional silencing [227]. The so-called locus control regions (LCRs) are regulatory DNA sequences that are situated many kilobases away from their cognate promoters and were suggested to perform specific chromatin remodelling activities [228]. The complete list of complexes can be found in appendix A.7.

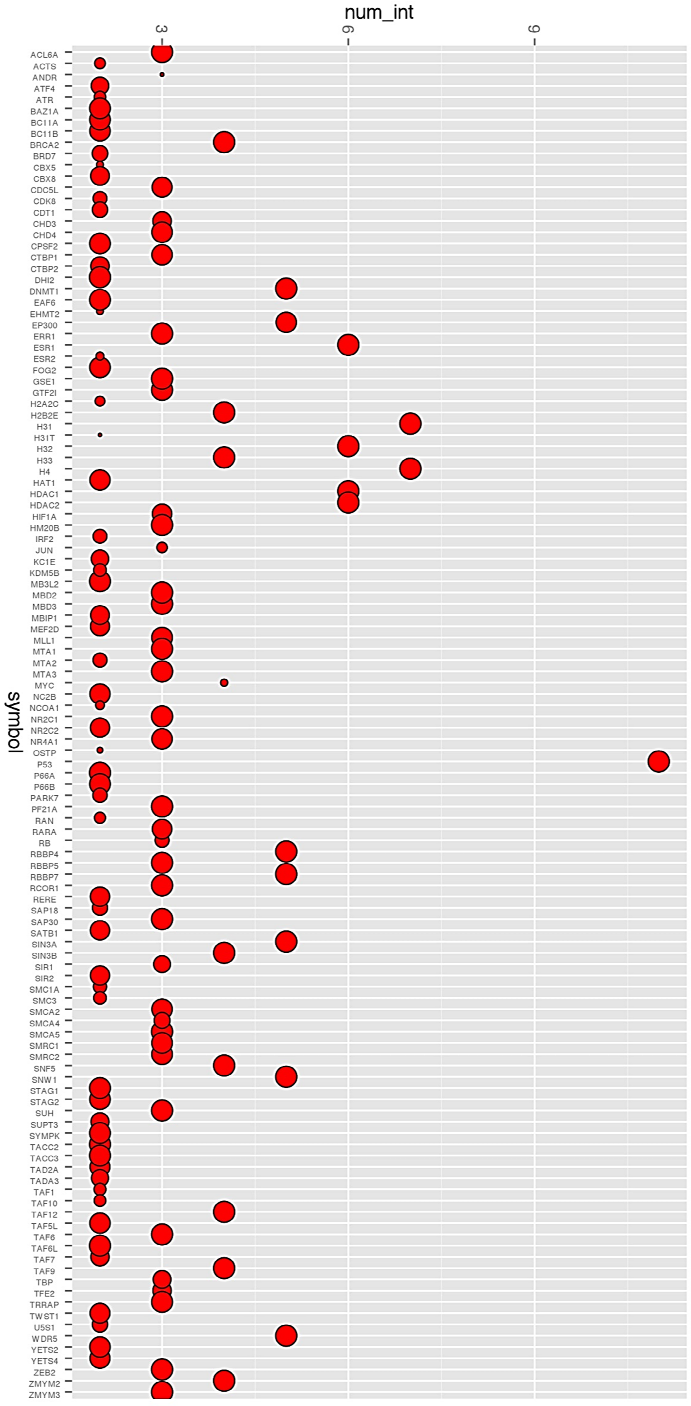

Figure 3.14: Protein-protein interactions of hit genes. On the x-axis the name of the protein/gene the hits are interacting with are shown, while the y-axis shows the number of interactions. The dot size represents the significance of the interactions (larger dot - higher significance). The graph is depicted in landscape format.

Cplx name	Cplx members	Cplx size	Total Hits	Num Hits	Cplx cov	p-value	Hits	Interactors	corr_p
LARC complex (LCR-associated remodelling complex)	P60709, O96019, O14497, Q14839, Q92785, Q8WXI9, Q13547, Q92769, P07910, Q9UBB5, O95983, O94776, Q09028, P51532, Q12824, Q92922, Q8TAQ2, Q92925, Q969G3	19	['O94776', 'Q92769', 'Q12824', 'O14497', 'Q8WXI9', 'Q9UBB5', 'O95983', 'O96019', 'P51532', 'Q09028', 'Q13547', 'Q14839', 'Q8TAQ2', 'Q92922', 'Q969G3']	15	0.79	7.22E-24	4	11	3.45E-21
SIN3-ING1b complex II	O96019, O14497, Q4LE39, Q13547, Q92769, Q9UK53, Q09028, Q16576, O00422, O75446, Q96ST3, P51532, Q12824, Q92922, Q8TAQ2, Q96GM5	16	['Q92769', 'Q12824', 'O14497', 'Q96GM5', 'O96019', 'P51532', 'Q09028', 'Q13547', 'Q16576', 'Q8TAQ2', 'Q92922', 'Q96ST3', 'Q9UK53']	13	0.81	4.09E-21	3	10	9.75E-19
BRM-SIN3A complex	O96019, O14497, Q13547, Q92769, O14744, Q09028, Q96ST3, P51531, Q12824, Q92922, Q8TAQ2, Q96GM5, Q92925, Q6STE5, Q969G3	15	['Q92769', 'Q12824', 'O14497', 'Q96GM5', 'O96019', 'P51531', 'Q09028', 'Q13547', 'Q8TAQ2', 'Q92922', 'Q969G3', 'Q96ST3']	12	0.80	2.05E-19	3	9	1.63E-17
NuA4/Tip60 HAT complex	O96019, Q9H0E9, Q9HAF1, Q9NPF5, Q96L91, Q9H2F5, Q92993, Q9NXR8, Q9UBU8, Q15014, Q9NV56, Q9Y265, Q9Y230, Q9Y4A5, O95619	15	['Q92993', 'Q9UBU8', 'Q9H0E9', 'O95619', 'O96019', 'Q15014', 'Q9H2F5', 'Q9HAF1', 'Q9NPF5', 'Q9NV56', 'Q9NXR8', 'Q9Y4A5']	12	0.80	2.05E-19	3	9	1.95E-17
WINAC complex	O96019, O14497, Q9UIG0, Q13111, P51531, P51532, Q12824, Q92922, Q8TAQ2, Q96GM5, Q969G3, Q9Y5B9, Q02880, P11473	14	['Q12824', 'Q9UIG0', 'O14497', 'Q96GM5', 'O96019', 'P51531', 'P51532', 'Q02880', 'Q8TAQ2', 'Q92922', 'Q969G3']	11	0.79	1.01E-17	3	8	5.33E-16

Table 3.8: ShRNA hit genes in protein complexes. List of complexes to which the shRNA targets could be assigned. Explanation of titles: cplx name, complex name; cplx members, complex members (Uniprot ID); cplx size, number of complex members; total hits, hits that are part of this complex (target genes and interaction partners); num hits, number of hits (= total hits); cplx cov, complex coverage - percentage of how much of the complex is covered by the total hits; p-value, how significant is this complex hit; hits, how many "real hits" (from the target gene list); interactors, how many interactors (genes of this complex that are interacting with target genes); corr_p, corrected p-value (multivariate testing).

3.3.9 Target gene selection for shRNA screen and selection of follow up targets

All hits from the shRNA screen were selected on the basis of the criteria explained in subsection 3.3.5. However, to further validate and to obtain a more focussed target list, some parameters were considered in addition:

- the greatest impact on alkaline phosphatase activity (decreasing or increasing)
- the effect on cell viability
- the number of hairpin structures generating a hit
- in which conditions the hit was obtained
- by comparing the known knockdown efficiencies of the hairpins generating the hit

- by comparing shRNA screen results to small molecule inhibitor screen results (see subsection 3.4).

By doing this, the following shortlist of candidate genes for further investigation evolved from the shRNA screen (table 3.9; for all knockdown data see appendix A.6.2).

3.3.10 Selected hits from shRNA screen

Gene symbol	Gene name	Gene ID	Information	Effect
KDM1A	Lysine-specific histone demethylase 1A	23028	Can act on mono- and dimethylated H3K4 and H3K9	↑
BRD4	Bromodomain containing 4	23476	Chromatin reader protein that recognises and binds acetylated histones	↓
JMJD8	Jumonji domain-containing protein 8	339123	Protein coding	↑
MORF4L1	Mortality factor 4 like 1	10933	Component of the NuA4 histone acetyltransferase (HAT) complex that is involved in transcriptional activation (acetylation of nucleosomal histones H4 and H2A)	↑
UBE2A	Ubiquitin-conjugating enzyme E2A	7319	Accepts ubiquitin from the E1 complex and catalyses its covalent attachment to other proteins	↑
PHIP	Pleckstrin homology domain interacting protein	55023	Probable regulator of the insulin and insulin-like growth factor signalling pathways	↑

Table 3.9: Selected hits from the shRNA screen. The effect on osteoblast differentiation for each gene is indicated by an arrow (↑, upregulating alkaline phosphatase activity; ↓, downregulating alkaline phosphatase activity).

BRD4

Bromodomain-containing protein 4 is a member of the bromodomain and extra-terminal (BET) family of chromatin modifying enzymes and in humans is encoded by the *BRD4* gene. BRD4 is a so called reader domain that recognises post-translational modification states of chromatin proteins, particularly ε-N-acetylation of lysine residues (Kac) on histone tails, a modification that is associated with open chromatin architecture and tran-

scriptional activation. Bromodomain-containing proteins function as components of larger complexes, and up to date there are over 40 diverse human proteins identified containing a total of 61 bromodomains (see subsection 1.4.3) [150]. Proteins of the BET family (BRD2, BRD3, BRD4, and BRDT) in addition share a similar architecture with two amino-terminal bromodomains and a carboxy-terminal recruitment domain. The knockdown of *BRD4* by hairpins 1 and 5 as shown in figure 3.15 led to a maximum decrease in alkaline phosphatase activity of about 50%. In all conditions and for both hairpins the cell viability did not appear to be impaired, supporting the hypothesis that the decrease in alkaline phosphatase activity presents a "real" decrease and is not due to a decrease in cell number.

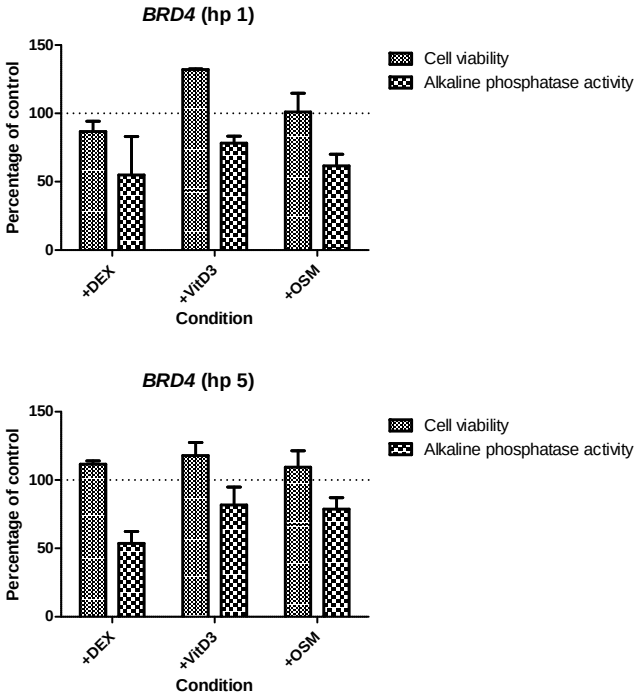

Figure 3.15: *BRD4* knockdown by hairpin 1 and hairpin 5. The x-axis shows the different conditions and the y-axis the percentage of control with 100% indicated by the dotted line. Information about conditions (= media compositions) can be found in appendix A.1. Cell viability as measured by Presto Blue® is displayed as dark grey columns and alkaline phosphatase activity as chequered columns.

KDM1A

KDM1A is a histone demethylase that demethylates both lysine 4 (H3K4me) and lysine 9 (H3K9me) of histone H3. By demethylating H3K4me, a specific histone mark for epigenetic transcriptional activation, KDM1A acts as a co-repressor, while for demethylation of H3K9me, a specific mark for epigenetic transcriptional repression, KDM1A acts as a co-activator. KDM1A and its paralog KDM1B are both FAD-dependent amine oxidases, which can act only on mono- and dimethylated lysines [130, 131]. Highlighting the importance of KDM1A for normal development, targeted deletion of murine *Kdm1a* results in early embryonic lethality [132], a fact that will be discussed further in chapter 5. KDM1A (also referred to as LSD1) can act on mono- and dimethylated H3K4 and H3K9, and KDM1B (also referred to as LSD2) acts only on mono- and dimethylated H3K4. The knockdown of *KDM1A* led to an increase in alkaline phosphatase activity of 200 to 1500% of the control throughout the conditions with no impairment of cell viability (figure 3.16).

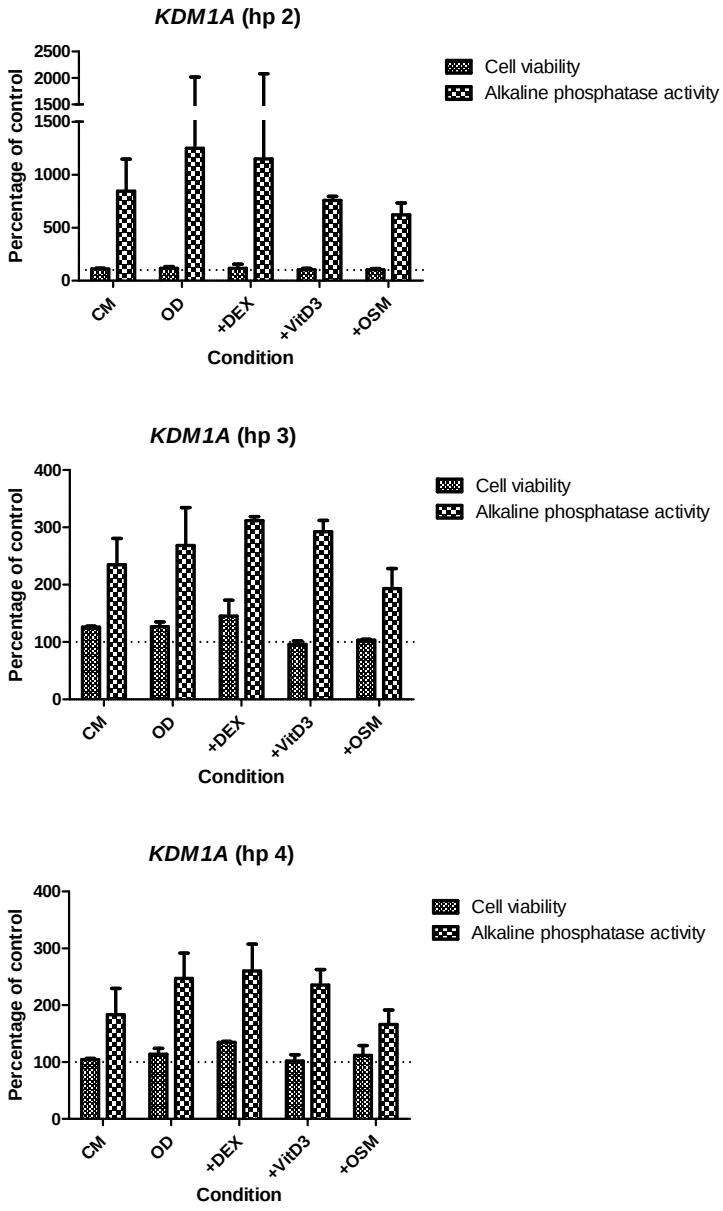

Figure 3.16: *KDM1A* knockdown by hairpins 2, 3 and 4. The x-axis shows the different conditions and the y-axis the percentage of control with 100% indicated by the dotted line. Information about conditions (= media compositions) can be found in appendix A.1. Cell viability as measured by Presto Blue® is displayed as dark grey columns and alkaline phosphatase activity as chequered columns.

JMJD8

Jumonji domain containing protein 8 is a member of the Jumonji gene family of histone demethylases involved in transcriptional repression and chromatin regulation. Many mem-

bers of the Jumonji C (JmjC) family utilise Iron(II) and 2-oxoglutarate as cofactors and catalyse lysine demethylation of histones through an oxidative reaction [135, 229]. Unlike KDM1A, which can only remove mono- and dimethyl lysine modifications, the JmjC-domain-containing histone demethylases (JHDMs) can remove all three histone lysine-methylation states [230]. Although the function of JMJD8 remains unknown, its knock-down in a cellular model for squamous cell carcinoma showed an inhibitory effect on cell proliferation [231]. *JMJD8* was one of the four target genes with two hairpins showing the same effect throughout all conditions. An increase in alkaline phosphatase activity of up to around 500% compared to the control could be seen for hairpin 3 and 4 (figure 3.17).

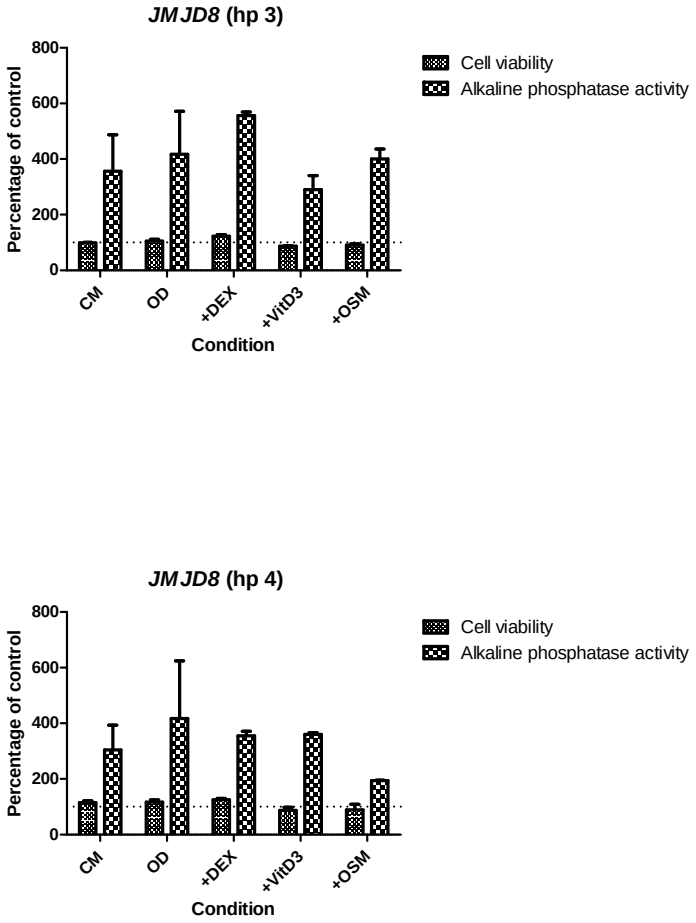

Figure 3.17: *JMJD8* knockdown by hairpin 3 and hairpin 4. The x-axis shows the different conditions and the y-axis the percentage of control with 100% indicated by the dotted line. Information about conditions (= media compositions) can be found in appendix A.1. Cell viability as measured by Presto Blue® is displayed as dark grey columns and alkaline phosphatase activity as chequered columns.

MORF4L1

Mortality factor 4 like protein 1 (MORF4L1) is a component of the NuA4 histone acetyltransferase (HAT) complex and involved in transcriptional activation by acetylation of H2A and H4 [232]. The same complex contains catalytic subunit KAT5/TIP60, which also evolved as a hit in the shRNA screen, although with an opposite effect compared to MORF4L1 (table 3.2). Known for playing a role in DNA repair of double strand breaks, a *Morf4l1* mouse knockout model shows abnormalities in organogenesis and de-

fects in DNA damage repair [233]. MORF4L1, or MRG15, has been reported to interact with MYST1 [234], retinoblastoma protein and MORF4 family-associated protein 1 (MRFAP1) [234,235], suggesting evidence for its activity as a transcriptional regulator in other complexes as well. *MORF4L1* is another gene whose knockdown leads to an increase in alkaline phosphatase activity with no decrease in cell viability (figure 3.18).

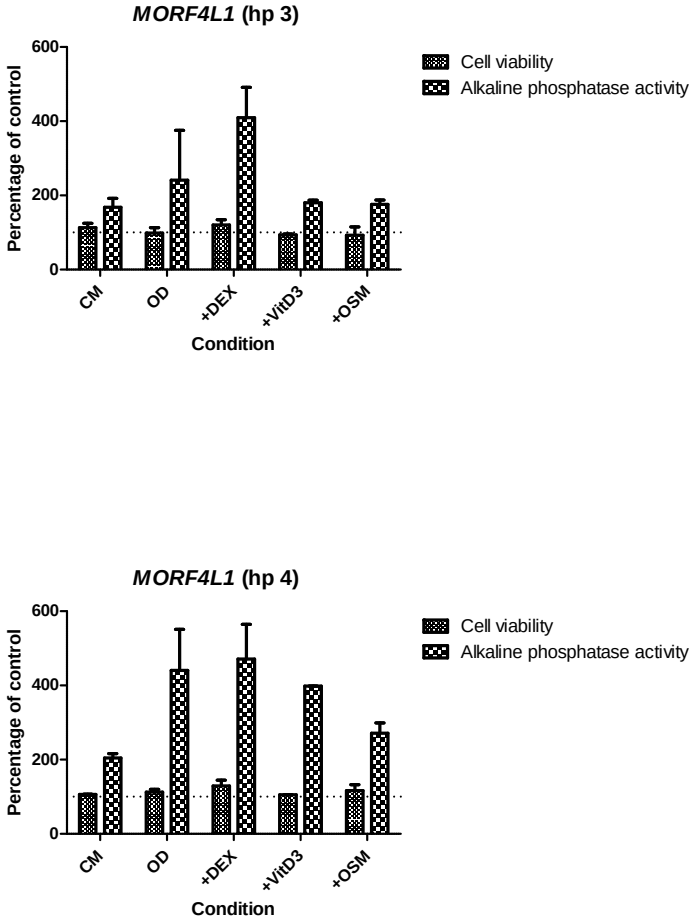

Figure 3.18: *MORF4L1* knockdown by hairpin 3 and hairpin 4. The x-axis shows the different conditions and the y-axis the percentage of control with 100% indicated by the dotted line. Information about conditions (= media compositions) can be found in appendix A.1. Cell viability as measured by Presto Blue® is displayed as dark grey columns and alkaline phosphatase activity as chequered columns.

PHIP

The Pleckstrin Homology Domain Interacting Protein (PHIP) comprises two bromodomains and modulates insulin signalling by binding the Pleckstrin Homology (PH) domain of insulin receptor substrate-1 [236, 237]. PHIP plays a role in pancreatic beta cell growth and survival [238], stimulates cell proliferation through regulation of cyclin transcription [238], and can exercise anti-apoptotic activity through AKT1 phosphorylation and activation [239]. Hairpin 3 knocking down *PHIP* showed an increase in alkaline phosphatase activity of up to 1200% compared to the control, with +DEX being the condition with the most prominent effect. Cell viability was not affected by the knockdown (figure 3.19).

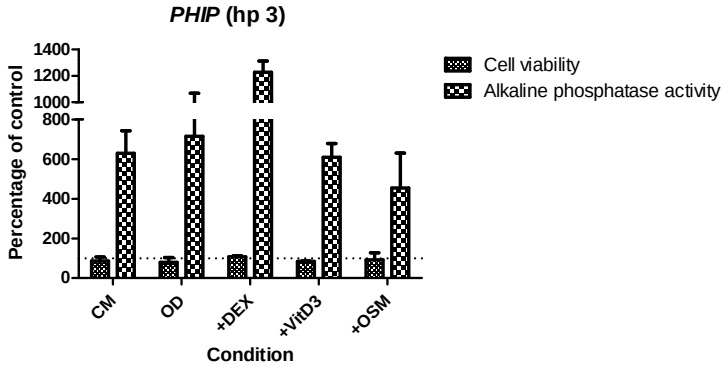

Figure 3.19: *PHIP* knockdown by hairpin 3. The x-axis shows the different conditions and the y-axis the percentage of control with 100% indicated by the dotted line. Information about conditions (= media compositions) can be found in appendix A.1. Cell viability as measured by Presto Blue® is displayed as dark grey columns and alkaline phosphatase activity as chequered columns.

UBE2A

Ubiquitin-conjugating enzyme E2A (UBE2A) was the one target fulfilling the hit selection criteria in all conditions, as discussed in subsection 3.3.5. UBE2A is a member of the E2 ubiquitin-conjugating enzyme family. It accepts ubiquitin from the E1 complex and catalyses its covalent attachment to other proteins. UBE2A has been shown to be required

for post-replicative DNA damage repair [240]. In association with the E3 enzyme, ubiquitin ligase BRE1, it was reported to play a role in transcriptional regulation. It catalyses monoubiquitination of histone H2B at lysine 120 (H2BK120ub1) which characterises a specific tag for epigenetic transcriptional activation, elongation by RNA polymerase II, telomeric silencing, and it is also a prerequisite for H3K4me and H3K79me formation [241]. *UBE2A* knockdown led to a consistent increase of alkaline phosphatase activity throughout the conditions with no impairment of cell viability. For detailed knockdown data see figure 3.8 and figure 3.9.

3.3.11 Validation of shRNA targets by locked nucleic acids knockdown

Locked nucleic acids (LNAs) were utilised as an orthogonal method to validate the shRNA findings, and in addition tested as another possibility to achieve long-term knockdown of gene targets. LNAs function in a similar manner to siRNA, but are believed to be more potent. The locked ribose conformation of an LNA nucleotide, modified with an methylene bridge connecting the 2' oxygen and the 4' carbon of the pentose, leads to an enhanced hybridisation affinity of the LNAs [242]. The locked oligonucleotides are used as antisense RNA to complement a specific mRNA sequence. Binding of the oligonucleotide to the target sequence creates a stretch of double stranded RNA, which cannot be translated and will be degraded. The applied oligonucleotides with a length of 8-15 base pairs are shorter than siRNAs and resistant to endonuclease activity and therefore more stable [243]. LNAs were designed specifically against the chosen targets by collaborators at Santaris (Copenhagen, Denmark) and were tested with regard to knockdown efficiency, effect on cell viability, and alkaline phosphatase activity. For knockdown efficiency and cell viability measurements, human mesenchymal stem cells were treated with LNAs at a concentration

of 5µM both on day 1 and day 5 before being assessed for cell viability and harvested for RNA extraction on day 7. With regard to alkaline phosphatase activity measurements cells were treated the same way (i.e. LNAs for seven days) before differentiation was induced. Medium was changed every other day and alkaline phosphatase activity was measured at day 7 of differentiation. RNA extraction and cDNA synthesis were performed as previously described (subsection 2.4.4). Expression of genes was tested using cDNA specific primers, targeting housekeeping genes Actin B, *GAPDH*, and target genes *KDM1A*, *UBE2A*, *BRD4*, *PHIP*, *JMJD8*, and *MORF4L1*. PCR was performed for 40 cycles of denaturation (95°C for 20s), annealing (95°C for 1s), and extension (60°C for 1min). The primer sequences can be found in appendix A.2.

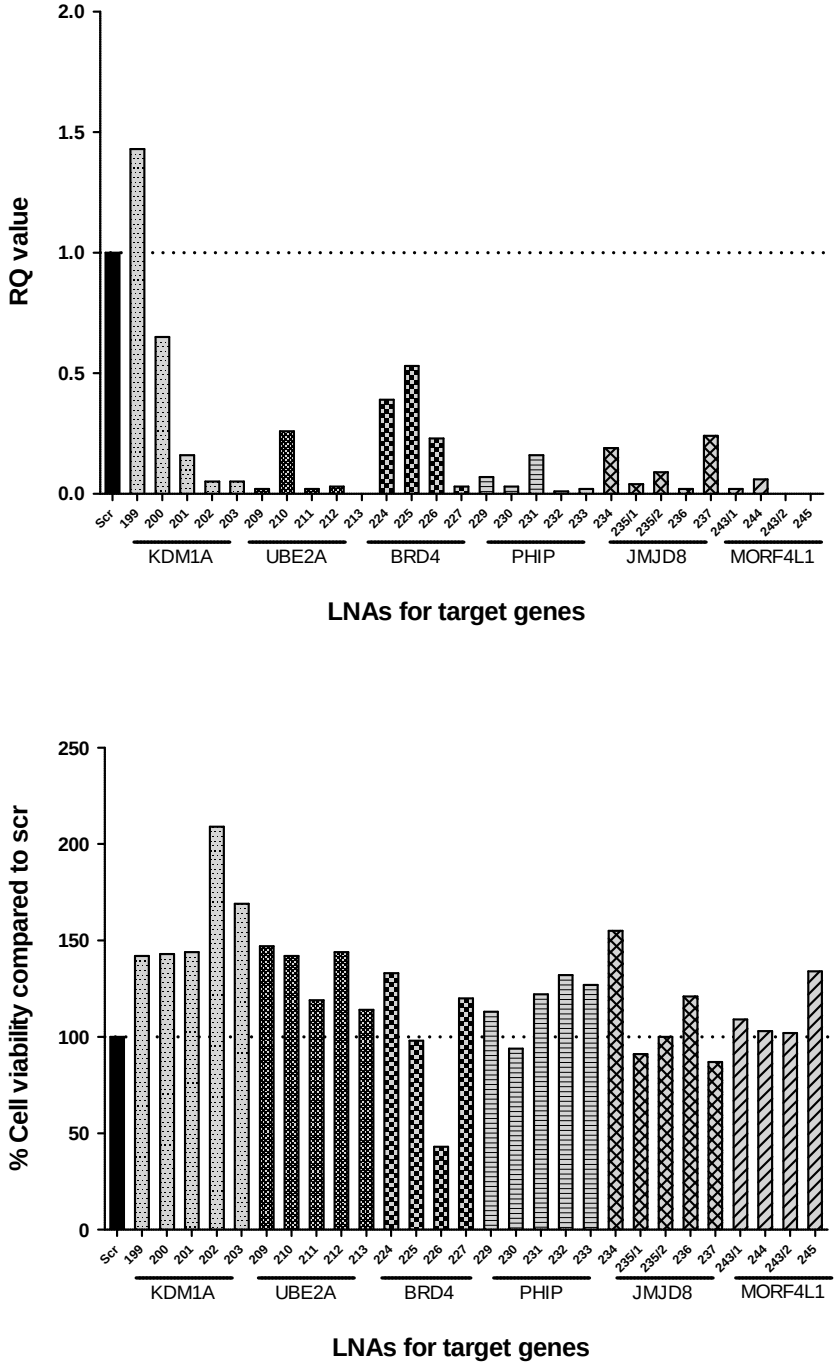

Figure 3.20: Locked nucleic acid knockdown of epigenetic target genes. Upper graph shows knockdown efficiency of various LNAs designed against the target genes as measured by qPCR and lower graph shows related cell viability values on day 7. For each gene, up to five LNAs were designed, and each knockdown was compared to the scrambled LNA control. Target genes are shown on the x-axis.

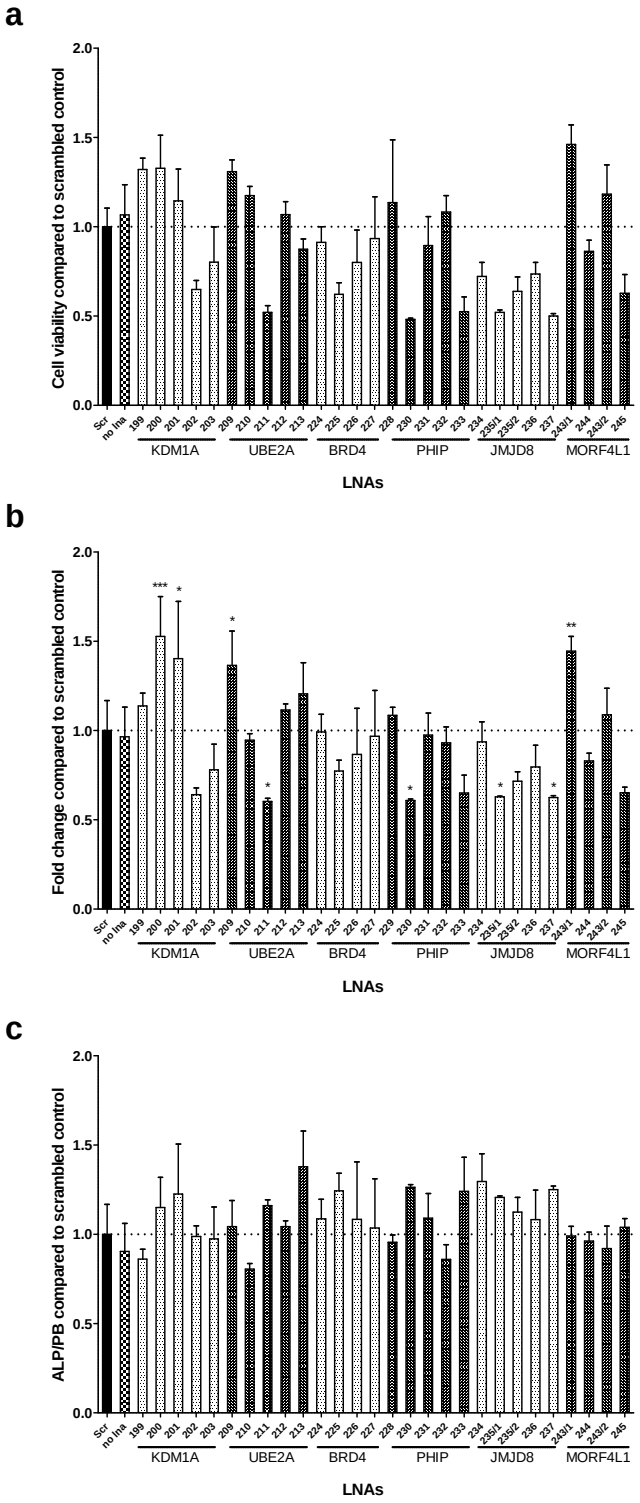

Figure 3.21: Locked nucleic acid knockdown of epigenetic target genes and its effect on alkaline phosphatase activity in human mesenchymal stem cells undergoing osteogenic differentiation. For each gene, up to five LNAs were tested, ALP activity was measured at day 7 of differentiation and compared to the scrambled LNA control (1=100%). Target genes including a no LNA control are shown on the x-axis. P-values were calculated using One-way ANOVA (Bonferroni post test - *** < 0.001, **<0.01, *<0.05). n=3

As it can be seen in figure 3.20, the produced LNAs showed a knockdown for almost all targets after 7 days of LNA treatment. Apart from three LNAs (LNA 238, 239, and 226) the cell viability was not impaired by the knockdown. When differentiation was induced for another 7 days, the cell viability was reduced for some of the LNAs as shown in 3.21 B. However, apart from *JMJD8*, there were at least two LNAs per target gene that did not reduced cell viability. With regard to the targets' effects on alkaline phosphatase activity, most of the LNAs reproduced a pattern similar to the one obtained in the shRNA screen, although to a lower extent. For *MORF4L1* and *BRD4* the effect observed with shRNA could not be reproduced and these targets require further optimisation of LNAs (figure 3.21).

3.4 Small molecule inhibitor screen

The second approach for interference with epigenetic modulators, besides the shRNA knockdown experiments, utilised small molecule inhibitors targeting epigenetic "writers", "erasers", and "readers" as well as other histone and chromatin modifying enzymes such as kinases and PARPs (Poly (ADP-ribose) polymerases). Various commercially available compounds, as well as compounds generated and/or provided by the Structural Genomics Consortium (SGC) were compiled into a epigenetic compound list which can be found in table 3.11. In total, 30 different compounds and control molecules were applied to human MSCs under different growth medium conditions as seen in table 3.10, with +DEX being the osteoblast differentiation- inducing factor.

Name	**Composition**
MSC	MesenPro-RS™ + 1% P/S
CM	DMEM F/12 + 15% FBS + 1% P/S + 1% NEAA + 2mM glutamine
OD	DMEM F/12 + 15% FBS + 1% P/S + 1% NEAA + 2mM glutamine + 50µg/ml ascorbic acid + 10mM beta-glycerophosphate
+DEX	DMEM F/12 + 15% FBS + 1% P/S + 1% NEAA + 2mM glutamine + 50µg/ml ascorbic acid + 10mM beta-glycerophosphate + 10nM dexamethasone

Table 3.10: Medium conditions for compound screen

Most of the compounds were used at a single concentration in 0.1% DMSO (table 3.11), and added to the medium every other day. If the initial screen showed a potential effect, dose-responses ranging from 0.04µM to 30µM were performed. Several compounds were targeting the same genes as some of the shRNAs. These were especially useful to conduct an orthogonal validation of shRNA targets and also to potentially distinguish between a catalytic and a structural role of the target gene in the phenotypic effect observed. The alkaline phosphatase assay was carried out as previously described (subsection 3.2.1) and minor adjustments made with regard to the facility can be found in appendix A.8. In

accordance with the selection criteria for the shRNA screen, the threshold for cell viability was set to ≥50% of the non-treated control. In the following sections, hits derived will be presented and further analysis will be shown for follow-up hits.

Compound name	Class - Target	Conc. in µM
DOT1L	Histone methyltransferase - DOT1L	7.5
SET7/9-1	Histone methyltransferase - SETD7	2.5
SET7/9-2	Histone methyltransferase - SETD7	2.5
SET7/9-3	Histone methyltransferase - SETD7	2.5
Chaetocin	Histone methyltransferase - SUV39H1	0.05
UNC0638	Histone methyltransferase - G9a/GLP	1
CXD101	HDAC	1
Valproic acid	HDAC - aliphatic acid compounds	1000
Entinostat	HDAC - ortho-amino anilides	0.5
Trichostatin A	HDAC - hydroxamic acids	0.5
SAHA	HDAC - hydroxamic acids - Class I & II	2.5
Belinostat	HDAC - hydroxamic acids	5
SRT1720	HDAC - SIRT1 activator	1
5-Aza-deoxy-cytidine	DNA methyltransferase (DNMT) - DNMT1/3	5
IOX1 (5COOH-8HQ)	Lysine demethylases	40
Methylstat	Histone demethylases	2.5
GSK J4	Lysine demethylases	10
GSK J5	Lysine demethylases - Negative control for J4	10
Tranylcypromine	Lysine demethylases -KDM1A	10
Rucaparib	Poly ADP ribose polymerase (PARP)	10
Olaparib	Poly ADP ribose polymerase (PARP)	1
5-Iodotubercidin	Kinase inhibitor - ATP mimetic - Haspin	1
K00135	Kinase inhibitor - ATP competitive - PIM	1
(+)-JQ1	Bromodomains	1
(-)-JQ1	Bromodomains (inactive stereoisomer)	1
PFI	Bromodomains	5
I-BET	Bromodomains	1
RVX-208	Bromodomains	5
IOX2	Bromodomains	10
UNC1215	L3MBTL3 methyllysine reader inhibitor	5

Table 3.11: List of small molecule inhibitors, their corresponding classes and if available, specific targets. The concentration applied is shown in the right column.

3.4.1 Results – Hits derived from small molecule inhibitor screen

The effect of compounds was assessed by both cell viability and alkaline phosphatase activity at 60mins after substrate addition. Criteria for hit selection were similar to the ones applied in the shRNA screen with cell viability to be ≥50% of the control. ALP activity had to be either below 80% or above 120% of the control. Hits derived in this way can be seen in the plot in figure 3.22 and in table 3.12.

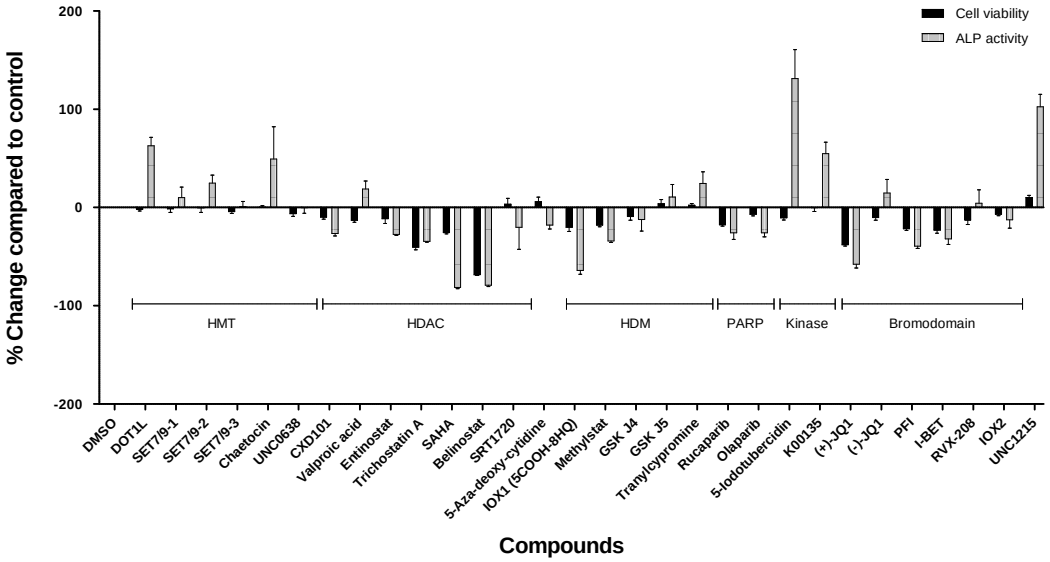

Figure 3.22: Compounds screened for effect on cell viability and alkaline phosphatase activity during dexamethasone-induced differentiation. Results are shown as percentage change compared to the DMSO control. The x-axis shows all compounds sorted according to their corresponding classes with cell viability depicted as black and ALP activity as dotted white columns. N = 4

Table 3.12 shows all compounds with their means and SD for cell viability and ALP activity. Compounds considered a hit by upregulating ALP activity to more than 120% are labelled in red and in bold, whereas compounds downregulating ALP activity to below 80% of the control are labelled in green and in bold. Only one compound, the HDAC inhibitor Belinostat, did not fulfil the cell viability threshold of 50% (grey).

	Cell viability		ALP activity		Dose-response
	Mean	SD	Mean	SD	
DMSO	100.0	0.00	100.0	0.00	
DOT1L	98.0	3.08	162.8	17.02	✓
SET7/9-1	98.5	6.94	110.0	21.75	
SET7/9-2	99.6	9.26	125.0	15.76	
SET7/9-3	95.7	3.57	101.0	10.37	
Chaetocin	100.5	3.02	149.4	65.79	
UNC0638	93.6	5.23	99.8	11.22	
CXD101	90.0	3.47	73.5	4.81	✓
Valproic acid	86.9	3.85	118.7	16.27	✓
Entinostat	88.6	9.47	72.7	2.43	
Trichostatin A	59.6	5.53	65.6	1.87	
SAHA	74.4	2.42	18.6	2.26	✓
Belinostat	31.6	1.58	20.8	2.60	
SRT1720	103.5	11.61	79.9	44.93	
5-Aza-deoxy-cytidine	106.1	9.07	82.0	7.75	
IOX1 (5COOH-8HQ)	79.9	8.65	35.9	7.51	
Methylstat	82.1	3.46	65.9	2.61	
GSK J4	90.8	7.23	87.9	23.83	
GSK J5	103.8	8.72	110.8	25.22	
Tranylcypromine	102.5	3.03	124.6	23.42	
Rucaparib	82.4	2.79	74.3	13.75	
Olaparib	93.2	3.42	74.2	8.21	
5-Iodotubercidin	89.4	4.19	231.2	59.30	✓
K00135	99.7	7.93	154.8	23.17	✓
(+)-JQ1	61.9	2.17	42.3	7.83	✓
(-)-JQ1	89.7	5.14	114.7	27.45	✓
PFI	78.2	3.28	60.6	4.49	
I-BET	76.9	5.89	67.9	11.02	
RVX-208	87.3	9.06	104.4	27.19	✓
IOX2	93.0	2.45	87.6	17.07	
UNC1215	110.2	4.37	202.4	25.64	

Table 3.12: List of small molecule inhibitor hits. Mean and SD for cell viability and alkaline phosphatase activity are given. Compounds considered a hit by upregulating ALP activity for more than 120% are labelled in red and in bold, and compounds downregulating ALP activity to below 80% of the control are labelled in green and in bold. Compounds selected for a dose-response experiment are indicated by a ticked box. N = 4

The inhibition of several methyltransferases led to an increase of alkaline phosphatase activity (as it can be seen for DOT1L, SET7/9-2, and chaetocin), whereas inhibition of bromodomains showed a decrease in alkaline phosphatase activity. Interestingly, the same epigenetic classes had already emerged as the classes comprising most hits in the shRNA screen, where 21 target genes could be assigned to bromodomains (largest hit group) and

11 target genes could be assigned to methyltransferases (third largest hit group).

3.4.2 Dose-response assays for selected small molecule inhibitor hits

Nine compounds (including the BET inihibitor control compound (-)-JQ1) were selected for a dose-response experiment as indicated in table 3.12. In this chapter the focus will be on four of the compounds that confirmed the initial trend: (+)-JQ1, K00135, 5-Iodotubercidin, and CXD101 (other dose-response results can be found in appendix A.9) In addition to these four, two other small molecule inhibitors that have already been published regards having an effect on osteoblast differentiation (valproic acid and SAHA) were used as "positive control" compounds to validate the utilised assay (see appendix A.9).

3.4.2.1 Bromodomain inhibitor (+)-JQ1

(+)-JQ1, a bromodomain inhibitor specific for BET protein family members [145], led to a reduction of alkaline phosphatase activity. Its inactive stereoisomer (-)-JQ1 did not show any response, providing evidence for specific bromodomain inhibition in osteoblast differentiation. Interestingly, two other compounds, PFI-1 (Pfizer, [244]) and I-BET (GSK, [245]), also targeting the BET family of proteins, showed a similar reducing effect on alkaline phosphatase activity (figure 3.22). For (+)-JQ1, the dose response showed a decreasing effect on cell viability even at low concentrations, however at all concentrations tested it never dropped far below the viability threshold of 50% (figure 3.23). Nevertheless, it became obvious that the initial concentration of 1µM could be decreased by a considerable amount without losing the effect of alkaline phosphatase reduction. In addition, the IC_{50} under dexamethasone treatment was calculated as 218nM, therefore for further long-term experiments an even lower concentration of 100nM was utilised. The

alkaline phosphatase activity at that concentration was still about 50% of the control (figure 3.23). With regard to cell viability, it also appeared that cells kept in a mesenchymal stem cell-like state (MSC medium) were more sensitive to compound treatment than cells undergoing directed differentiation into osteoblasts (+DEX) or cells given the opportunity to leave the stem cell state and differentiate (CM and OD medium).

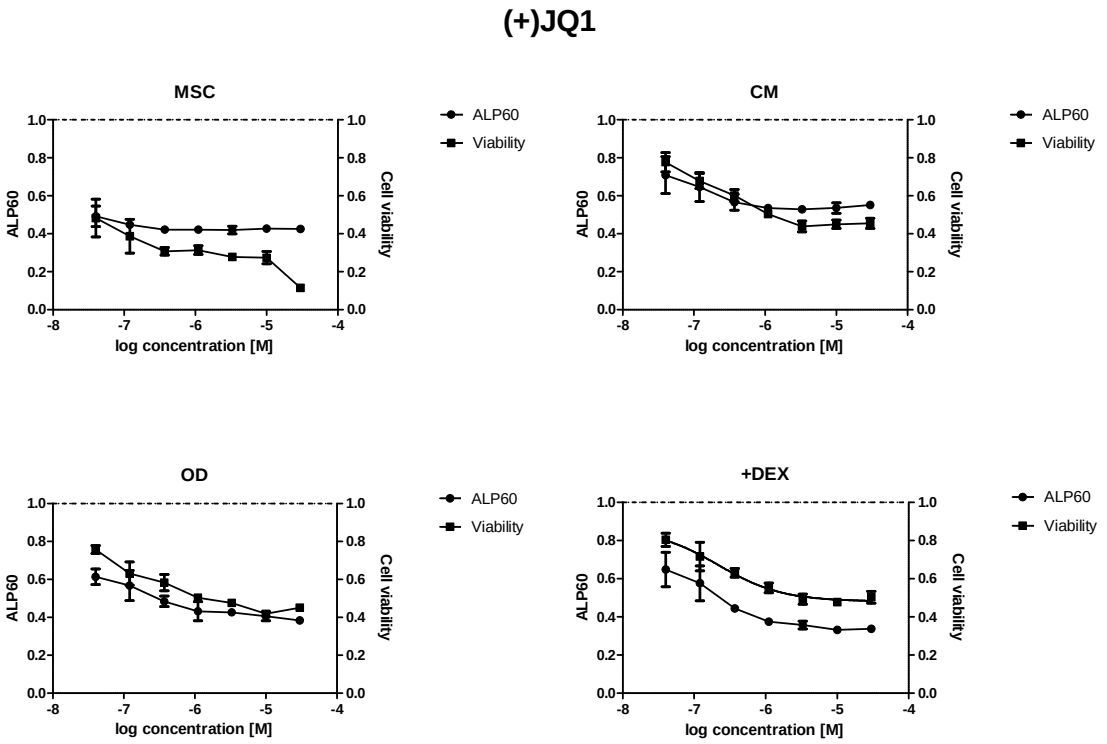

Figure 3.23: Dose response curves under (+)-JQ1 treatment. The x-axis shows applied concentrations in log [M], left y-axis shows level of alkaline phosphatase activity compared to the control (=1), right y-axis shows level of cell viability compared to the control (=1). 1 indicates 100% (of the control). Doses ranged from 0.04µM to 30µM in 0.1% DMSO. Medium was changed on day 5 of culture and compounds were replenished. After 7 days of culture, both cell viability and alkaline phosphatase activity were assessed.

In addition to (+)-JQ1, PFI-I, and I-BET, two other small molecules developed as BET bromodomain inhibitors, RVX-208 and bromosporine, which were not included in the initial compound screen, became available during the course of this project. Bromosporine showed a decreasing effect on alkaline phosphatase (figure 3.25), whereas RVX-208, a compound already in Phase II clinical trial, did not show a decrease (figure 3.24). With regard

to both the alkaline phosphatase and cell viability curves being almost identical, the effect seen under bromosporine treatment might however also be a toxic dose-dependent reduction. RVX-208 was previously reported to increase the production of APOA-I protein which is used to produce high-density lipoprotein (HDL) particles. HDL particles are transport forms for cholesterol from peripheral tissue to the liver, an effect of importance in atherosclerosis and cardiovascular disease (CVD) [246]. Interestingly, another publication reported that RVX-208 is specific for second bromodomains (BD2) (for more information, see chapter 4) and that BD2 inhibition only modestly affects BET-dependent gene transcription [247]. As (+)-JQ1 was shown to be more specific for BD1 and bromosporine to be similarly effective on BD1 and BD2, this could potentially suggest that bromodomain 1 (BD1) is playing a more important role in the regulation of alkaline phosphatase activity in differentiating osteoblasts.

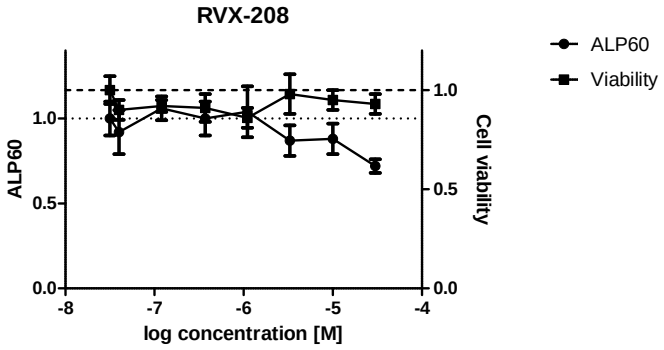

Figure 3.24: Dose response curve under RVX-208 treatment. The x-axis shows applied concentrations in log [M], left y-axis shows level of alkaline phosphatase activity compared to the control (=1), right y-axis shows level of cell viability compared to the control (=1). 1 indicates 100% (of the control). Doses ranged from 0.04µM to 30µM in 0.1% DMSO. Medium was changed on day 5 of culture and compounds were replenished. After 7 days of culture, both cell viability and alkaline phosphatase activity were run.

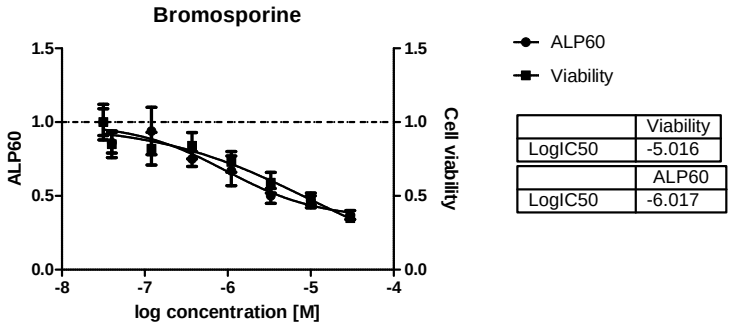

Figure 3.25: Dose response curve under bromosporine treatment. The x-axis shows applied concentrations in log [M], left y-axis shows level of alkaline phosphatase activity compared to the control (=1), right y-axis shows level of cell viability compared to the control (=1). 1 indicates 100% (of the control). Doses ranged from 0.04µM to 30µM in 0.1% DMSO. Medium was changed on day 5 of culture and compounds were replenished. After 7 days of culture, both cell viability and alkaline phosphatase activity were assessed.

3.4.2.2 Kinase inhibitors – K00135 and 5-Iodotubercidin

Two compounds inhibiting kinases displayed an increasing effect on alkaline phosphatase activity (table 3.12). **PIM1** inhibitor K00135, a member of the imidazo[1,2-b]pyridazines class and previously identified as inhibitor for PIM kinases [248], showed a promoting effect on ALP activity and no effect on cell viability up to 1µM concentration in all four conditions tested (LogIC_{50} under dexamethasone treatment = -4.459; figure 3.26). *PIM-1* encodes a serine/threonine kinase, which belongs to the group of calcium/calmodulin-regulated kinases (CAMK), is widely expressed in tissues and cell types, ranging from bone marrow, prostate, to epithelial cells, and was reported to be overexpressed in cell cultures isolated from human tumours [249]. Its main function is in cell cycle progression, apoptosis, and transcriptional activation, and it was shown to regulate RANKL-induced osteoclastogenesis via NF-kB activation and NFATc1 induction [250]. Transcription of *PIM-1* is mediated by binding of STAT3, a transcription factor whose signalling has been shown to play a vital role in MSC osteogenic differentiation [192]. Two other Pim kinases, PIM-2 and PIM-3 have been shown to be structurally and functionally similar [249, 251].

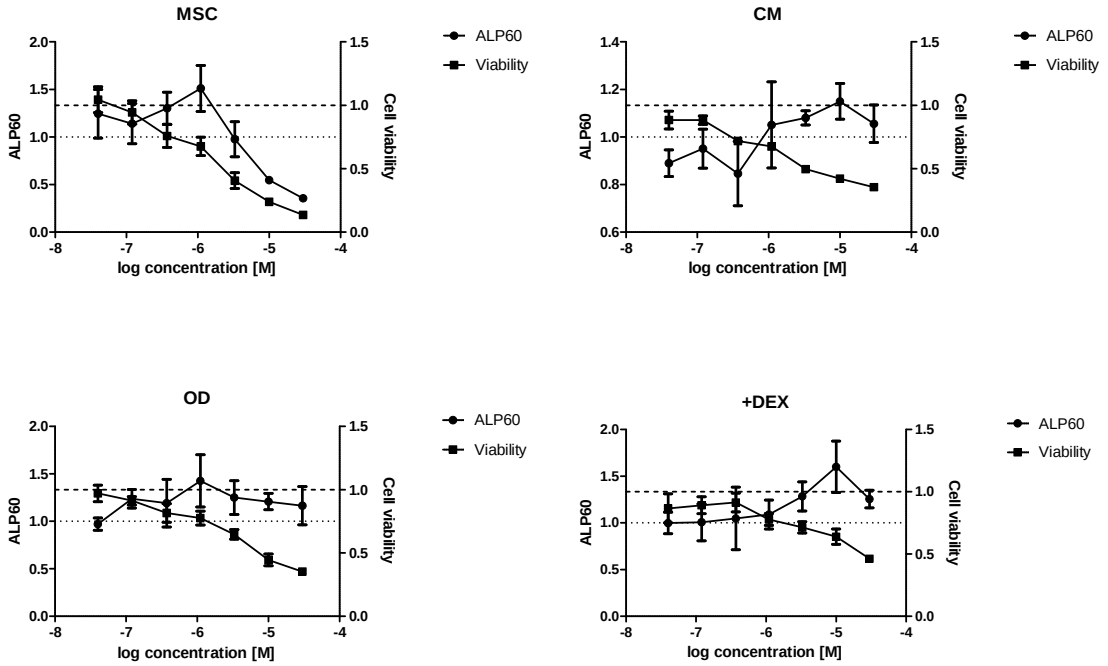

Figure 3.26: Dose response curves under K00135 treatment. The x-axis shows applied concentrations in log [M], left y-axis shows level of alkaline phosphatase activity compared to the control (=1), right y-axis shows level of cell viability compared to the control (=1). 1 indicates 100% (of the control). Doses ranged from 0.04µM to 30µM in 0.1% DMSO. Medium was changed on day 5 of culture and compounds were replenished. After 7 days of culture, both cell viability and alkaline phosphatase activity were assessed.

5-Iodotubercidin has previously been shown to be a **Haspin** inhibitor, targeting the ATP-binding site [252]. Haspin is a serine/threonine protein kinase (also known as germ cell–specific gene 2 protein/GSG2 or haploid germ cell–specific nuclear protein kinase) that phosphorylates Thr3 on histone 3 at centromeres during mitosis [253, 254]. Thereby it positions the kinase Aurora B that is part of the chromosomal passenger complex (CPC), at the centromeres [252], a process that is required for correct spindle-kinetochore attachment, proper chromatid cohesion, metaphase alignment and normal progression through the cell cycle [255, 256]. Treatment with 5-Iodotubercidin led to an increase in alkaline phosphatase activity to about 200% in three out of four conditions (MSC, OD, +DEX) and even in CM to an increase of about 50% (figure 3.27). Cell viability remained stable

(70-100% of the DMSO control) up to a concentration of 1µM, and again, similar to their reaction to BET inhibitors, hMSCs kept in stem cell medium also seemed to be more sensitive to compound treatment with kinase inhibitors ($LogIC_{50}$ under dexamethasone treatment = -5.435). The pressure to remain in a stem cell state could potentially leave cells more prone to undergo apoptosis under compound treatment.

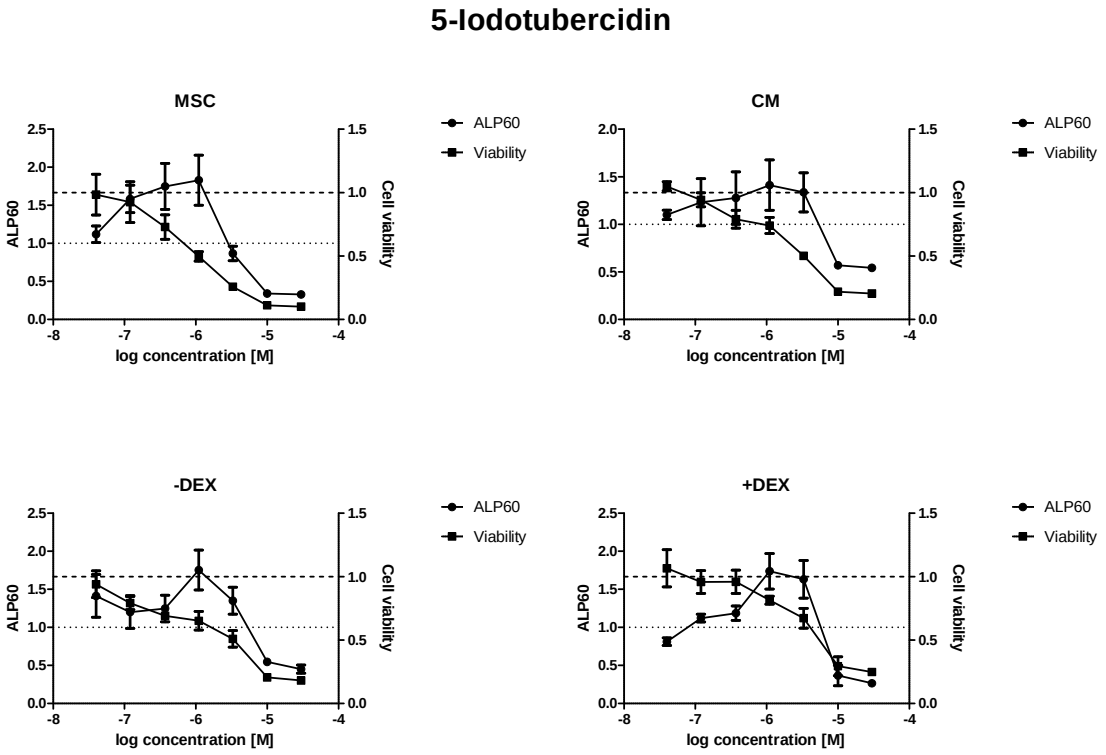

Figure 3.27: Dose response curves under 5-Iodotubercidin treatment. The x-axis shows applied concentrations in log [M], left y-axis shows level of alkaline phosphatase activity compared to the control (=1) , right y-axis shows level of cell viability compared to the control (=1). 1 indicates 100% (of the control). Doses ranged from 0.04µM to 30µM in 0.1% DMSO. Medium was changed on day 5 of culture and compounds were replenished. After 7 days of culture, both cell viability and alkaline phosphatase assay were run.

3.4.2.3 HDAC-inhibitor CXD-101

CXD-101 is a histone deacetylase inhibitor developed by AstraZeneca. HDACs and development of inhibitors are interesting targets for cancer therapy, as they control a wide variety of mechanisms involved in tumour cell growth and division, but because they are

ubiquitously expressed, their clinical utility has been difficult to determine. Nevertheless, CXD-101 is planned to soon enter phase I clinical trials in advanced cancer patients with solid tumours, lymphoma, and myeloma.

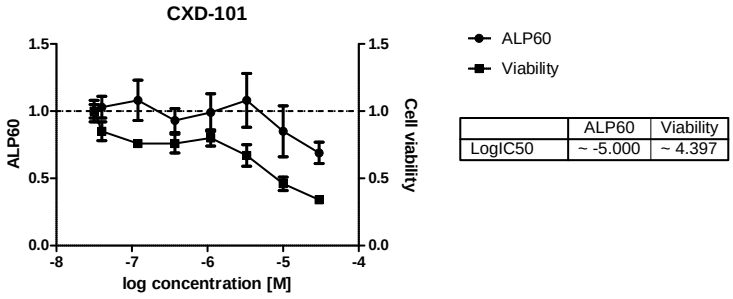

Figure 3.28: Dose response curves under CXD-101 treatment. The x-axis shows applied concentrations in log [M], left y-axis shows level of alkaline phosphatase activity compared to the control (=1), right y-axis shows level of cell viability compared to the control (=1). 1 indicates 100% (of the control). Doses ranged from 0.04µM to 30µM in 0.1% DMSO. Medium was changed on day 5 of culture and compounds were replenished. After 7 days of culture, both cell viability and alkaline phosphatase assay were performed.

For doses up to 1µM, cells showed a slight reduction in cell viability down to 70% of the control, but almost no response with regard to ALP activity, thus not confirming the initial finding. Concentrations over 1µM led to a toxic effect and related decrease in both cell viability and alkaline phosphatase activity, with the IC_{50} at approximately 10µM (figure 3.28). With no effect on alkaline phosphatase activity in the non-toxic range, this compound was not further considered.

3.4.3 Selected hits from small molecule inhibitor screen

Compounds provide an easy-to use tool for long-term experiments. Therefore, having a potent compound for the most interesting targets is very desirable. With different BET inhibitors showing a similar effect, BRD4 (and the most potent compound (+)-JQ1) was chosen as a follow-up target from the compound screen. In addition, the promising results achieved by kinase inhibition led to the decision to select the two compounds K00135

(Pim1 inhibitor) and 5-Iodotubercidin (Haspin inhibitor) for further investigation in the future.

3.5 Final selection of two follow-up targets – BRD4 and KDM1A

With the aim to further assess the initial findings, two targets were selected for more in-depth analysis of their effect on osteoblast differentiation. These were BRD4 and KDM1A, which will be discussed in detail in the following chapters. They were chosen based on all aforementioned criteria, and also with the thought in mind that further analysis of one gene each for the up- and downregulating modifiers would be of particular interest. In addition, having access to a specific compound targeting BRD4 opened many more possibilities for analyses (chapter 4). For KDM1A, the compound tranylcypromine showed a similar result as observed in the shRNA knockdown experiments, supporting the selection of KDM1A as a follow-up target. In addition, a transgenic mouse model was available (kindly provided by Professor Roland Schuele, University of Freiburg), offering unique opportunities to study the *in vivo* effect of KDM1A on bone development. During the course of this project, a new small molecule inhibitor targeting KDM1A became available as well, and data on this subproject can be found in chapter 5. For other targets an initial follow-up analysis was carried out as shown in the data on locked nucleic acids and dose-response assays, with the intent to confirm our previous findings from the shRNA knockdown and small molecule inhibition experiments and to assess new ways of manipulation. The other listed targets will be followed up in the future, for these see the future directions in chapter 6.

3.6 Conclusion and discussion

With the aim to identify epigenetic modulators involved in osteoblast differentiation of human mesenchymal stem cells, two different approaches - short hairpin knockdown and small molecule inhibition - were utilised. The shRNA screen led to 89 hit genes identified having an effect on alkaline phosphatase activity, while the small molecule inhibition experiments identified 19 potential targets. Knockdown or inhibition of approximately 70% of the targets led to a downregulation of alkaline phosphatase activity. Six target genes from the shRNA screen and eight target genes from the small molecule screen, respectively, were selected for further investigation. Orthogonal knockdown validation by locked nucleic acids and small-molecule dose-response experiments were carried out before two target genes, namely *BRD4* and *KDM1A*, were selected for further analysis. As illustrated in the overview graphic at the beginning of this chapter, the initially long list of genes assessed was consecutively narrowed down to produce a target hit list, eventually leading to a focussed number of hits that will be further analysed in the following chapters. Approaches as carried out in this thesis, addressing a large number of genes, offer great opportunities in identifying a number of target genes involved in a process but also comprise the risk of missing out on potential other targets due to stringent selection criteria. The number of hits obtained in this work provides a good basis for assessing relationships between different modifiers as well as direct effects on osteoblast differentiation. The networks and pathways identified using IPA already gave an insight into the possible complexes playing a role in osteoblast development. However, the calculations and connections made by IPA are all based on knowledge currently available from publications, therefore it is more likely to identify pathways involved for which a lot of work has already been published and much is known about interactions and connections, rather

than identifying new interactions that might potentially be discovered within the data set that was uploaded. Therefore, all hits require confirmation and thorough assessment, as discussed in future directions (chapter 6), and as already done for two genes with regard to their direct effect on osteoblast differentiation (chapter 4 and 5). With regard to the tools applied, particularly the short hairpins, some of the hits might indeed prove not to be verifiable. For instance, the knockdown efficiencies of most of the applied hairpins were previously assessed in other cell lines such as HEK (human embryonic kidney) and HeLA (cervix cancer cells), but not in mesenchymal stem cells. Hairpin efficiencies reported by TRC ranged from 0% remaining target RNA to RNA levels higher than the "original" level, and both, but particularly the latter should be regarded with caution. Higher values could first of all only be caused by experimental errors, but could also be due to inadequate or no knockdown at all, and might cause a cell response leading to increased transcription of a target gene. The knockdown efficiency required for an effect is unknown and for some targets it might be sufficient to reduce the number of transcripts available, whereas for others a full knockdown might be required; however, this could also be cell type-specific. Furthermore, depending on the half-life of a protein, the knockdown of a target mRNA might not even lead to an effect as it does not affect already present proteins.

Although specifically designed against particular targets, shRNAs could also have off-target effects, both specific and non-specific. Specific off-target effects can be caused by partial sequence complementarity to non-target RNAs, leading to off-target suppression. Non-specific responses could be due to cellular toxicities caused by the integrated nucleotide construct or due to an immune response caused by the viral entry. However, shRNAs are thought to not have as many off-target effects as e.g. siRNAs or small molecule inhibitors. Compared to siRNA, this could be due to the fact that shRNAs are integrated

into the genome and transcribed in the nucleus, allowing further cell-specific processing. Compounds instead are usually not protein-specific but rather targeted against a class of proteins. As seen in the list of small molecules in table 3.11, many compounds are known to inhibit the entire protein class of e.g. HDACs or bromodomains. If a compound is targeted against a particular domain, the presence of this domain in a number of proteins increases the likelihood for non-specific effects (for a detailed view on the presence of e.g. bromodomains in proteins, see figure 4.2 in chapter 4). Other compounds might not have been sufficiently active or concentrated to cause an effect. In general, the application of compounds has to be carefully assessed, as toxicity effects could mask a specific effect. As seen for example for bromosporine, it is likely that the reduction in alkaline phosphatase was rather caused by compound toxicity and not related to a direct effect on bromodomains. It is difficult to tell whether also an increase in alkaline phosphatase could be due to a decrease in cell viability and a possible increase in apoptosis. It has been suggested that alkaline phosphatase could be released in consequence of cell death [257], however, for the applied compounds leading to an increase of ALP in this work, an increase could only be observed for low compound concentrations with almost no effect on cell viability. At very high concentrations of approximately 10µM, when cell viability was reduced to below 50% of the control, a decrease could also be seen for the alkaline phosphatase activity. However, for compound K00135 a reduction in cell viability to 50% showed an increase in alkaline phosphatase activity of 20%. The application of locked nucleic acids (LNAs) on the other hand did not seem to affect the cell viability to the same extentl, however, in this case the targets were already chosen based on sufficient cell viability values as assessed in the previous shRNA screen. LNAs will therefore be a valuable tool for further analysis of the selected target genes.

The main target classes emerging from this chapter were bromodomains (BRDs) and PHDs, both so-called "reader" domains, with bromodomains recognising acetylated lysines and PH domains recognising methylated lysines. Lysine acetylation is a reversible post-translational modification of proteins and plays a key role in regulation of gene expression and chromatin remodelling [258]. Reader domains are important not only for recognition of these chromatin marks, but also for the assembly of transcription regulatory complexes. Performing an effector role, they often act with other protein-interaction modules to guarantee a high level of targeting specificity. Readers typically provide an accessible surface, in the case of BRDs a largely hydrophobic acetyl lysine binding site, that can accommodate a modified histone residue; they determine the modification (acetylation vs methylation), or state specificity (e.g. level of methylation of lysines); and they interact with the flanking sequence of the modified amino acid in order to distinguish sequence context [259]. For lineage determination and stem cell differentiation, the recognition of epigenetic marks on relevant genes such as key osteogenic transcription factors is essential, and one of the here identified reader domains will be presented in the next chapter.

4 The role of bromodomain containing protein 4 (BRD4) in osteoblast differentiation

Bromodomain-containing protein 4 was already briefly introduced in the previous chapter and partly in the introduction (subsections 1.4.3 and 3.3.10) but will be presented in more detail here.

4.1 Background

Bromodomain-containing protein 4 (BRD4) is a member of the bromodomain and extra-terminal (BET) subfamily of human bromodomains. These proteins are so-called "reader" domains that selectively recognise acetylated lysine (KAc) residues on histones. By associating with these chromatin marks, bromodomains can recruit other factors in order to facilitate transcriptional activation [154]. In co-crystal structures with acetyl-lysine residue containing peptides it was shown that the acetylated lysine residue is recognised by a central hydrophobic cavity within the bromodomain module and is anchored by a hydrogen bond to an asparagine residue (figure 4.1) [153].

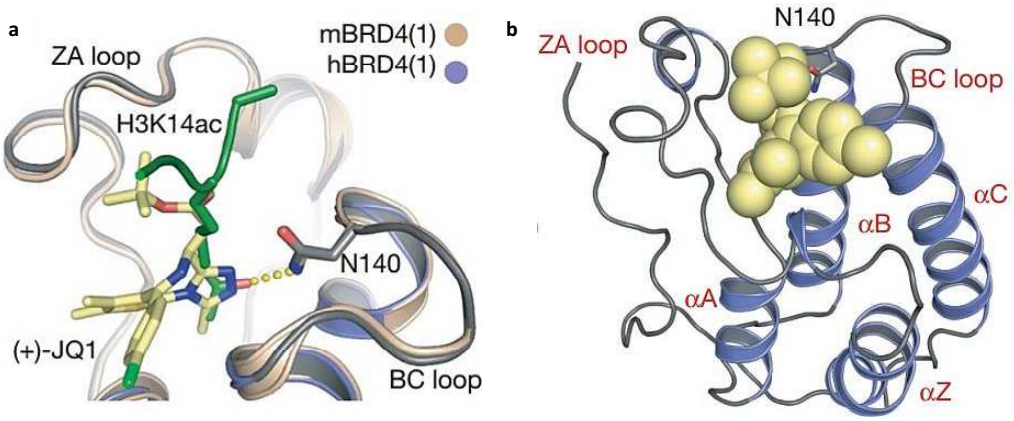

Figure 4.1: Structural analysis of BRD4 and (+)-JQ1 complexes. a, Superimposition of the mouse BRD4(1)–H3K14ac peptide complex with the human BRD4(1)–(+)-JQ1 complex structure. Yellow dots are indicating the hydrogen bond formed to the conserved asparagine residue (N140). b, Ribbon diagram of the human BRD4(1) with (+)-JQ1. The main structural elements and motives are labelled. Adapted from [152]

To date, there are 61 known unique human bromodomains that cluster into eight distinct families based on structural similarity (figure 4.2). All members of the BET subfamily have two bromodomains, bromodomain 1 (BD1) and 2 (BD2).

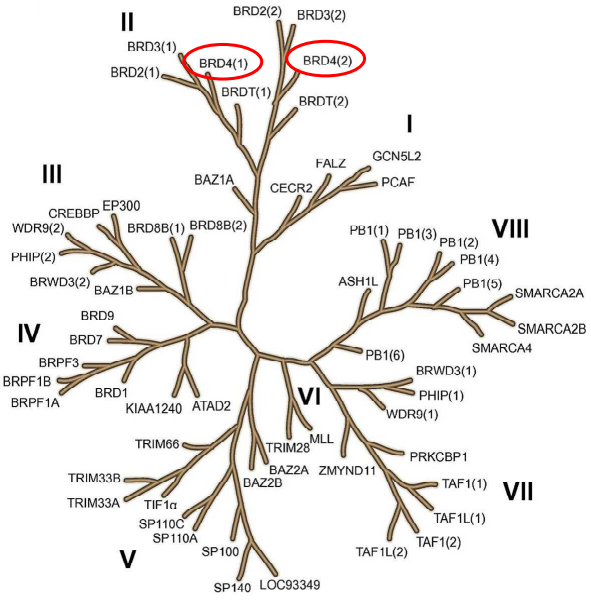

Figure 4.2: Structure based phylogenetic tree of the human bromodomain family. The different families are named by Roman numbers (I–VIII). The two bromodomains of BRD4 are circled in red. Adapted from [260].

Recently it has been reported that bromodomains not only recognise acetylated sequences but also combinations of marks within the flanking regions [151]. Filippakopoulos et al. observed a strong influence of neighbouring PTMs, such as phosphorylation, on recognition of BRD target sites. Their work suggests that combinatorial motifs rather than single PTMs determine the cellular outcome of processes regulated by epigenetic reader domains. This hypothesis is supported by the network analysis of epigenetic target hits (subsection 3.3.7), showing tight interlinkage between different modifiers and the complexes they work within (subsection 3.3.8).

BRD4 has been shown to ensure immediate gene expression in daughter cells following mitosis by marking cell cycle genes that regulate M/G1 transition [261]. By interacting with the positive transcription elongation factor P-TEFb it allows for immediate *de novo* gene transcription through activation of RNA Polymerase II [154,262], and thereby functions as a global transcriptional co-activator [153]. BRD4 has also been reported to be involved in the development of a rare and aggressive malignant epithelial tumour called NUT (nuclear protein in testis) midline carcinoma (NMC) that is characterised by a translocation of the *NUT* gene [263]. The most common translocation involving the *NUT* gene is the t(15;19) (q14;p13.1) translocation which fuses the *NUT* gene on chromosome 15 to the *BRD4* gene, leading to expression of the two amino-terminal bromodomains as an in-frame chimaera with the NUT protein [264, 265]. In about one third of cases, *NUT* is fused to *BRD3* on chromosome 9 instead. Recent data suggests that the *BRD-NUT* fusion oncogene associates with chromatin and interferes with epithelial and squamous differentiation thereby contributing to carcinogenesis [266]. Consequently, the BET proteins were of great interest as potential drug targets, initially for NMC, but later extended also to other cancer types. In 2010, a cell-permeable small molecule that binds competitively to acetyl-lysine

recognition motifs, or bromodomains, was developed [152]. The compound (+)-JQ1 was shown to bind BRD4, displacing it from chromatin and inhibiting its role in complex assembly (figure 4.1). In this initial publication, treatment with (+)-JQ1 prompted squamous differentiation and growth arrest in NMC [151]. Following this, other publications reported that inhibiting bromodomains could be a way of targeting MYC dependence in cancer [267]. Inhibition of the interaction between BET bromodomains and the *MYC* gene promoter was shown to reduce MYC transcription and protein levels, resulting in G1 arrest and extensive apoptosis in a variety of leukaemia, myeloma and lymphoma cell lines [220, 244, 267, 268]. In the last four years, other BET targeting compounds were developed (PFI-1, I-BET, RVX-208, Bromosporine) and have been described in chapter 3.

4.2 Recapitulation of earlier results and aim of this study

In this study, I set out to investigate the mechanism by which BRD4 influences osteoblast differentiation. BRD4 was chosen as a follow-up target based on its consistency in reducing alkaline phosphatase activity (chapter 3). ALP activity was decreased in both shRNA and small molecule inhibitor screens using three different compounds that target the BET family and specifically BRD4.

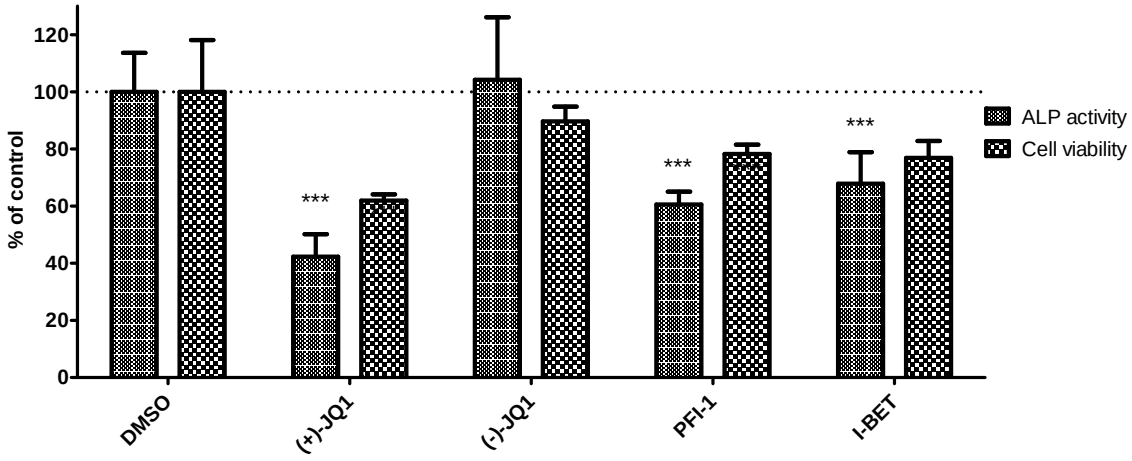

Figure 4.3: Effect of BET compounds on cell viability and alkaline phosphatase activity. Cell viability as measured by Presto Blue® is displayed as chequered columns and alkaline phosphatase activity as dark grey columns. P-values were calculated using One-way ANOVA (Dunnett's post test - *** < 0.001, **<0.01, *<0.05).

All BET inhibitors led to a significant decrease in ALP activity, with (+)-JQ1 showing the largest decrease. Its inactive stereoisomer (-)-JQ1 did not show an effect on ALP activity with only a negligible reduction in cell viability (figures 4.3 and 4.4).

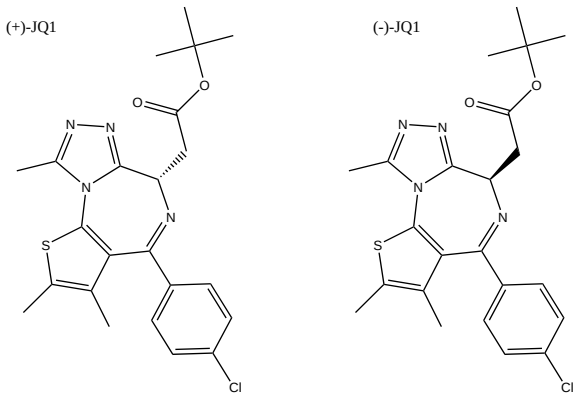

Figure 4.4: Chemical structure of the active enantiomer (+)-JQ1 and the inactive stereoisomer (-)-JQ1. Adapted from JQ1/SGCBD01 Data Sheet.

Generally speaking, the cell viability appeared to be more negatively affected under compound treatment than under shRNA treatment as seen in figure 3.15. Knockdown of *BRD4* led to a decrease in ALP activity with virtually no impairment of cell viability but rather showing a slight increase (figure 3.15). The knockdown effect seemed to be

more prominent under dexamethasone treatment than under 1,25-dihydroxyvitamin D_3 or oncostatin M treatment. A stable cell viability result was essential in order to consider the decrease in ALP activity as a valid result, and not just a reflection of a reduction in cell viability.

4.3 Materials and Methods

4.3.1 Cell culture

Human mesenchymal stem cells from two different donors (female donor, 21 years old; male donor, 19 years old) were obtained at passage 2 and were cultured in MesenPRO-RS™ (Life Technologies), a reduced serum (2%) medium formulated to support the growth of MSCs in culture. The cells were utilised for experiments up to a maximum of 8 passages. To induce osteogenesis, cells were treated as previously described (chapter 2).

4.3.2 Long-term differentiation under (+)-JQ1 treatment

Both hMSC lines were utilised to assess the effect of (+)-JQ1 over long term differentiation of four weeks. From earlier dose-response experiments, a long-term dose of 100nM (+)-JQ1 was derived, lower than the IC_{50} (IC_{50} = 218nM) with the aim to have minimal effects on cell viability. Cells were treated for four weeks and compound was added together with fresh medium every other day.

4.3.3 RNA extraction and cDNA synthesis

As previously described (subsection 2.4.4). Expression of genes was tested using cDNA specific primers, targeting housekeeping genes Actin B, *GAPDH*, osteoblast genes *RUNX2*,

Osterix (*OSX*), bone sialoprotein (*IBSP*), collagen 1A1 (*COL1A1*), osteocalcin (*BGLAP*), osteonectin (*SPARC*), and alkaline phosphatase (*ALPL*). PCR was performed for 40 cycles of denaturation (95°C for 20s), annealing (95°C for 1s), and extension (60°C for 1min). The primer sequences can be found in appendix A.2.

4.3.4 Alizarin Red S staining

As previously described (subsection 2.4.7).

4.3.5 Oil Red O staining

Oil Red O is a lysochrome, a fat-soluble dye, used for visualisation of lipids and neutral triglycerides in cell layers. Cells were washed twice in PBS and fixed in 4% PFA for 20-30mins. Fixative was removed and cells were washed with 60% isopropanol for 5mins at room temperature. Isopropanol was removed and cells were allowed to dry completely before Oil Red O solution (8.5mM) was added for 10mins at room temperature. Solution was removed and cells were immediately washed four times in ddH_2O. Lipid deposits were observed under microscope and plates were scanned.

4.4 Results

4.4.1 The effect of (+)-JQ1 on cell proliferation

Treatment with 100nM (+)-JQ1 for four weeks showed an effect on proliferation of cells in both mesenchymal stem cell medium (MSC) and complete differentiation medium (+DEX) (figure 4.5). Cells appeared less dense under (+)-JQ1 treatment, whereas for the cells without (+)-JQ1 treatment, cell alignment and interlinkage of cells could be observed.

Up to seven days into treatment, both treated and non-treated cells appeared similar, however, after 14 days of differentiation or cultivation in MSC medium, a reduction in cell density in (+)-JQ1 treated cells became apparent. MSC medium was used as a control to give an indication of the general effect on cell growth and proliferation under (+)-JQ1 treatment. In the controls, a parallel alignment of cells could be observed in MSC medium, while cells in differentiation medium grew in random orientation.

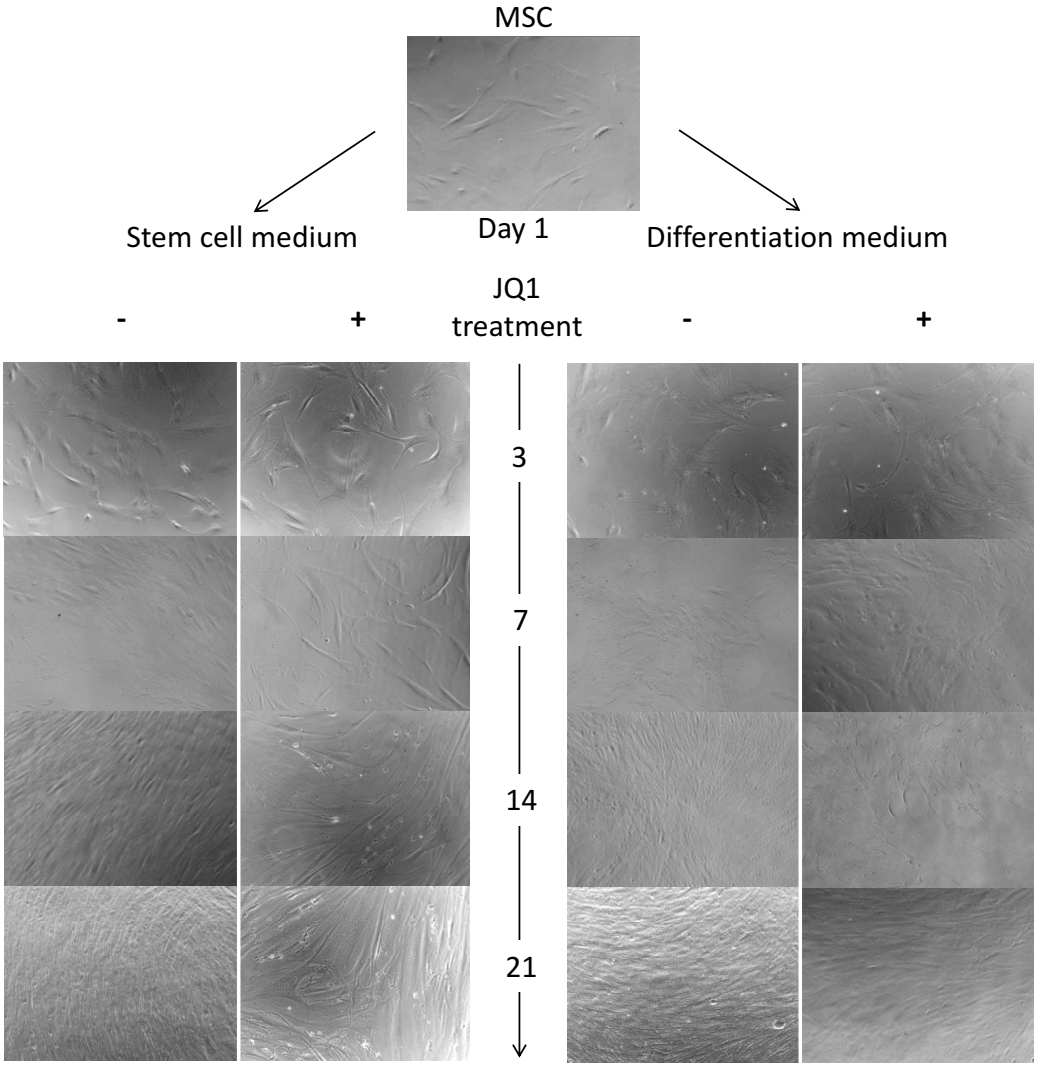

Figure 4.5: Bright-field microscopy images showing the effect of 100nM (+)-JQ1 treatment for 4 weeks in either stem cell medium or osteogenic differentiation medium. Numbers in the middle indicate the day of the experiment, + and - signs with or without (+)-JQ1 treatment. N $\geq$ 16 for two different cell lines, representative images chosen (10x objective).

4.4.2 The effect of (+)-JQ1 on osteoblastic gene expression

In the process of osteogenic differentiation MSCs lose their stem cell markers and upregulate expression of osteoblastic genes. Changes in gene expression under treatment with (+)-JQ1 were assessed by both qPCR and microarray and a set of osteoblastic genes was analysed. Eleven RNA samples were selected for microarray analysis using the HumanHT-12v4 Expression BeadChip targeting >47,000 probes. General gene expression profiles and hierarchical clustering can be found in subsection 4.4.3 and in appendix A.10. With regard to the osteoblast expression profiles of the utilised MSCs (chapter 2), the usually highly expressed genes *APOD*, *DARC*, *OMD*, and *BMP6* were downregulated under (+)-JQ1 treatment as assessed on day 21 of differentiation. For *APOD* and *DARC*, a 40-fold difference in gene expression was observed. Likewise, osteoblast transcription factor *RUNX2*, as well as the main component of mineralised bone matrix, collagen 1, were downregulated. In addition, expression of later osteoblastic markers and matrix proteins such as periostin and osteocalcin was reduced in (+)-JQ1 treated cells (figure 4.6 and table 4.3). *CADM3* (cell adhesion molecule 3), a gene involved in cell-cell adhesion showed a decrease by almost 5-fold, suggesting that the difference in cell density might be due to missing adhesion molecules and lack of matrix formation.

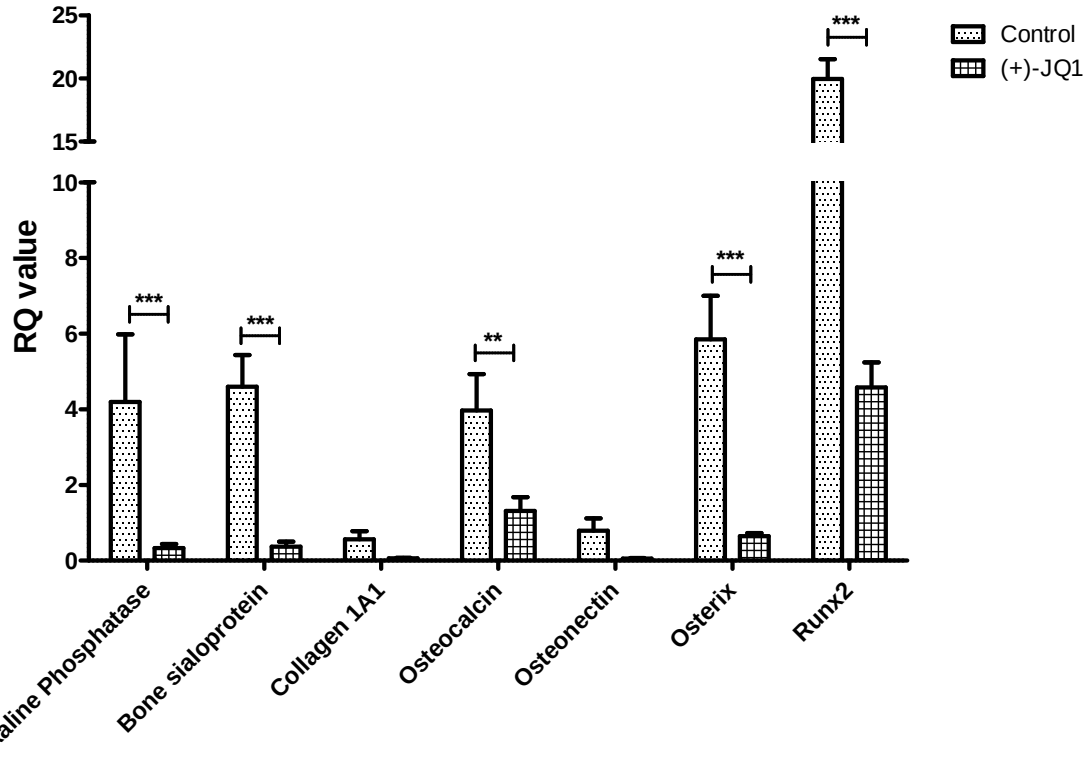

Figure 4.6: Changes in osteoblast gene expression under (+)-JQ1 treatment. Gene expression was measured by qPCR on day 7 of differentiation and treatment is shown as comparison to the non-treated control and normalised to day 1 (stem cell state). Expression of alkaline phosphatase (*ALPL*), bone sialoprotein (*IBSP*), collagen 1A1 (*COL1A1*), osteocalcin (*BGLAP*), osteonectin (*SPARC*), Osterix (*OSX*), and *RUNX2* are shown. P-values were calculated using One-way ANOVA (Bonferroni post test - *** $<$ 0.001, **$<$0.01, *$<$0.05).

4.4.3 Hierarchical clustering of genes expressed under (+)-JQ1 treatment

Microarrays are a useful tool to study gene expression on a genomic scale, generating a large amount of expression data. To facilitate dealing with experiments of this complexity and scope, various analysis tools are available, enabling techniques such as clustering. Here, a microarray data analysis tool, MeV: MultiExperiment Viewer (TM4) and the software R were used [269, 270]. Hierarchical clustering identifies genes that are expressed similarly in response to treatment. Pairs of genes that are most similar are joined together one after another until all genes are joined into one cluster. Known osteoblast marker signature genes were presented in the previous section, here a more comprehensive gene expression analysis is shown. With the aim to only include stably regulated genes, only genes regulated more than two-fold compared to the control at two different time points during treatment were con-

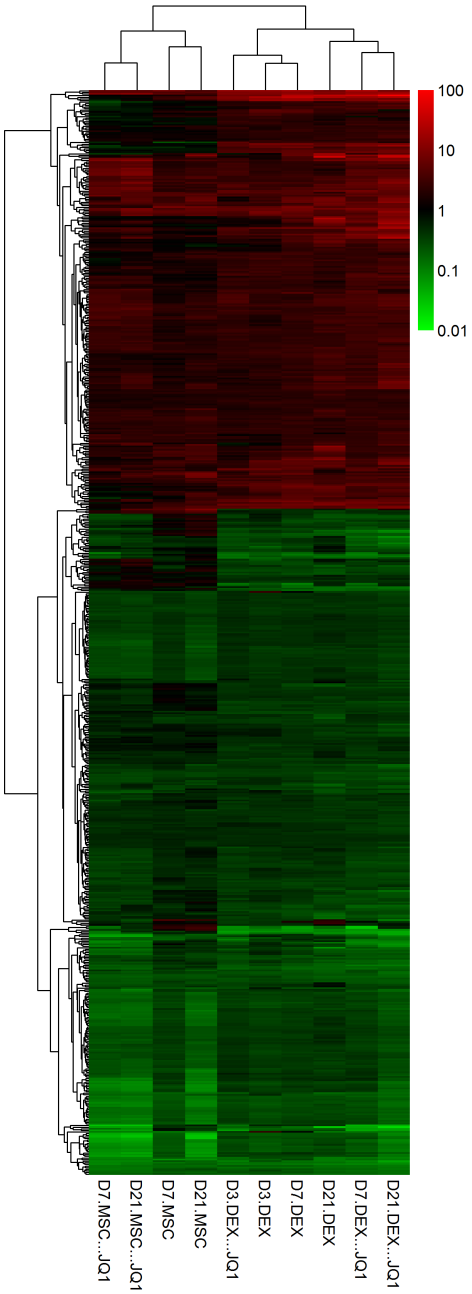

Figure 4.7: Hierarchical clustering of all genes regulated for at least two time points in Dex and Dex + (+)-JQ1. By joining or "clustering" similarly expressed genes into groups of genes that respond similarly to treatment can be identified. Here, gene and sample clustering was carried out. Above each column, the condition and treatment are indicated. Expression ranges from green (low) to red (high).

sidered. Time points assessed were day 3, day 7, and day 21 for DEX and DEX (+)-JQ1. In doing this, 672 genes were included in the cluster analysis. The most obvious difference in gene expression was observed between cells under MSC treatment compared to those under dexamethasone treatment, which can be expected with regard to significant changes in gene expression under differentiation conditions (figure 4.7). Similarly, genes upregulated at a later stage of differentiation (day 21) showed a distinct expression pattern compared to earlier time points. Some of these genes might be related to prolonged time in culture, for instance *EFEMP1* (EGF Containing Fibulin-Like Extracellular Matrix Protein 1) was found, a gene involved in cell adhesion providing and stabilising extracellular matrix [271]. Cells in MSC medium under (+)-JQ1 treatment showed lower expression of the genes that were expressed in the control cells, indicating that (+)-JQ1 may also affect stem cell maintenance. For Dex-induced differentiation, the expression of genes related to osteogenic differentiation also showed a reduction under (+)-JQ1 treatment. However, the majority of the genes upregulated by Dex treatment were also regulated in the same direction under (+)-JQ1 treatment, but to a lower degree (figure 4.7 and table 4.1). It could also be the case that regulation of genes only occurred at a later time point or at a slower rate under (+)-JQ1 treatment, leading to a delay in gene expression compared to the non-treated control. (+)-JQ1 treatment itself led to an upregulation of a number of genes, which can be seen in more detail in table 4.2.

In order to identify genes that might be specifically upregulated or downregulated due to (+)-JQ1 treatment, the fifty highest upregulated genes for both Dex treatment and Dex + (+)-JQ1 treatment were listed separately. Seventeen genes were shared between the 50 highest upregulated genes in Dex and Dex + (+)-JQ1. The complete microarray dataset can be found in appendix A.10.

SYMBOL	REFSEQ_ID	D7 MSC	D21 MSC	D7 MSC + JQ1	D21 MSC + JQ1	D3 DEX	D7 DEX	D21 DEX	D3 DEX + JQ1	D7 DEX + JQ1	D21 DEX + JQ1
CADM3	NM_021189.2	0.97	1.01	1.01	1.01	1.11	7.24	66.10	1.05	1.29	13.51
IFITM1	NM_003641.3	1.83	4.27	1.25	1.62	1.51	3.58	51.57	1.20	5.68	36.52
APOD	NM_001647.2	1.07	1.31	0.92	0.99	1.28	2.29	46.19	1.02	1.02	1.95
DARC	NM_002036.2	1.02	1.00	0.95	1.08	1.12	5.83	40.96	1.03	1.16	8.30
SAA1	NM_199161.1	1.47	2.01	1.01	1.12	7.53	27.25	34.48	7.89	40.52	96.73
SUSD2	NM_019601.3	1.09	0.97	1.02	0.98	2.04	2.94	23.06	1.41	4.37	9.81
PPP1R14A	NM_033256.1	2.69	5.19	0.89	1.32	21.77	34.15	21.88	10.50	16.22	22.43
FBLN1	NM_001996.2	0.96	0.59	0.40	0.38	1.52	2.35	19.90	0.96	1.29	6.02
IL8	NM_000584.2	0.60	3.57	0.54	1.43	2.09	2.57	19.33	1.62	1.30	3.51
IGFBP2	NM_000597.2	1.31	10.66	1.32	2.86	1.56	6.20	18.25	1.77	12.48	32.74
ALPL	NM_000478.3	1.87	4.99	0.35	0.41	1.09	5.94	17.82	0.70	2.29	5.17
EPSTI1	NM_033255.2	2.63	3.36	1.27	1.36	2.11	3.79	13.61	1.49	2.22	2.22
GPM6B	NM_001001995.1	0.98	1.01	1.05	0.96	1.24	2.41	13.58	1.02	1.42	1.98
OLFML2A	NM_182487.2	1.67	1.61	1.17	1.50	1.41	4.88	12.14	1.40	5.53	12.42
CLEC3B	NM_003278.1	1.45	1.78	1.92	3.46	1.23	3.95	11.66	1.30	7.37	15.04
AOX1	NM_001159.3	1.75	4.21	1.19	1.21	2.75	7.13	10.93	1.48	3.73	6.37
CRYAB	NM_001885.1	1.52	2.00	0.47	1.39	15.96	16.40	10.83	6.59	9.62	12.87
CEBPD	NM_005195.3	4.03	4.70	5.32	5.58	10.68	12.95	10.83	9.71	14.89	16.46
ITGA10	NM_003637.3	2.78	2.76	1.27	1.85	6.33	7.35	10.16	7.02	6.13	4.33
CYP1B1	NM_000104.2	5.25	3.22	10.49	12.84	10.46	13.86	9.69	10.52	16.41	20.14
UBA7	NM_003335.2	3.68	3.51	2.03	1.93	2.24	3.26	9.31	1.76	2.62	2.55
ZBTB16	NM_006006.4	0.96	0.92	0.91	0.99	2.38	4.86	9.10	2.31	6.13	8.25
GPM6B	NM_001001995.1	0.98	0.94	0.93	0.94	1.11	2.25	8.80	0.96	1.13	1.68
TNS3	NM_022748.10	2.47	3.54	0.71	1.02	3.83	5.62	8.72	3.24	8.29	8.25
HRASLS3	NM_007069.2	3.55	5.98	5.35	8.71	6.91	8.00	8.43	5.80	10.02	9.06
IFI35	NM_005533.2	2.34	3.40	1.97	1.83	1.59	2.16	8.37	1.71	2.61	2.57
UBE2L6	NM_004223.3	4.13	4.78	4.67	3.88	2.45	2.80	8.30	2.81	4.72	5.78
EFEMP1	NM_004105.3	2.74	6.12	1.56	4.85	3.16	5.91	8.27	1.43	3.53	9.77
EFEMP1	NM_004105.3	2.72	7.21	2.14	5.31	2.40	6.48	8.11	1.15	3.62	9.90
AKR1C3	NM_003739.4	3.41	3.87	10.00	12.66	2.13	3.78	8.09	2.94	8.17	11.79
LOC645638	XR_040455.1	8.26	3.77	5.78	5.22	13.92	18.81	8.04	13.93	21.01	7.47
PLAC9	NM_001012973.1	1.59	3.49	1.19	2.87	2.87	4.60	7.94	1.73	2.31	4.21
FBLN1	NM_006486.2	0.90	0.60	0.20	0.18	1.60	2.29	7.50	0.97	1.37	4.05
CRISPLD2	NM_031476.2	1.66	0.75	3.81	3.79	7.19	8.38	7.44	4.49	10.19	23.01
LEPR	NM_001003679.1	1.12	1.38	1.78	2.30	1.24	2.15	7.44	1.47	3.97	21.42
DUSP23	NM_017823.3	1.22	1.27	0.76	0.84	4.81	7.84	7.06	2.97	3.21	4.25
WFDC1	NM_021197.2	1.16	1.62	0.96	1.07	4.66	9.26	7.05	1.04	1.12	1.39
ABCC3	NM_003786.2	1.74	1.20	1.50	1.54	3.94	5.76	7.04	3.89	9.71	11.85
TMTC1	NM_175861.2	0.99	1.34	1.31	1.64	1.73	4.02	6.98	1.79	3.49	5.16
EFEMP1	NM_001039348.1	2.51	5.58	1.68	4.34	2.57	5.25	6.81	1.07	3.19	7.45
KIAA0367	NM_015225.1	3.01	4.31	3.50	4.47	3.52	5.89	6.79	2.76	6.13	12.88
C13orf15	NM_014059.2	2.92	4.80	0.85	0.94	13.73	17.19	6.66	10.19	9.93	6.44
ALDH3B1	NM_000694.2	1.98	2.23	5.31	5.44	4.05	4.50	6.56	5.66	8.04	5.47
ADM	NM_001124.1	4.56	2.91	1.94	2.25	2.38	4.21	6.53	2.25	5.25	6.41
HSPB2	NM_001541.2	1.48	1.85	1.09	1.54	4.69	5.75	6.43	2.07	3.00	3.37
TIMP4	NM_003256.2	1.05	0.97	1.08	1.10	1.65	2.22	6.43	1.34	1.58	2.09
SVEP1	NM_153366.2	1.59	1.34	2.08	4.98	2.94	3.77	6.40	2.53	7.63	24.20
DCN	NM_133503.2	0.93	1.03	0.39	0.92	6.19	5.69	6.21	4.93	9.78	16.09
ZBTB16	NM_001018011.1	1.01	1.07	1.02	1.05	2.00	3.02	6.21	1.98	3.84	5.86
ANKRD35	NM_144698.2	2.76	1.75	2.29	2.83	4.32	4.41	6.01	2.03	2.49	2.93

Table 4.1: 50 highest upregulated genes in DEX compared to gene expression in MSC, MSC + (+)-JQ1, and DEX + (+)-JQ1 for day 3, 7, and 21. Expression ranges from green (low) to red (high). MSC, mesenchymal stem cell medium; DEX, complete osteogenic differentiation medium containing dexamethasone; +JQ1, addition of (+)-JQ1.

As discussed above, it appeared that many of the normally upregulated genes under Dex treatment were also upregulated under Dex + (+)-JQ1 treatment, however, there seemed to be a slight delay in gene expression as well as a lower general expression level (table 4.1). Generally speaking, (+)-JQ1 treatment, led to an increase in expression of a number of genes that were not expressed to the same level in the control cells. As it can be seen in table 4.2, the gene with the highest expression under (+)-JQ1 treatment, *SAA1* (serum amyloid A1, a member of the serum amyloid A family of apolipoproteins) was upregulated by almost three-fold under (+)-JQ1 treatment compared to Dex alone. The SAA family of proteins represents major acute phase reactants in response to inflammation and tissue

injury. Prolonged expression or overexpression of *SAA1* has been reported to potentially play a role in degenerative diseases such as rheumatoid arthritis (RA) [272]. *IFITM1* (interferon-induced transmembrane protein 1) was another highly upregulated gene under dexamethasone (51.57-fold) and dexamethasone + (+)-JQ1 treatment (36.52-fold). In human alveolar-derived bone marrow stromal cells (AD-BMSCs), IFITM1 increases osteoblast differentiation through RUNX2 and its knockdown was reported to lead to a decrease in bone specific markers such as ALP, collagen type 1A1, bone sialoprotein, osteocalcin, Osterix, and to a reduction in calcium accumulation [273]. This decrease in *IFITM1* induction under (+)-JQ1 treatment might involve a similar mechanisms in bone marrow-derived stem cells as utilised here. The third highest expressed gene under (+)-JQ1 treatment, *IGFBP2* (insulin-like growth factor binding protein 2), was also the tenth highest under Dex treatment. IGFBP2 is a member of the highly conserved family of IGFBPs regulating the effects of IGFs. IGFBPs circulate or reside locally in the extracellular space including the bone marrow micro-environment. IGFBP2 was shown to increase during rapid neonatal growth and at the time of peak bone acquisition, and Kawai et al. postulated that IGFBP2 increases bone mass through the activity of its heparin-binding domain (HBD) [274, 275]. Interestingly, *IGFBP2*, as well as a number of other genes in this table (*TPD52L1*, *EPDR1*; table 4.2), are known to be involved in calcium-dependent processes and signalling, and were higher expressed under Dex + (+)-JQ1 treatment. (+)-JQ1 could potentially interfere with the mineral deposition capacity of osteoblastic cells, leading to excess calcium in the matrix. On this basis, the mineralisation potential of (+)-JQ1 treated cells will be assessed in the next section.

SYMBOL	REFSEQ_ID	D7 MSC	D21 MSC	D7 MSC + JQ1	D21 MSC + JQ1	D3 DEX	D7 DEX	D21 DEX	D3 DEX + JQ1	D7 DEX + JQ1	D21 DEX + JQ1
SAA1	NM_199161.1	1.47	2.01	1.01	1.12	7.53	27.25	34.48	7.89	40.52	96.73
IFITM1	NM_003641.3	1.83	4.27	1.25	1.62	1.51	3.58	51.57	1.20	5.68	36.52
IGFBP2	NM_000597.2	1.31	10.66	1.32	2.86	1.56	6.20	18.25	1.77	12.48	32.74
SVEP1	NM_153366.2	1.59	1.34	2.08	4.98	2.94	3.77	6.40	2.53	7.63	24.20
CRISPLD2	NM_031476.2	1.66	0.75	3.81	3.79	7.19	8.38	7.44	4.49	10.19	23.01
PPP1R14A	NM_033256.1	2.69	5.19	0.89	1.32	21.77	34.15	21.88	10.50	16.22	22.43
LEPR	NM_001003679.1	1.12	1.38	1.78	2.30	1.24	2.15	7.44	1.47	3.97	21.42
CYP1B1	NM_000104.2	5.25	3.22	10.49	12.84	10.46	13.86	9.69	10.52	16.41	20.14
CEBPD	NM_005195.3	4.03	4.70	5.32	5.58	10.68	12.95	10.83	9.71	14.89	16.46
DCN	NM_133503.2	0.93	1.03	0.39	0.92	6.19	5.69	6.21	4.93	9.78	16.09
C10ORF10	NM_007021.2	1.73	3.42	1.53	2.69	2.03	3.17	5.20	2.36	7.84	15.89
SAA1	NM_000331.3	1.12	1.08	1.02	1.08	1.68	3.02	4.20	1.62	4.74	15.42
CLEC3B	NM_003278.1	1.45	1.78	1.92	3.46	1.23	3.95	11.66	1.30	7.37	15.04
TPD52L1	NM_001003396.1	5.95	5.64	2.85	7.03	9.03	6.58	4.27	4.09	5.28	14.90
KIAA0367	NM_015225.1	3.01	4.31	3.50	4.47	3.52	5.89	6.79	2.76	6.13	12.88
CRYAB	NM_001885.1	1.52	2.00	0.47	1.39	15.96	16.40	10.83	6.59	9.62	12.87
OLFML2A	NM_182487.2	1.67	1.61	1.17	1.50	1.41	4.88	12.14	1.40	5.53	12.42
ABCC3	NM_003786.2	1.74	1.20	1.50	1.54	3.94	5.76	7.04	3.89	9.71	11.85
AKR1C3	NM_003739.4	3.41	3.87	10.00	12.66	2.13	3.78	8.09	2.94	8.17	11.79
EPDR1	NM_017549.3	2.26	3.82	4.94	9.45	3.66	3.44	2.97	3.17	5.87	11.12
SORBS2	NM_003603.4	3.94	4.65	1.20	1.80	7.24	6.47	4.66	5.49	8.01	10.81
C10ORF54	NM_022153.1	5.11	6.29	4.96	8.55	6.14	7.66	4.08	5.69	6.81	10.43
RASD1	NM_016084.3	0.80	0.79	1.49	1.46	1.67	2.21	5.93	1.14	3.05	10.29
GPC4	NM_001448.2	3.19	5.40	2.14	6.72	4.83	5.85	3.37	3.63	5.13	10.08
EFEMP1	NM_004105.3	2.72	7.21	2.14	5.31	2.40	6.48	8.11	1.15	3.62	9.90
SUSD2	NM_019601.3	1.09	0.97	1.02	0.98	2.04	2.94	23.06	1.41	4.37	9.81
TPD52L1	NM_001003397.1	4.41	4.70	2.36	5.55	7.73	5.22	3.86	3.53	3.80	9.81
EFEMP1	NM_004105.3	2.74	6.12	1.56	4.85	3.16	5.91	8.27	1.43	3.53	9.77
GAS1	NM_002048.1	3.11	2.18	1.46	1.71	4.38	5.48	4.93	2.38	2.97	9.49
ASAP3	NM_017707.2	3.32	2.35	3.90	5.54	2.35	2.34	2.94	2.33	4.40	9.35
SORBS2	NM_003603.4	3.05	4.59	1.23	1.74	5.72	6.36	4.01	4.50	6.86	9.35
IMPA2	NM_014214.1	0.94	0.77	0.94	1.30	8.36	8.66	4.92	4.63	7.95	9.28
HRASLS3	NM_007069.2	3.55	5.98	5.35	8.71	6.91	8.00	8.43	5.80	10.02	9.06
TXNIP	NM_006472.2	2.01	2.15	7.11	7.22	1.38	3.29	4.72	2.52	9.61	8.81
ANGPT1	NM_001146.3	3.65	3.42	1.52	1.98	4.86	5.60	5.31	2.07	3.52	8.77
PPAP2A	NM_176895.1	1.61	1.69	2.16	3.50	2.16	2.23	2.41	2.04	2.47	8.51
ZBTB16	NM_006006.4	0.96	0.92	0.91	0.99	2.38	4.86	9.10	2.31	6.13	8.25
TNS3	NM_022748.10	2.47	3.54	0.71	1.02	3.83	5.62	8.72	3.24	8.29	8.25
C1RL	NM_016546.1	2.38	2.40	3.29	3.76	2.50	2.54	3.97	2.47	5.06	8.14
TRNP1	NM_001013642.2	1.19	1.02	1.67	2.32	2.20	2.97	3.91	3.46	5.96	7.83
LOC645638	XR_040455.1	8.26	3.77	5.78	5.22	13.92	18.81	8.04	13.93	21.01	7.47
EFEMP1	NM_001039348.1	2.51	5.58	1.68	4.34	2.57	5.25	6.81	1.07	3.19	7.45
ADARB1	NM_015833.2	0.83	0.81	0.84	0.78	4.42	5.53	4.39	4.06	7.17	7.42
FTH1	NM_002032.2	1.96	2.52	4.03	4.62	2.56	2.34	4.20	4.83	5.31	7.37
PROS1	NM_000313.1	1.44	2.40	2.72	3.37	1.80	2.70	4.35	1.40	3.37	7.30
FKBP5	NM_004117.2	0.71	0.74	1.00	1.00	3.97	5.43	5.12	4.15	4.99	7.30
HCFC1R1	NM_001002018.1	2.81	2.21	4.88	5.23	2.82	2.59	5.07	4.22	6.14	7.23
CFH	NM_001014975.1	1.80	3.23	2.06	3.28	1.89	3.06	4.05	1.87	4.57	7.03
CFH	NM_001014975.1	1.75	3.00	1.88	2.83	2.08	3.15	3.65	1.94	4.02	6.81
RCAN2	NM_005822.2	1.91	1.69	2.88	3.82	2.53	2.87	3.00	4.32	10.01	6.71

Table 4.2: 50 highest upregulated genes in Dex + (+)-JQ1 compared to gene expression in MSC, MSC+JQ1, and DEX for day 3, 7, and 21. Expression ranges from green (low) to red (high). MSC, mesenchymal stem cell medium; DEX, complete osteogenic differentiation medium containing dexamethasone; +JQ1, addition of (+)-JQ1.

As discussed in subsection 4.4.2, osteoblast-related genes normally expressed during Dex-induced differentiation were downregulated under (+)-JQ1 treatment, as shown in the previous graphs and summarised here in table 4.3. The microarray analysis was in accordance with results obtained by qPCR analysis. Interestingly, genes involved in the interplay of osteoblast and adipose tissue showed an increase in expression with (+)-JQ1 treatment. Transcript variants of the leptin receptor (*LEP-R*) were highly upregulated by Dex + (+)-JQ1 compared to Dex alone (table 4.3), whereas leptin levels were only slightly higher. Leptin induced signalling requires the transcription factor signal transducer and activator of transcription 3 (STAT3), and STAT3 itself was also upregulated

during (+)-JQ1 treatment.

ProbeID	SYMBOL	DEFINITION	REFSEQ_ID	D3 DEX	D7 DEX	D21 DEX	D3 DEX +JQ1	D7 DEX +JQ1	D21 DEX +JQ1
6100356	**ALPL**	H.sapiens alkaline phosphatase, liver/bone/kidney (ALPL), transcript variant 1, mRNA.	NM_000478.3	1.09	5.94	17.82	0.70	2.29	5.17
50192	**DARC**	H.sapiens Duffy blood group, chemokine receptor (DARC), transcript variant 2, mRNA.	NM_002036.2	1.12	5.83	40.96	1.03	1.16	8.30
7150634	**APOD**	H.sapiens apolipoprotein D (APOD), mRNA.	NM_001647.2	1.28	2.29	46.19	1.02	1.02	1.95
3450446	**CADM3**	H.sapiens cell adhesion molecule 3 (CADM3), mRNA.	NM_021189.2	1.11	7.24	66.10	1.05	1.29	13.51
4610246	**OMD**	H.sapiens osteomodulin (OMD), mRNA.	NM_005014.1	2.04	2.18	5.09	1.05	0.96	1.32
510246	**POSTN**	H.sapiens periostin, osteoblast specific factor (POSTN), mRNA.	NM_006475.1	1.34	1.37	1.43	0.86	0.16	0.11
6980064	**BMP6**	H.sapiens bone morphogenetic protein 6 (BMP6), mRNA.	NM_001718.4	6.02	7.66	2.60	2.89	4.57	4.23
6960142	**COL1A1**	H. sapiens collagen, type I, alpha 1 (COL1A1), mRNA.	NM_000088.3	0.96	1.08	0.94	0.95	0.61	0.52
2680382	**LEPR**	H.sapiens leptin receptor (LEPR), transcript variant 2, mRNA.	NM_001003679.1	1.24	2.15	7.44	1.47	3.97	21.42
1940196	**LEPR**	H.sapiens leptin receptor (LEPR), transcript variant 2, mRNA.	NM_001003679.1	1.04	1.23	2.60	1.08	1.64	6.02
3400747	**LEPR**	H.sapiens leptin receptor (LEPR), transcript variant 1, mRNA.	NM_002303.3	1.03	1.18	1.70	1.05	1.52	2.72
6480348	**LEPR**	H.sapiens leptin receptor (LEPR), transcript variant 2, mRNA.	NM_001003679.1	1.07	1.27	2.06	1.18	1.76	4.57
1940156	**LEPR**	H.sapiens leptin receptor (LEPR), transcript variant 3, mRNA.	NM_001003680.1	1.18	1.52	2.84	1.13	2.26	7.13

Table 4.3: Fold changes in gene expression of bone-related genes under (+)-JQ1 treatment. Gene expression on day 3, 7, and 21 normalised to day 1 is shown. +JQ1 indicates (+)-JQ1 treatment. Gene expression range is indicated by colour change green (low) to red (high).

When the microarray data was subjected to the previously mentioned IPA analysis, an interesting finding was made: under (+)-JQ1 treatment, the second largest network calculated was "Lipid Metabolism, Small Molecule Biochemistry, Developmental Disorder" (table 4.4). 22 genes upregulated under Dex + (+)-JQ1 treatment were part of this network as shown in figure 4.8. Furthermore, looking at canonical pathways involved, "PPARa/RXRa Activation" turned out to be the third most likely one, a pathway that did not come up under Dex treatment alone (table 4.9). The left part of the network (figure 4.8), including peroxisome proliferator-activated receptor alpha (PPARα), acetyl-coenzyme A acyltransferase 1 (ACAA1), acyl-CoA dehydrogenase family member 11 (ACAD11), solute carrier family 27 (fatty acid transporter) member 1 (SLC27A1), as well as cytochrome B5 reductase 3 (CYB5R3), represents the lipid metabolism part of the network, whereas the right part involves genes that are known to be upregulated in response to oxidative stress. Treatment with (+)-JQ1 and the observed change in proliferation could indeed be related to a stress-response, and the upregulation of genes such as glutathione S-transferase kappa

1 (GSTK1), aldo-keto reductase family 1 member C3 (AKR1C3), NAD(P)H dehydrogenase quinone 1 (NQO1), amongst others, indicate the involvement of a cellular defence mechanism (table 4.9). Genes upregulated in this pathway can be seen in table 4.5.

ID	Molecules in Network	Score	Focus Molecules	Top Diseases and Functions
1	ALDH, ALDH3A2, ALDH3B1, ALDH4A1, ALDH6A1, ALPL, AMPK, ARL6IP5, BNIP3L, DHRS3, DUSP1, EIF4A2, FKBP5, FSH, GDE1, ITPK1, LEPR, LEPROT, Lh, LRRC32, Mapk, MT1X, PC, Pde, PDE5A, phosphatase, PLCE1, PPAP2A, PRUNE2, RNASET2, STOM, STRADB, TNS3, TPD52L1, TPRA1	46	28	Hereditary Disorder, Neurological Disease, Carbohydrate Metabolism
2	ACAA1, ACAD11, ADM, AKR1C3, AKR1C4, Aldose Reductase, BBS1, BBS2, BCAT2, BRE, CYB5R3, DCXR, GFPT2, glutathione peroxidase, GPX4, GST, GSTA4, GSTK1, MUC1, NADH or NADPH:quinone oxidoreductase, NFkB (complex), NGFRAP1, NQO1, OSBPL10, peptidase, PI3K (family), PPARα-RXRα, PXR ligand-PXR-Retinoic acid-RXRα, RNF141, SLC27A1, SLC2A5, SLC2A6, T3-TR-RXR, UBA7, VGLL3	39	25	Lipid Metabolism, Small Molecule Biochemistry, Developmental Disorder
3	20s proteasome, BCR (complex), C1q, CFH, CYBRD1, Cyclin A, DCN, DDIT4, DECR2, E2f, EPAS1, FHL1, FOS, GAMT, GBA, GOT, HIST1H2AC, LAMP2, LPCAT3, NCK, NFIL3, NIPSNAP1, OMA1, OPTN, p70 S6k, Pias, PTX3, Rab11, SELENBP1, Sos, STAT1/3/5 dimer, TUBB2B, TXNIP, ZBTB16, ZMYM6	34	23	Renal and Urological Disease, Cardiovascular Disease, Pulmonary Hypertension

Table 4.4: The three top gene networks under Dex + (+)-JQ1 treatment as calculated by IPA. To rank the networks, a score is computed according to the fit of that network to the genes that were uploaded. The score is derived from a p-value and indicates the likelihood of the focus genes in a network being found together by random chance. The p-value is calculated using Fisher's exact test.

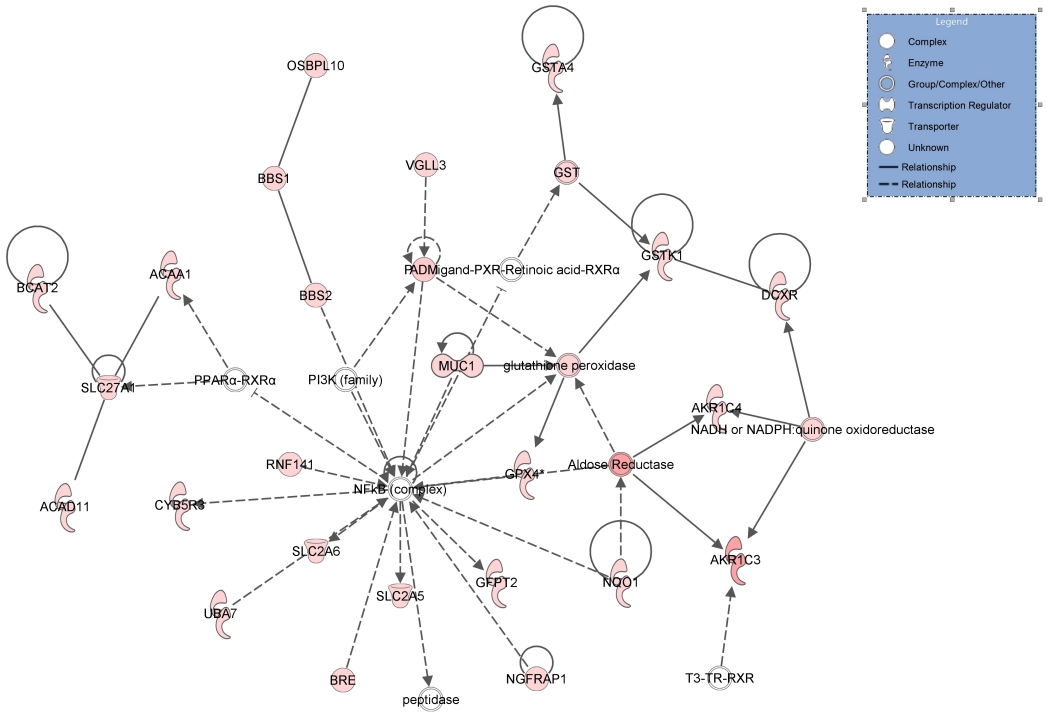

Figure 4.8: Network "Lipid Metabolism, Small Molecule Biochemistry, Developmental Disorder", comprising 22 genes upregulated during Dex + (+)JQ1 treatment as shown in red. Network of potentially interacting proteins was identified and placed into node-edge diagrams comprised of focus molecules (microarray-identified genes) and other interacting molecules. A direct relationship between two genes is indicated by a solid line, whereas an indirect relationship is indicated by a dashed line.

Gene symbol	Entrez Gene Name	Fold Change	Location	Type(s)
ABCA1	ATP-binding cassette, sub-family A (ABC1), member 1	4.69	Plasma Membrane	transporter
ACAA1	acetyl-CoA acyltransferase 1	2.07	Cytoplasm	enzyme
ADCY4	adenylate cyclase 4	4.3	Plasma Membrane	enzyme
ADCY9	adenylate cyclase 9	2.1	Other	other
MAPK3	mitogen-activated protein kinase 3	2.28	Other	other
NFKBIA	nuclear factor of kappa light polypeptide gene enhancer in B-cells inhibitor, alpha	2.26	Cytoplasm	transcription regulator
PLCD1	phospholipase C, delta 1	2.21	Cytoplasm	enzyme
PLCE1	phospholipase C, epsilon 1	2.48	Cytoplasm	enzyme
RRAS	related RAS viral (r-ras) oncogene homolog	2.3	Cytoplasm	enzyme
SLC27A1	solute carrier family 27 (fatty acid transporter), member 1	2.58	Plasma Membrane	transporter
SMAD3	SMAD family member 3	3.25	Nucleus	transcription regulator
TGFBR3	transforming growth factor, beta receptor III	3.47	Plasma Membrane	kinase

Table 4.5: Genes included in the canonical pathway "PPARa/RXRa Activation" as derived from microarray data and calculated by IPA. Gene expression values are shown as fold change, and type of gene and cellular location are indicated.

4.4.4 (+)-JQ1 inhibits bone matrix mineralisation

One of the key factors that determines why bone can form its rigid structure is the hardening of the matrix, accomplished primarily by deposition of inorganic hydroxyapatite ($Ca_5(PO_4)_3(OH)$) and organic collagen. The matrix also contains various growth factors

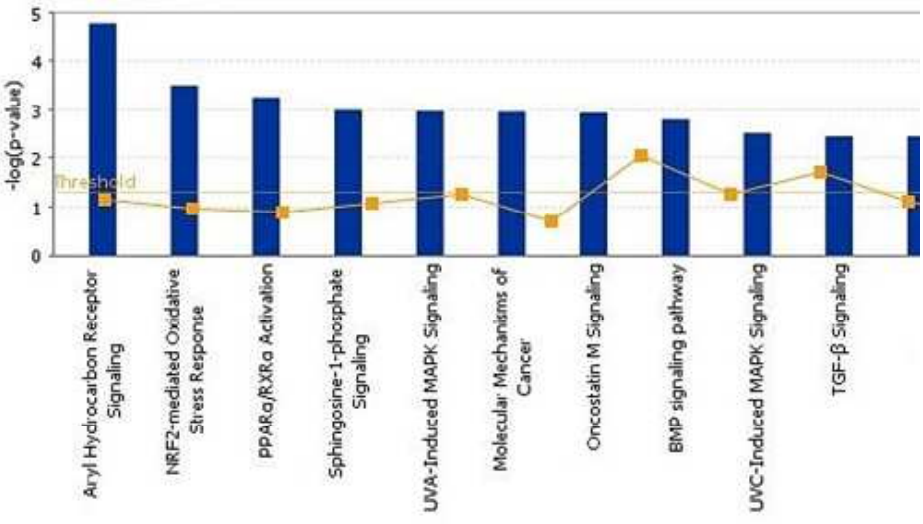

Ingenuity Canonical Pathways	-log(p-value)	Ratio	Molecules
Aryl Hydrocarbon Receptor Signalling	4.77E00	8.07E-02	*FOS, CTSD, ALDH4A1, ALDH3A2, GSTA4, MAPK3, HSPB2, NQO1, NFIB, ALDH3B1, ALDH6A1, CYP1B1, GSTK1*
NRF2-mediated Oxidative Stress Response	3.49E00	6.77E-02	*RRAS, MAPK3, GSTA4, ACTA2, NQO1, FOS, CAT, AOX1, FKBP5, PRKD1, FTH1, GSTK1, EPHX1*
PPARα/RXRα Activation	3.25E00	6.28E-02	*PLCD1, ADCY9, PLCE1, NFKBIA, ACAA1, RRAS, MAPK3, ADCY4, SMAD3, TGFBR3, SLC27A1, ABCA1*
Sphingosine-1-phosphate Signalling	2.99E00	7.5E-02	*PLCD1, ADCY9, NAAA, PLCE1, MAPK3, ADCY4, SMPD1, FNBP1, PDGFRB*
UVA-Induced MAPK Signalling	2.96E00	8.7E-02	*PLCD1, BCL2L1, FOS, PLCE1, RRAS, MAPK3, SMPD1, STAT1*
Molecular Mechanisms of Cancer	2.96E00	4.76E-02	*ADCY9, FYN, LRP5, BMP4, APH1B, RRAS, MAPK3, ADCY4, SMAD3, SMAD6, HIF1A, BCL2L1, FOS, NFKBIA, BMP6, FNBP1, PRKD1, BMP1*
Oncostatin M Signalling	2.93E00	1.43E-01	*EPAS1, RRAS, MAPK3, PLAU, STAT1*
BMP signalling pathway	2.8E00	8.75E-02	*ZNF423, BMP4, RRAS, MAPK3, SMAD6, BMP6, BMP1*
UVC-Induced MAPK Signalling	2.51E00	1.19E-01	*FOS, RRAS, MAPK3, SMPD1, PRKD1*
TGF-β Signalling	2.44E00	7.87E-02	*ZNF423, FOS, BMP4, RRAS, MAPK3, SMAD3, SMAD6*

Figure 4.9: Overview of canonical pathways affected by BET protein inhibition: The most statistically significant canonical pathways identified in the microarray data of Dex + (+)-JQ1 treatment. Upper figure, Pathways are ranked according to their p-value (-log) (blue bars) and the ratio of list genes found in each pathway over the total number of genes in that pathway (ratio, orange squares). The threshold line corresponds to a p-value of 0.05. The ratio is calculated as the number of genes in a given pathway that meet the cut-off criteria, divided by total number of genes that make up that pathway. Lower table, List of canonical pathways and corresponding molecules.

such as osteocalcin, osteonectin, osteopontin, bone sialoprotein and glycosaminoglycans (GAGs). The matrix is first laid down as unmineralised osteoid secreted by osteoblasts, which mineralises once osteoblasts start secreting vesicles containing alkaline phosphatase. The vesicles serve as calcification sites for the bone matrix, while the enzyme activity provides phosphate groups and thereby allows their deposition. Accumulation of inorganic phosphate and Ca^{2+} lead to the formation of hydroxyapatite. The differentiation medium used in this work is supplemented with two components that support mineralisation - ascorbic acid and beta-glycerophosphate. The latter serves as a source of phosphate, while ascorbic acid is a known co-factor for assisting in collagen synthesis [276].

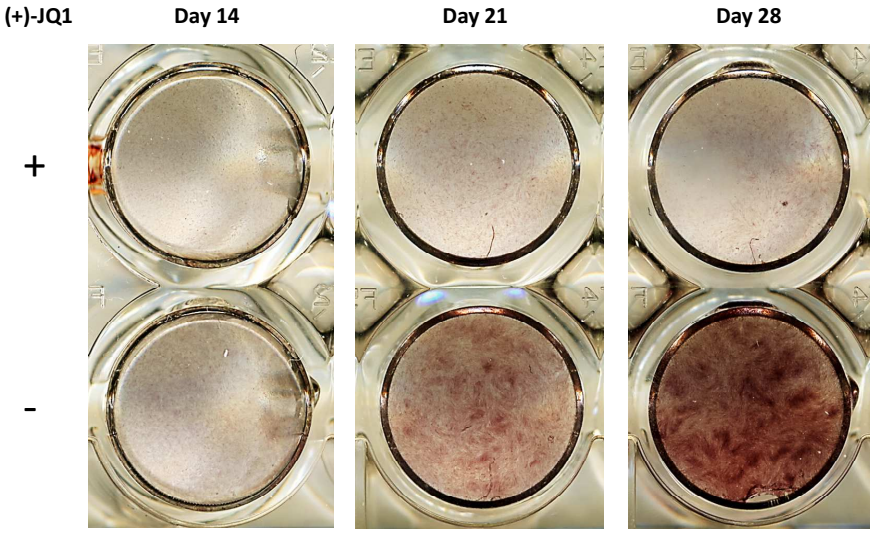

Figure 4.10: Alizarin Red S staining for calcium detection on human bone marrow-derived MSCs undergoing osteoblast differentiation with or without (+)-JQ1 treatment (100nM). Representative images chosen for day 14 to day 28. N = 4

Mineralisation can be assessed by a number of methods including Alizarin Red S and Von Kossa staining. Alizarin Red S (ARS) staining determines the presence of calcium deposition, while Von Kossa staining detects phosphate using a precipitation reaction in which silver ions react with phosphate in the matrix [277–279]. Alizarin Red S staining

was chosen for this work as it can not only be visualised under the microscope but is also versatile since the dye can be extracted from the stained monolayer and assayed by colorimetric detection at 405nm. Under treatment with (+)-JQ1 for four weeks, an inhibition of matrix mineralisation at all stages of osteogenesis was observed. Human MSCs treated with Dex showed first indications of mineralisation at 14 days after induction, with maximal mineralisation observed at day 28. Under (+)-JQ1 application almost no calcium deposition was observed in both mesenchymal stem cell lines used (figure 4.10 A). Quantification of ARS staining by acetic acid extraction of calcium yielded a significant decrease ($p < 0.01$) for day 28 of differentiation (figure 4.11 B).

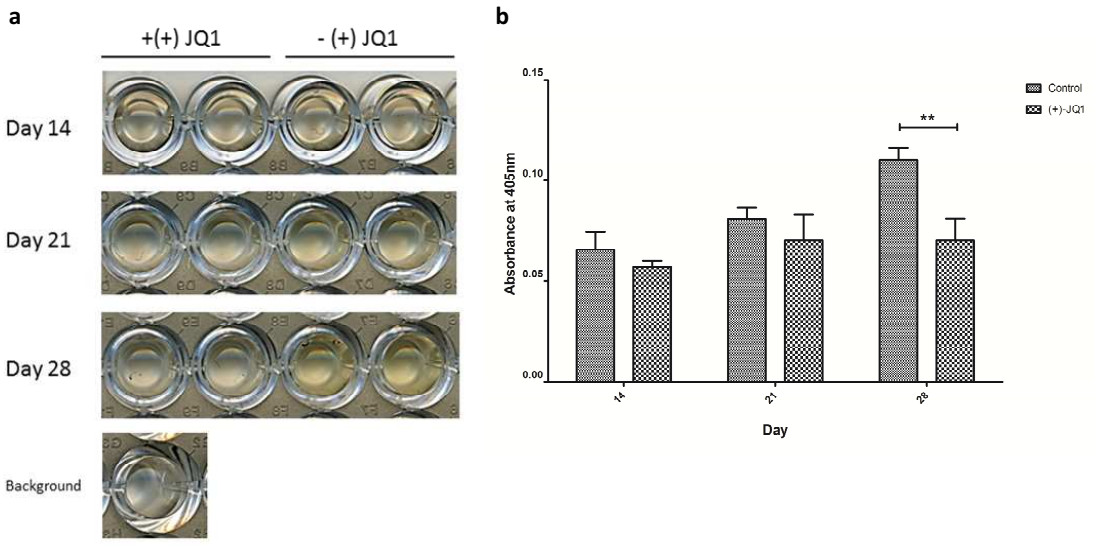

Figure 4.11: Alizarin Red S quantification by acetic acid extraction from human bone marrow-derived MSCs undergoing osteoblast differentiation with or without (+)-JQ1 treatment on day 14, 21, and 28 (A). The dye was extracted and determined by measuring absorbance at 405nm (B). P-value calculated by unpaired t-tests; **<0.01. Representative duplicate images chosen for day 14 to 28. N= 4

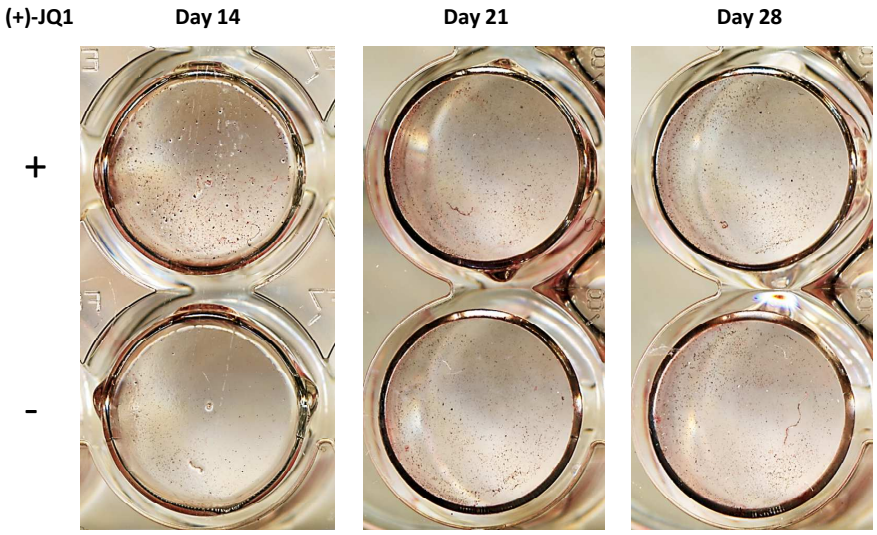

Figure 4.12: Oil Red O staining of human bone marrow-derived MSCs undergoing dexamethasone-induced osteoblast differentiation with or without (+)-JQ1 treatment for four weeks. Representative images chosen for day 14 to day 28.

4.4.5 Oil Red O staining to determine adipogenic differentiation potential

Human MSCs have the potential to differentiate into three main lineages - osteoblasts, adipocytes, and chondrocytes. As outlined in the introduction, the lineage determination is tightly regulated.

In the previous sections findings that could potentially point towards an imbalance of or even shift from osteogenesis were discussed. To test whether the restricted mineralisation potential of cells treated with (+)-JQ1 might be due to a treatment-caused shift in lineage determination towards adipogenesis, Oil Red O staining was carried out. No obvious lipid staining could be observed, however, under the microscope a small number of lipid deposits could be seen in the (+)-JQ1 treated cells, particularly on day 14 (figure 4.12).

4.4.6 (+)-JQ1 treatment of primary bone marrow-derived patient cells

All the above findings were made in homogeneous, commercially available primary mesenchymal stem cell lines undergoing differentiation. In order to validate these in primary patient cells, a bone marrow sample from a male patient (age 55) with osteoarthritis undergoing a total hip replacement was kindly provided by Dr. Philippa Hulley (NDORMS). The cells were obtained from the Oxford Musculoskeletal BioBank (OMB) and collected with informed donor consent in full compliance with National and Institutional ethical requirements, the United Kingdom Human Tissue Act, and the Declaration of Helsinki. The cells were previously shown to express alkaline phosphatase and form bone nodules (personal communication with Allahdad Zarei, unpublished data). Cells were seeded at 30,000 cells per well in a 48 well plate and cultured for four weeks until confluency was reached. DEX differentiation medium was applied and (+)-JQ1 was added for seven days at six different doses ranging from 0 to 3.3µM. After seven days of differentiation cell viability was measured using Presto Blue® and protein lysates were collected. Protein concentration was determined using the Pierce BCA Protein Assay (Thermo Scientific) and 10µl of lysate was used for the alkaline phosphatase assay (figure 4.13).

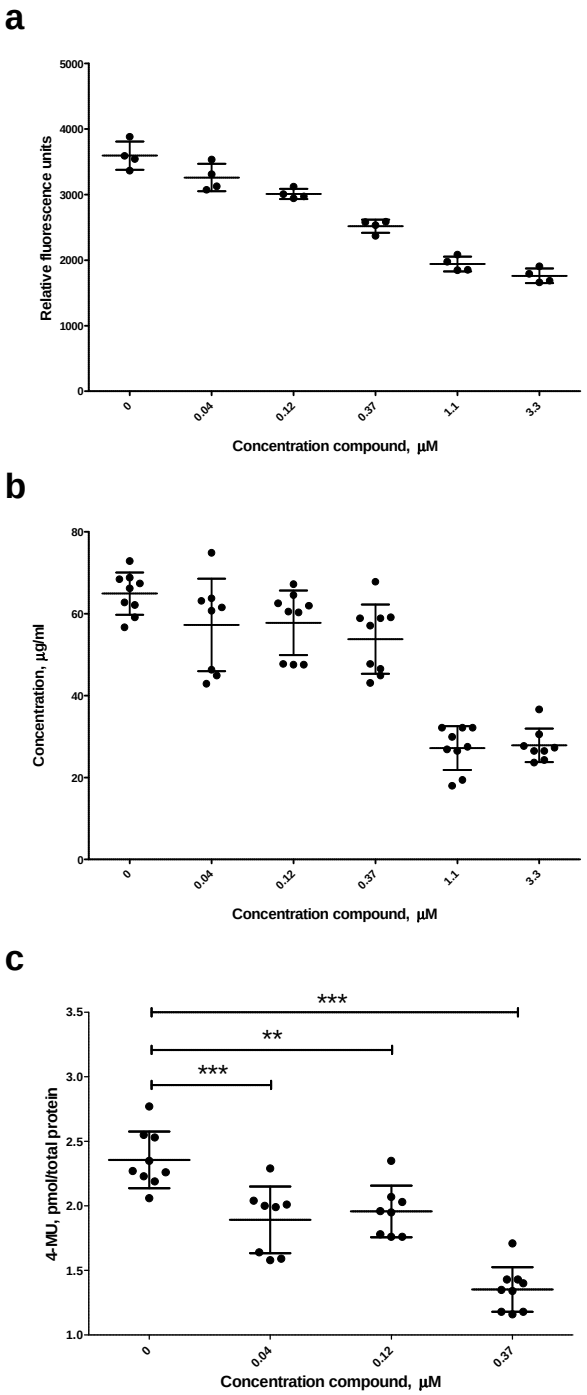

Figure 4.13: (+)-JQ1 treatment of primary cells. (+)-JQ1 doses applied are shown on the x-axis. a, Cell viability as measured by Presto Blue® after seven days of differentiation, fluorescence measurement values are shown on the y-axis. N = 4. b, Protein levels as measured by protein assay. Protein concentration in µg/ml is plotted on the y-axis. N = 3 (technical replicates shown). c, Alkaline phosphatase activity was measured at 120mins after substrate addition, and alkaline phosphatase product 4-MU in µg/ml normalised to total protein content is plotted on the y-axis. N = 3 (technical replicates shown); p-values were calculated using One-way ANOVA (Bonferroni post test - *** < 0.001, **<0.01, *<0.05).

Cell viability was observed to drop in a dose-dependent relation, whereas total protein levels remained constant over a range of concentrations until decreasing to almost half of the control levels at concentrations over 1µM (figure 4.13). With regard to cell viability concentrations over 1µM were not further considered. Alkaline phosphatase activity showed a significant decline at 40nM and a reduction by almost half at 370nM (figure 4.13). Again, to ensure that the reduction in ALP activity was not simply due to a decrease in cell number, the activity was normalised to the total protein concentration measured for the sample. These findings were in accordance with the results obtained in commercially available MSC lines, showing that the effect of (+)-JQ1 on ALP can also be reproduced in patient primary cells.

4.5 Conclusion and discussion

Follow-up studies on BRD4, identified in the initial screen as inhibitor of osteoblast formation, were performed using a chemical biology approach. Various compounds were available for use in experiments, with (+)-JQ1 being the most potent one; in addition, an inactive stereoisomer of the compound allowed rigorous assessment of on-target effects. In the shRNA screen BRD4 did not meet all selection criteria to be automatically selected as a hit, however, it was manually identified after taking additional selection criteria into account such as extent of change in alkaline phosphatase activity, consistence in hairpins and duplicates, etc. (for all criteria see subsections 3.3.5 and 3.3.9). Two hairpins (hairpin 1 and 5) showed a decreasing effect on alkaline phosphatase activity with almost no effect on cell viability. The selection of available compounds (including (+)-JQ1, I-BET, PFI-1, and bromosporine) used to inhibit the BET protein family member also showed a reduction in alkaline phosphatase activity, however with a dose-dependent effect on cell

viability. In addition, the fact that the (-)-JQ1 stereoisomer did not decrease ALP activity supported the specific effect of the (+)-JQ1 compound (for (-)-JQ1 dose-response see appendix A.9). The cell viability issue was overcome by obtaining a dose-response for (+)-JQ1, leading to the concentration of choice (100nM) for long-term treatment. A reduction in gene expression for a set of osteoblast genes was observed in qPCR and microarray experiments. *RUNX2*, *BMP6*, *ALPL*, *BGLAP*, *SPARC*, *APOD*, *DARC*, *OMD*, *COL1A1*, periostin (*POSTN*), and *IBSP* showed a reduced expression under (+)-JQ1 treatment, with up to 40-fold changes. In contrast, expression of genes involved in adipogenesis showed an increase in expression levels, indicating that BRD4 might constitute an important switch between osteoblast and adipocyte cell fate. In addition, matrix formation and mineralisation were impaired under BET protein inhibition, with (+)-JQ1 treatment leading to a significant decrease in calcium deposition as assessed by ARS staining and quantification. The effect of (+)-JQ1 was also tested on primary cells obtained from a bone marrow sample and confirmed the decreasing effect on alkaline phosphatase activity. Overall, BRD4 proved to be a reliable hit with different knockdown and inhibition techniques leading to consistent results in reduction of ALP activity. However, an important point to consider was the associated reduction in cell viability. We had to ensure that the decrease in alkaline phosphatase activity under compound treatment was not simply due to a decrease in cell viability and proliferation. To try to avoid this we determined a dose that did not impair cell viability, here a dose of half the IC_{50} value was applied. Also, by allowing cells to grow to confluency before inducing differentiation, cell proliferation is expected to remain minimal throughout the treatment time. After differentiation induction, cells transition into the differentiation phase very quickly and stop proliferating. In addition, for all experiments the cell viability was assessed before ALP activity was mea-

Bromodomain	KD/nM (ITC)	Tm shift °C
BRD2 (1)	128±6.5	6.5 ± 0.1
BRD2 (2)	nt	8.0 ± 0.01
BRD3 (1)	59.5 ± 3.1	8.3 ±0.1
BRD3 (2)	82.0 ±5.3	8.4 ± 0.01
BRD4 (1)	49.0 ± 2.4	9.4 ± 0.07
BRD4 (2)	90.1 ± 4.6	7.4 ± 0.1
BRDT (1)	190.1 ± 7.6	3.9 ± 0.1
BRDT (2)	nt	nt
CREBBP	nd	1.0 ± 0.1

Table 4.6: (+)-JQ1 selectivity within BET protein target family. Both bromodomains for each family member are shown (BD(1) and BD(2)). Dissociation constants (KD) as measured by isothermal titration calorimetry (ITC) and thermal shift assay results are presented. nt=not tested, nd=not detected. Adapted from http://www.thesgc.org/chemical-probes/JQ1

sured, allowing normalisation of enzyme activity to cell viability. In some cases when also the protein concentration was determined, ALP activity was normalised to total protein content. Generally speaking, the cell viability seemed to be more negatively affected when treating with compounds than with shRNA. This could be due to downstream effects of the BRD4 inhibition, but could also be caused by the fact that the compounds are targeting all BET proteins (although with different efficiencies) whereas the knockdown was only targeting *BRD4* or other single members of the BET protein family. This was another factor we had to consider – is the effect we were seeing with (+)-JQ1 treatment due to specific BRD4 inhibition or could it also be caused by another member of the BET protein family such as BRDT? BRDT is the testis-specific bromodomain protein and is located on chromosome 1, thus also expressed in females. In the shRNA screen, two hairpins for *BRDT* also showed a decreasing effect on alkaline phosphatase activity in dexamethasone-induced differentiation. However, the selectivity for (+)-JQ1 was previously published and the compound was shown to have a higher affinity for BRD4, especially towards its first bromodomain BD1 (table 4.6) [151].

Nevertheless, this does not exclude BRDT as a potential target or "participant" in the

observed effect. Interestingly, the International Mouse Phenotyping Consortium (IMPC) recently published data on a *Brdt* homozygous knockout mouse, showing a "skeleton phenotype" for both sexes. The knockout showed a decreased number of lumbar vertebrae as well as an increased number of sacral vertebrae. Moreover, vertebral transformation was observed for these mice, a process that can occur between spinal morphological segments (for *Brdt* knockouts transformation of L6 to S1, C7 to T1, T7 to T8, and TX to L1). It is also called transitional vertebrae as one vertebra has indeterminate characteristics and features of vertebrae from adjacent vertebral segments. In humans, this type of abnormality is quite common, with a reported prevalence of 4%–30%, and the majority of patients are asymptomatic. Lumbosacral transitional vertebrae in the lower back are sometimes associated with back pain and sciatica, however [280]. These findings in mice would suggest that Brdt is involved in generating a "normal" skeleton phenotype, however, the abnormalities are very specific for certain bone types and do not point towards a general role of BRDT in mesenchymal stem cell differentiation, osteoblast maturation, and bone formation. The stage of differentiation at which an epigenetic modulator might play a role is another interesting aspect and could make an important difference to experimental findings. If a modulator is directly targeting for instance the main osteoblast transcription factor RUNX2, does this imply that it only needs to be affected once in order to start or inhibit the differentiation process? If it is on the other hand regulating the transcription of a "secondary" gene, for example a matrix protein, does the modulator need to be inhibited throughout the differentiation time? For BRD4, this was an important assumption to be made - as bromodomains are "reader" domains and selectively recognise acetylated lysine (Kac) residues on histones without changing them. Does BRD4 change one initial process or reaction, or do bromodomains play a permanent role in osteoblast differentiation?

Could the lack of matrix mineralisation as shown here be due to a constant inhibition of certain matrix protein gene transcription and expression? For this chapter, we decided to apply (+)-JQ1 throughout the differentiation time to constantly inhibit BRD4. The compound was refreshed every other day to avoid loss of effect due to compound instability. Not knowing how exactly BRD4 is regulating osteoblast transcription or even where it is binding at chromatin sites, it is difficult to assess whether the effect on osteoblast differentiation and matrix formation is direct or indirect. Available genome analysis tools were used to identify potential binding sites for BRD4 on genes in mesenchymal stem cells or cells undergoing differentiation. For *RUNX2*, a potential binding site could be identified, however only for transcript variant 3. Eventually only chromatin immunoprecipitation (ChIP) analysis will allow assignment of exact binding sites for BRD4, an analysis that is still ongoing for this work. A recent publication showed that BRD4 does bind to H3K27 acetylated rich sites on *RUNX2*, but not in the promoter region [281].

The changes in gene expression that were observed under (+)-JQ1 treatment showed a reduction in expression for a number of osteoblast-related genes. Although the reduction in the key osteoblast transcription factor *RUNX2* itself could theoretically be sufficient to inhibit differentiation, other key genes such as *BMP6* showed a decrease in expression levels. Both these proteins can induce the transcriptional program required for osteogenic differentiation, thus BRD4 inhibition could potentially occur via multiple different pathways. Another interesting gene is the extracellular matrix component periostin (POSTN), which was shown to modulate cell adhesion, proliferation, and differentiation, as well as cell–matrix interaction by binding to cell surface receptors [282]. Its involvement in collagen folding and cross-linking is crucial for matrix assembly and therefore bone strength. Under (+)-JQ1 treatment, periostin expression was virtually abolished, which is another

factor that may explain the lack of matrix formation and mineralisation. Marker genes for all stages of osteoblast differentiation, early alkaline phosphatase (4-fold downregulation), mid-stage marker bone sialoprotein (16-fold) as well as late marker osteocalcin (13-fold) showed a reduction in expression under (+)-JQ1 treatment. This suggests a consistent downregulation of osteoblast differentiation. As seen in the hierarchical clustering, many other genes not directly related to osteoblast differentiation were also shown to be downregulated under (+)-JQ1 treatment. This could however also be due in part to a change in proliferation and cell cycle, especially in the case of MSCs where treatment with (+)-JQ1 delayed expression of some osteogenic genes. On the other hand, a number of genes that were upregulated under (+)-JQ1 treatment pointed to a role of calcium ion processes including cell signalling, adhesion and binding. *IGFBP2*, *TPD52L1*, *EPDR*, as well as *SVEP1* seemed to more highly expressed under (+)-JQ1 treatment and one could speculate if the lack of mineralisation and calcium depositions as shown by ARS staining is leading to a compensation mechanism for the usage of calcium. A reduction of alkaline phosphatase and the subsequent lack of phosphate ions could potentially lead to an abundance of free calcium without calcification sites to attach to.

Another interesting finding was the upregulation of a range of genes characterising lipid metabolism and adipose signalling pathways (canonical pathway "PPARa/RXRa Activation"). The 3-fold upregulation for each of the transcript variants of the leptin receptor (*LEPR*) appears significant, whereas leptin itself, a 16kDa adipokine secreted by adipose tissue, was only slightly elevated during (+)-JQ1 treatment. *STAT3*, a downstream target of leptin receptor signalling, also showed an increase in expression, however, this could also be happening through other cellular signals, such as other cytokine-induced signalling. Leptin receptor signalling has been shown to play a role in osteoblast regulation,

as osteoblasts express the long and short forms of the leptin receptor whose activation generates the aforementioned signal transduction via STAT3 phosphorylation. The addition of leptin to human marrow stromal cells was reported to enhance their osteoblast differentiation potential and inhibit differentiation into adipocytes [205]. However, in knockout animal models for leptin or leptin receptor deficiencies, reports are contradictory. Steppan et al. reported a decrease in bone mineral density (BMD) for mice lacking leptin, suggesting a supporting effect of leptin on bone [283]. Ducy et al. analysed two knockout models for both leptin and the leptin receptor, and both mutant mice had an increased bone formation, suggesting leptin as an inhibitor of bone formation [284]. Therefore, the role of leptin and its receptor still remains to be elucidated, as well as their involvement in response to (+)-JQ1 treatment. It could be speculated that (+)-JQ1 treatment is not simply inhibiting osteogenesis but actually promoting adipogenesis. That said, Oil Red O staining data (for day 14-28) did not directly support a switch to adipogenesis as only small lipid deposits could be observed. However, with medium supporting osteoblast development a clear change to adipogenesis cannot be expected. It is conceivable that under latent differentiation choices, as observed between osteoblasts and adipocytes, MSCs that are prevented from one lineage might choose another, closely related lineage if forced by compound treatment. (+)-JQ1 treatment might close the door to one lineage but open another one. This is a possibility that needs to be thoroughly assessed, as with regard to potential tissue engineering applications trans-lineage-differentiation of cells is not necessarily desired. An elegant way to address this question would be the use of mass cytometry, a single-cell multiparametric protein detection technology. Generally similar to flow cytometry and fluorescence-activated cell sorting (FACS), the antibodies used in this process are labelled with isotopic probes, allowing simultaneous measurement of a wide

range of parameters without causing any spectral overlap. Applying this method to test different epigenetic modulator targeting compounds on mesenchymal stem cells and assess their effect on lineage determination by investigating a set of antibodies for each lineage (adipogenic, chondrogenic, and osteogenic markers) could be an elegant way of answering this question.

Some of the tools used in this study in order to assess lineage determination have their limitations. As discussed in chapter 3, the alkaline phosphatase assay is an easy-to-use assay giving an indication of early osteoblastogenesis. However, ALP is also expressed in other cell types, although to a lower level, and therefore not unique to osteoblasts. In our case this did not pose a problem as most of the work was carried out on commercially available and validated cell lines of human mesenchymal origin, thus limiting the risk of mixed populations of cells. For candidate genes, the initial alkaline phosphatase assay was also followed by a thorough assessment of other bone markers. Nonetheless, when primary cells are used, mixed populations of cells can involve the risk of contamination by other cell types also expressing ALP, for instance fibroblasts [285].

5 The effect of lysine-specific demethylase 1A (KDM1A) on human mesenchymal stem cell differentiation and murine bone development

Lysine (K)-specific demethylase 1A was discovered by Shi et al. in 2004 [131], followed shortly by others [132], demonstrating the ability of the amine oxidase KDM1A/LSD1 to demethylate lysine 4 on histone H3 in a flavin adenine dinucleotide (FAD)-dependent reaction. In the beginning of this chapter, a brief summary of the data on *KDM1A* obtained in the shRNA screen followed by a literature review will be given. As main results, the work on human mesenchymal stem cells treated with a KDM1A inhibitor, as well as on a mouse model carrying a transgenic mutation of *Kdm1a* will be presented.

5.1 Background

KDM1A and its paralog KDM1B are both FAD-dependent amine oxidases, which act only on mono- and dimethylated lysine residues. KDM1A (also referred to as LSD1) can act on mono- and dimethylated H3K4 and H3K9, and KDM1B (also referred to as LSD2) acts only on mono- and dimethylated H3K4 [131, 132]. KDM1A is known to work within several chromatin modifying deacetylases complexes, though its intrinsic function is a demethylase activity [286]. It has been shown to interact directly with several proteins such as CoREST, which enables KDM1A to demethylate nucleosomes and protects it from proteasomal degradation [287, 288], the androgen receptor (AR), which changes KDM1A specificity from demethylating H3K4 towards H3K9 [132], and BHC80, which inhibits (CoREST-)KDM1A mediated demethylation activity [289]. KDM1A co-localises and interacts with Jumonji C (JMJC) domain-containing protein JMJD2C (KDM4C), a his-

tone tri-demethylase, and both demethylases cooperatively stimulate androgen receptor-dependent gene transcription [290]. In addition, all three proteins, KDM1A, JMJD2C, and AR, assemble on chromatin to remove methyl groups from mono-, di- and tri-methylated H3K9, and thereby taking advantage of their distinct substrate specificities. KDM1A has also been reported to promote oestrogen receptor activation by demethylating both promoter and enhancer sites [291]. Generally, the ability of KDM1A to demethylate H3K4 as well as H3K9 allows it to function both as a transcriptional co-repressor or co-activator (figure 5.1).

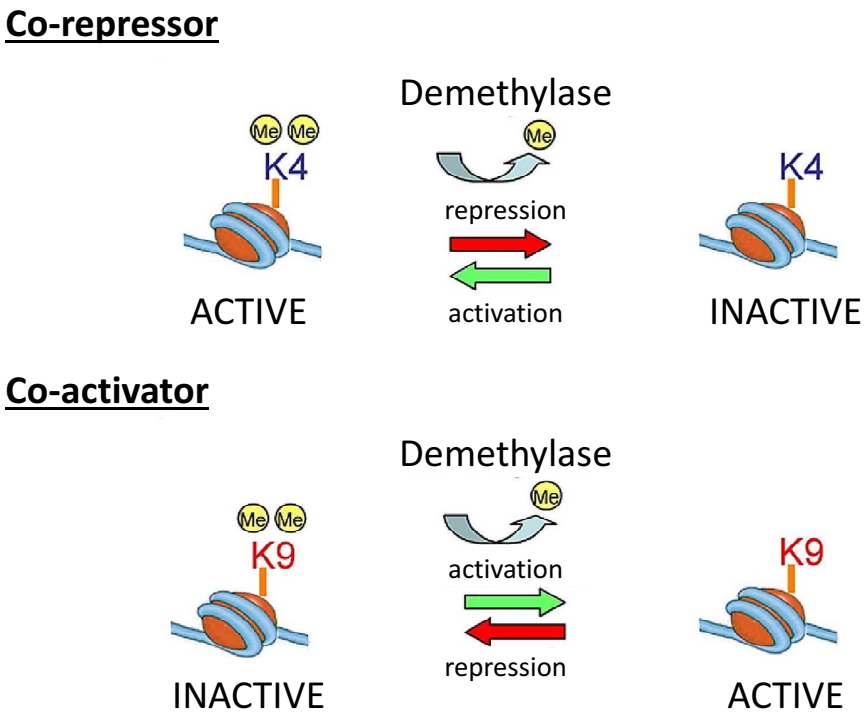

Figure 5.1: KDM1A functions in regulation of gene expression. KDM1A acts as a co-repressor by demethylating H3K4me, a specific tag for epigenetic transcriptional activation. Demethylation of H3K9me, a specific tag for epigenetic transcriptional repression, requires KDM1A as a co-activator. Adapted from [286].

In demethylating H3K4me, a specific tag for epigenetic transcriptional activation, KDM1A acts as a co-repressor, while for demethylation of H3K9me, a specific tag for epigenetic transcriptional repression, KDM1A acts as a co-activator. KDM1A has several func-

tional regions: a Swi3p, Rsc8p and Moira (SWIRM) domain, an FAD-binding motif, and an amine oxidase domain (figure 5.2). The combination of these three domains was predicted to mediate specific protein-protein interactions in the assembly of chromatin-protein complexes by altering charge distribution between histones and other chromosomal proteins [292, 293].

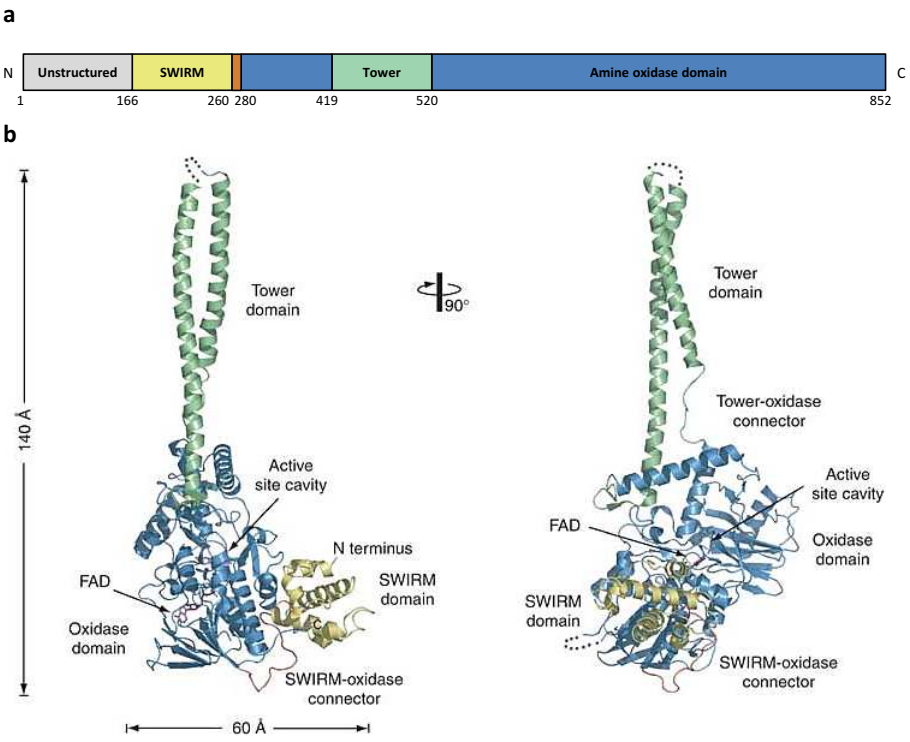

Figure 5.2: Domain organisation and crystal structure of KDM1A in ribbon representation with indicated dimensions (90°-rotated structure is shown on the right). Colours indicate: yellow, SWIRM domain; red, SWIRM-oxidase connector; blue, oxidase domain; green, helical insertion. Adapted from [292].

Being part of essential chromatin targeting complexes, KDM1A is involved in many processes, influencing transcription of target genes as well as regulating DNA methylation and p53 function [294, 295]. It is no surprise that with these multiple mechanisms, overexpression of KDM1A is implicated in many cancer types promoting carcinogenesis, including prostate [132,296] and breast cancer [297], non-small cell lung cancer (NSCLC) [298], blad-

der cancer [299], and neuroblastoma [300]. Although a desired target in cancer therapy, there is a lack of potent inhibitors of KDM1A. The monoamine oxidase inhibitor tranylcypromine was the first to be reported, however it was shown to lack specificity [301].

In recent years, three companies developed small molecule inhibitors, which are currently in clinical trials. Oryzon Genomics S.A. has the KDM1A inhibitor ORY-1001 already in Phase I/IIa trials for acute myelogenous leukemia (AML) [302], while GlaxoSmithKline has various KDM1A inhibitors in preclinical development to treat AML [303]. Salarius Pharmaceuticals LLC has a presumably selective KDM1A inhibitor SP-2528 in preclinical development for cancer [304]. However, considering the functioning of KDM1A in protein complexes, pan-histone demethylase inhibitors simultaneously targeting Jumonji C and lysine-specific demethylases, as in the case for JMJD2C and KDM1A, might be more promising and have already been shown to display higher anticancer activities by leading to growth arrest and apoptosis [305]. In mice, the targeted whole body deletion of *Kdm1a* was reported to result in early embryonic lethality [133]. Foster et al. showed that the gene is essential for embryonic development in the mouse beyond embryonic day 6.5, possibly being involved in regulation of expression and appropriate timing of key developmental regulators. Nevertheless, transcriptional regulation by demethylation does not seem to be the only role of KDM1A. Only recently it was suggested that KDM1A might also play a role in DNA damage response (DDR), by being recruited directly to the site of DNA damage and resulting in a reduction of H3K4 dimethylation in a KDM1A-dependent manner [306].

5.2 Aim of this study

The work described in this chapter aims at elucidating the mechanisms of the second selected follow-up gene identified in the shRNA screen in osteoblast differentiation. In

the screen detailed in chapter 3, knockdown of *KDM1A* by shRNA led to an increase in alkaline phosphatase activity of up to 20-fold (figure 3.16). Here, a new small molecule inhibitor of KDM1A was tested in osteoblast differentiation assays and the expression of osteoblast-related genes was assessed. Furthermore, a transgenic mouse model of *Kdm1a* that became available during this thesis work (kindly provided by Professor Roland Schuele at the University of Freiburg Medical Center, Germany) was studied to investigate the effect of Kdm1a on murine bone development, using both phenotypic analysis of bone and cell-based assays. Interestingly, a study on murine pre-adipocytes had previously shown that the knockdown of *Kdm1a* resulted in markedly decreased adipogenic differentiation, suggesting that Kdm1a is playing a role in the maintenance of methylation status of adipogenic genes [307]. Based on this information and our own preliminary data from the shRNA screen, we hypothesise that mice deficient in *Kdm1a* would have more or denser bone. Moreover, would transgenic mice with an overexpression of Kdm1a have less bone or exhibit lower bone mineral density (BMD)?

5.3 Materials and Methods

5.3.1 Mouse tissue preparation

Mice were sacrificed in Freiburg, Germany, where fur was removed and the lower body parts (not including soft tissue organs) beginning from below the rib cage (from L1 lumbar vertebrae) were transferred into Dulbecco's modified Eagle's medium (DMEM) and shipped at 4°C (delivery within 24 hours). The right leg was removed and bones were isolated and cleaned from soft tissue. The left leg and spine were fixed in formalin for 48 hours and transferred into 70% EtOH for long-term storage and microCT (computed tomography) scanning (figure 5.3).

Figure 5.3: Mouse tissue preparation. Images of preparation, from top left to right bottom: Mouse parts were received and prepared approximately 24 hours after sacrifice. Right leg was removed by rotating out the femoral head. Bones were isolated and cleaned from tissue. Left leg and spine were fixed in formalin for 48 hours and then transferred into 70% EtOH for long-term storage and for microCT scanning. Bones (femur and tibia) from right leg were each cut open at both ends with a sterile scalpel. Using a syringe bone marrow was gently flushed out applying medium pressure. Bones were then used for cell isolation from compact bone (bone chips).

5.3.2 Bone marrow flush

Bones (femur and tibia) from right leg were cut open at both ends with a sterile scalpel. A syringe containing 3ml of basic (mouse) medium (α-MEM containing 10% FBS, 1% P/S, and 2mM glutamine; see appendix A.1) was attached to one end of the bone and the bone marrow was gently flushed out by applying medium pressure. Each bone was flushed approximately three times from each side and all flush contents were gently dispersed into the medium. Cells were counted using Trypan blue (Life Technologies).

5.3.3 MicroCT analysis of mouse long bones

Fixed long bones were prepared as described and stored in 70% EtOH. Each mouse leg was scanned using Skyscan 1174 (Bruker, Belgium) compact microCT scanner, at 50kV, 800µA, 8.3µm isometric voxel resolution, 0.7 degree rotation step, and with a 0.5mm Aluminium filter. The scans were reconstructed using NRecon software from Skyscan. Various measurements and selections were made: a trabecular region of interest (ROI) of 160 slices was identified, by drawing to exclude the bone cortex and include trabecular bone between the growth plate and the diaphysis of the tibia. This represented approximately 1.32mm in length, starting from just below the growth plate. Images were obtained and 3D parameter analysis was performed using Skyscan CT Analyzer software version 1.9.3.0. Trabecular bone volume was measured by setting a threshold for trabecular bone of 80 units corresponding to a BMD of 0.32 g/cm^3. An assessment of total bone content was performed by including both cortical and trabecular bone for a region of 3mm in length, starting from just below the growth plate. Bone volume was measured by setting a threshold for bone of 80 units corresponding to a bone mineral density of 0.32 g/cm^3. For BMD measurements, a cortical selection of 100 slices was performed, by drawing to exclude the trabeculae in a region of the diaphysis of the tibia. This represented approx. 0.8mm in length, at a distance of approximately 3.8mm from the growth plate. Images were obtained and 3D parameter analysis was performed using Skyscan CT Analyzer software version 1.9.3.0. Cortical bone volume was measured by setting a threshold for trabecular bone of 100 units corresponding to a BMD of 0.44 g/cm^3. Bone volume (BV), tissue volume (TV), and bone mineral density (BMD) were determined. For an illustration of different measurement regions see figure 5.4.

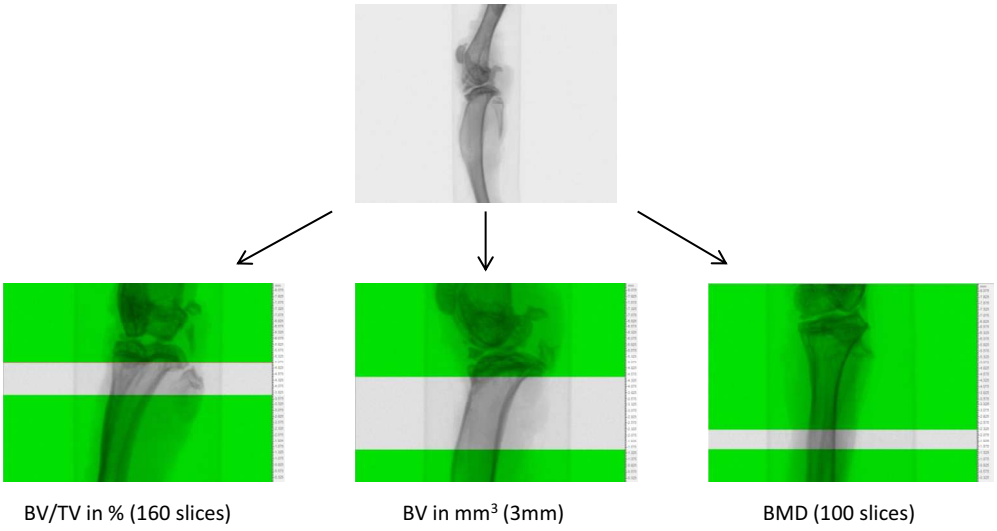

Figure 5.4: MicroCT scan of mouse bones - different measurement areas. Bone volume (BV), tissue volume (TV), bone mineral density (BMD) and connectivity density were determined in different parts of the mouse bone. The grey area indicates the selected area.

5.3.4 Isolation and culture of cells from mouse cortical bone

Using a scalpel, bones were broken into small pieces of approximately 2-3mm in size. Bone fragments were rinsed vigorously in PBS before being incubated in collagenase II solution (2mg/ml) in serum free DMEM for 1 hour at 37°C in a shaking incubator. Collagenase solution was decanted and bone fragments were washed twice in DMEM containing 10% FBS. Bone chips (both femur and tibia from one leg) were plated into one well of a 12 well plate containing medium composed of DMEM, 10% FBS, and 50µg/ml ascorbic acid. Medium was replaced every other day and at each medium change the bone chips were moved around the plate. Cells became visible before 5 days of culture. When confluent, cells were passaged and used for experiments, e.g. alkaline phosphatase assay.

5.3.5 RNA extraction and cDNA synthesis

As previously described (subsection 2.4.4). Expression of genes was tested using cDNA specific primers, targeting housekeeping genes Actin B, *GAPDH*, osteoblast genes *RUNX2*, Osterix (*OSX*), bone sialoprotein (*IBSP*), osteocalcin (*BGLAP*), osteonectin (*SPARC*), and alkaline phosphatase (*ALPL*), and *KDM1A*. PCR was performed for 40 cycles of denaturation (95°C for 20s), annealing (95°C for 1s), and extension (60°C for 1min). The primer sequences can be found in appendix A.2.

5.4 Results

5.4.1 Treatment of human mesenchymal stem cells with a small molecule inhibitor targeting KDM1A leads to an increase in osteoblast gene expression

During the course of this work, a small molecule inhibitor from GSK became available (GSK690, see figure 5.6). The potency of this compound was assessed by a dose-response experiment on human mesenchymal stem cells. Inhibition of KDM1A for one week with addition of the GSK690 compound every other day led to an increase in alkaline phosphatase activity with no impairment of cell viability up to compound concentrations of 10µM. Indeed, the cell viability increased under inhibitor treatment up to 130% of the non-treated control (figure 5.5).

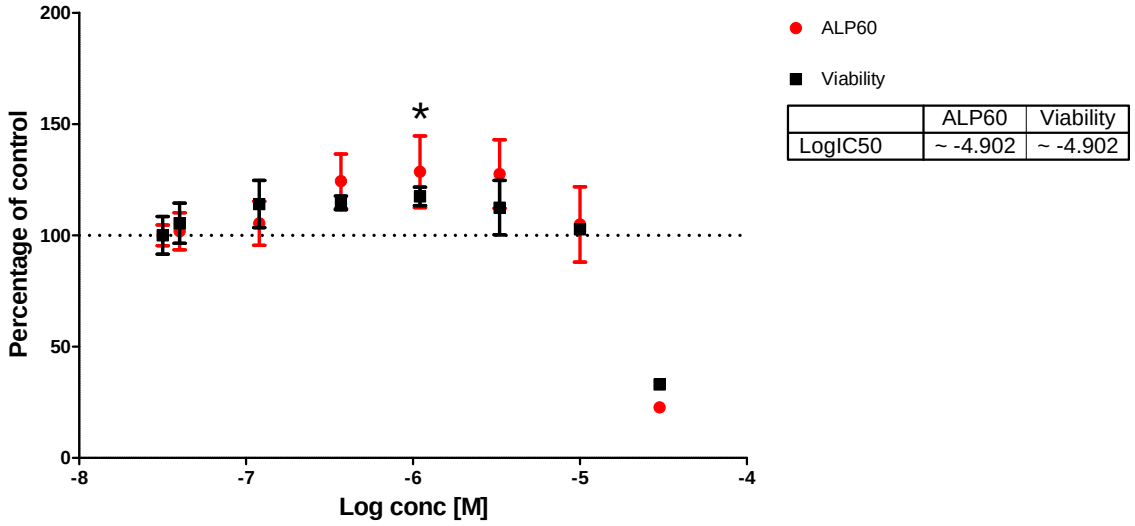

Figure 5.5: Dose response curve using the GSK690 inhibitor. Doses ranged from 0 to 30µM and compound was applied for one week (added with three media changes). P-values for alkaline phosphatase activity were calculated using One-way ANOVA (Dunnett's test - * < 0.05).

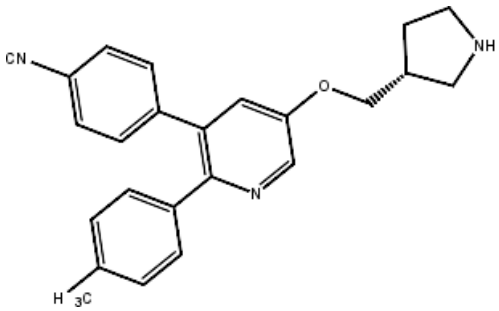

Figure 5.6: Structure of the GSK690 inhibitor

When applied to human mesenchymal stem cells (male and female cell lines) undergoing differentiation for two weeks, treatment with the inhibitor led to a significant increase of bone sialoprotein (*IBSP*) and a 2-fold increase in alkaline phosphatase expression on day 7 of differentiation (figure 5.7). IBSP is a major structural protein of the bone matrix and constitutes approximately 12% of the non-collagenous proteins in human bone. With regard to alkaline phosphatase expression and activity (as shown above), pharmacological inhibition using GSK690 was not as potent as molecular knockdown using shRNA. The female cell line, as displayed in the lower graph of figure 5.7, also showed a slight increase of *RUNX2* and osteocalcin (*BGLAP*) expression compared to the non-treated control as seen on day 7. The target gene *KDM1A* itself was not affected or only

showed a slightly higher expression level on day 7.

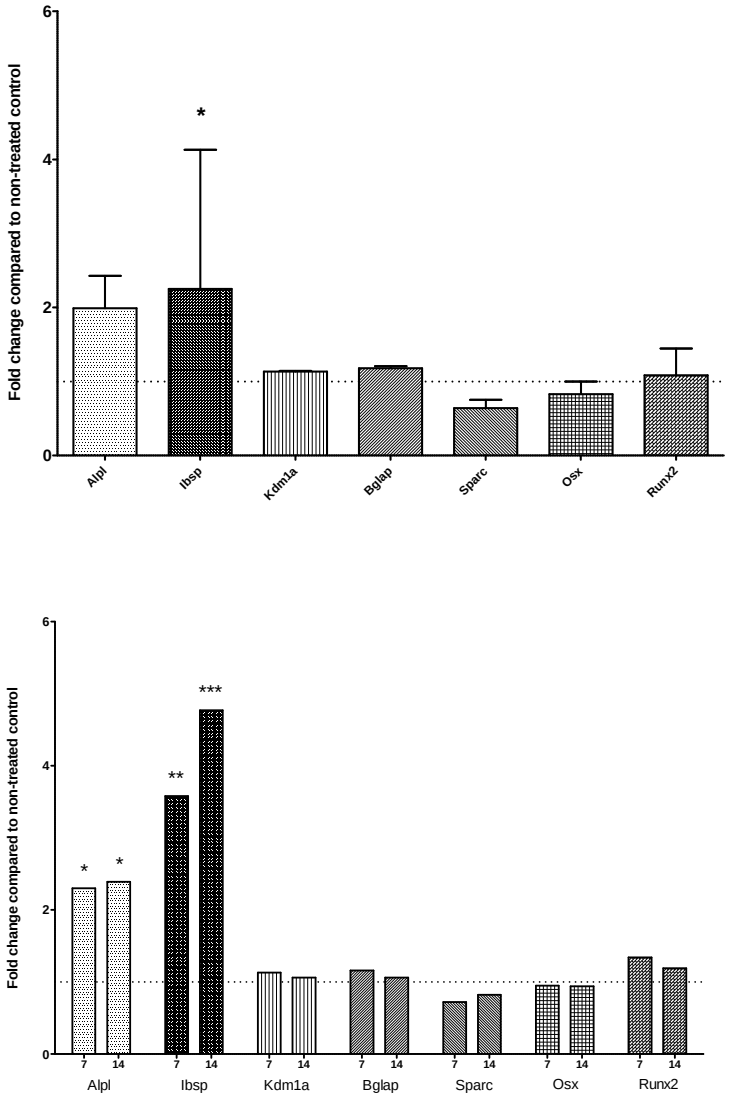

Figure 5.7: Osteoblast gene expression under KDM1A inhibitor (GSK690) treatment. Levels of alkaline phosphatase (*ALPL*), bone sialoprotein (*IBSP*), *KDM1A*, osteocalcin (*BGLAP*), osteonectin (*SPARC*), Osterix (*OSX*), and *RUNX2* were assessed as indicated on the x-axis and shown as fold changes on the y-axis. The upper graph shows gene expression on day 7 for two different cell lines (male and female origin). The lower graph shows gene expression for the female cell line on day 7 and day 14 of treatment. All changes are shown compared to the non-treated DMSO control. Level of DMSO control is indicated by dotted line (=1). P-values were calculated using One-way ANOVA (Bonferroni post test - *** < 0.001, **<0.01, *<0.05).

5.4.2 The transgenic mouse model of *Kdm1a*

Transgenic mice overexpressing Kdm1a approximately 2-fold were bred on an FVB background (personal communication with Roland Schuele). The transgenic mice were generated using pronucleus microinjection and the transgene is driven by the Rosa26 promoter. All mice were assigned to different age cohorts in order to allow a matched comparison. The age difference in the youngest cohort constituted up to four weeks of age, and was slightly expanded in the older cohorts (table 5.1). In this study, mostly females were used and it was ensured that all female mice were not previously used for breeding, as this would affect calcium levels and therefore bone homoeostasis. Two transgenic male mice were analysed (table 5.1 and figure 5.8), but were not included in other data tables or figures. Comparing male mice, with naturally more bone than female mice, to female mice with a transgenic mutation or potential knockout would skew the data; nevertheless it was useful to get baseline values for male mice bone content.

Mouse number	Age in weeks	Genotype	Gender
207	12	Transgenic	Female
208	12	Transgenic	Female
209	12	Transgenic	Female
201	13	Wildtype	Female
202	13	Wildtype	Female
203	13	Transgenic	Female
195	16	Wildtype	Female
196	16	Wildtype	Female
171	74	Transgenic	Female
172	74	Wildtype	Female
133	84	Transgenic	Female
129	86	Wildtype	Female
118	89	Transgenic	Female
119	89	Wildtype	Female
98	99	Wildtype	Male
100	99	Wildtype	Male
88	106	Transgenic	Female
61	116	Wildtype	Female
43	120	Transgenic	Female
44	120	Transgenic	Female
12	128	Wildtype	Female
13	128	Transgenic	Female

Table 5.1: List of transgenic mice and related wild types. Mouse numbers as obtained by collaborator; age cohorts are indicated by colour – green, younger cohort; yellow, middle cohort; red, older cohort; genotype, and gender.

5.4.3 Transgenic mice overexpressing Kdm1a show a significant decrease in trabecular bone volume and bone mineral density

The transgenic mice and their matched controls were grouped into three different cohorts as it can be seen in table 5.1 and figure 5.8. With an ascending age order from left to right a decrease in the ratio of BV to TV in the trabecular region could be observed (figure 5.9). BV/TV represents the ratio (%) of bone volume in comparison to the total tissue volume, i.e. it indicates the fraction of a given volume of interest that is occupied by mineralised bone. Conversely, the BV itself, as measured in 3mm bone starting from below the tibial growth plate, did not show an age-dependent change to such extent (figure 5.8). However,

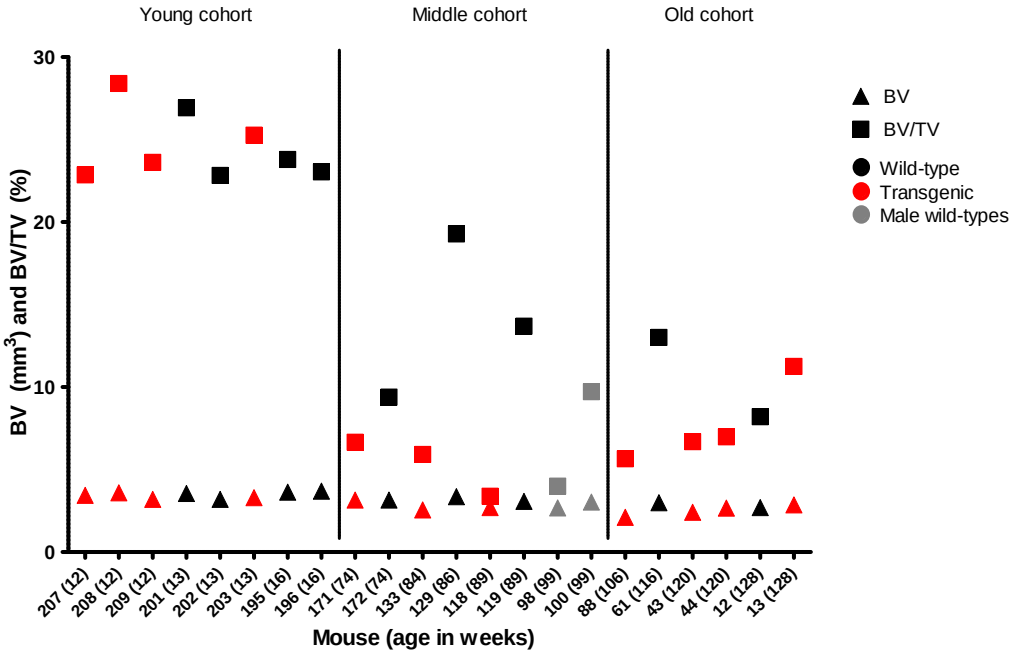

Figure 5.8: BV and BV/TV in different mouse age cohorts. Black symbols represent wild type mice, red symbols represent transgenic mice. In addition, grey symbols are male wild types. Squares represent BV/TV and triangles represent BV.

when comparing BVs of transgenic mice and wild type mice in the middle-aged cohort, the transgenic mice showed on average approximately 15% less total bone volume (in 3mm bone) and only a third of the trabecular bone volume (BV/TV) of wild type mice. Although significance levels ($p<0.05$) were not reached in other age cohorts, it appeared as if a similar general trend could be observed (figure 5.9). Only the young cohort showed a contrasting result with transgenic mice having slightly more trabecular bone volume than the wild type.

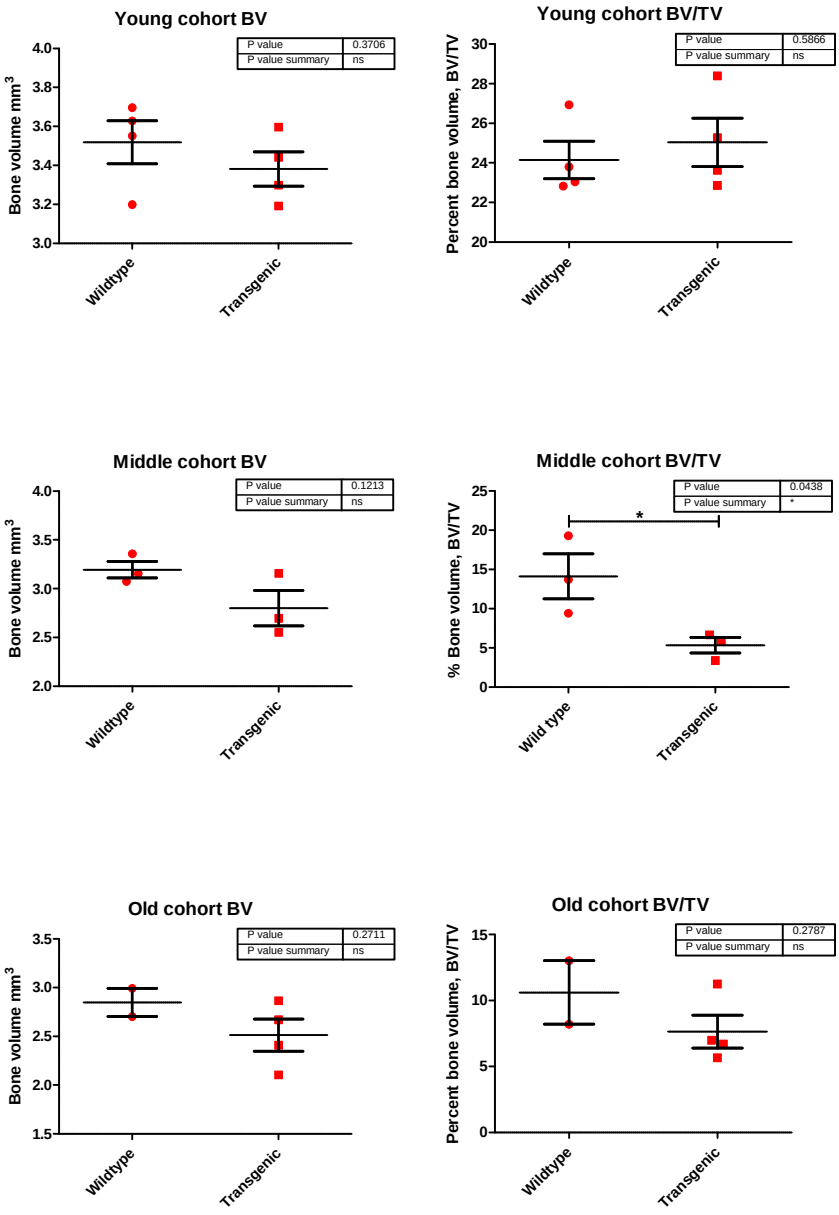

Figure 5.9: BV and BV/TV values as measured for transgenic and wild type mice. The bone value (BV) is specified as mm^3 and the trabecular bone volume as percentage (BV/TV). P-values were calculated with unpaired t-tests. * < 0.05

For illustration (figure 5.10), the trabecular region of transgenic mouse 118 and wild type mouse 119 was rendered using the volume rendering program ImageVis3D (developed by the NIH/NIGMS Center for Integrative Biomedical Computing (CIBC) at the University of Utah). The difference in trabecular volume can be seen in figure 5.8.

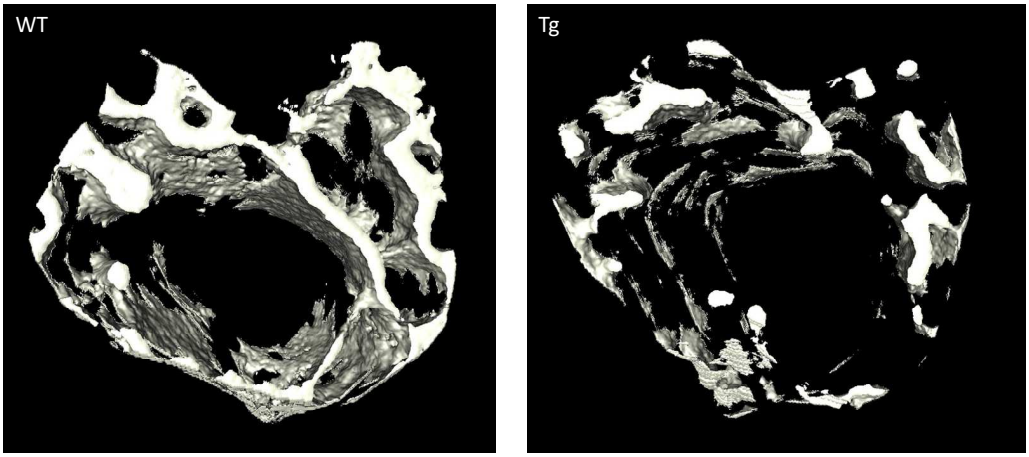

Figure 5.10: Three-dimensional rendered images from MicroCT scanned regions of tibial metaphysis (1.3mm) showed decreased bone volume in the trabecular region of transgenic mice compared to wild type mice.

5.4.3.1 Assessment of bone mineral density

Bone mineral density is defined as the amount and density of minerals, such as calcium and hydroxyapatite, in the bone, and correlates with bone strength and its ability to bear weight. The BMD was measured using a CT scan and expressed as g/cm^3. Using microCT analysis, the BMD can be determined for two different areas: the trabecular region, containing bone and soft tissue (medullary BMD), or only the calcified bone tissue, the cortical region (volumetric BMD). Here, only the cortical region was assessed for BMD. Two reference phantoms with a known mass concentration were used for calibration (0.25 and 0.75 g/cm^3). By linking these mass concentrations with measured x-ray attenuation, a calibration can be made that allows inferring the density from measured attenuation coefficients. Transgenic mice of the youngest cohort showed a significantly lower BMD than the wild type controls with means of 0.84 g/cm^3 for the wild type and 0.8 g/cm^3 for the transgenic mice. Mice in the middle cohort did not show a similar difference in BMD, but here only a smaller set of mice could be assessed (figure 5.11).

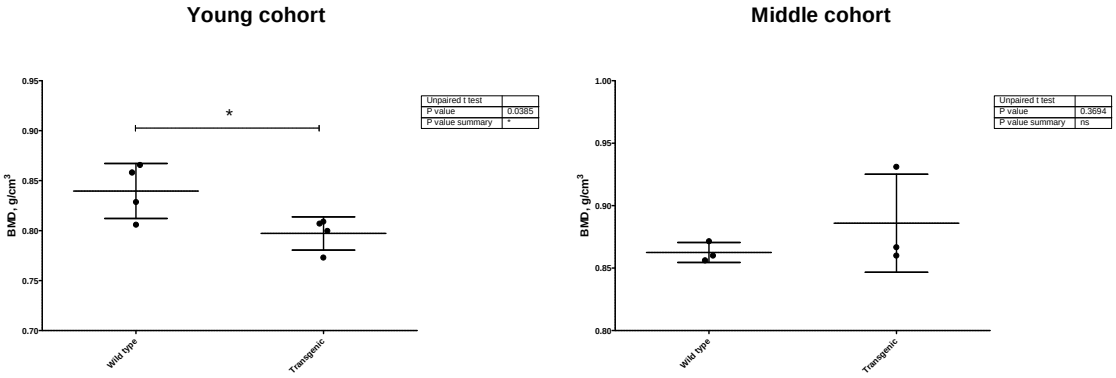

Figure 5.11: Bone mineral density measurement of young (left) and middle (right) cohort transgenic mice. P-values were calculated with unpaired t-tests. * < 0.05

5.4.3.2 Alkaline phosphatase activity measurement in bone chip derived cells

Cells derived from bone chips were cultured in differentiation medium containing dexamethasone for one week before being analysed for alkaline phosphatase activity. When plotted against the bone mineral density of the same mouse, an interesting cross-like pattern was observed: mice of the young transgenic cohort had a higher activity of alkaline phosphatase compared to the wild type control, but conversely, their BMD was significantly lower (figure 5.12). In the middle-aged cohort, this effect was not observed (data not shown).

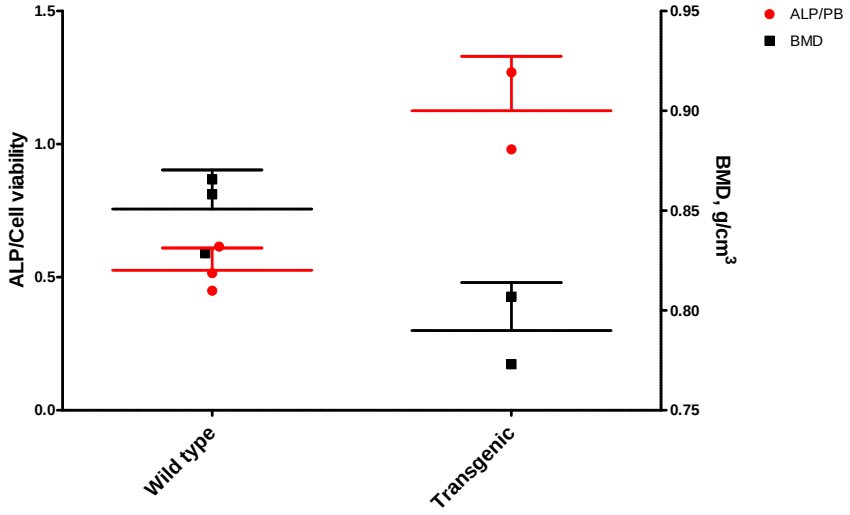

Figure 5.12: Comparison of bone mineral density (BMD) and alkaline phosphatase (ALP)/cell viability (PB) ratio in young cohort transgenic and wild type mice. The activity of ALP normalised to cell viability is shown on the left y-axis, and the BMD on the right y-axis. Red dots indicate ALP levels, and black squares the BMD.

5.5 Conclusion and discussion

Lysine (K)-specific demethylase 1A was a particularly interesting target to work on, as the results from the shRNA screen and small molecule inhibitor screen could not only be validated using a new small molecule inhibitor (GSK690), but also in a transgenic mouse model. In parallel with the *KDM1A*-targeting short hairpin RNAs, the compound tranylcypromine was initially tested in the small molecule inhibitor screen (at a concentration of 10µM) and in both approaches KDM1A was identified as a hit. The non-selective monoamine oxidase inhibitor tranylcypromine was previously shown to also serve as an H3K4 demethylase inhibitor [308], which also increased ALP activity by 25% with no effect on cell viability (chapter 3). However, the compound lacks specificity and is likely inhibiting other monoamine oxidases [301]. A presumably more specific compound targeting KDM1A, GSK690, became available during the course of this work, and was tested on mesenchymal stem cells undergoing osteoblast differentiation as well as on osteoclast differentiation. The effect on MSCs showed a result similar to tranylcypromine, with an increase in ALP activity of around 25% and no detrimental effect on cell viability up to 10µM. In osteoclast differentiation experiments, the compound GSK690 led to a slight decrease in osteoclast number when applied at concentrations of 2 and 5µM, but not at 0.5 µM. Furthermore, although osteoclasts were present in small numbers at higher concentrations, no bone resorption was observed (personal communication with Na Wu, DPhil student). Treatment with GSK690, compared to short hairpin-induced knockout, did not show an increase in ALP activity to the same extent (+25% with the compound compared to up to +1400% with short hairpins). This could however be due to the different biology of compound treatment. KDM1A with its structural features comprising active site, SWIRM domain, and Tower domain, has a range of structural components to be targeted.

It was previously speculated that the Tower domain functions as a connector for other proteins whose binding modulates the size of the active site and allosterically regulates the catalytic activity [292].

Compared to complete knockdown with shRNAs such mechanistic features may remain available under GSK690 treatment, and allow for additional forms of regulation to occur, leading to a less prominent change in alkaline phosphatase activity. Recent suggestions indicate that the repertoire of KMD1A interference may be expanded, predicting that the interface between the SWIRM domain and the amine oxidase domain, as well as the Tower domain, could represent new targets for molecular probes to block association of KDM1A/CoREST with chromatin or other protein partners [309]. Although different in extent, the increase seen in alkaline phosphatase was consistent for both shRNA knockdown and small molecule inhibition. It can be speculated whether the inhibition of a demethylase per se can lead directly to such an increase in ALP activity, or if it is rather a secondary effect based on changes in osteogenic transcription factor levels and related changes in osteoblast gene expression. In a study analysing the relationship between alkaline phosphatase gene expression and the methylation of a CpG island located in its proximal region, the degree of methylation in the CpG island was inversely associated with the transcriptional levels of *ALPL* in the studied cells (primary human osteoblasts (hOBs), the osteoblastic cell line MG-63, and the mammary cell line MCF-7) [310]. The authors also analysed osteocytes, which do not express alkaline phosphatase, and in which the CpG island was highly methylated, whereas lining osteoblasts showed an intermediate degree of methylation. These results suggest a role of DNA methylation in the regulation of ALPL expression at an early stage of osteoblast development, which could also play a role in the differentiation of MSCs into osteoblasts. Although KDM1A has pri-

marily been shown to demethylate histones H3K4 and H3K9, it was suggested that it is also required for maintenance of global DNA methylation. Wang et al. showed that in mouse ES cells, loss of KDM1A correlates with a decrease in DNA methyltransferase 1 (DNMT1), as a result of reduced DNMT1 stability due to lack of demethylation by KDM1A [311]. Likewise, the knockdown of *KDM1A* in MSCs could potentially lead to instability of DNMT1 and corresponding decrease of methylation at promoters of osteoblast related genes such as alkaline phosphatase. In yet another study analysing the expression of several histone demethylases and methyltransferases during adipogenesis, Musri et al. suggested that KDM1A acts to maintain a permissive state of chromatin in the promoter of CCAAT/enhancer-binding protein alpha (CEBPA) by opposing the action of a H3K9 methyltransferase [307]. Knockdown of *KDM1A* resulted in decreased differentiation of pre-adipocytes, whereas knockdown of H3K9 methyltransferase SETDB1 produced the opposite results, favouring differentiation. Interestingly, a similar finding was made in this study, with the knockdown of *SETDB1* leading to a decrease in alkaline phosphatase activity (table 3.2), while knockdown of *KDM1A* increased alkaline phosphatase activity, thus promoting osteogenesis. These findings indicate that the histone methylation status of osteogenic as well as adipogenic genes and the expression and function of the proteins involved in its maintenance play a crucial role in differentiation, particularly with regard to lineage determination in MSCs.

The opportunity to translate findings from *in vitro* models to an *in vivo* environment offered a great addition to the previously performed work. A mouse model to study the overexpression of Kdm1a allowed a first insight into the gene's role in skeletal development. The differences observed in trabecular bone volume, total bone volume, and BMD in the transgenic mice showed a general trend towards a reduction in transgenic mice.

In the young cohort, the consistent reduction in these three parameters was opposed by an increase in alkaline phosphatase as compared to the control. This is an interesting finding and it can be speculated that a lack of mineralisation as seen by BMD reduction is causing a "feedback signalling" leading to an increased activity of alkaline phosphatase. In addition, younger mice with a higher rate of bone remodelling might be more capable of dealing with the effects of a genetic mutation on the skeletal system than older mice. However, this could only be tested in a small number of mice and will have to be repeated in order to prove this hypothesis. Results on osteoclast formation from bone marrow-derived cells from transgenic mice showed no difference in osteoclast number, suggesting that the differences observed were not caused by increased osteoclast formation (data not shown). Further analysis is planned for this transgenic model (chapter 6). In addition, a KDM1A overexpression model for a mesenchymal stem cell line is currently being developed, allowing verification of the observed effect in a cell line. With regard to the differences in bone mineral density, biomechanical analysis such as bend testing could give further information about bone strength and mechanical properties, and the previously scanned bones could be used for this analysis. In addition, histological analyses of bone tissue could give an insight into extracellular matrix formation and cellular distribution in these mice. To confirm changes in alkaline phosphatase expression and activity, alkaline phosphatase could not only be measured in the cells obtained from the mice, but also in the mouse serum; here calcium levels could also be assessed, potentially indicating the rate of bone turnover. With regard to the mouse line used, future experiments will likely be on another genetic background for which both transgenic mice and heterozygous knockout mice are available and for which an intensified collaboration is planned (chapter 6).

6 Discussion and future perspectives

Mesenchymal stem cells are the focus of intensive efforts directed at the development of cell-based therapies; however the lack of knowledge regarding their identity and function limits their envisioned therapeutic potential. In order to overcome this issue, a much better understanding of their nature and mechanisms underlying their lineage determination properties is required. The aim of this thesis was to identify and characterise the epigenetic mechanisms underlying the differentiation of human mesenchymal stem cells into osteoblasts. Here, I provide the first systematic attempt to study epigenetic mechanisms affecting osteoblast differentiation of MSCs. A short list of targets that potentially influence and direct differentiation was generated, of which two target genes were assessed in more detail. In addition, we also provide a list of epigenetic tool compounds tested on mesenchymal stem cells undergoing osteoblast differentiation. These molecules can be utilised further to explore epigenetic mechanisms underlying bone biology and potentially bone diseases. The first objective of this thesis (chapter 2) was to validate published osteoblast differentiation protocols on human MSCs. Available protocols generate a varied response and osteoblasts with different phenotypic characteristics; therefore we aimed to assess the effect of different induction methods with regard to epigenetic factors. An assay determining osteoblast differentiation by measuring alkaline phosphatase activity was employed to screen short hairpin RNAs and small molecule inhibitors (chapter 3). Over 100 stringently selected hits were derived from both shRNA and compound screens, generating a first insight into the role of different epigenetic factors and a solid foundation for further target analysis. Two identified targets, BRD4 and KDM1A, were investigated in further detail to understand phenotypic effects and for both initial results could be confirmed using orthogonal approaches. The opportunity to observe the effect of KDM1A

on bone formation not only independently *in vitro*, but also *in vivo* offers even further possibilities for analysis, and in the future, we will also assess a heterozygous knockout model of *Kdm1a*. Furthermore, we are currently establishing conditional knockout cell lines both for bone marrow derived cells and in addition for osteoblast-like cells derived from bone chips. These cell types will offer the unique possibility to assess whether the effect of Kdm1a is developmental, taking effect in the early stages of differentiation from mesenchymal stem cells to osteoblasts, or if it is a continuous effect also influencing mature osteoblasts.

The application of stem cells in (bone) tissue engineering is still in its infancy as many factors remain unknown, and for the generation of healthy and viable tissue, a number of prerequisites have to be fulfilled. Successful tissue engineering requires not only active and responsive stem cells, but also inducive soluble signals and an extracellular matrix or scaffold, and the combination of the three is not easily achieved [6]. The lack of knowledge regarding the biology of bone marrow-derived mesenchymal stem cells as a source for tissue is a major limitation, as well as the intrinsic restrictions such as tissue origin, availability of cells, as well as cell ageing. In recent years there has been a growing interest in investigating the role of epigenetic modifications in these factors and I presented a literature review on epigenetics involved in osteoblast differentiation in the introduction to this thesis.

Here, I would now like to contrast findings made in this thesis with already published data. In my work, the "reader" domains BRDs and PHDs emerged as major target classes of modulators potentially involved in osteoblast differentiation, however, not much is known about them with regard to published data. The gap in research and publications on "reader" domains might mainly be due to a lack of knowledge regarding these domains, for which only recently potent compounds have been developed (see chapters 3 and 4). Fur-

thermore, for modifications performed by "writers" and "erasers", more opportunities for investigation are present, such as antibodies against certain histone marks, whereas "readers" require more downstream-focussed analysis. The pan-HDAC inhibitor trichostatin A, as presented in subsection 1.4.4, was reported to promote osteoblast differentiation in both adipose-derived MSCs and in BMP-9-mediated osteogenic differentiation of mouse MSCs by increasing RUNX2, ALP, and BGLAP [156]. In our bone marrow-derived and dexamethasone-induced differentiation model, these findings could not be confirmed, and TSA led to a decrease in ALP activity. This first example already shows the difference the tissue origin and the method of differentiation induction can have on the outcome of epigenetic manipulation. Another pan-HDAC inhibitor, SAHA, was reported to decrease gene expression of immature osteoblasts when applied to murine bone marrow-derived adherent cells in vitro, while mature osteoblasts appeared to be resistant to HDAC inhibition [161]. The undifferentiated MSCs utilised in this thesis showed the same results as murine MSCs, supporting the hypothesis that the response of osteoblasts to SAHA is dependent on their differentiation state. The depletion of demethylases *KDM4B* and *KDM6B* by knockdown, as reported by Ye at al., is supposed to reduce osteogenic differentiation, and indeed also in this work, the knockdown of *KDM6B* led to a decrease in ALP activity [162]. However, the shRNA-caused decrease was at the border of significance to categorise *KDM6B* as a target gene. To review our finding, we re-assessed the effect of *KDM6B* knockdown on ALP activity by using locked nucleic acids (LNAs). Here, in addition to our three differentiation induction methods, we also employed BMP-2 and the dimer BMP-4/-7 as inducers, as used in the original publication [162]. And indeed, a higher degree of ALP activity suppression could be observed under BMP-induced differentiation, suggesting that KDM6B-regulated induction of ALP might initially be regulated by BMPs

(data not shown) [162, 312]. The significance of the choice of differentiation induction is also illustrated by the effect of the demethylase NO66 on osteogenic differentiation, as demonstrated by Sinha et al. [163]. In the original publication employing BMP-2-induced differentiation of pre-osteoblasts, the knockdown of NO66 led to accelerated osteoblast differentiation and mineralisation, whereas in our dexamethasone-induced model, it led to a decrease in ALP activity. These examples illustrate the difference the choice of differentiation inducers can have on phenotypic outcomes. Indeed, when a similar induction method is applied, better consistency can be observed. In dexamethasone-induced differentiation of murine mesenchymal stem cells, the knockdown of *Setdb1* severely impaired osteoblast differentiation [166], and also in this work, the knockdown of *SETDB1* led to a decrease in ALP activity under dexamethasone treatment. On the other hand, DNA methyltransferase inhibitor 5-aza-deoxy-cytidine was shown to significantly facilitate osteogenic differentiation when MSCs were pre-treated with the compound for 24 hours prior to osteogenic induction with dexamethasone. Although the same inducer was applied in our work, here at least three other parameters could potentially lead to a difference: the timing of compound treatment (prior to induction vs. together with induction medium), compound concentration (in Zhou et al. [167], 5-azacytidine was applied at a concentration of 10µM, in our study only 5µM were used), and age of cell donor (cells employed in the study from El-Serafi et al. were obtained from donors aged 60-92 [168] , compared to 21 years old in hour study). Furthermore, another factor playing a role is the donor gender - in this work two commercially available cell lines of female and male origin and of approximately the same age (19 and 21 years old, respectively) were employed, and already between the two genders a different response to compound treatment was observed (GSK690, see chapter 5). As this was obviously only a small sample number it does not

allow definite conclusions, however, it also supports the hypothesis that differences in response to treatments or differences in differentiation potential can be caused by a variety of factors.

In summary, these examples demonstrate how different parameters can change the outcome of an experiment and furthermore illustrate how the aforementioned limitations and challenges of MSC differentiation and epigenetic modification analysis are affected by the complexity of parameters involved in differentiation. With our work, we aimed at elucidating the unique effects of various inducers, applying glucocorticoid-induced differentiation, 1,25-dihydroxyvitamin D_3-induced differentiation, as well as differentiation induced by cytokines, analysing pro-inflammatory conditions. We therefore kept all other parameters, such as cell origin, donor age, and other supplements, constant, and the only wilfully applied difference was the change in the main inducer. As presented in chapter 3, many of the derived target genes were unique for one inducing condition, however, no particular pattern with regard to epigenetic domain distribution was observed. In addition, a number of target genes were identified in all of the inducing conditions, suggesting that these genes might play a generic role in osteoblast differentiation independent of the induction method. Within the scope of this thesis, more variable conditions and cells from different tissue origins could not be assessed, but as discussed above, these parameters can have a huge impact on the differentiation outcome. This thesis' work described parts of the parameters that have to be thoroughly assessed before mesenchymal stem cells can be safely applied in tissue engineered-therapies, however I would like take the opportunity and describe ideas for further investigation.

With limited availability of MSCs from bone marrow, the far more abundant adipose tissue-derived cells are likely to gain importance in cell-based tissue engineering. But in

order to ensure the applicability of MSCs from other tissue origins, a better understanding of how differentiation of cells from different sources is achieved is crucial. Screening of epigenetic modulators as performed in this thesis presents an opportunity to generate epigenetic profiles of cells from different origins. Mesenchymal stem cells from different sources, such as bone marrow, adipose tissue, umbilical cord, or dental tissue, could be assessed for the effect of epigenetic modulators involved in osteoblast differentiation. Different responses to e.g. small molecule inhibitors of epigenetic modulators might potentially point towards a tissue-specific difference in osteoblast differentiation and would allow better choice of tissue origin with regard to certain applications. These epigenetic analyses should not only include knockdown and inhibition screenings of epigenetic modulators, but also genome wide analysis of e.g. methylation status [313], or small non-coding RNA expression [314]. Although this is a huge task, obtaining something like an "epigenetic map" for MSCs from different sources, applying various differentiation methods, for e.g. osteogenesis, chondrogenesis, or adipogenesis, could revolutionise the application of MSCs in regenerative medicine. In addition, investigation of the discrete epigenetic profiles of MSCs from different origins as well as of differentiated cells such as osteoblasts and adipocytes could help understanding the disruption of the balance between osteogenic and adipogenic differentiation of MSCs as seen in osteoporosis [315]. A better understanding of how this balance is regulated under normal conditions is highly desirable and might offer new opportunities for therapeutic interventions. Especially for age-related musculoskeletal diseases, a clear understanding of the potential of MSCs can be helpful. With regard to MSCs and ageing, generating a comprehensive epigenetic profile of MSCs from different age groups can provide an important insight into age-related changes in cell potency [316]. Would some of the epigenetic modulators potentially not show an effect anymore, or are

cells derived from certain age groups more sensitive to treatment than others? Being aware of the potential and limitations of cells from each origin and furthermore, knowing about the underlying epigenetic differences and potentially being able to manipulate them, could open new doors for MSC-based tissue engineering. Identifying characteristics for each tissue-derived cell type would facilitate the classification of cells into different potency categories for generating e.g. osteoblasts, or chondrocytes.

The key components for studies like this are potent and selective tool compounds that can be utilised for manipulation and potential treatment. However, the potential of epigenetic modulators as drug targets is often limited because of their wide-spread function. Off-target effects of epigenetics modulating compounds are likely to happen as these modulators have a broad spectrum of effects with specific roles in almost every tissue type. In addition, many epigenetic modulators contain similar domains which make it even more difficult to obtain specific targeting. This was already discussed for the example of (+)-JQ1 and bromodomains in the BET family of proteins (chapter 4), as well as for the monoamine oxidase inhibitor tranylcypromine that in addition to its intended targets monoamine oxidase A (MaoA) and MaoB also targets KDM1 enzymes belonging to the same subfamily of monoamine oxidases (chapter 5). In addition, it was recently discovered that also kinase inhibitors can bind to the active site of BET bromodomain BD1, suggesting that bromodomains are also potential off-targets of diverse kinase inhibitors [317]. Selective and potent compounds are not only important as tools to study the mechanics of epigenetic modifications, but also with regard to potential therapeutic applications and as drug targets. With regard to already tested compounds in cancer therapies (chapter 1), the scientific community is striving to develop more potent and more specific compounds against epigenetic targets not only, but primarily, in cancer biology. The key question is

how specific a compound can be after all, and it is also debatable how specific a compound must be. If a disease requires the inhibition of a certain set of targets of the same protein class, a less specific compound might be desirable, given that other off-target class effects can be prevented. For instance, for cancer cells the main goal is the elimination of proliferating and metastasising cells, which might be more easily achieved using a compound with a broad spectrum of effects. This could of course also be the aim for bone cells, for instance in skeletal pathologies with extensive bone growth such as Fibrodysplasia ossificans progressiva (FOP), or in bone cancer such as the Ewing sarcoma family of tumours, where bone formation and cell proliferation inhibitors would be of great interest. Nevertheless, a selective compound allows better defined assessment of cellular processes and is therefore the main goal of drug development. In addition, the development and improvement of protein- and cell-based assays to determine the selectivity and activity of a compound are equally important.

Once a selective and potent drug is developed, one other important factor is the targeting of the drug. As discussed for off-target effects, also off-tissue effects are unwanted. For our target BRD4, functions in many tissue types are established, thus its application to target e.g. excessive bone formation would be hindered by the risk of off-tissue effects. One way of targeting drugs specifically to bone and avoid widespread off-tissue effects is the coupling of drugs to bone-targeting devices such as bisphosphonates, which are synthetic compounds that are used to inhibit bone resorption in osteoporosis [318]. The effects of nitrogen-containing bisphosphonates consist of an inhibition of bone resorption and an inhibition of calcification. While the latter effect is the consequence of a physical-chemical inhibition of calcium phosphate crystal formation, the former is caused by a decrease in osteoclast activity due to apoptosis and the destruction of the osteoclastic cytoskeleton [318].

Bisphosphonates mimic the structure of pyrophosphate, thereby inhibiting activation of enzymes that utilise pyrophosphate. Farnesyl pyrophosphate synthase (FPPS) is a key enzyme in the mevalonate pathway and its inhibition leads to the loss of prenylated proteins that are essential for osteoclast function [319,320]. Bisphosphonates adsorb very effectively to hydroxyapatite, the crystalline form of calcium and phosphate in bone, and therefore accumulate to a high concentration in bone. A proportion of bisphosphonates that are absorbed is incorporated into bone, while the remaining fraction is excreted unchanged by the kidney. Using bisphosphonates as a carrier for drugs targeted to bone, the risk of off-tissue effects for epigenetic inhibitors could eventually be minimised by increasing the local drug concentration at its intended target site. A similar approach (i.e. tagging of bisphosphonates to a target-ligand scaffold) was already published for prostaglandins and estradiol [321, 322]. Prostaglandins are investigated for application as bone growth stimulator in treatment of osteoporosis and were coupled to bisphosphonates [321]. The conjugates were shown to be well tolerated and offer potential for sustained release and dual synergistic activity through their selective bone targeting, bone resorption inhibition and local release of the active component. Other potential coupling mechanisms are the linkage to tetracycline, which is known to avidly bind to hydroxyapatite [323], or linkage to oligopeptides, such as repeating sequences of aspartate and serine ($(\mathrm{AspSerSer})_6$) which were shown to selectively target bone-formation surfaces [324]. All of these methods are however at the beginning of development and have so far only been tested in animal models.

Consequently, the main focus is yet on developing selective drugs that allow systemic control without adverse effects, an essential factor for the therapeutic use of compounds. Although adverse effects might be more tolerable in diseases such as final stage cancer,

in chronic diseases like rheumatoid arthritis they are undesired. The control of the tissue environment under inflammatory diseases is crucial, and in the bone and joint environment this includes not only osteoblasts, but also osteoclasts, and other cell types such as T cells, B cells, macrophages, and synovial fibroblasts. Before administering a drug that could potentially influence any of the involved cell components, it should be thoroughly assessed for its effect on these different cell types. In the future, we aim to systematically identify epigenetic mechanisms that underlie and control the complex stem cell and inflammatory environment that leads to destruction of bone tissue in arthritis and other musculoskeletal conditions. The work started in this thesis lays the foundation to answer the question if there are epigenetic factors that can be used to understand the spectrum of musculoskeletal pathologies, e.g. bone loss in rheumatoid arthritis (RA) or bone formation and ossification in ankylosing spondylitis (AS). These diseases are characterised by an inflammatory environment and are only an example for the multitude of effects of inflammation on the bone environment, and show that different inflammatory environments against a specific genetic make-up can lead to different outcomes (i.e. excessive bone resorption as seen in RA, and excessive bone formation and fusion of bone in AS) in different autoimmune diseases. Although anti-TNFα therapy is highly effective in these conditions, it is a chronic and costly treatment that does not cure the disease. Validation of potential drug targets to reverse bone loss or prevent bone formation is therefore highly desirable. The two identified targets presented in this thesis (BRD4 and KDM1A), as well as a rich shortlist of further targets support the hypothesis that in principle epigenetic modulators can be possible candidates for novel therapeutic intervention strategies. Intended future work will analyse the complex relationships between different cell types involved in inflammation and the function of chromatin and DNA modifications among

the bone environment elements. We will continue to systematically investigate the potential of epigenetic mechanisms that control mesenchymal stem cell behaviour in relation to inflammation, ageing, and tissue regeneration, building on the technical platforms and identified targets in the work that led to this thesis.

References

[1] T W Bauer and G F Muschler. Bone graft materials. An overview of the basic science. *Clin Orthop Relat Res*, (371):10–27, 2000.

[2] J S Silber, D G Anderson, S D Daffner, B T Brislin, J M Leland, A S Hilibrand, A R Vaccaro, and T J Albert. Donor site morbidity after anterior iliac crest bone harvest for single-level anterior cervical discectomy and fusion. *Spine (Phila Pa 1976)*, 28(2):134–139, 2003.

[3] G E Friedlaender, C R Perry, J D Cole, S D Cook, G Cierny, G F Muschler, G A Zych, J H Calhoun, A J LaForte, and S Yin. Osteogenic protein-1 (bone morphogenetic protein-7) in the treatment of tibial nonunions. *J Bone Joint Surg Am*, 83-A Suppl(Pt 2):S151–8, 2001.

[4] S Govender, C Csimma, H K Genant, A Valentin-Opran, Y Amit, R Arbel, H Aro, D Atar, M Bishay, M G Borner, P Chiron, P Choong, J Cinats, B Courtenay, R Feibel, B Geulette, C Gravel, N Haas, M Raschke, E Hammacher, D van der Velde, P Hardy, M Holt, C Josten, R L Ketterl, B Lindeque, G Lob, H Mathevon, G McCoy, D Marsh, R Miller, E Munting, S Oevre, L Nordsletten, A Patel, A Pohl, W Rennie, P Reynders, P M Rommens, J Rondia, W C Rossouw, P J Daneel, S Ruff, A Ruter, S Santavirta, T A Schildhauer, C Gekle, R Schnettler, D Segal, H Seiler, R B Snowdowne, J Stapert, G Taglang, R Verdonk, L Vogels, A Weckbach, A Wentzensen, and T Wisniewski. Recombinant human bone morphogenetic protein-2 for treatment of open tibial fractures: a prospective, controlled, randomized study of four hundred and fifty patients. *J Bone Joint Surg Am*, 84-A(12):2123–2134, 2002.

[5] W R Moore, S E Graves, and G I Bain. Synthetic bone graft substitutes. *ANZ J Surg*, 71(6):354–361, 2001.

[6] T Morishita, K Honoki, H Ohgushi, N Kotobuki, A Matsushima, and Y Takakura. Tissue engineering approach to the treatment of bone tumors: three cases of cultured bone grafts derived from patients' mesenchymal stem cells. *Artif Organs*, 30(2):115–118, 2006.

[7] J A Inzana, D Olvera, S M Fuller, J P Kelly, O A Graeve, E M Schwarz, S L Kates, and H A Awad. 3D printing of composite calcium phosphate and collagen scaffolds for bone regeneration. *Biomaterials*, 35(13):4026–4034, 2014.

[8] R Tavakoli-darestani, A Manafi-rasi, and A Kamrani-rad. Dexamethasone-loaded hydroxyapatite enhances bone regeneration in rat calvarial defects. *Mol Biol Rep*, 41(1):423–428, 2014.

[9] W Xiao, H Fu, M N Rahaman, Y Liu, and B S Bal. Hollow hydroxyapatite microspheres: a novel bioactive and osteoconductive carrier for controlled release of bone morphogenetic protein-2 in bone regeneration. *Acta Biomater*, 9(9):8374–8383, 2013.

[10] A Hima Bindu and B Srilatha. Potency of Various Types of Stem Cells and their Transplantation. *Stem Cell Research & Therapy*, 1(3), 2011.

[11] M Jones. Stem cells diagram. *Wikimedia Commons [CC-BY-SA-2.5]*, 2006.

[12] K Takahashi and S Yamanaka. Induction of pluripotent stem cells from mouse embryonic and adult fibroblast cultures by defined factors. *Cell*, 126(4):663–676, 2006.

[13] N Rotter, J Oder, P Schlenke, U Lindner, F Bohrnsen, J Kramer, J Rohwedel, R Huss, S Brandau, B Wollenberg, and S Lang. Isolation and characterization of adult stem cells from human salivary glands. *Stem Cells Dev*, 17(3):509–518, 2008.

[14] M Z Ratajczak, B Machalinski, W Wojakowski, J Ratajczak, and M Kucia. A hypothesis for an embryonic origin of pluripotent Oct-4(+) stem cells in adult bone marrow and other tissues. *Leukemia*, 21(5):860–867, 2007.

[15] Y Y Dan and G C Yeoh. Liver stem cells: a scientific and clinical perspective. *J Gastroenterol Hepatol*, 23(5):687–698, 2008.

[16] E Messina, L De Angelis, G Frati, S Morrone, S Chimenti, F Fiordaliso, M Salio, M Battaglia, M V Latronico, M Coletta, E Vivarelli, L Frati, G Cossu, and A Giacomello. Isolation and expansion of adult cardiac stem cells from human and murine heart. *Circ Res*, 95(9):911–921, 2004.

[17] S Massberg, P Schaerli, I Knezevic-Maramica, M Kollnberger, N Tubo, E A Moseman, I V Huff, T Junt, A J Wagers, I B Mazo, and U H von Andrian. Immunosurveillance by hematopoietic progenitor cells trafficking through blood, lymph, and peripheral tissues. *Cell*, 131(5):994–1008, 2007.

[18] C A Roufosse, N C Direkze, W R Otto, and N A Wright. Circulating mesenchymal stem cells. *Int J Biochem Cell Biol*, 36(4):585–597, 2004.

[19] J A Thomson, J Itskovitz-Eldor, S S Shapiro, M A Waknitz, J J Swiergiel, V S Marshall, and J M Jones. Embryonic stem cell lines derived from human blastocysts. *Science*, 282(5391):1145–1147, 1998.

[20] M J Sandel. Embryo ethics–the moral logic of stem-cell research. *N Engl J Med*, 351(3):207–209, 2004.

[21] K Takahashi, K Okita, M Nakagawa, and S Yamanaka. Induction of pluripotent stem cells from fibroblast cultures. *Nat Protoc*, 2(12):3081–3089, 2007.

[22] N Maherali, R Sridharan, W Xie, J Utikal, S Eminli, K Arnold, M Stadtfeld, R Yachechko, J Tchieu, R Jaenisch, K Plath, and K Hochedlinger. Directly reprogrammed fibroblasts show global epigenetic remodeling and widespread tissue contribution. *Cell Stem Cell*, 1(1):55–70, 2007.

[23] M Wernig, A Meissner, R Foreman, T Brambrink, M Ku, K Hochedlinger, B E Bernstein, and R Jaenisch. In vitro reprogramming of fibroblasts into a pluripotent ES-cell-like state. *Nature*, 448(7151):318–324, 2007.

[24] R Lister, M Pelizzola, Y S Kida, R D Hawkins, J R Nery, G Hon, J Antosiewicz-Bourget, R O'Malley, R Castanon, S Klugman, M Downes, R Yu, R Stewart, B Ren, J A Thomson, R M Evans, and J R Ecker. Hotspots of aberrant epigenomic reprogramming in human induced pluripotent stem cells. *Nature*, 471(7336):68–73, 2011.

[25] A Martinez-Fernandez, T J Nelson, and A Terzic. Nuclear reprogramming strategy modulates differentiation potential of induced pluripotent stem cells. *J Cardiovasc Transl Res*, 4(2):131–137, 2011.

[26] A Bird. DNA methylation patterns and epigenetic memory. *Genes Dev*, 16(1):6–21, 2002.

[27] M C Marchetto, G W Yeo, O Kainohana, M Marsala, F H Gage, and A R Muotri. Transcriptional signature and memory retention of human-induced pluripotent stem cells. *PLoS One*, 4(9):e7076, 2009.

[28] F Liu, Y Akiyama, S Tai, K Maruyama, Y Kawaguchi, K Muramatsu, and K Yamaguchi. Changes in the expression of CD106, osteogenic genes, and transcription factors involved in the osteogenic differentiation of human bone marrow mesenchymal stem cells. *J Bone Miner Metab*, 26(4):312–320, 2008.

[29] S Halfon, N Abramov, B Grinblat, and I Ginis. Markers distinguishing mesenchymal stem cells from fibroblasts are downregulated with passaging. *Stem Cells Dev*, 20(1):53–66, 2011.

[30] A J Friedenstein, R K Chailakhjan, and K S Lalykina. The development of fibroblast colonies in monolayer cultures of guinea-pig bone marrow and spleen cells. *Cell Tissue Kinet*, 3(4):393–403, 1970.

[31] A Uccelli, L Moretta, and V Pistoia. Mesenchymal stem cells in health and disease. *Nat Rev Immunol*, 8(9):726–736, 2008.

[32] A I Caplan. Mesenchymal stem cells. *J Orthop Res*, 9(5):641–650, 1991.

[33] P Bianco, P G Robey, and P J Simmons. Mesenchymal stem cells: revisiting history, concepts, and assays. *Cell Stem Cell*, 2(4):313–319, 2008.

[34] P Bianco, P G Robey, I Saggio, and M Riminucci. "Mesenchymal" stem cells in human bone marrow (skeletal stem cells): a critical discussion of their nature, identity, and significance in incurable skeletal disease. *Hum Gene Ther*, 21(9):1057–1066, 2010.

[35] P Bianco, X Cao, P S Frenette, J J Mao, P G Robey, P J Simmons, and C Y Wang. The meaning, the sense and the significance: translating the science of mesenchymal stem cells into medicine. *Nat Med*, 19(1):35–42, 2013.

[36] R Abdi, P Fiorina, C N Adra, M Atkinson, and M H Sayegh. Immunomodulation by mesenchymal stem cells: a potential therapeutic strategy for type 1 diabetes. *Diabetes*, 57(7):1759–1767, 2008.

[37] S M Melief, J J Zwaginga, W E Fibbe, and H Roelofs. Adipose tissue-derived multipotent stromal cells have a higher immunomodulatory capacity than their bone marrow-derived counterparts. *Stem Cells Transl Med*, 2(6):455–463, 2013.

[38] F Barry and M Murphy. Mesenchymal stem cells in joint disease and repair. *Nat Rev Rheumatol*, 2013.

[39] M M Bonab, K Alimoghaddam, F Talebian, S H Ghaffari, A Ghavamzadeh, and B Nikbin. Aging of mesenchymal stem cell in vitro. *BMC Cell Biol*, 7:14, 2006.

[40] S Sethe, A Scutt, and A Stolzing. Aging of mesenchymal stem cells. *Ageing Res Rev*, 5(1):91–116, 2006.

[41] V Sottile, A Thomson, and J McWhir. In vitro osteogenic differentiation of human ES cells. *Cloning Stem Cells*, 5(2):149–155, 2003.

[42] S L Cheng, S F Zhang, and L V Avioli. Expression of bone matrix proteins during dexamethasone-induced mineralization of human bone marrow stromal cells. *J Cell Biochem*, 61(2):182–193, 1996.

[43] J E Phillips, C A Gersbach, A M Wojtowicz, and A J Garcia. Glucocorticoid-induced osteogenesis is negatively regulated by Runx2/Cbfa1 serine phosphorylation. *J Cell Sci*, 119(Pt 3):581–591, 2006.

[44] B W Phillips, N Belmonte, C Vernochet, G Ailhaud, and C Dani. Compactin enhances osteogenesis in murine embryonic stem cells. *Biochem Biophys Res Commun*, 284(2):478–484, 2001.

[45] J Kawaguchi, P J Mee, and A G Smith. Osteogenic and chondrogenic differentiation of embryonic stem cells in response to specific growth factors. *Bone*, 36(5):758–769, 2005.

[46] N I zur Nieden, G Kempka, and H J Ahr. In vitro differentiation of embryonic stem cells into mineralized osteoblasts. *Differentiation*, 71(1):18–27, 2003.

[47] P Malladi, Y Xu, G P Yang, and M T Longaker. Functions of vitamin D, retinoic acid, and dexamethasone in mouse adipose-derived mesenchymal cells. *Tissue Eng*, 12(7):2031–2040, 2006.

[48] P Guihard, Y Danger, B Brounais, E David, R Brion, J Delecrin, C D Richards, S Chevalier, F Redini, D Heymann, H Gascan, and F Blanchard. Induction of osteogenesis in mesenchymal stem cells by activated monocytes/macrophages depends on oncostatin M signaling. *Stem Cells*, 30(4):762–772, 2012.

[49] M J Lee, S C Heo, S H Shin, Y W Kwon, E K Do, D S Suh, M S Yoon, and J H Kim. Oncostatin M promotes mesenchymal stem cell-stimulated tumor growth through a paracrine mechanism involving periostin and TGFBI. *Int J Biochem Cell Biol*, 45(8):1869–1877, 2013.

[50] A I Caplan and S P Bruder. Mesenchymal stem cells: building blocks for molecular medicine in the 21st century. *Trends Mol Med*, 7(6):259–264, 2001.

[51] P Ducy, R Zhang, V Geoffroy, A L Ridall, and G Karsenty. Osf2/Cbfa1: a transcriptional activator of osteoblast differentiation. *Cell*, 89(5):747–754, 1997.

[52] K Nakashima, X Zhou, G Kunkel, Z Zhang, J M Deng, R R Behringer, and B de Crombrugghe. The novel zinc finger-containing transcription factor osterix is required for osteoblast differentiation and bone formation. *Cell*, 108(1):17–29, 2002.

[53] L F Bonewald. The amazing osteocyte. *J Bone Miner Res*, 26(2):229–238, 2011.

[54] J P Bilezikian, L G Raisz, and T J Martin. Principles of Bone Biology, Vol 1, 3rd Edition. *Principles of Bone Biology, Vol 1, 3rd Edition*, pages 1–968, 2008.

[55] N K Lee, H Sowa, E Hinoi, M Ferron, J D Ahn, C Confavreux, R Dacquin, P J Mee, M D McKee, D Y Jung, Z Zhang, J K Kim, F Mauvais-Jarvis, P Ducy, and G Karsenty. Endocrine regulation of energy metabolism by the skeleton. *Cell*, 130(3):456–469, 2007.

[56] G Karsenty and M Ferron. The contribution of bone to whole-organism physiology. *Nature*, 481(7381):314–320, 2012.

[57] Mark S.K. Chong Yuchun Liu Mahesh Choolani Chao Le Meng Bao, Erin Y. Teo and Jerry K.Y. Chan. *Regenerative Medicine and Tissue Engineering*. InTech, May 2013.

[58] T D White, Michael T Black, and Pieter A Folkens. *Human osteology*. Academic Press, San Diego, Calif., 3rd edition, 2012.

[59] Lauren Vedder Ackerman, Harlan J Spjut, and Murray R Abell. *Bones and joints*. Number no 17. Williams & Wilkins, Baltimore, 1976.

[60] F Long. Building strong bones: molecular regulation of the osteoblast lineage. *Nat Rev Mol Cell Biol*, 13(1):27–38, 2012.

[61] J C Crockett, M J Rogers, F P Coxon, L J Hocking, and M H Helfrich. Bone remodelling at a glance. *J Cell Sci*, 124(Pt 7):991–998, 2011.

[62] N Rucci. Molecular biology of bone remodelling. *Clin Cases Miner Bone Metab*, 5(1):49–56, 2008.

[63] J Salo, P Lehenkari, M Mulari, K Metsikko, and H K Vaananen. Removal of osteoclast bone resorption products by transcytosis. *Science*, 276(5310):270–273, 1997.

[64] L G Raisz. Pathogenesis of osteoporosis: concepts, conflicts, and prospects. *J Clin Invest*, 115(12):3318–3325, 2005.

[65] F Rauch and F H Glorieux. Osteogenesis imperfecta. *Lancet*, 363(9418):1377–1385, 2004.

[66] Iain B McInnes and Georg Schett. The pathogenesis of rheumatoid arthritis. *The New England journal of medicine*, 365(23):2205–19, December 2011.

[67] J Sieper, J Braun, M Rudwaleit, A Boonen, and A Zink. Ankylosing spondylitis: an overview. *Ann Rheum Dis*, 61(90003):8iii–18, November 2002.

[68] J A Buckwalter and J A Martin. Osteoarthritis. *Adv Drug Deliv Rev*, 58(2):150–167, 2006.

[69] E M Shore, M Xu, G J Feldman, D A Fenstermacher, T J Cho, I H Choi, J M Connor, P Delai, D L Glaser, M LeMerrer, R Morhart, J G Rogers, R Smith, J T Triffitt, J A Urtizberea, M Zasloff, M A Brown, and F S Kaplan. A recurrent mutation in the BMP type I receptor ACVR1 causes inherited and sporadic fibrodysplasia ossificans progressiva. *Nat Genet*, 38(5):525–527, 2006.

[70] K A Petrie, W H Lee, A N Bullock, J J Pointon, R Smith, R G Russell, M A Brown, B P Wordsworth, and J T Triffitt. Novel mutations in ACVR1 result in atypical features in two fibrodysplasia ossificans progressiva patients. *PLoS One*, 4(3):e5005, 2009.

[71] T Komori. Regulation of osteoblast differentiation by transcription factors. *J Cell Biochem*, 99(5):1233–1239, 2006.

[72] T P Hill, D Spater, M M Taketo, W Birchmeier, and C Hartmann. Canonical Wnt/beta-catenin signaling prevents osteoblasts from differentiating into chondrocytes. *Dev Cell*, 8(5):727–738, 2005.

[73] G Rawadi, B Vayssiere, F Dunn, R Baron, and S Roman-Roman. BMP-2 controls alkaline phosphatase expression and osteoblast mineralization by a Wnt autocrine loop. *J Bone Miner Res*, 18(10):1842–1853, 2003.

[74] K S Lee, H J Kim, Q L Li, X Z Chi, C Ueta, T Komori, J M Wozney, E G Kim, J Y Choi, H M Ryoo, and S C Bae. Runx2 is a common target of transforming growth factor beta1 and bone morphogenetic protein 2, and cooperation between Runx2 and Smad5 induces osteoblast-specific gene expression in the pluripotent mesenchymal precursor cell line C2C12. *Mol Cell Biol*, 20(23):8783–8792, 2000.

[75] J Pratap, J J Wixted, T Gaur, S K Zaidi, J Dobson, K D Gokul, S Hussain, A J van Wijnen, J L Stein, G S Stein, and J B Lian. Runx2 transcriptional activation of Indian Hedgehog and a downstream bone metastatic pathway in breast cancer cells. *Cancer Res*, 68(19):7795–7802, 2008.

[76] T Takarada, E Hinoi, R Nakazato, H Ochi, C Xu, A Tsuchikane, S Takeda, G Karsenty, T Abe, H Kiyonari, and Y Yoneda. An analysis of skeletal development in osteoblast-specific and chondrocyte-specific runt-related transcription factor-2 (Runx2) knockout mice. *J Bone Miner Res*, 28(10):2064–2069, 2013.

[77] D L Diefenderfer, A M Osyczka, G C Reilly, and P S Leboy. BMP responsiveness in human mesenchymal stem cells. *Connect Tissue Res*, 44 Suppl 1:305–311, 2003.

[78] V Viereck, H Siggelkow, S Tauber, D Raddatz, N Schutze, and M Hufner. Differential regulation of Cbfa1/Runx2 and osteocalcin gene expression by vitamin-D3, dexamethasone, and local growth factors in primary human osteoblasts. *J Cell Biochem*, 86(2):348–356, 2002.

[79] B Kuske, V Savkovic, and N I zur Nieden. Improved media compositions for the differentiation of embryonic stem cells into osteoblasts and chondrocytes. *Methods Mol Biol*, 690:195–215, 2011.

[80] A Moustakas, S Souchelnytskyi, and C H Heldin. Smad regulation in TGF-beta signal transduction. *J Cell Sci*, 114(Pt 24):4359–4369, 2001.

[81] R S Weinstein. Glucocorticoid-induced osteoporosis. *Rev Endocr Metab Disord*, 2(1):65–73, 2001.

[82] P A Price and S A Baukol. 1,25-Dihydroxyvitamin D3 increases synthesis of the vitamin K-dependent bone protein by osteosarcoma cells. *J Biol Chem*, 255(24):11660–11663, 1980.

[83] C W Prince and W T Butler. 1,25-Dihydroxyvitamin D3 regulates the biosynthesis of osteopontin, a bone-derived cell attachment protein, in clonal osteoblast-like osteosarcoma cells. *Coll Relat Res*, 7(4):305–313, 1987.

[84] S Takeda, T Yoshizawa, Y Nagai, H Yamato, S Fukumoto, K Sekine, S Kato, T Matsumoto, and T Fujita. Stimulation of osteoclast formation by 1,25-dihydroxyvitamin D requires its binding to vitamin D receptor (VDR) in osteoblastic cells: studies using VDR knockout mice. *Endocrinology*, 140(2):1005–1008, 1999.

[85] F Long. Building strong bones: molecular regulation of the osteoblast lineage. *Nat Rev Mol Cell Biol*, 13(1):27–38, 2012.

[86] A W James. Review of Signaling Pathways Governing MSC Osteogenic and Adipogenic Differentiation. *Scientifica (Cairo)*, 2013:684736, 2013.

[87] D I Becker, S U Toverud, D A Ontjes, and C W Cooper. Circulating calcitonin in lactating women. *J Endocrinol Invest*, 2(2):159–164, 1979.

[88] S Granholm, P Lundberg, and U H Lerner. Calcitonin inhibits osteoclast formation in mouse haematopoetic cells independently of transcriptional regulation by receptor activator of NF-{kappa}B and c-Fms. *J Endocrinol*, 195(3):415–427, 2007.

[89] T Matsui, N Kuramitsu, H Yano, and R Kawashima. Suppressive effect of calcitonin on intestinal absorption of calcium and phosphorus in sheep. *Endocrinol Jpn*, 30(4):485–490, 1983.

[90] M Cochran, M Peacock, G Sachs, and B E Nordin. Renal effects of calcitonin. *Br Med J*, 1(5689):135–137, 1970.

[91] P Jaeger, W Jones, T L Clemens, and J P Hayslett. Evidence that calcitonin stimulates 1,25-dihydroxyvitamin D production and intestinal absorption of calcium in vivo. *J Clin Invest*, 78(2):456–461, 1986.

[92] S Minear, P Leucht, J Jiang, B Liu, A Zeng, C Fuerer, R Nusse, and J A Helms. Wnt proteins promote bone regeneration. *Sci Transl Med*, 2(29):29ra30, 2010.

[93] A Shimoyama, M Wada, F Ikeda, K Hata, T Matsubara, A Nifuji, M Noda, K Amano, A Yamaguchi, R Nishimura, and T Yoneda. Ihh/Gli2 signaling promotes osteoblast differentiation by regulating Runx2 expression and function. *Mol Biol Cell*, 18(7):2411–2418, 2007.

[94] H Hu, M J Hilton, X Tu, K Yu, D M Ornitz, and F Long. Sequential roles of Hedgehog and Wnt signaling in osteoblast development. *Development*, 132(1):49–60, 2005.

[95] C Nusslein-Volhard and E Wieschaus. Mutations affecting segment number and polarity in Drosophila. *Nature*, 287(5785):795–801, 1980.

[96] R Nusse and H E Varmus. Wnt genes. *Cell*, 69(7):1073–1087, 1992.

[97] J Briscoe and P P Therond. The mechanisms of Hedgehog signalling and its roles in development and disease. *Nat Rev Mol Cell Biol*, 14(7):416–429, 2013.

[98] T Yuasa, H Kataoka, N Kinto, M Iwamoto, M Enomoto-Iwamoto, S Iemura, N Ueno, Y Shibata, H Kurosawa, and A Yamaguchi. Sonic hedgehog is involved in osteoblast differentiation by cooperating with BMP-2. *J Cell Physiol*, 193(2):225–232, 2002.

[99] O Levy, E Ruvinov, T Reem, Y Granot, and S Cohen. Highly efficient osteogenic differentiation of human mesenchymal stem cells by eradication of STAT3 signaling. *Int J Biochem Cell Biol*, 42(11):1823–1830, 2010.

[100] Y Mikami, M Asano, M J Honda, and M Takagi. Bone morphogenetic protein 2 and dexamethasone synergistically increase alkaline phosphatase levels through JAK/STAT signaling in C3H10T1/2 cells. *J Cell Physiol*, 223(1):123–133, 2010.

[101] P J Marie. Fibroblast growth factor signaling controlling bone formation: an update. *Gene*, 498(1):1–4, 2012.

[102] D M Ornitz and P J Marie. FGF signaling pathways in endochondral and intramembranous bone development and human genetic disease. *Genes Dev*, 16(12):1446–1465, 2002.

[103] M J Hilton, X Tu, X Wu, S Bai, H Zhao, T Kobayashi, H M Kronenberg, S L Teitelbaum, F P Ross, R Kopan, and F Long. Notch signaling maintains bone marrow mesenchymal progenitors by suppressing osteoblast differentiation. *Nat Med*, 14(3):306–314, 2008.

[104] K Ting, H Vastardis, J B Mulliken, C Soo, A Tieu, H Do, E Kwong, C N Bertolami, H Kawamoto, S Kuroda, and M T Longaker. Human NELL-1 expressed in unilateral coronal synostosis. *J Bone Miner Res*, 14(1):80–89, 1999.

[105] S S Lu, X Zhang, C Soo, T Hsu, A Napoli, T Aghaloo, B M Wu, P Tsou, K Ting, and J C Wang. The osteoinductive properties of Nell-1 in a rat spinal fusion model. *Spine J*, 7(1):50–60, 2007.

[106] T Aghaloo, C M Cowan, Y F Chou, X Zhang, H Lee, S Miao, N Hong, S Kuroda, B Wu, K Ting, and C Soo. Nell-1-induced bone regeneration in calvarial defects. *Am J Pathol*, 169(3):903–915, 2006.

[107] R K Siu, S S Lu, W Li, J Whang, G McNeill, X Zhang, B M Wu, A S Turner, H B Seim 3rd, P Hoang, J C Wang, A A Gertzman, K Ting, and C Soo. Nell-1 protein promotes bone formation in a sheep spinal fusion model. *Tissue Eng Part A*, 17(7-8):1123–1135, 2011.

[108] A W James, A Pan, M Chiang, J N Zara, X Zhang, K Ting, and C Soo. A new function of Nell-1 protein in repressing adipogenic differentiation. *Biochem Biophys Res Commun*, 411(1):126–131, 2011.

[109] C H Waddington. *The strategy of the genes; a discussion of some aspects of theoretical biology.* Allen & Unwin, London„ 1957.

[110] V E A Russo. Epigenetic mechanisms of gene regulation. *Cold Spring Harbor Laboratory Press*, 1996.

[111] E J Richards. Inherited epigenetic variation–revisiting soft inheritance. *Nat Rev Genet*, 7(5):395–401, 2006.

[112] J M Harp, B L Hanson, D E Timm, and G J Bunick. Asymmetries in the nucleosome core particle at 2.5 A resolution. *Acta Crystallogr D Biol Crystallogr*, 56(Pt 12):1513–1534, 2000.

[113] K Luger, A W Mader, R K Richmond, D F Sargent, and T J Richmond. Crystal structure of the nucleosome core particle at 2.8 A resolution. *Nature*, 389(6648):251–260, 1997.

[114] G Arents and E N Moudrianakis. The histone fold: a ubiquitous architectural motif utilized in DNA compaction and protein dimerization. *Proc Natl Acad Sci U S A*, 92(24):11170–11174, 1995.

[115] S Gonzalo. Chromatin Structure. *URL:http://biochem.slu.edu [20 April 2014]*, 2014.

[116] T Kouzarides. Chromatin modifications and their function. *Cell*, 128(4):693–705, 2007.

[117] M Jakovcevski and S Akbarian. Epigenetic mechanisms in neurological disease. *Nat Med*, 18(8):1194–1204, 2012.

[118] E L Putiri and K D Robertson. Epigenetic mechanisms and genome stability. *Clin Epigenetics*, 2(2):299–314, 2011.

[119] E L Greer and Y Shi. Histone methylation: a dynamic mark in health, disease and inheritance. *Nat Rev Genet*, 13(5):343–357, 2012.

[120] V E MacDonald and L J Howe. Histone acetylation: where to go and how to get there. *Epigenetics*, 4(3):139–143, 2009.

[121] R Lu and G G Wang. Tudor: a versatile family of histone methylation 'readers'. *Trends Biochem Sci*, 38(11):546–555, 2013.

[122] H N Du. Transcription, DNA damage and beyond: the roles of histone ubiquitination and deubiquitination. *Curr Protein Pept Sci*, 13(5):447–466, 2012.

[123] D Rossetto, N Avvakumov, and J Cote. Histone phosphorylation: a chromatin modification involved in diverse nuclear events. *Epigenetics*, 7(10):1098–1108, 2012.

[124] K Iqbal, S G Jin, G P Pfeifer, and P E Szabo. Reprogramming of the paternal genome upon fertilization involves genome-wide oxidation of 5-methylcytosine. *Proc Natl Acad Sci U S A*, 108(9):3642–3647, 2011.

[125] R A Copeland, M P Moyer, and V M Richon. Targeting genetic alterations in protein methyltransferases for personalized cancer therapeutics. *Oncogene*, 32(8):939–946, 2013.

[126] Y Wang, Y Li, J I Toth, M D Petroski, Z Zhang, and J C Zhao. N6-methyladenosine modification destabilizes developmental regulators in embryonic stem cells. *Nat Cell Biol*, 16(2):191–198, 2014.

[127] G Zheng, J A Dahl, Y Niu, Y Fu, A Klungland, Y G Yang, and C He. Sprouts of RNA epigenetics: the discovery of mammalian RNA demethylases. *RNA Biol*, 10(6):915–918, 2013.

[128] K D Robertson, E Uzvolgyi, G Liang, C Talmadge, J Sumegi, F A Gonzales, and P A Jones. The human DNA methyltransferases (DNMTs) 1, 3a and 3b: coordinate mRNA expression in normal tissues and overexpression in tumors. *Nucleic Acids Res*, 27(11):2291–2298, 1999.

[129] E Ballestar and A P Wolffe. Methyl-CpG-binding proteins. Targeting specific gene repression. *Eur J Biochem*, 268(1):1–6, 2001.

[130] M T Pedersen and K Helin. Histone demethylases in development and disease. *Trends Cell Biol*, 20(11):662–671, 2010.

[131] Y Shi, F Lan, C Matson, P Mulligan, J R Whetstine, P A Cole, and R A Casero. Histone demethylation mediated by the nuclear amine oxidase homolog LSD1. *Cell*, 119(7):941–953, 2004.

[132] E Metzger, M Wissmann, N Yin, J M Muller, R Schneider, A H Peters, T Gunther, R Buettner, and R Schule. LSD1 demethylates repressive histone marks to promote androgen-receptor-dependent transcription. *Nature*, 437(7057):436–439, 2005.

[133] C T Foster, O M Dovey, L Lezina, J L Luo, T W Gant, N Barlev, A Bradley, and S M Cowley. Lysine-specific demethylase 1 regulates the embryonic transcriptome and CoREST stability. *Mol Cell Biol*, 30(20):4851–4863, 2010.

[134] Y Wang, J Wysocka, J Sayegh, Y H Lee, J R Perlin, L Leonelli, L S Sonbuchner, C H McDonald, R G Cook, Y Dou, R G Roeder, S Clarke, M R Stallcup, C D Allis, and S A Coonrod. Human PAD4 regulates histone arginine methylation levels via demethylimination. *Science*, 306(5694):279–283, 2004.

[135] G L Cuthbert, S Daujat, A W Snowden, H Erdjument-Bromage, T Hagiwara, M Yamada, R Schneider, P D Gregory, P Tempst, A J Bannister, and T Kouzarides. Histone deimination antagonizes arginine methylation. *Cell*, 118(5):545–553, 2004.

[136] Y Tsukada, J Fang, H Erdjument-Bromage, M E Warren, C H Borchers, P Tempst, and Y Zhang. Histone demethylation by a family of JmjC domain-containing proteins. *Nature*, 439(7078):811–816, 2006.

[137] T Takeuchi, Y Yamazaki, Y Katoh-Fukui, R Tsuchiya, S Kondo, J Motoyama, and T Higashinakagawa. Gene trap capture of a novel mouse gene, jumonji, required for neural tube formation. *Genes Dev*, 9(10):1211–1222, 1995.

[138] K K Lee and J L Workman. Histone acetyltransferase complexes: one size doesn't fit all. *Nat Rev Mol Cell Biol*, 8(4):284–295, 2007.

[139] M Dokmanovic, C Clarke, and P A Marks. Histone deacetylase inhibitors: overview and perspectives. *Mol Cancer Res*, 5(10):981–989, 2007.

[140] M Yoshida, M Kijima, M Akita, and T Beppu. Potent and specific inhibition of mammalian histone deacetylase both in vivo and in vitro by trichostatin A. *J Biol Chem*, 265(28):17174–17179, 1990.

[141] G Blander and L Guarente. The Sir2 family of protein deacetylases. *Annu Rev Biochem*, 73:417–435, 2004.

[142] B J North and E Verdin. Sirtuins: Sir2-related NAD-dependent protein deacetylases. *Genome Biol*, 5(5):224, 2004.

[143] L Gao, M A Cueto, F Asselbergs, and P Atadja. Cloning and functional characterization of HDAC11, a novel member of the human histone deacetylase family. *J Biol Chem*, 277(28):25748–25755, 2002.

[144] H Hess-Stumpp. Histone deacetylase inhibitors and cancer: from cell biology to the clinic. *Eur J Cell Biol*, 84(2-3):109–121, 2005.

[145] R Somech, S Izraeli, and J Simon A. Histone deacetylase inhibitors–a new tool to treat cancer. *Cancer Treat Rev*, 30(5):461–472, 2004.

[146] J S Carew, F J Giles, and S T Nawrocki. Histone deacetylase inhibitors: mechanisms of cell death and promise in combination cancer therapy. *Cancer Lett*, 269(1):7–17, 2008.

[147] W W Hancock, T Akimova, U H Beier, Y Liu, and L Wang. HDAC inhibitor therapy in autoimmunity and transplantation. *Ann Rheum Dis*, 71 Suppl 2:i46–54, 2012.

[148] L Zeng and M M Zhou. Bromodomain: an acetyl-lysine binding domain. *FEBS Lett*, 513(1):124–128, 2002.

[149] R Marmorstein and S L Berger. Structure and function of bromodomains in chromatin-regulating complexes. *Gene*, 272(1-2):1–9, 2001.

[150] S Muller, P Filippakopoulos, and S Knapp. Bromodomains as therapeutic targets. *Expert Rev Mol Med*, 13:e29, 2011.

[151] P Filippakopoulos, S Picaud, M Mangos, T Keates, J P Lambert, D Barsyte-Lovejoy, I Felletar, R Volkmer, S Muller, T Pawson, A C Gingras, C H Arrowsmith, and S Knapp. Histone recognition and large-scale structural analysis of the human bromodomain family. *Cell*, 149(1):214–231, 2012.

[152] P Filippakopoulos, J Qi, S Picaud, Y Shen, W B Smith, O Fedorov, E M Morse, T Keates, T T Hickman, I Felletar, M Philpott, S Munro, M R McKeown, Y Wang, A L Christie, N West, M J Cameron, B Schwartz, T D Heightman, N La Thangue, C A French, O Wiest, A L Kung, S Knapp, and J E Bradner. Selective inhibition of BET bromodomains. *Nature*, 468(7327):1067–1073, 2010.

[153] D J Owen, P Ornaghi, J C Yang, N Lowe, P R Evans, P Ballario, D Neuhaus, P Filetici, and A A Travers. The structural basis for the recognition of acetylated histone H4 by the bromodomain of histone acetyltransferase gcn5p. *EMBO J*, 19(22):6141–6149, 2000.

[154] Z Yang, J H Yik, R Chen, N He, M K Jang, K Ozato, and Q Zhou. Recruitment of P-TEFb for stimulation of transcriptional elongation by the bromodomain protein Brd4. *Mol Cell*, 19(4):535–545, 2005.

[155] Z Yang, N He, and Q Zhou. Brd4 recruits P-TEFb to chromosomes at late mitosis to promote G1 gene expression and cell cycle progression. *Mol Cell Biol*, 28(3):967–976, 2008.

[156] P Maroni, A T Brini, E Arrigoni, L de Girolamo, S Niada, E Matteucci, P Bendinelli, and M A Desiderio. Chemical and genetic blockade of HDACs enhances osteogenic differentiation of human adipose tissue-derived stem cells by oppositely affecting osteogenic and adipogenic transcription factors. *Biochem Biophys Res Commun*, 428(2):271–277, 2012.

[157] N Hu, C Wang, X Liang, L Yin, X Luo, B Liu, H Zhang, W Shui, G Nan, N Wang, N Wu, X Chen, Y He, S Wen, F Deng, Z Liao, H H Luu, R C Haydon, T C He, and W Huang. Inhibition of Histone Deacetylases Potentiates BMP9-Induced Osteogenic

Signaling in Mouse Mesenchymal Stem Cells. *Cell Physiol Biochem*, 32(2):486–498, 2013.

[158] T M Schroeder, R A Kahler, X Li, and J J Westendorf. Histone deacetylase 3 interacts with runx2 to repress the osteocalcin promoter and regulate osteoblast differentiation. *J Biol Chem*, 279(40):41998–42007, 2004.

[159] M E McGee-Lawrence, E W Bradley, A Dudakovic, S W Carlson, Z C Ryan, R Kumar, M Dadsetan, M J Yaszemski, Q Chen, K N An, and J J Westendorf. Histone deacetylase 3 is required for maintenance of bone mass during aging. *Bone*, 52(1):296–307, 2013.

[160] L Pham, B Kaiser, A Romsa, T Schwarz, R Gopalakrishnan, E D Jensen, and K C Mansky. HDAC3 and HDAC7 have opposite effects on osteoclast differentiation. *J Biol Chem*, 286(14):12056–12065, 2011.

[161] M E McGee-Lawrence, A L McCleary-Wheeler, F J Secreto, D F Razidlo, M Zhang, B A Stensgard, X Li, G S Stein, J B Lian, and J J Westendorf. Suberoylanilide hydroxamic acid (SAHA; vorinostat) causes bone loss by inhibiting immature osteoblasts. *Bone*, 48(5):1117–1126, 2011.

[162] L Ye, Z Fan, B Yu, J Chang, K Al Hezaimi, X Zhou, N H Park, and C Y Wang. Histone Demethylases KDM4B and KDM6B Promotes Osteogenic Differentiation of Human MSCs. *Cell Stem Cell*, 11(1):50–61, 2012.

[163] K M Sinha, H Yasuda, M M Coombes, S Y Dent, and B de Crombrugghe. Regulation of the osteoblast-specific transcription factor Osterix by NO66, a Jumonji family histone demethylase. *EMBO J*, 29(1):68–79, 2010.

[164] S Hemming, D Cakouros, S Isenmann, L Cooper, D Menicanin, A Zannettino, and S Gronthos. EZH2 and KDM6A act as an epigenetic switch to regulate mesenchymal stem cell lineage specification. *Stem Cells*, 2013.

[165] Y Wei, Y H Chen, L Y Li, J Lang, S P Yeh, B Shi, C C Yang, J Y Yang, C Y Lin, C C Lai, and M C Hung. CDK1-dependent phosphorylation of EZH2 suppresses methylation of H3K27 and promotes osteogenic differentiation of human mesenchymal stem cells. *Nat Cell Biol*, 13(1):87–94, 2011.

[166] K A Lawson, C J Teteak, J Gao, N Li, J Hacquebord, A Ghatan, A Zielinska-Kwiatkowska, G Song, H A Chansky, and L Yang. ESET histone methyltransferase regulates osteoblastic differentiation of mesenchymal stem cells during postnatal bone development. *FEBS Lett*, 2013.

[167] G S Zhou, X L Zhang, J P Wu, R P Zhang, L X Xiang, L C Dai, and J Z Shao. 5-Azacytidine facilitates osteogenic gene expression and differentiation of mesenchymal stem cells by alteration in DNA methylation. *Cytotechnology*, 2009.

[168] A T El-Serafi, R O Oreffo, and H I Roach. Epigenetic modifiers influence lineage commitment of human bone marrow stromal cells: Differential effects of 5-aza-deoxycytidine and trichostatin A. *Differentiation*, 81(1):35–41, 2011.

[169] N R Jorgensen, Z Henriksen, O H Sorensen, and R Civitelli. Dexamethasone, BMP-2, and 1,25-dihydroxyvitamin D enhance a more differentiated osteoblast phenotype: validation of an in vitro model for human bone marrow-derived primary osteoblasts. *Steroids*, 69(4):219–226, 2004.

[170] G Mazziotti, A Angeli, J P Bilezikian, E Canalis, and A Giustina. Glucocorticoid-induced osteoporosis: an update. *Trends Endocrinol Metab*, 17(4):144–149, 2006.

[171] E Canalis and A M Delany. Mechanisms of glucocorticoid action in bone. *Neuroendocrine Immune Basis of the Rheumatic Diseases Ii, Proceedings*, 966:73–81, 2002.

[172] I V Arutyunyan, A A Rzhaninova, A V Volkov, and D V Goldstein. Effect of dexamethasone on differentiation of multipotent stromal cells from human adipose tissue. *Bull Exp Biol Med*, 147(4):503–508, 2009.

[173] S L Cheng, J W Yang, L Rifas, S F Zhang, and L V Avioli. Differentiation of human bone marrow osteogenic stromal cells in vitro: induction of the osteoblast phenotype by dexamethasone. *Endocrinology*, 134(1):277–286, 1994.

[174] M Eijken, M Koedam, M van Driel, C J Buurman, H A Pols, and J P van Leeuwen. The essential role of glucocorticoids for proper human osteoblast differentiation and matrix mineralization. *Mol Cell Endocrinol*, 248(1-2):87–93, 2006.

[175] A Dostert and T Heinzel. Negative glucocorticoid receptor response elements and their role in glucocorticoid action. *Curr Pharm Des*, 10(23):2807–2816, 2004.

[176] G Pelaia, A Vatrella, G Cuda, R Maselli, and S A Marsico. Molecular mechanisms of corticosteroid actions in chronic inflammatory airway diseases. *Life Sci*, 72(14):1549–1561, 2003.

[177] A A Hidalgo, K K Deeb, J W Pike, C S Johnson, and D L Trump. Dexamethasone Enhances 1{alpha},25-Dihydroxyvitamin D3 Effects by Increasing Vitamin D Receptor Transcription. *J Biol Chem*, 286(42):36228–36237, 2011.

[178] C G Bellows, Y H Wang, J N Heersche, and J E Aubin. 1,25-dihydroxyvitamin D3 stimulates adipocyte differentiation in cultures of fetal rat calvaria cells: comparison with the effects of dexamethasone. *Endocrinology*, 134(5):2221–2229, 1994.

[179] K A Kelly and J M Gimble. 1,25-Dihydroxy vitamin D3 inhibits adipocyte differentiation and gene expression in murine bone marrow stromal cell clones and primary cultures. *Endocrinology*, 139(5):2622–2628, 1998.

[180] M van Driel, H A Pols, and J P van Leeuwen. Osteoblast differentiation and control by vitamin D and vitamin D metabolites. *Curr Pharm Des*, 10(21):2535–2555, 2004.

[181] H Skjodt, J A Gallagher, J N Beresford, M Couch, J W Poser, and R G Russell. Vitamin D metabolites regulate osteocalcin synthesis and proliferation of human bone cells in vitro. *J Endocrinol*, 105(3):391–396, 1985.

[182] J N Beresford, C J Joyner, C Devlin, and J T Triffitt. The effects of dexamethasone and 1,25-dihydroxyvitamin D3 on osteogenic differentiation of human marrow stromal cells in vitro. *Arch Oral Biol*, 39(11):941–947, 1994.

[183] Y C Li, A E Pirro, M Amling, G Delling, R Baron, R Bronson, and M B Demay. Targeted ablation of the vitamin D receptor: an animal model of vitamin D-dependent rickets type II with alopecia. *Proc Natl Acad Sci U S A*, 94(18):9831–9835, 1997.

[184] M R Haussler, G K Whitfield, C A Haussler, J C Hsieh, P D Thompson, S H Selznick, C E Dominguez, and P W Jurutka. The nuclear vitamin D receptor: biological and molecular regulatory properties revealed. *J Bone Miner Res*, 13(3):325–349, 1998.

[185] A H Reddi. Role of morphogenetic proteins in skeletal tissue engineering and regeneration. *Nat Biotechnol*, 16(3):247–252, 1998.

[186] M Fujii, K Takeda, T Imamura, H Aoki, T K Sampath, S Enomoto, M Kawabata, M Kato, H Ichijo, and K Miyazono. Roles of bone morphogenetic protein type I receptors and Smad proteins in osteoblast and chondroblast differentiation. *Mol Biol Cell*, 10(11):3801–3813, 1999.

[187] T Ebisawa, K Tada, I Kitajima, K Tojo, T K Sampath, M Kawabata, K Miyazono, and T Imamura. Characterization of bone morphogenetic protein-6 signaling pathways in osteoblast differentiation. *J Cell Sci*, 112 (Pt 2:3519–3527, 1999.

[188] C F Lai and S L Cheng. Signal transductions induced by bone morphogenetic protein-2 and transforming growth factor-beta in normal human osteoblastic cells. *J Biol Chem*, 277(18):15514–15522, 2002.

[189] Y Chen, H C Whetstone, A Youn, P Nadesan, E C Chow, A C Lin, and B A Alman. Beta-catenin signaling pathway is crucial for bone morphogenetic protein 2 to induce new bone formation. *J Biol Chem*, 282(1):526–533, 2007.

[190] I S Kim, Y M Song, T H Cho, Y D Park, K B Lee, I Noh, F Weber, and S J Hwang. In vitro response of primary human bone marrow stromal cells to recombinant human bone morphogenic protein-2 in the early and late stages of osteoblast differentiation. *Dev Growth Differ*, 50(7):553–564, 2008.

[191] F J Hughes, W Turner, G Belibasakis, and G Martuscelli. Effects of growth factors and cytokines on osteoblast differentiation. *Periodontology 2000*, 41:48–72, 2006.

[192] C D Richards. The Enigmatic Cytokine Oncostatin M and Roles in Disease. *ISRN Inflamm*, 2013:512103, 2013.

[193] V Nicolaidou, M M Wong, A N Redpath, A Ersek, D F Baban, L M Williams, A P Cope, and N J Horwood. Monocytes Induce STAT3 Activation in Human Mesenchymal Stem Cells to Promote Osteoblast Formation. *PLoS One*, 7(7):e39871, 2012.

[194] C Chipoy, M Berreur, S Couillaud, G Pradal, F Vallette, C Colombeix, F Redini, D Heymann, and F Blanchard. Downregulation of osteoblast markers and induction of the glial fibrillary acidic protein by oncostatin M in osteosarcoma cells require PKCdelta and STAT3. *J Bone Miner Res*, 19(11):1850–1861, 2004.

[195] S Kawauchi, H Terasaki, M Katano, J Murase, Y Masuda, T Tamura, and M Shimadzu. Quality control and monitoring for the isolation process of mesenchymal stem cells and their differentiation into osteoblasts. *Genet Test Mol Biomarkers*, 14(2):269–282, 2010.

[196] M Ishii, C Koike, A Igarashi, K Yamanaka, H Pan, Y Higashi, H Kawaguchi, M Sugiyama, N Kamata, T Iwata, T Matsubara, K Nakamura, H Kurihara, K Tsuji, and Y Kato. Molecular markers distinguish bone marrow mesenchymal stem cells from fibroblasts. *Biochem Biophys Res Commun*, 332(1):297–303, 2005.

[197] Y Sasaki, H Negishi, R Koyama, N Anbo, K Ohori, M Idogawa, H Mita, M Toyota, K Imai, Y Shinomura, and T Tokino. p53 family members regulate the expression of the apolipoprotein D gene. *J Biol Chem*, 284(2):872–883, 2009.

[198] Z Liu, G Q Chang, and S F Leibowitz. Apolipoprotein D interacts with the long-form leptin receptor: a hypothalamic function in the control of energy homeostasis. *FASEB J*, 15(7):1329–1331, 2001.

[199] T Shingai, W Ikeda, S Kakunaga, K Morimoto, K Takekuni, S Itoh, K Satoh, M Takeuchi, T Imai, M Monden, and Y Takai. Implications of nectin-like molecule-2/IGSF4/RA175/SgIGSF/TSLC1/SynCAM1 in cell-cell adhesion and transmembrane protein localization in epithelial cells. *J Biol Chem*, 278(37):35421–35427, 2003.

[200] B Edderkaoui, D J Baylink, W G Beamer, J E Wergedal, R Porte, A Chaudhuri, and S Mohan. Identification of mouse Duffy antigen receptor for chemokines (Darc) as a BMD QTL gene. *Genome Res*, 17(5):577–585, 2007.

[201] A P Rehn, A M Chalk, and M Wendel. Differential regulation of osteoadherin (OSAD) by TGF-beta1 and BMP-2. *Biochem Biophys Res Commun*, 349(3):1057–1064, 2006.

[202] E S Tasheva, B Klocke, and G W Conrad. Analysis of transcriptional regulation of the small leucine rich proteoglycans. *Mol Vis*, 10:758–772, 2004.

[203] K Ninomiya, T Miyamoto, J Imai, N Fujita, T Suzuki, R Iwasaki, M Yagi, S Watanabe, Y Toyama, and T Suda. Osteoclastic activity induces osteomodulin expression in osteoblasts. *Biochem Biophys Res Commun*, 362(2):460–466, 2007.

[204] K Sivasubramaniyan, A Harichandan, S Schumann, M Sobiesiak, C Lengerke, A Maurer, H Kalbacher, and H J Buhring. Prospective isolation of mesenchymal stem cells from human bone marrow using novel antibodies directed against Sushi domain containing 2. *Stem Cells Dev*, 22(13):1944–1954, 2013.

[205] T Thomas, F Gori, S Khosla, M D Jensen, B Burguera, and B L Riggs. Leptin acts on human marrow stromal cells to enhance differentiation to osteoblasts and to inhibit differentiation to adipocytes. *Endocrinology*, 140(4):1630–1638, 1999.

[206] E L Scheller, J Song, M I Dishowitz, F N Soki, K D Hankenson, and P H Krebsbach. Leptin functions peripherally to regulate differentiation of mesenchymal progenitor cells. *Stem Cells*, 28(6):1071–1080, 2010.

[207] IPA. The [networks, functional analyses, etc.] were generated through the use of IPA (Ingenuity Systems, www.ingenuity.com).

[208] J C Prior. Progesterone as a bone-trophic hormone. *Endocr Rev*, 11(2):386–398, 1990.

[209] V Seifert-Klauss and J C Prior. Progesterone and bone: actions promoting bone health in women. *J Osteoporos*, 2010:845180, 2010.

[210] H N Fernley and P G Walker. Kinetic behaviour of calf-intestinal alkaline phosphatase with 4-methylumbelliferyl phosphate. *Biochem J*, 97(1):95–103, 1965.

[211] A Fire, S Xu, M K Montgomery, S A Kostas, S E Driver, and C C Mello. Potent and specific genetic interference by double-stranded RNA in Caenorhabditis elegans. *Nature*, 391(6669):806–811, 1998.

[212] D J Obbard, K H Gordon, A H Buck, and F M Jiggins. The evolution of RNAi as a defence against viruses and transposable elements. *Philos Trans R Soc Lond B Biol Sci*, 364(1513):99–115, 2009.

[213] S A Stewart, D M Dykxhoorn, D Palliser, H Mizuno, E Y Yu, D S An, D M Sabatini, I S Chen, W C Hahn, P A Sharp, R A Weinberg, and C D Novina. Lentivirus-delivered stable gene silencing by RNAi in primary cells. *RNA*, 9(4):493–501, 2003.

[214] D Cojocari. ShRNA lentivirus. *Wikimedia Commons [CC BY-SA 3.0]*, 2009.

[215] Y Deng, C C Wang, K W Choy, Q Du, J Chen, Q Wang, T K Chung, and T Tang. Therapeutic potentials of gene silencing by RNA interference: Principles, challenges, and new strategies. *Gene*, 2014.

[216] S A Miller, S E Mohn, and A S Weinmann. Jmjd3 and UTX play a demethylase-independent role in chromatin remodeling to regulate T-box family member-dependent gene expression. *Mol Cell*, 40(4):594–605, 2010.

[217] D E Root, N Hacohen, W C Hahn, E S Lander, and D M Sabatini. Genome-scale loss-of-function screening with a lentiviral RNAi library. *Nat Methods*, 3(9):715–719, 2006.

[218] H E Davis, M Rosinski, J R Morgan, and M L Yarmush. Charged polymers modulate retrovirus transduction via membrane charge neutralization and virus aggregation. *Biophys J*, 86(2):1234–1242, 2004.

[219] W A Warr. Scientific workflow systems: Pipeline Pilot and KNIME. *J Comput Aided Mol Des*, 26(7):801–804, 2012.

[220] J E Delmore, G C Issa, M E Lemieux, P B Rahl, J Shi, H M Jacobs, E Kastritis, T Gilpatrick, R M Paranal, J Qi, M Chesi, A C Schinzel, M R McKeown, T P Heffernan, C R Vakoc, P L Bergsagel, I M Ghobrial, P G Richardson, R A Young, W C Hahn, K C Anderson, A L Kung, J E Bradner, and C S Mitsiades. BET bromodomain inhibition as a therapeutic strategy to target c-Myc. *Cell*, 146(6):904–917, 2011.

[221] S T Su, H Y Ying, Y K Chiu, F R Lin, M Y Chen, and K I Lin. Involvement of histone demethylase LSD1 in Blimp-1-mediated gene repression during plasma cell differentiation. *Mol Cell Biol*, 29(6):1421–1431, 2009.

[222] J Chang, Z Wang, E Tang, Z Fan, L McCauley, R Franceschi, K Guan, P H Krebsbach, and C Y Wang. Inhibition of osteoblastic bone formation by nuclear factor-kappaB. *Nat Med*, 15(6):682–689, 2009.

[223] Y Q Yang, Y Y Tan, R Wong, A Wenden, L K Zhang, and A B Rabie. The role of vascular endothelial growth factor in ossification. *Int J Oral Sci*, 4(2):64–68, 2012.

[224] J Lou, Y Tu, S Li, and P R Manske. Involvement of ERK in BMP-2 induced osteoblastic differentiation of mesenchymal progenitor cell line C3H10T1/2. *Biochemical and biophysical research communications*, 268(3):757–62, February 2000.

[225] Y L Yao and W M Yang. The metastasis-associated proteins 1 and 2 form distinct protein complexes with histone deacetylase activity. *J Biol Chem*, 278(43):42560–42568, 2003.

[226] A Ruepp, B Waegele, M Lechner, B Brauner, I Dunger-Kaltenbach, G Fobo, G Frishman, C Montrone, and H W Mewes. CORUM: the comprehensive resource of mammalian protein complexes–2009. *Nucleic Acids Res*, 38(Database issue):D497–501, 2010.

[227] L Huang, H Fu, C M Lin, A L Conner, Y Zhang, and M I Aladjem. Prevention of transcriptional silencing by a replicator-binding complex consisting of SWI/SNF, MeCP1, and hnRNP C1/C2. *Mol Cell Biol*, 31(16):3472–3484, 2011.

[228] M C Mahajan, G J Narlikar, G Boyapaty, R E Kingston, and S M Weissman. Heterogeneous nuclear ribonucleoprotein C1/C2, MeCP1, and SWI/SNF form a chromatin remodeling complex at the beta-globin locus control region. *Proc Natl Acad Sci U S A*, 102(42):15012–15017, 2005.

[229] C Johansson, A Tumber, K Che, P Cain, R Nowak, C Gileadi, and U Oppermann. The roles of Jumonji-type oxygenases in human disease. *Epigenomics*, 6(1):89–120, 2014.

[230] R J Klose, E M Kallin, and Y Zhang. JmjC-domain-containing proteins and histone demethylation. *Nat Rev Genet*, 7(9):715–727, 2006.

[231] X Ding, H Pan, J Li, Q Zhong, X Chen, S M Dry, and C Y Wang. Epigenetic activation of AP1 promotes squamous cell carcinoma metastasis. *Sci Signal*, 6(273):ra28 1–13, S0–15, 2013.

[232] Y Doyon and J Cote. The highly conserved and multifunctional NuA4 HAT complex. *Curr Opin Genet Dev*, 14(2):147–154, 2004.

[233] A N Pena and O M Pereira-Smith. The role of the MORF/MRG family of genes in cell growth, differentiation, DNA repair, and thereby aging. *Ann N Y Acad Sci*, 1100:299–305, 2007.

[234] P S Pardo, J K Leung, J C Lucchesi, and O M Pereira-Smith. MRG15, a novel chromodomain protein, is present in two distinct multiprotein complexes involved in transcriptional activation. *J Biol Chem*, 277(52):50860–50866, 2002.

[235] J K Leung, N Berube, S Venable, S Ahmed, N Timchenko, and O M Pereira-Smith. MRG15 activates the B-myb promoter through formation of a nuclear complex with the retinoblastoma protein and the novel protein PAM14. *J Biol Chem*, 276(42):39171–39178, 2001.

[236] J Farhang-Fallah, V K Randhawa, A Nimnual, A Klip, D Bar-Sagi, and M Rozakis-Adcock. The pleckstrin homology (PH) domain-interacting protein couples the insulin receptor substrate 1 PH domain to insulin signaling pathways leading to mitogenesis and GLUT4 translocation. *Mol Cell Biol*, 22(20):7325–7336, 2002.

[237] J Farhang-Fallah, X Yin, G Trentin, A M Cheng, and M Rozakis-Adcock. Cloning and characterization of PHIP, a novel insulin receptor substrate-1 pleckstrin homology domain interacting protein. *J Biol Chem*, 275(51):40492–40497, 2000.

[238] A Podcheko, P Northcott, G Bikopoulos, A Lee, S R Bommareddi, J A Kushner, J Farhang-Fallah, and M Rozakis-Adcock. Identification of a WD40 repeat-containing isoform of PHIP as a novel regulator of beta-cell growth and survival. *Mol Cell Biol*, 27(18):6484–6496, 2007.

[239] L Yenush, C Zanella, T Uchida, D Bernal, and M F White. The pleckstrin homology and phosphotyrosine binding domains of insulin receptor substrate 1 mediate inhibition of apoptosis by insulin. *Mol Cell Biol*, 18(11):6784–6794, 1998.

[240] M H Koken, J W Hoogerbrugge, I Jasper-Dekker, J de Wit, R Willemsen, H P Roest, J A Grootegoed, and J H Hoeijmakers. Expression of the ubiquitin-conjugating DNA repair enzymes HHR6A and B suggests a role in spermatogenesis and chromatin modification. *Dev Biol*, 173(1):119–132, 1996.

[241] J Kim, S B Hake, and R G Roeder. The human homolog of yeast BRE1 functions as a transcriptional coactivator through direct activator interactions. *Mol Cell*, 20(5):759–770, 2005.

[242] H Kaur, A Arora, J Wengel, and S Maiti. Thermodynamic, counterion, and hydration effects for the incorporation of locked nucleic acid nucleotides into DNA duplexes. *Biochemistry*, 45(23):7347–7355, 2006.

[243] B Vester and J Wengel. LNA (locked nucleic acid): high-affinity targeting of complementary RNA and DNA. *Biochemistry*, 43(42):13233–13241, 2004.

[244] S Picaud, D Da Costa, A Thanasopoulou, P Filippakopoulos, P V Fish, M Philpott, O Fedorov, P Brennan, M E Bunnage, D R Owen, J E Bradner, P Taniere, B O'Sullivan, S Muller, J Schwaller, T Stankovic, and S Knapp. PFI-1, a highly selective protein interaction inhibitor, targeting BET Bromodomains. *Cancer Res*, 73(11):3336–3346, 2013.

[245] E Nicodeme, K L Jeffrey, U Schaefer, S Beinke, S Dewell, C W Chung, R Chandwani, I Marazzi, P Wilson, H Coste, J White, J Kirilovsky, C M Rice, J M Lora, R K Prinjha, K Lee, and A Tarakhovsky. Suppression of inflammation by a synthetic histone mimic. *Nature*, 468(7327):1119–1123, 2010.

[246] D Bailey, R Jahagirdar, A Gordon, A Hafiane, S Campbell, S Chatur, G S Wagner, H C Hansen, F S Chiacchia, J Johansson, L Krimbou, N C Wong, and J Genest. RVX-208: a small molecule that increases apolipoprotein A-I and high-density lipoprotein cholesterol in vitro and in vivo. *J Am Coll Cardiol*, 55(23):2580–2589, 2010.

[247] S Picaud, C Wells, I Felletar, D Brotherton, S Martin, P Savitsky, B Diez-Dacal, M Philpott, C Bountra, H Lingard, O Fedorov, S Muller, P E Brennan, S Knapp, and P Filippakopoulos. RVX-208, an inhibitor of BET transcriptional regulators with selectivity for the second bromodomain. *Proc Natl Acad Sci U S A*, 2013.

[248] V Pogacic, A N Bullock, O Fedorov, P Filippakopoulos, C Gasser, A Biondi, S Meyer-Monard, S Knapp, and J Schwaller. Structural analysis identifies imidazo[1,2-b]pyridazines as PIM kinase inhibitors with in vitro antileukemic activity. *Cancer Res*, 67(14):6916–6924, 2007.

[249] M Bachmann and T Moroy. The serine/threonine kinase Pim-1. *Int J Biochem Cell Biol*, 37(4):726–730, 2005.

[250] K Kim, J H Kim, B U Youn, H M Jin, and N Kim. Pim-1 regulates RANKL-induced osteoclastogenesis via NF-kappaB activation and NFATc1 induction. *J Immunol*, 185(12):7460–7466, 2010.

[251] M Bachmann, C Kosan, P X Xing, M Montenarh, I Hoffmann, and T Moroy. The oncogenic serine/threonine kinase Pim-1 directly phosphorylates and activates the G2/M specific phosphatase Cdc25C. *Int J Biochem Cell Biol*, 38(3):430–443, 2006.

[252] A De Antoni, S Maffini, S Knapp, A Musacchio, and S Santaguida. A small-molecule inhibitor of Haspin alters the kinetochore functions of Aurora B. *J Cell Biol*, 199(2):269–284, 2012.

[253] J M Higgins. Haspin: a newly discovered regulator of mitotic chromosome behavior. *Chromosoma*, 119(2):137–147, 2010.

[254] J Eswaran, D Patnaik, P Filippakopoulos, F Wang, R L Stein, J W Murray, J M Higgins, and S Knapp. Structure and functional characterization of the atypical human kinase haspin. *Proc Natl Acad Sci U S A*, 106(48):20198–20203, 2009.

[255] F Wang, J Dai, J R Daum, E Niedzialkowska, B Banerjee, P T Stukenberg, G J Gorbsky, and J M Higgins. Histone H3 Thr-3 phosphorylation by Haspin positions Aurora B at centromeres in mitosis. *Science*, 330(6001):231–235, 2010.

[256] T U Tanaka, M J Stark, and K Tanaka. Kinetochore capture and bi-orientation on the mitotic spindle. *Nat Rev Mol Cell Biol*, 6(12):929–942, 2005.

[257] J R Farley and B Stilt-Coffing. Apoptosis may determine the release of skeletal alkaline phosphatase activity from human osteoblast-line cells. *Calcif Tissue Int*, 68(1):43–52, 2001.

[258] Chunaram Choudhary, Chanchal Kumar, Florian Gnad, Michael L Nielsen, Michael Rehman, Tobias C Walther, Jesper V Olsen, and Matthias Mann. Lysine acetylation

targets protein complexes and co-regulates major cellular functions. *Science (New York, N.Y.)*, 325(5942):834–40, August 2009.

[259] Miyong Yun, Jun Wu, Jerry L Workman, and Bing Li. Readers of histone modifications. *Cell research*, 21(4):564–78, April 2011.

[260] P Filippakopoulos and S Knapp. The bromodomain interaction module. *FEBS Lett*, 586(17):2692–2704, 2012.

[261] A Dey, A Nishiyama, T Karpova, J McNally, and K Ozato. Brd4 marks select genes on mitotic chromatin and directs postmitotic transcription. *Mol Biol Cell*, 20(23):4899–4909, 2009.

[262] M K Jang, K Mochizuki, M Zhou, H S Jeong, J N Brady, and K Ozato. The bromodomain protein Brd4 is a positive regulatory component of P-TEFb and stimulates RNA polymerase II-dependent transcription. *Mol Cell*, 19(4):523–534, 2005.

[263] E B Stelow. A review of NUT midline carcinoma. *Head Neck Pathol*, 5(1):31–35, 2011.

[264] C A French, I Miyoshi, J C Aster, I Kubonishi, T G Kroll, P Dal Cin, S O Vargas, A R Perez-Atayde, and J A Fletcher. BRD4 bromodomain gene rearrangement in aggressive carcinoma with translocation t(15;19). *Am J Pathol*, 159(6):1987–1992, 2001.

[265] C A French, I Miyoshi, I Kubonishi, H E Grier, A R Perez-Atayde, and J A Fletcher. BRD4-NUT fusion oncogene: a novel mechanism in aggressive carcinoma. *Cancer Res*, 63(2):304–307, 2003.

[266] C A French, C L Ramirez, J Kolmakova, T T Hickman, M J Cameron, M E Thyne, J L Kutok, J A Toretsky, A K Tadavarthy, U R Kees, J A Fletcher, and J C Aster. BRD-NUT oncoproteins: a family of closely related nuclear proteins that block epithelial differentiation and maintain the growth of carcinoma cells. *Oncogene*, 27(15):2237–2242, 2008.

[267] J A Mertz, A R Conery, B M Bryant, P Sandy, S Balasubramanian, D A Mele, L Bergeron, and R J Sims 3rd. Targeting MYC dependence in cancer by inhibiting BET bromodomains. *Proc Natl Acad Sci U S A*, 108(40):16669–16674, 2011.

[268] A R Grayson, E M Walsh, M J Cameron, J Godec, T Ashworth, J M Ambrose, A B Aserlind, H Wang, G I Evan, M J Kluk, J E Bradner, J C Aster, and C A French. MYC, a downstream target of BRD-NUT, is necessary and sufficient for the blockade of differentiation in NUT midline carcinoma. *Oncogene*, 2013.

[269] A I Saeed, V Sharov, J White, J Li, W Liang, N Bhagabati, J Braisted, M Klapa, T Currier, M Thiagarajan, A Sturn, M Snuffin, A Rezantsev, D Popov, A Ryltsov, E Kostukovich, I Borisovsky, Z Liu, A Vinsavich, V Trush, and J Quackenbush. TM4: a free, open-source system for microarray data management and analysis. *BioTechniques*, 34(2):374–8, February 2003.

[270] Ross Ihaka and Robert Gentleman. R: A Language for Data Analysis and Graphics. *Journal of Computational and Graphical Statistics*, 5(3):299–314, 1996.

[271] W S Argraves, L M Greene, M A Cooley, and W M Gallagher. Fibulins: physiological and disease perspectives. *EMBO Rep*, 4(12):1127–1131, 2003.

[272] C M Uhlar and A S Whitehead. Serum amyloid A, the major vertebrate acute-phase reactant. *Eur J Biochem*, 265(2):501–523, 1999.

[273] B S Kim, H J Kim, J S Kim, Y O You, H Zadeh, H I Shin, S J Lee, Y J Park, T Takata, S H Pi, J Lee, and H K You. IFITM1 increases osteogenesis through Runx2 in human alveolar-derived bone marrow stromal cells. *Bone*, 51(3):506–514, 2012.

[274] M Kawai, A C Breggia, V E DeMambro, X Shen, E Canalis, M L Bouxsein, W G Beamer, D R Clemmons, and C J Rosen. The heparin-binding domain of IGFBP-2 has insulin-like growth factor binding-independent biologic activity in the growing skeleton. *J Biol Chem*, 286(16):14670–14680, 2011.

[275] S M Firth and R C Baxter. Cellular actions of the insulin-like growth factor binding proteins. *Endocr Rev*, 23(6):824–854, 2002.

[276] S Murad, D Grove, K A Lindberg, G Reynolds, A Sivarajah, and S R Pinnell. Regulation of collagen synthesis by ascorbic acid. *Proc Natl Acad Sci U S A*, 78(5):2879–2882, 1981.

[277] H Puchtler, S N Meloan, and M S Terry. On the history and mechanism of alizarin and alizarin red S stains for calcium. *J Histochem Cytochem*, 17(2):110–124, 1969.

[278] C A Gregory, W G Gunn, A Peister, and D J Prockop. An Alizarin red-based assay of mineralization by adherent cells in culture: comparison with cetylpyridinium chloride extraction. *Anal Biochem*, 329(1):77–84, 2004.

[279] H Puchtler and S N Meloan. Demonstration of phosphates in calcium deposits: a modification of von Kossa's reaction. *Histochemistry*, 56(3-4):177–185, 1978.

[280] G P Konin and D M Walz. Lumbosacral transitional vertebrae: classification, imaging findings, and clinical relevance. *AJNR Am J Neuroradiol*, 31(10):1778–1786, 2010.

[281] F Lamoureux, M Baud'huin, L Rodriguez Calleja, C Jacques, M Berreur, F Redini, F Lecanda, J E Bradner, D Heymann, and B Ory. Selective inhibition of BET bromodomain epigenetic signalling interferes with the bone-associated tumour vicious cycle. *Nat Commun*, 5:3511, 2014.

[282] B Merle and P Garnero. The multiple facets of periostin in bone metabolism. *Osteoporos Int*, 23(4):1199–1212, 2012.

[283] C M Steppan, D T Crawford, K L Chidsey-Frink, H Ke, and A G Swick. Leptin is a potent stimulator of bone growth in ob/ob mice. *Regul Pept*, 92(1-3):73–78, 2000.

[284] P Ducy, M Amling, S Takeda, M Priemel, A F Schilling, F T Beil, J Shen, C Vinson, J M Rueger, and G Karsenty. Leptin inhibits bone formation through a hypothalamic relay: a central control of bone mass. *Cell*, 100(2):197–207, 2000.

[285] Y Murakami, T Kojima, T Nagasawa, H Kobayashi, and I Ishikawa. Novel isolation of alkaline phosphatase-positive subpopulation from periodontal ligament fibroblasts. *J Periodontol*, 74(6):780–786, 2003.

[286] J Wysocka, T A Milne, and C D Allis. Taking LSD 1 to a new high. *Cell*, 122(5):654–658, 2005.

[287] R Baron and N A Vellore. LSD1/CoREST is an allosteric nanoscale clamp regulated by H3-histone-tail molecular recognition. *Proc Natl Acad Sci U S A*, 109(31):12509–12514, 2012.

[288] M Yang, C B Gocke, X Luo, D Borek, D R Tomchick, M Machius, Z Otwinowski, and H Yu. Structural basis for CoREST-dependent demethylation of nucleosomes by the human LSD1 histone demethylase. *Mol Cell*, 23(3):377–387, 2006.

[289] Y J Shi, C Matson, F Lan, S Iwase, T Baba, and Y Shi. Regulation of LSD1 histone demethylase activity by its associated factors. *Mol Cell*, 19(6):857–864, 2005.

[290] M Wissmann, N Yin, J M Muller, H Greschik, B D Fodor, T Jenuwein, C Vogler, R Schneider, T Gunther, R Buettner, E Metzger, and R Schule. Cooperative demethylation by JMJD2C and LSD1 promotes androgen receptor-dependent gene expression. *Nat Cell Biol*, 9(3):347–353, 2007.

[291] B Perillo, M N Ombra, A Bertoni, C Cuozzo, S Sacchetti, A Sasso, L Chiariotti, A Malorni, C Abbondanza, and E V Avvedimento. DNA oxidation as triggered by H3K9me2 demethylation drives estrogen-induced gene expression. *Science*, 319(5860):202–206, 2008.

[292] P Stavropoulos, G Blobel, and A Hoelz. Crystal structure and mechanism of human lysine-specific demethylase-1. *Nat Struct Mol Biol*, 13(7):626–632, 2006.

[293] L Aravind and L M Iyer. The SWIRM domain: a conserved module found in chromosomal proteins points to novel chromatin-modifying activities. *Genome Biol*, 3(8):RESEARCH0039, 2002.

[294] J Wang, S Hevi, J K Kurash, H Lei, F Gay, J Bajko, H Su, W Sun, H Chang, G Xu, F Gaudet, E Li, and T Chen. The lysine demethylase LSD1 (KDM1) is required for maintenance of global DNA methylation. *Nat Genet*, 41(1):125–129, 2009.

[295] J Huang, R Sengupta, A B Espejo, M G Lee, J A Dorsey, M Richter, S Opravil, R Shiekhattar, M T Bedford, T Jenuwein, and S L Berger. p53 is regulated by the lysine demethylase LSD1. *Nature*, 449(7158):105–108, 2007.

[296] V Kashyap, S Ahmad, E M Nilsson, L Helczynski, S Kenna, J L Persson, L J Gudas, and N P Mongan. The lysine specific demethylase-1 (LSD1/KDM1A) regulates VEGF-A expression in prostate cancer. *Mol Oncol*, 7(3):555–566, 2013.

[297] Y Wang, H Zhang, Y Chen, Y Sun, F Yang, W Yu, J Liang, L Sun, X Yang, L Shi, R Li, Y Li, Y Zhang, Q Li, X Yi, and Y Shang. LSD1 is a subunit of the NuRD complex and targets the metastasis programs in breast cancer. *Cell*, 138(4):660–672, 2009.

[298] T Lv, D Yuan, X Miao, Y Lv, P Zhan, X Shen, and Y Song. Over-expression of LSD1 promotes proliferation, migration and invasion in non-small cell lung cancer. *PLoS One*, 7(4):e35065, 2012.

[299] E C Kauffman, B D Robinson, M J Downes, L G Powell, M M Lee, D S Scherr, L J Gudas, and N P Mongan. Role of androgen receptor and associated lysine-demethylase coregulators, LSD1 and JMJD2A, in localized and advanced human bladder cancer. *Mol Carcinog*, 50(12):931–944, 2011.

[300] J H Schulte, S Lim, A Schramm, N Friedrichs, J Koster, R Versteeg, I Ora, K Pajtler, L Klein-Hitpass, S Kuhfittig-Kulle, E Metzger, R Schule, A Eggert, R Buettner, and J Kirfel. Lysine-specific demethylase 1 is strongly expressed in poorly differentiated neuroblastoma: implications for therapy. *Cancer Res*, 69(5):2065–2071, 2009.

[301] T Schenk, W C Chen, S Gollner, L Howell, L Jin, K Hebestreit, H U Klein, A C Popescu, A Burnett, K Mills, R A Casero Jr., L Marton, P Woster, M D Minden, M Dugas, J C Wang, J E Dick, C Muller-Tidow, K Petrie, and A Zelent. Inhibition of the LSD1 (KDM1A) demethylase reactivates the all-trans-retinoic acid differentiation pathway in acute myeloid leukemia. *Nat Med*, 18(4):605–611, 2012.

[302] Oryzon Genomics. ORYZON initiates clinical development of ORY-1001, a novel LSD1 inhibitor, in patients with acute myeloid leukemia. *URL:http://www.oryzon.com [20 April 2014]*, 2014.

[303] H Mohammad. Inhibition of LSD1 as a therapeutic strategy for the treatment of acute myeloid leukemia. *55th American Society of Hematology Meeting and Exhibition*, 2013.

[304] Salarius Pharmaceuticals. SP-2528, an inhibitor of lysine-specific demethylase 1 (LSD1). *URL:http://www.pharmaconnections.com [20 October 2014]*, 2012.

[305] D Rotili, S Tomassi, M Conte, R Benedetti, M Tortorici, G Ciossani, S Valente, B Marrocco, D Labella, E Novellino, A Mattevi, L Altucci, A Tumber, C Yapp, O N King, R J Hopkinson, A Kawamura, C J Schofield, and A Mai. Pan-histone demethylase inhibitors simultaneously targeting jumonji C and lysine-specific demethylases display high anticancer activities. *J Med Chem*, 57(1):42–55, 2014.

[306] N Mosammaparast, H Kim, B Laurent, Y Zhao, H J Lim, M C Majid, S Dango, Y Luo, K Hempel, M E Sowa, S P Gygi, H Steen, J W Harper, B Yankner, and Y Shi. The histone demethylase LSD1/KDM1A promotes the DNA damage response. *J Cell Biol*, 203(3):457–470, 2013.

[307] M M Musri, M C Carmona, F A Hanzu, P Kaliman, R Gomis, and M Parrizas. Histone demethylase LSD1 regulates adipogenesis. *J Biol Chem*, 285(39):30034–30041, 2010.

[308] M G Lee, C Wynder, D M Schmidt, D G McCafferty, and R Shiekhattar. Histone H3 lysine 4 demethylation is a target of nonselective antidepressive medications. *Chem Biol*, 13(6):563–567, 2006.

[309] J C Robertson, N C Hurley, M Tortorici, G Ciossani, M T Borrello, N A Vellore, A Ganesan, A Mattevi, and R Baron. Expanding the druggable space of the LSD1/CoREST epigenetic target: new potential binding regions for drug-like molecules, peptides, protein partners, and chromatin. *PLoS Comput Biol*, 9(7):e1003158, 2013.

[310] Jesús Delgado-Calle, Carolina Sañudo, Lydia Sánchez-Verde, Raúl J García-Renedo, Jana Arozamena, and José A Riancho. Epigenetic regulation of alkaline phosphatase in human cells of the osteoblastic lineage. *Bone*, 49(4):830–8, October 2011.

[311] Jing Wang, Sarah Hevi, Julia K Kurash, Hong Lei, Frédérique Gay, Jeffrey Bajko, Hui Su, Weitao Sun, Hua Chang, Guoliang Xu, François Gaudet, En Li, and Taiping Chen. The lysine demethylase LSD1 (KDM1) is required for maintenance of global DNA methylation. *Nature genetics*, 41(1):125–9, January 2009.

[312] Juan Xu, Bo Yu, Christine Hong, and Cun-Yu Wang. KDM6B epigenetically regulates odontogenic differentiation of dental mesenchymal stem cells. *International journal of oral science*, 5(4):200–5, December 2013.

[313] Shaun D Fouse, Raman O Nagarajan, and Joseph F Costello. Genome-scale DNA methylation analysis. *Epigenomics*, 2(1):105–17, February 2010.

[314] John S Mattick and Igor V Makunin. Non-coding RNA. *Human molecular genetics*, 15 Spec No:R17–29, April 2006.

[315] Mark E Nuttall and Jeffrey M Gimble. Controlling the balance between osteoblastogenesis and adipogenesis and the consequent therapeutic implications. *Current opinion in pharmacology*, 4(3):290–4, June 2004.

[316] Lyle Armstrong, Jumana Al-Aama, Miodrag Stojkovic, and Majlinda Lako. The epigenetic contribution to stem cell ageing - can we rejuvenate our older cells? *Stem cells (Dayton, Ohio)*, April 2014.

[317] S W Ember, J Y Zhu, S H Olesen, M P Martin, A Becker, N Berndt, G I Georg, and E Schonbrunn. The acetyl-lysine binding site of bromodomain-containing protein 4 (BRD4) interacts with diverse kinase inhibitors. *ACS Chem Biol*, 2014.

[318] Herbert Fleisch. Development of bisphosphonates. *Breast cancer research : BCR*, 4(1):30–4, January 2002.

[319] R G Russell, N B Watts, F H Ebetino, and M J Rogers. Mechanisms of action of bisphosphonates: similarities and differences and their potential influence on clinical efficacy. *Osteoporos Int*, 19(6):733–759, 2008.

[320] Kathryn L Kavanagh, Kunde Guo, James E Dunford, Xiaoqiu Wu, Stefan Knapp, Frank H Ebetino, Michael J Rogers, R Graham G Russell, and Udo Oppermann. The molecular mechanism of nitrogen-containing bisphosphonates as antiosteoporosis drugs. *Proceedings of the National Academy of Sciences of the United States of America*, 103(20):7829–34, May 2006.

[321] Steve Arns, Romelo Gibe, Anne Moreau, M Monzur Morshed, and Robert N Young. Design and synthesis of novel bone-targeting dual-action pro-drugs for the treatment and reversal of osteoporosis. *Bioorganic & medicinal chemistry*, 20(6):2131–40, March 2012.

[322] F. Bauss, A. Esswein, K. Reiff, G. Sponer, and B. Müller-Beckmann. Effect of 17β-estradiol-bisphosphonate conjugates, potential bone-seeking estrogen pro-drugs, on 17β-estradiol serum kinetics and bone mass in rats. *Calcified Tissue International*, 59(3):168–173, September 1996.

[323] Jason R Neale, Natali B Richter, Kevyn E Merten, K Grant Taylor, Sujan Singh, Leonard C Waite, Nicole K Emery, Ned B Smith, Jian Cai, and William M Pierce. Bone selective effect of an estradiol conjugate with a novel tetracycline-derived bone-targeting agent. *Bioorganic & medicinal chemistry letters*, 19(3):680–3, February 2009.

[324] Ge Zhang, Baosheng Guo, Heng Wu, Tao Tang, Bao-Ting Zhang, Lizhen Zheng, Yixin He, Zhijun Yang, Xiaohua Pan, Heelum Chow, Kinwah To, Yaping Li, Dahu Li, Xinluan Wang, Yixiang Wang, Kwongman Lee, Zhibo Hou, Nan Dong, Gang Li, Kwoksui Leung, Leungkim Hung, Fuchu He, Lingqiang Zhang, and Ling Qin. A delivery system targeting bone formation surfaces to facilitate RNAi-based anabolic therapy. *Nature medicine*, 18(2):307–14, February 2012.

A Appendix

A.1 Reagents and media compositions

All reagents unless otherwise stated were from Sigma-Aldrich (Poole, UK). Different formulations of standard medium were purchased from Life Technologies. Human mesenchymal stem cells were purchased from Lonza (Basel, Switzerland) and expanded previously to obtain a high enough cell stock to be used for all related experiments. The standard medium for hMSC growth and expansion was MesenPRO-RS™. When cells reached approximately 70% confluency in either culture vessel, the medium was replaced with either of the following media: control medium (CM: DMEM/F12 supplemented with 10% fetal bovine serum (FBS), 1% penicillin/streptomycin (P/S), 1% non-essential amino acids (NEAA), 2mM glutamine); incomplete osteogenic differentiation medium (OD: DMEM/F12 supplemented with 10% FBS, 1% P/S, 1% NEAA, 2mM glutamine, 50µg/ml ascorbic acid, 10mM beta-glycerophosphate); or complete osteogenic differentiation medium containing either of the inducers dexamethasone (+DEX), 1α,25-Dihydroxyvitamin D_3 (+VitD3), oncostatin M (+OSM), or BMP-2 (+BMP) (DMEM/F12 supplemented with 10% FBS, 1% P/S, 1% NEAA, 2mM glutamine, 50µg/ml ascorbic acid, 10mM beta-glycerophosphate, with either 10nM dexamethasone, 1nM 1α,25-Dihydroxyvitamin D_3, 10ng/ml oncostatin M). The different concentrations of inducers used for the initial validation of the alkaline phosphatase assay can be found in chapter 2. 1% penicillin/streptomycin equals 100 units of penicillin and 0.1mg/ml streptomycin. The MEM Non-essential Amino Acid Solution (NEAA) is a 100x solution and was used as a 1x solution.

Name	Composition
MSC	MesenPro-RS™ + 1% P/S
CM	DMEM F/12 + 15% FBS + 1% P/S + 1% NEAA + 2mM glutamine
OD	DMEM F/12 + 15% FBS + 1% P/S + 1% NEAA + 2mM glutamine + 50µg/ml ascorbic acid + 10mM beta-glycerophosphate
+DEX	DMEM F/12 + 15% FBS + 1% P/S + 1% NEAA + 2mM glutamine + 50µg/ml ascorbic acid + 10mM beta-glycerophosphate + 10nM dexamethasone
+VitD3	DMEM F/12 + 15% FBS + 1% P/S + 1% NEAA + 2mM glutamine + 50µg/ml ascorbic acid + 10mM beta-glycerophosphate + 1nM 1,25-dihydroxyvitamin D_3
+OSM	DMEM F/12 + 15% FBS + 1% P/S + 1% NEAA + 2mM glutamine + 50µg/ml ascorbic acid + 10mM beta-glycerophosphate + 10ng/ml OSM
+BMP	DMEM F/12 + 15% FBS + 1% P/S + 1% NEAA + 2mM glutamine + 50µg/ml ascorbic acid + 10mM beta-glycerophosphate + 100ng/ml BMP2
Basic mouse medium	α-MEM + 10% FBS + 1% P/S + 2mM glutamine
Bone chip medium	DMEM + 10% FBS + 50µg/ml ascorbic acid

Table A.1: Media compositions used in this thesis

A.2 Primer sequences for qPCR

Gene	Forward primer sequence	Reverse primer sequence
ALP	ACTGGTACTCAGACAACGAGAT	ACGTCAATGTCCCTGATGTTATG
IBSP	GAACCTCGTGGGGACAATTAC	CATCATAGCCATCGTAGCCTTG
COL1A1	GAGGGCCAAGACGAAGACATC	CAGATCACGTCATCGCACAAC
BGLAP	GGCGCTACCTGTATCAATGG	GTGGTCAGCCAACTCGTCA
RUNX2	TCAACGATCTGAGATTTGTGGG	GGGGAGGATTTGTGAAGACGG
BRD4	GAGCTACCCACAGAAGAAACC	GAGTCGATGCTTGAGTTGTGTT
JMJD8	CAGGTTGCTGGCTTCGTTTG	CCCACTCGGTGAAGTTGTTGT
KDM1A	GTGGACGAGTTGCCACATTTC	TGACCACAGCCATAGGATTCC
MORF4L1	AGCAATGTTGGCTTATACACCTC	AGCTTTCCGATGGTACTCAGG
PHIP	GGGGCAGATGGCACTATTTGT	CTTCCCGTCGCCAGAAACATT
UBE2A	GGAGTCCAACCTATGATGTGTCT	CATATTCCCGTTTGTTCTCCTGG

Table A.2: Primer sequences

The following primers were purchased from Qiagen: Osterix, Hs_SP7_1_SG QuantiTect Primer Assay; Osteonectin, Hs_SPARC_1_SG QuantiTect Primer Assay; Gapdh, Hs_GAPDH_2_SG QuantiTect Primer Assay (200) and Actin B, Hs_ACTB_2_SG QuantiTect Primer Assay.

A.3 Dexamethasone-induced gene expression - microarray data

Gene symbol	Entrez Gene Name	Fold Change	Location	Type(s)
APOD	apolipoprotein D	16.27	Extracellular Space	transporter
CADM3	cell adhesion molecule 3	15.30	Plasma Membrane	other
SUSD2	sushi domain containing 2	12.09	Extracellular Space	other
DARC	Duffy blood group, chemokine receptor	11.29	Plasma Membrane	G-protein coupled receptor
OLFML2A	olfactomedin-like 2A	10.12	Extracellular Space	other
OMD	osteomodulin	9.20	Extracellular Space	other
FAM167A	family with sequence similarity 167, member A	8.57	unknown	other
LEPR	leptin receptor	8.38	Plasma Membrane	transmembrane receptor
FAM167A	family with sequence similarity 167, member A	8.20	unknown	other
BMP6	bone morphogenetic protein 6	7.93	Extracellular Space	growth factor
CRISPLD2	cysteine-rich secretory protein LCCL domain containing 2	7.70	Cytoplasm	other
WFDC1	WAP four-disulfide core domain 1	7.58	Extracellular Space	other
FBLN1	fibulin 1	7.37	Extracellular Space	other
DUSP23	dual specificity phosphatase 23	6.70	Cytoplasm	phosphatase
FKBP5	FK506 binding protein 5	6.42	Nucleus	enzyme
TMTC1	transmembrane and tetratricopeptide repeat containing 1	5.51	Cytoplasm	other
EPSTI1	epithelial stromal interaction 1 (breast)	5.45	unknown	other
IMPA2	inositol(myo)-1(or 4)-monophosphatase 2	5.34	Cytoplasm	phosphatase
IFITM1	interferon induced transmembrane protein 1	5.21	Plasma Membrane	other
TRNP1	TMF1-regulated nuclear protein 1	4.88	unknown	other
MME	membrane metallo-endopeptidase	4.86	Plasma Membrane	peptidase
KIAA1644	KIAA1644	4.77	unknown	other
PTGS2	prostaglandin-endoperoxide synthase 2	4.73	Cytoplasm	enzyme
CD14	CD14 molecule	4.44	Plasma Membrane	transmembrane receptor
ZBTB16	zinc finger and BTB domain containing 16	4.21	Nucleus	transcription regulator
DBC1	deleted in bladder cancer 1	4.19	Nucleus	peptidase
FBLN1	fibulin 1	4.15	Extracellular Space	other
ZFP36	zinc finger protein 36, C3H type, homolog (mouse)	4.11	Nucleus	transcription regulator
RASD1	RAS, dexamethasone-induced 1	3.96	Cytoplasm	enzyme
LEPR	leptin receptor	3.76	Plasma Membrane	transmembrane receptor
RPS6KA2	ribosomal protein S6 kinase, 90kDa, polypeptide 2	3.71	Nucleus	kinase
ZFP36L2	zinc finger protein 36, C3H type-like 2	3.69	Nucleus	transcription regulator
KCNT2	potassium channel, subfamily T, member 2	3.68	Plasma Membrane	ion channel
A4GALT	alpha 1,4-galactosyltransferase	3.39	Cytoplasm	enzyme
FBN2	fibrillin 2	3.29	Extracellular Space	other
ZBTB16	zinc finger and BTB domain containing 16	3.27	Nucleus	transcription regulator
TYMP	thymidine phosphorylase	3.22	Extracellular Space	growth factor
ALDH3B1	aldehyde dehydrogenase 3 family, member B1	3.16	Cytoplasm	enzyme
PTGER2	prostaglandin E receptor 2 (subtype EP2), 53kDa	3.16	Plasma Membrane	G-protein coupled receptor
SORT1	sortilin 1	3.07	Plasma Membrane	transmembrane receptor
PRKD1	protein kinase D1	3.01	Cytoplasm	kinase
NPTX1	neuronal pentraxin I	3.01	Extracellular Space	other
C1RL	complement component 1, r subcomponent-like	3.00	Extracellular Space	peptidase
FTH1	ferritin, heavy polypeptide 1	2.97	Cytoplasm	enzyme
SLC44A1	solute carrier family 44, member 1	2.93	Plasma Membrane	transporter
FZD4	frizzled family receptor 4	2.91	Plasma Membrane	G-protein coupled receptor
ANKRD35	ankyrin repeat domain 35	2.88	unknown	other
IFITM3	interferon induced transmembrane protein 3	2.84	Plasma Membrane	other
CLEC3B	C-type lectin domain family 3, member B	2.83	Extracellular Space	other
CORIN	corin, serine peptidase	2.83	Plasma Membrane	peptidase
PHACTR2	phosphatase and actin regulator 2	2.83	unknown	other
GCNT1	glucosaminyl (N-acetyl) transferase 1, core 2	2.81	Cytoplasm	enzyme
C10orf54	chromosome 10 open reading frame 54	2.78	unknown	other
LEPROT	leptin receptor overlapping transcript	2.70	Plasma Membrane	other
IRS2	insulin receptor substrate 2	2.68	Cytoplasm	enzyme
LHFP	lipoma HMGIC fusion partner	2.65	unknown	other
GALNT1	UDP-N-acetyl-alpha-D-galactosamine:polypeptide N-acetylgalactosaminyltransferase 1	2.62	Cytoplasm	enzyme
RNASET2	ribonuclease T2	2.61	Cytoplasm	enzyme
OSBPL10	oxysterol binding protein-like 10	2.59	unknown	other
KLHL5	kelch-like 5 (Drosophila)	2.58	Extracellular Space	other
TGIF1	TGFB-induced factor homeobox 1	2.57	Nucleus	transcription regulator
AKR1C4	aldo-keto reductase family 1, member C4	2.56	Cytoplasm	enzyme
ALPL	alkaline phosphatase, liver/bone/kidney	2.52	Plasma Membrane	phosphatase
IGFBP6	insulin-like growth factor binding protein 6	2.50	Extracellular Space	other
ARL6IP5	ADP-ribosylation-like factor 6 interacting protein 5	2.47	Cytoplasm	other
KCNK6	potassium channel, subfamily K, member 6	2.47	Plasma Membrane	ion channel
ITPK1	inositol-tetrakisphosphate 1-kinase	2.46	Cytoplasm	kinase
LPAR1	lysophosphatidic acid receptor 1	2.44	Plasma Membrane	G-protein coupled receptor
KANK1	KN motif and ankyrin repeat domains 1	2.41	Nucleus	transcription regulator
NELF	nasal embryonic LHRH factor	2.41	Extracellular Space	other
PPAP2B	phosphatidic acid phosphatase type 2B	2.41	Plasma Membrane	phosphatase
TCEA3	transcription elongation factor A (SII), 3	2.41	Nucleus	transcription regulator
VGLL3	vestigial like 3 (Drosophila)	2.38	unknown	other
HSPB2	heat shock 27kDa protein 2	2.37	Cytoplasm	other
OSBPL5	oxysterol binding protein-like 5	2.35	Cytoplasm	other
SIRPA	signal-regulatory protein alpha	2.34	Plasma Membrane	phosphatase
NFKBIA	nuclear factor of kappa light polypeptide gene enhancer in B-cells inhibitor, alpha	2.32	Cytoplasm	transcription regulator
MGLL	monoglyceride lipase	2.30	Plasma Membrane	enzyme
ANPEP	alanyl (membrane) aminopeptidase	2.30	Plasma Membrane	peptidase
CKB	creatine kinase, brain	2.29	Cytoplasm	kinase
MUC1	mucin 1, cell surface associated	2.29	Plasma Membrane	transcription regulator
S100A10	S100 calcium binding protein A10	2.29	Cytoplasm	other
DBNDD2	dysbindin (dystrobrevin binding protein 1) domain containing 2	2.28	Cytoplasm	other
TCEAL4	transcription elongation factor A (SII)-like 4	2.27	unknown	other

Table A.3: Dexamethasone-induced gene expression - microarray data I

Gene symbol	Entrez Gene Name	Fold Change	Location	Type(s)
CST3	cystatin C	2.25	Extracellular Space	other
IFITM2	interferon induced transmembrane protein 2	2.25	Plasma Membrane	other
SSB	Sjogren syndrome antigen B (autoantigen La)	2.25	Nucleus	enzyme
SAA1	serum amyloid A1	2.25	Extracellular Space	other
TWIST1	twist homolog 1 (Drosophila)	2.23	Nucleus	transcription regulator
STAT2	signal transducer and activator of transcription 2, 113kDa	2.20	Nucleus	transcription regulator
TSC22D3	TSC22 domain family, member 3	2.19	Nucleus	other
CFD	complement factor D (adipsin)	2.18	Extracellular Space	peptidase
PCDH18	protocadherin 18	2.18	Extracellular Space	other
HTRA1	HtrA serine peptidase 1	2.16	Extracellular Space	peptidase
ADARB1	adenosine deaminase, RNA-specific, B1	2.13	Nucleus	enzyme
TGIF1	TGFB-induced factor homeobox 1	2.13	Nucleus	transcription regulator
MGST1	microsomal glutathione S-transferase 1	2.10	Cytoplasm	enzyme
RAB11FIP1	RAB11 family interacting protein 1 (class I)	2.10	Cytoplasm	other
PLXNA2	plexin A2	2.09	Plasma Membrane	transmembrane receptor
OSBPL5	oxysterol binding protein-like 5	2.08	Cytoplasm	other
TOB1	transducer of ERBB2, 1	2.08	Nucleus	transcription regulator
COL8A1	collagen, type VIII, alpha 1	2.07	Extracellular Space	other
DUSP5	dual specificity phosphatase 5	2.06	Nucleus	phosphatase
TRAF3IP2	TRAF3 interacting protein 2	2.06	Cytoplasm	other
PON2	paraoxonase 2	2.05	Plasma Membrane	enzyme
PYGB	phosphorylase, glycogen; brain	2.05	Cytoplasm	enzyme
CCND3	cyclin D3	2.04	Nucleus	other
LOC645638	WDNM1-like pseudogene	2.03	unknown	other
ADAP1	ArfGAP with dual PH domains 1	2.02	Nucleus	other
PTPRG	protein tyrosine phosphatase, receptor type, G	2.02	Plasma Membrane	phosphatase
FUCA1	fucosidase, alpha-L- 1, tissue	1.98	Cytoplasm	enzyme
SDF2L1	stromal cell-derived factor 2-like 1	-1.96	Cytoplasm	other
GPER	G protein-coupled estrogen receptor 1	-2.00	Plasma Membrane	G-protein coupled receptor
NET1	neuroepithelial cell transforming 1	-2.00	Nucleus	other
ABL1	c-abl oncogene 1, non-receptor tyrosine kinase	-2.04	Nucleus	kinase
FAM176A	family with sequence similarity 176, member A	-2.04	Plasma Membrane	other
PLAUR	plasminogen activator, urokinase receptor	-2.04	Plasma Membrane	transmembrane receptor
SQLE	squalene epoxidase	-2.04	Cytoplasm	enzyme
STC1	stanniocalcin 1	-2.04	Extracellular Space	kinase
ISLR	immunoglobulin superfamily containing leucine-rich repeat	-2.08	Extracellular Space	other
PLAUR	plasminogen activator, urokinase receptor	-2.08	Plasma Membrane	transmembrane receptor
PSPH	phosphoserine phosphatase	-2.08	Cytoplasm	phosphatase
ATXN1	ataxin 1	-2.13	Nucleus	transcription regulator
POSTN	periostin, osteoblast specific factor	-2.13	Extracellular Space	other
SERPINH1	serpin peptidase inhibitor, clade H (heat shock protein 47), member 1, (collagen binding protein 1)	-2.13	Extracellular Space	other
SMYD3	SET and MYND domain containing 3	-2.17	Nucleus	enzyme
CSRNP1	cysteine-serine-rich nuclear protein 1	-2.22	Nucleus	transcription regulator
DOCK10	dedicator of cytokinesis 10	-2.22	unknown	other
FAM101B	family with sequence similarity 101, member B	-2.22	unknown	other
PBX3	pre-B-cell leukemia homeobox 3	-2.22	Nucleus	transcription regulator
RHOJ	ras homolog family member J	-2.27	Cytoplasm	enzyme
AEBP1	AE binding protein 1	-2.33	Nucleus	peptidase
KRT19	keratin 19	-2.33	Cytoplasm	other
NT5DC2	5'-nucleotidase domain containing 2	-2.44	unknown	other
PAMR1	peptidase domain containing associated with muscle regeneration 1	-2.44	Extracellular Space	peptidase
MMP2	matrix metallopeptidase 2 (gelatinase A, 72kDa gelatinase, 72kDa type IV collagenase)	-2.50	Extracellular Space	peptidase
NTM	neurotrimin	-2.50	Plasma Membrane	other
TSPAN13	tetraspanin 13	-2.50	Plasma Membrane	other
LRRC17	leucine rich repeat containing 17	-2.56	Extracellular Space	other
OCIAD2	OCIA domain containing 2	-2.56	Cytoplasm	other
TMEM2	transmembrane protein 2	-2.56	unknown	other
TUFT1	tuftelin 1	-2.56	Extracellular Space	other
CAP2	CAP, adenylate cyclase-associated protein, 2 (yeast)	-2.63	Plasma Membrane	other
PCDH19	protocadherin 19	-2.63	Extracellular Space	other
PTK7	PTK7 protein tyrosine kinase 7	-2.63	Plasma Membrane	kinase
PLAU	plasminogen activator, urokinase	-2.64	Extracellular Space	peptidase
MARCKSL1	MARCKS-like 1	-2.70	Cytoplasm	other
NTM	neurotrimin	-2.70	Plasma Membrane	other
RAB3B	RAB3B, member RAS oncogene family	-2.70	Cytoplasm	enzyme
TNFRSF10D	tumor necrosis factor receptor superfamily, member 10d, decoy with truncated death domain	-2.70	Plasma Membrane	transmembrane receptor
BCAT1	branched chain amino-acid transaminase 1, cytosolic	-2.78	Cytoplasm	enzyme
DACT1	dapper, antagonist of beta-catenin, homolog 1 (Xenopus laevis)	-2.78	Cytoplasm	other
ESM1	endothelial cell-specific molecule 1	-2.78	Extracellular Space	growth factor
EXTL1	exostoses (multiple)-like 1	-2.78	Cytoplasm	enzyme
HAS2	hyaluronan synthase 2	-2.78	Plasma Membrane	enzyme
SPHK1	sphingosine kinase 1	-2.78	Cytoplasm	kinase
TNC	tenascin C	-2.78	Extracellular Space	other
IL11	interleukin 11	-2.86	Extracellular Space	cytokine
CLDN11	claudin 11	-2.94	Plasma Membrane	other
LDB2	LIM domain binding 2	-2.94	Nucleus	transcription regulator
FLG	filaggrin	-3.03	Cytoplasm	other
HS3ST3A1	heparan sulfate (glucosamine) 3-O-sulfotransferase 3A1	-3.03	Cytoplasm	enzyme
SOX9	SRY (sex determining region Y)-box 9	-3.13	Nucleus	transcription regulator
SERTAD4-AS1	SERTAD4 antisense RNA 1	-3.23	unknown	other
TNC	tenascin C	-3.23	Extracellular Space	other
P4HA2	prolyl 4-hydroxylase, alpha polypeptide II	-3.33	Cytoplasm	enzyme
PTPRF	protein tyrosine phosphatase, receptor type, F	-3.57	Plasma Membrane	phosphatase
CDKN2B	cyclin-dependent kinase inhibitor 2B (p15, inhibits CDK4)	-3.85	Nucleus	transcription regulator
LARGE	like-glycosyltransferase	-4.00	Cytoplasm	enzyme
OXTR	oxytocin receptor	-4.00	Plasma Membrane	G-protein coupled receptor
P4HA2	prolyl 4-hydroxylase, alpha polypeptide II	-4.00	Cytoplasm	enzyme
CDH2	cadherin 2, type 1, N-cadherin (neuronal)	-4.55	Plasma Membrane	other
PTPRF	protein tyrosine phosphatase, receptor type, F	-5.26	Plasma Membrane	phosphatase
IGFBP5	insulin-like growth factor binding protein 5	-7.14	Extracellular Space	other

Table A.4: Dexamethasone-induced gene expression - microarray data II

A.4 Alkaline phosphatase assay validation

The validity of both alkaline phosphatase acitivity and cell viability assays was tested by applying the assay substrates to different cell numbers, thereby ensuring the accuracy of the test regarding a linear relation of signal to cell number (figure A.1). The activity of alkaline phosphatase was measured by using the substrate 4-methylumbelliferyl phosphate (4-MUP) and a commercially available 4-MU standard was used to test the fluorescence stability of the reaction product in the lysis buffer over time. Alkaline phosphatase activity of the cells and the conversion of the substrate during the assay were measured at 0, 30, and 60 minutes after substrate addition. The same time points were used for the validation and the results showed a reliable stable linear relationship of fluorescence of different 4-MU concentrations (figure A.2).

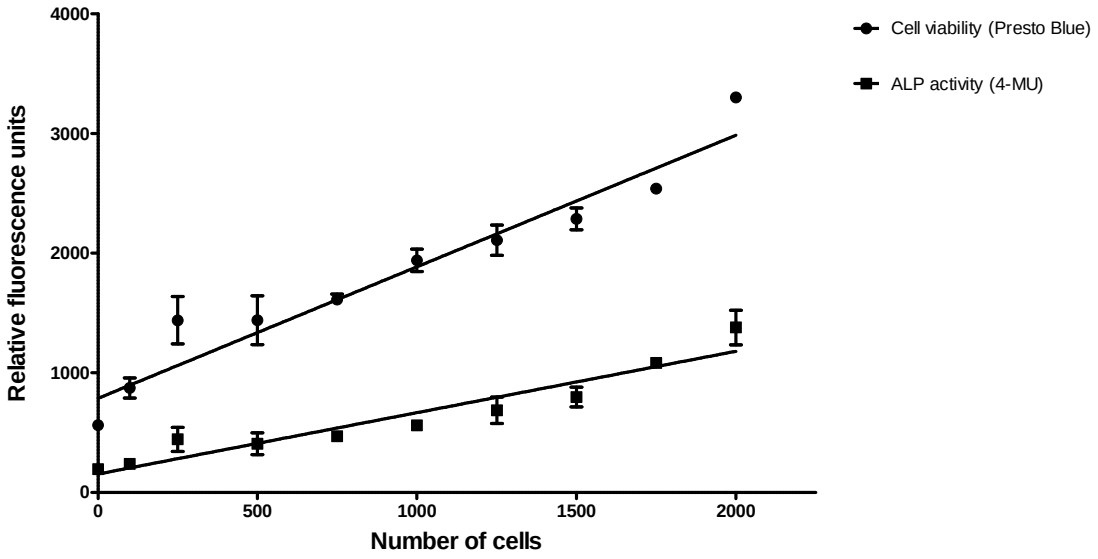

Figure A.1: Correlation of cell number to RFUs of Presto Blue® and ALP assay. Cells from 0-2000 cells per well were seeded and differentiated for 7 days when cell viability and alkaline phosphatase activity were assessed. N=3

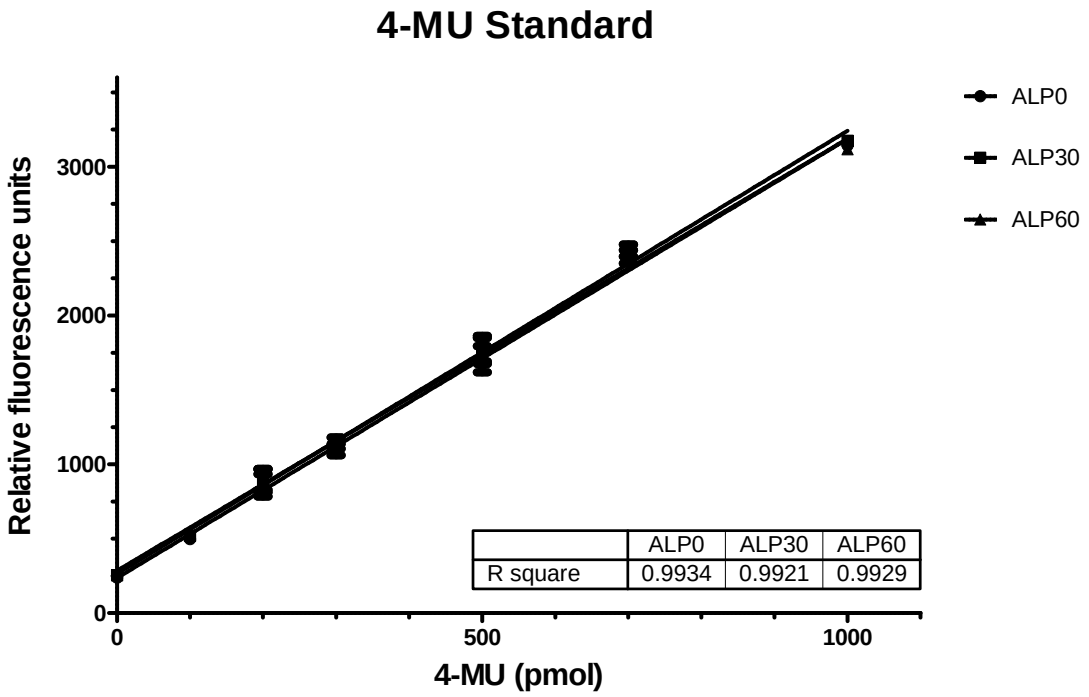

Figure A.2: Validation of alkaline phosphatase substrate stability. Fluorescence of 4-MU standard concentrations was assessed at 0, 30, and 60 minutes post substrate addition. Linear regression calculation confirmed stable product fluorescence over time.

A.5 Setup short hairpin RNA screen

A.5.1 PLACEBO Platform

At PLACEBO, a platform containing instrumentation for both high-throughput and high-content screening of small molecules was available (figure A.3). The system held two robotic arms installed in a biosafety enclosure and allowed the fully automated handling of 96 and 384 well plate formats. Different liquid transfer options included acoustic and pipet-based transfer and bulk dispensing for the addition of cells, medium, and other reagents to the plates. Plates could be sealed automatically and incubated at temperatures between 25 and 50°C. A plate washer in the system allowed implementation of assay steps requiring aspiration of liquid, e.g. washes with phosphate buffered saline (PBS), and a fluorescence plate reader provided the basis for the assay fluorescence measurements. Overall the platform allowed handling of cells and plates by the robot for most of the time, performing standardised processes and allowing a consistent treatment avoiding experimental errors introduced by the scientist (for equipment list see table A.5).

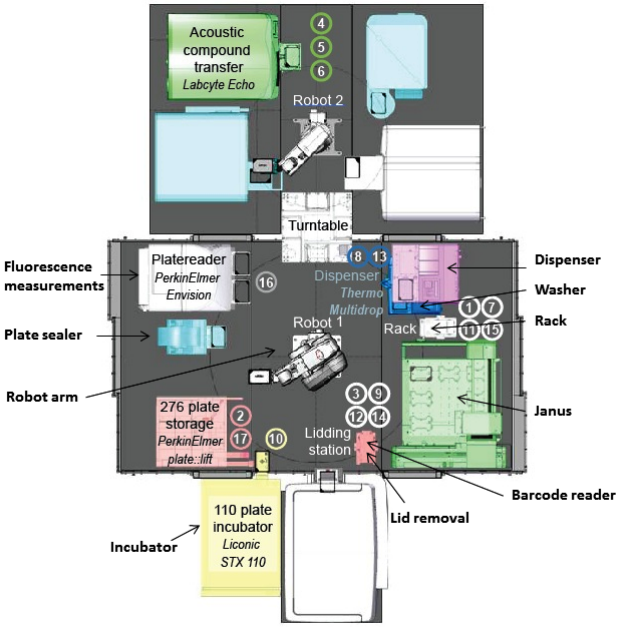

Figure A.3: Platform setup at PLACEBO Vienna

Equipment	Tasks
Dispenser	Cell seeding; medium dispensing ; shaking of plate and substrate dispensing during assay
Envision (Fluorescence plate reader)	Fluorescence reads for both cell viability and alkaline phosphatase assays
Incubator	Plate storage and incubation during ALP reaction
JANUS	All pipetting processes: virus distribution, medium removal, Presto Blue® and lysis buffer addition during assay
Plate sealer	Sealing of virus plates
Robot	All plate handling
Washer	PBS washes during assay

Table A.5: List of equipment present in the PLACEBO platform with corresponding tasks performed during the screen.

The platform was controlled by an programme called Plateworks (perkin elmer - plate::works™ automation control and scheduling software) and had an additional sub-operating system for e.g. the pipet-based transfer unit Janus (figure A.3).

A.5.2 Vector maps for viral plasmids

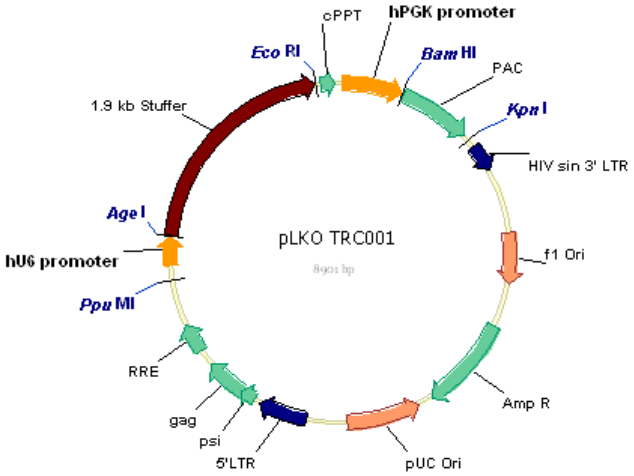

Figure A.4: Vector map pLKO TRC001 (length: 8901 bp)

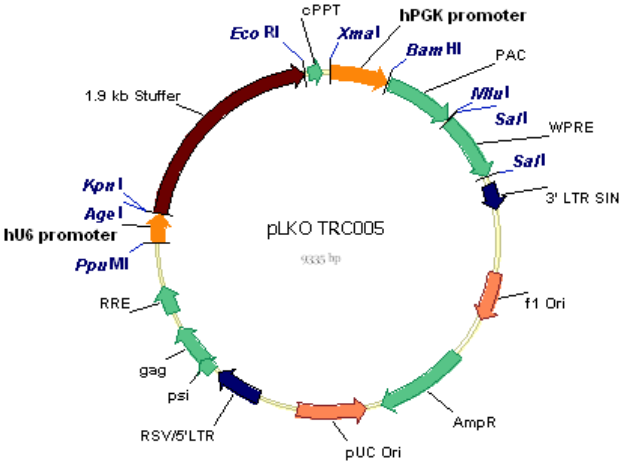

Figure A.5: Vector map pLKO TRC005 (length: 9335 bp)

A.5.3 Assay optimisation with regard to PLACEBO facility

The majority of the tasks were handled by a robot, performing standardised processes and allowing a consistent treatment avoiding human errors. However, settings like speed of dispensing or aspiration of medium or PBS, tip depths with regard to size of the wells, amounts of volumes removed and/or added and related concentrations, had to be tested and adjusted beforehand. Timings with regard to the assay were optimised and a set of eight plates per assay run turned out to be the most time-efficient and allowed previously determined incubation times (30mins for the cell viability assay, 15mins for cell lysis, and 60mins for ALP assay (including three measurements at T_0, T_{30}, and T_{60}); for more detail see later in this section). Also, some adjustments/optimisations had to be made with regard to the assay protocol. To ensure that live cells could still be in a sterile environment while other cells were already lysed, the cell lysis protocol had to be changed (several options with or without spinning, with or without transfer of protein lysates, etc. were tested; data not shown). Here, the cells were lysed directly in the 384 well plates at room temperature, shaken on a plate shaker and the lysate was used for the assay. This ensured that all steps could be handled inside the sterile platform compartment and that the plates did not need to leave the enclosed environment. Using this procedure, sufficient lysis was ensured and alkaline phosphatase activity could be clearly detected.

Protocols

In order to have most of the work consistently carried out by the robot and within the sterile enclosure, protocols for both equipment and software were developed, tested and optimised for the following parts of the experiment:

1. Cell seeding

2. Virus transduction

3. Puromycin selection

4. Induction of differentiation

5. Change of culture medium

6. Readout of osteoblast differentiation using alkaline phosphatase assay

Some of these will be shown and explained in the following sections.

Virus transduction

The shRNA library existed in 96 well plates. Therefore, four 96 well plates were used to fill one 384 well plate (figure A.6).

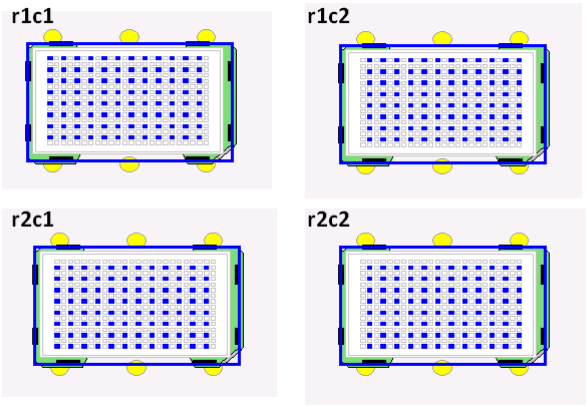

Figure A.6: Setup for virus distribution. Four virus plates are added into one 384 well plate and each filled ¼ of a quadrant.

Each hairpin was tested in five medium conditions (CM, control medium; OD, basic osteogenic medium lacking the main inducer; +DEX, complete osteogenic medium containing dexamethasone; +VitD3, complete osteogenic medium containing 1,25-dihydroxyvitamin D_3; +OSM, complete osteogenic medium containing oncostatin M). Consequently, a total of sixty 384 well plates was assessed. For the initial steps of transduction and selection, all cells were kept in MSC medium to ensure similar conditions for the hairpin integration

before the various differentiation methods were applied. A general layout of the platform protocol for the lentivirus distribution can be seen in figure A.7. All steps were carried out by the robot arm, and tip boxes were automatically renewed. The pull-down menu on the left gives an indication of the precise settings used for this application.

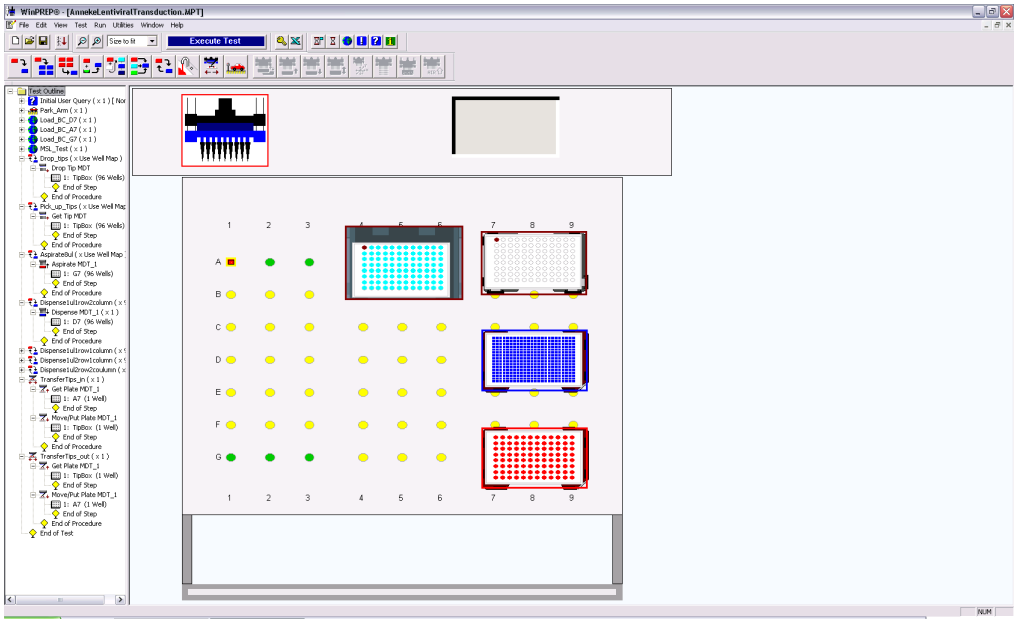

Figure A.7: JANUS setup for lentivirus transduction

Puromycin selection

The selection with puromycin was undertaken 36 hours after transduction, for this 5µg/ml puromycin was added together with new medium. Only the cells with successfully integrated hairpins exhibited a puromycin resistance and therefore survived the selection, which led to a homogeneous population of cells with the desired knockdown.

Induction of differentiation and medium change

One day after selection the medium containing puromycin was removed and replaced by osteogenic differentiation medium. In previous experiments, the duration of 24 hours was

shown to be long enough to eliminate the non-transfected cells. Culture medium was then changed again on day 3 and 5.

Alkaline phosphatase assay

All motions of the assay were performed by the robot. The procedure was as follows:

1. Plate was removed from incubator, lid was removed, barcode was read and plate transferred onto JANUS.
2. Janus aspirated 20µl of Presto Blue® from adjacent plate and dispensed 4x5µl in a 384 well plate (5µl in 50µl medium, 1:10 of substrate).
3. Plate got lid back on and was returned to incubator for 30 minutes incubation at 37°C.
4. Plate was removed from incubator, lid was removed and fluorescence measured in Envision (exc. 535, em 580, gain 1, 1%).
5. Plate was transferred onto the rack or directly to the washer and washed 3x with PBS.
6. Plate was transferred to JANUS and 10µl of CelLytic M™ containing 2% protease inhibitor were added (JANUS aspirated 40µl and dispensed 10µl each).
7. Plate got lid back on and was incubated on rack for 15 mins at room temperature.
8. Plate was transferred onto dispenser and shaken for 30 sec at 10 Hertz.
9. Substrate 4-MUP (30µl 4-MUP and 10µl TRIS, 50mM, pH8) was added by dispenser.
10. Plate was measured in Envision: exc. 340, em 520, gain 1 = ALP T_0 mins.

11. Lid got back on and plate was incubated in incubator for 30 mins at 37°C.

12. Plate was measured as in 10) (lid removed) = ALP T_{30} mins.

13. Another 30 mins incubation at 37°C (lid on).

14. Plate was measured as in 10) (lid removed) = ALP T_{60} mins.

Eight sample plates were run per set, so all procedures had to be staggered. It was ensured that all critical incubation times were adhered to. Each set of eight plates took approximately 2 ½ hours to process.

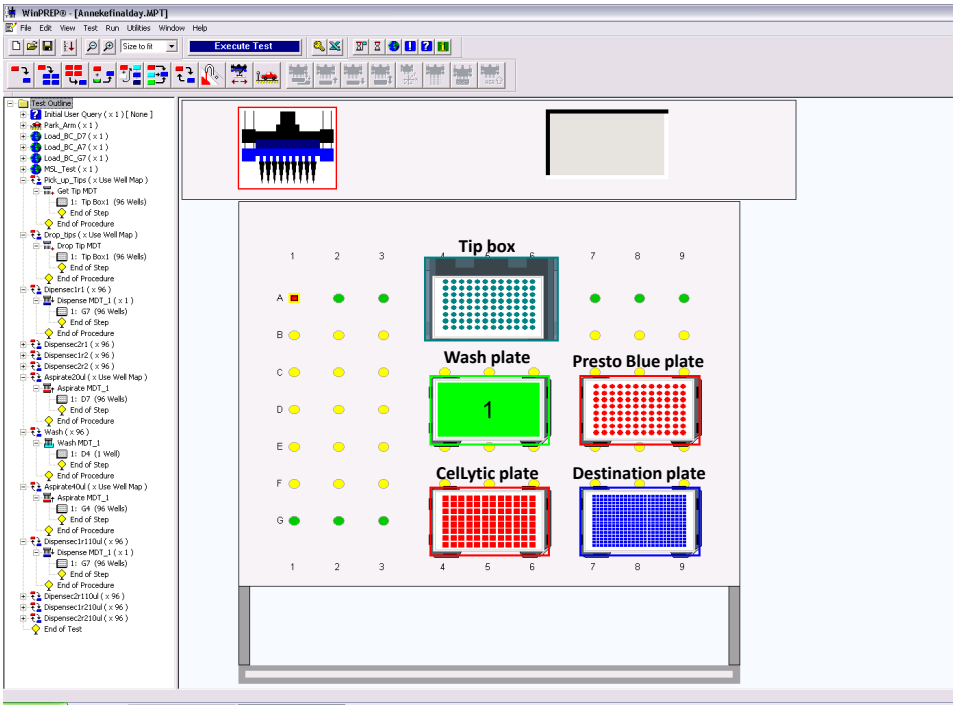

Figure A.8: JANUS setup for alkaline phosphatase assay

A.6 shRNA targets

A.6.1 Gene list

RefSeq	Gene symbol	Preferred Gene Name
NM_000383	*AIRE*	Autoimmune Polyendocrinopathy Candidiasis Ectodermal Dystrophy
NM_003488	*AKAP1*	Akinase Anchor Protein 1
NM_024810	*ALG13*	Asparaginelinked Glycosylation 13 Homolog
NM_006015	*ARID1A*	AT Rich Interactive Domain 1A
NM_002892	*ARID4A*	Retinoblastoma Binding Protein 1
NM_016374	*ARID4B*	AT Rich Interactive Domain 4B
NM_014034	*ASF1A*	ASF1 Antisilencing Function 1 Homolog A
NM_018154	*ASF1B*	CCG1interacting Factor AII
NM_018489	*ASH1L*	Ash1 (Absent, Small, Or Homeotic)Like
NM_014109	*ATAD2*	ATPase Family, AAA Domain Containing 2
NM_003600	*AURKA*	IPL1related Kinase|AuroraA|Aurorarelated Kinase 1
NM_004217	*AURKB*	Aurora1|AuroraB|Serine/Threonine Kinase 12
NM_003160	*AURKC*	Aurora/IPL1related Kinase 3|Aurora/IPL1/EG2 Protein 2|Serine/Threonine Kinase 13
NM_013448	*BAZ1A*	Bromodomain Adjacent To Zinc Finger Domain, 1A
NM_023005	*BAZ1B*	Bromodomain Adjacent To Zinc Finger Domain, 1B
NM_013449	*BAZ2A*	Bromodomain Adjacent To Zinc Finger Domain, 2A
NM_013450	*BAZ2B*	Bromodomain Adjacent To Zinc Finger Domain, 2B
NM_004459	*BPTF*	Bromodomain And PHD Domain Transcription Factor
NM_014577	*BRD1*	BR140like|Bromodomain Containing Protein 1
NM_005104	*BRD2*	Bromodomaincontaining 2|Female Sterile Homeoticrelated Gene 1
NM_007371	*BRD3*	RING3like|Bromodomain Containing Protein 3
NM_058243	*BRD4*	Bromodomaincontaining 4|Bromodomaincontaining Protein 4
NM_013263	*BRD7*	Bromodomain Protein|Bromodomaincontaining 7
NM_006696	*BRD8*	Skeletal Muscle Abundant Protein 2|Thyroid Hormone Receptor Coactivating Protein
NM_023924	*BRD9*	Rhabdomyosarcoma Antigen MURMS40.8|Sarcoma Antigen NYSAR29
NM_001726	*BRDT*	Testisspecific Bromodomain Protein
NM_004634	*BRPF1*	Bromodomain And PHD Fingercontaining Protein 1
XM_166450	*BRPF3*	Bromodomain And PHD Fingercontaining Protein 3
NM_018963	*BRWD1*	WD Repeat Domain 9
NM_153252	*BRWD3*	Bromo Domaincontaining Protein Disrupted In Leukemia
NM_006806	*BTG3*	Bcell Translocation Gene 3|Abundant In Neuroepithelium Area
NM_024644	*C14orf169*	MYCassociated Protein With JmjC Domain
NM_152382	*C2orf60*	hypothetical protein LOC129450
NM_023925	*CAPRIN2*	C1q domain containing 1
NM_199141	*CARM1*	coactivatorassociated arginine methyltransferase1
NM_032647	*CBX2*	chromobox homolog 2
NM_007276	*CBX3*	chromobox homolog 3
NM_003655	*CBX4*	chromobox homolog 4
NM_012117	*CBX5*	chromobox homolog 5
NM_014292	*CBX6*	chromobox homolog 6
NM_175709	*CBX7*	chromobox homolog 7
NM_020649	*CBX8*	chromobox homolog 8
NM_004824	*CDYL*	CDYlike, autosomal|bA620A17.2 (chromodomain protein, Y chromosomelike)
NM_152342	*CDYL2*	chromodomain Ylike protein 2
NM_031413	*CECR2*	Cat Eye Syndrome Chromosome Region, Candidate 2
NM_005483	*CHAF1A*	chromatin assembly factor I (150 kDa)
NM_005441	*CHAF1B*	CAF1 subunit B, chromatin assembly factor 1 subunit B
NM_001270	*CHD1*	chromodomain helicase DNA binding protein 1
NM_001271	*CHD2*	chromodomain helicase DNA binding protein 2
NM_001005271	*CHD3*	chromodomain helicase DNA binding protein 3
NM_001273	*CHD4*	chromodomain helicase DNA binding protein 4
NM_015557	*CHD5*	chromodomain helicase DNA binding protein 5
NM_032221	*CHD6*	chromodomain helicase DNA binding protein 6
XM_098762	*CHD7*	chromodomain helicase DNA binding protein 7
XM_370738	*CHD8*	chromodomain helicase DNA binding protein 8
NM_025134	*CHD9*	chromodomain helicase DNA binding protein 9
NM_020412	*CHMP1B*	charged multivesicular body protein 1B
NM_014453	*CHMP2A*	charged multivesicular body protein 2A
NM_176812	*CHMP4B*	charged multivesicular body protein 4B
NM_152284	*CHMP4C*	charged multivesicular body protein 4C
NM_017444	*CHRAC1*	histone fold protein
NM_004898	*CLOCK*	circadian locomoter output cycles kaput protein|clock

Table A.6: ShRNA gene target list as provided by PLACEBO - part I

RefSeq	Gene symbol	Preferred Gene Name
NM_004380	*CREBBP*	CREB binding protein
NM_014593	*CXXC1*	CpG binding protein|DNAbinding protein with PHD finger and CXXC domain
NM_022105	*DIDO1*	death associated transcription factor 1
NM_001379	*DNMT1*	DNA methyltransferase 1
NM_022552	*DNMT3A*	DNA MTase HsaIIIA|DNA cytosine methyltransferase 3 alpha
NM_006892	*DNMT3B*	DNA MTase HsaIIIB|DNA cytosine5 methyltransferase 3 beta
NM_013369	*DNMT3L*	cytosine5methyltransferase 3like protein
NM_004647	*DPF1*	Neurod4 (rat) homolog
NM_006268	*DPF2*	apoptosis response zinc finger protein|requiem
NM_012074	*DPF3*	2810403B03Rik|cerd4 (mouse) homolog
NM_003797	*EED*	WD protein associating with integrin cytoplasmic tails 1
NM_024757	*EHMT1*	G9a like protein|euchromatic histone methyltransferase 1
NM_025256	*EHMT2*	G9A histone methyltransferase|HLAB associated transcript 8|ankyrin repeatcontaining protein
NM_018091	*ELP3*	elongation protein 3 homolog
EMPTY	*EMPTY*	EMPTY
NM_001429	*EP300*	E1Aassociated protein p300|E1Abinding protein, 300kD|histone acetyltransferase p300
NM_025209	*EPC1*	enhancer of polycomb 1
NM_015630	*EPC2*	enhancer of polycomb homolog 2
NM_001991	*EZH1*	enhancer of zeste homolog 1
NM_004456	*EZH2*	enhancer of zeste 2
NM_019085	*FBXL19*	jumonji C domaincontaining histone demethylase 1C
NM_012167	*FBXO11*	Fbox only protein 11|ubiquitin protein ligase E3 component nrecognin 6
NM_017769	*G2E3*	G2/Mphase specific E3 ubiquitin ligase
clonetechGfp	*GFP*	green fluorescent protein
NM_003642	*HAT1*	histone acetyltransferase 1
NM_004964	*HDAC1*	histone deacetylase 1
NM_032019	*HDAC10*	histone deacetylase 10
NM_024827	*HDAC11*	histone deacetylase 11
NM_001527	*HDAC2*	histone deacetylase 2
NM_003883	*HDAC3*	histone deacetylase 3
NM_006037	*HDAC4*	histone deacetylase 4
NM_005474	*HDAC5*	histone deacetylase 5
NM_006044	*HDAC6*	histone deacetylase 6
NM_015401	*HDAC7*	histone deacetylase 7
NM_018486	*HDAC8*	histone deacetylase 8
NM_014707	*HDAC9*	histone deacetylase 9
NM_017902	*HIF1AN*	factor inhibiting HIF1
NM_003325	*HIRA*	HIR (histone cell cycle regulation defective) homolog A
NM_005144	*HR*	hairless protein
NM_024610	*HSPBAP1*	HSPB (heat shock 27kD) associated protein 1
NM_005537	*ING1*	inhibitor of growth family, member 1
NM_001564	*ING2*	inhibitor of growth family, member 2
NM_019071	*ING3*	inhibitor of growth family, member 3
NM_032329	*ING5*	inhibitor of growth family, member 5
NM_020395	*INTS12*	PHD finger protein 22
NM_004973	*JARID2*	jumonji homolog|jumonji, AT rich interactive domain 2 protein
NM_030647	*JHDM1D*	jumonji C domain containing histone demethylase 1 homolog D
NM_004241	*JMJD1C*	thyroid receptor interacting protein 8
NM_023007	*JMJD4*	jumonji domain containing 4
NM_024773	*JMJD5*	jumonji domain containing 5
NM_015167	*JMJD6*	jumonji domain containing 6
NM_005090	*JMJD7*	jumonji domain containing 7
NM_001005920	*JMJD8*	jumonji domain containing 8
NM_021078	*KAT2A*	GCN5 (general control of aminoacid synthesis, yeast, homolog)like 2
NM_003884	*KAT2B*	CREBBPassociated factor
NM_006388	*KAT5*	HIV1 Tat interactive protein, 60kDa|Kacetyltransferase 5
NM_015013	*KDM1A*	lysine (K)specific demethylase 1|lysinespecific histone demethylase 1
XM_173173	*KDM1B*	amine oxidase, flavin containing 1
NM_012308	*KDM2A*	Fbox protein FBL11|jumonji C domaincontaining histone demethylase 1A
NM_001005366	*KDM2B*	jumonji C domaincontaining histone demethylase 1B
NM_018433	*KDM3A*	jumonji C domaincontaining histone demethylase 2A
NM_016604	*KDM3B*	nuclear protein 5qNCA
NM_014663	*KDM4A*	jumonji C domaincontaining histone demethylase 3A
NM_015015	*KDM4B*	jumonji C domaincontaining histone demethylase 4B
NM_015061	*KDM4C*	lysine (K)-specific demethylase 4C
NM_018039	*KDM4D*	lysine (K)-specific demethylase 4D
NM_005056	*KDM5A*	Jumonji, AT rich interactive domain 1A (RBP2like)|retinoblastoma binding protein 2
NM_006618	*KDM5B*	Jumonji, AT rich interactive domain 1B (RBP2like)
NM_004187	*KDM5C*	Jumonji, AT rich interactive domain 1C (RBP2like)

Table A.7: ShRNA gene target list as provided by PLACEBO - part II

RefSeq	Gene symbol	Preferred Gene Name
NM_004653	*KDM5D*	Jumonji, AT rich interactive domain 1D (RBP2like)
NM_021140	*KDM6A*	ubiquitouslytranscribed TPR gene on the X chromosome
NM_001080424	*KDM6B*	lysine (K)-specific demethylase 6B
lacZ	*lacZ*	lacZ
NM_002296	*LBR*	integral nuclear envelope inner membrane protein
NM_002384	*MBD1*	methyl-CpG binding domain protein 1
NM_003927	*MBD2*	methyl-CpG binding domain protein 2
NM_003926	*MBD3*	methyl-CpG binding domain protein 3
NM_003925	*MBD4*	methyl-CpG binding domain protein 4
NM_018328	*MBD5*	methyl-CpG binding domain protein 5
NM_052897	*MBD6*	methyl-CpG binding domain protein 6
NM_005241	*MECOM*	AML1EVI1 fusion protein|oncogene EVI1
NM_004992	*MECP2*	methyl CpG binding protein 2
NM_032778	*MINA*	mineral dust induced gene protein
NM_005933	*MLL*	CDK6/MLL fusion protein
NM_003482	*MLL2*	trinucleotide repeat containing 21
NM_021230	*MLL3*	histonelysine Nmethyltransferase, H3 lysine4 specific
NM_014727	*MLL4*	WW domain binding protein 7
NM_018682	*MLL5*	myeloid/lymphoid or mixedlineage leukemia 5
NM_004641	*MLLT10*	myeloid/lymphoid or mixedlineage leukemia (trithorax (Drosophila) homolog); translocated to, 10
NM_005937	*MLLT6*	Myeloid/lymphoid or mixedlineage leukemia, translocated to, 6
NM_006791	*MORF4L1*	MORFrelated gene 15
NM_017520	*MPHOSPH8*	Mphase phosphoprotein, mpp
NM_006800	*MSL3*	drosophila MSL3like 1
NM_004689	*MTA1*	metastasis associated gene 1 protein
NM_004739	*MTA2*	metastasis associated gene 1like 1
XM_038567	*MTA3*	metastasis associated family, member 3
NM_007358	*MTF2*	metal response elementbinding transcription factor 2
NM_032188	*MYST1*	histone acetyltransferase MYST1
NM_007067	*MYST2*	histone acetyltransferase
NM_006766	*MYST3*	Monocytic leukemia zinc finger protein
NM_012330	*MYST4*	histone acetyltransferase
NM_004537	*NAP1L1*	nucleosome assembly protein 1-like 1
NM_021963	*NAP1L2*	nucleosome assembly protein 1-like 1
NM_004538	*NAP1L3*	nucleosome assembly protein 1-like 3
NM_005969	*NAP1L4*	nucleosome assembly protein 1-like 2
NM_153757	*NAP1L5*	nucleosome assembly protein 1-like 5
NM_014293	*NPTXR*	neuronal pentraxin receptor
NM_022455	*NSD1*	androgen receptorassociated coregulator 267
NM_012387	*PADI4*	PADIH protein|peptidyl arginine deiminase, type V
NM_018165	*PBRM1*	polybromo 1
pgw	*pgw*	(toxic)
NM_004427	*PHC2*	early development regulator 2 (homolog of polyhomeotic 2)
NM_024947	*PHC3*	early development regulator 3
NM_002636	*PHF1*	PHD finger protein 1
NM_018288	*PHF10*	PHD finger protein 10
NM_016119	*PHF11*	PHD finger protein 11
NM_020889	*PHF12*	PHD finger protein 12
NM_153812	*PHF13*	PHD finger protein 13
XM_376578	*PHF14*	PHD finger protein 14
NM_015288	*PHF15*	PHD finger protein 15
NM_014735	*PHF16*	PHD finger protein 16
NM_024900	*PHF17*	PHD protein Jade1
NM_015651	*PHF19*	polycomb like 3
NM_005392	*PHF2*	jumonji C domaincontaining histone demethylase 1E
NM_016436	*PHF20*	gliomaexpressed antigen 2
NM_016018	*PHF20L1*	PHD finger protein 20-like 1
NM_016621	*PHF21A*	BRAF35/HDAC2 complex
NM_138415	*PHF21B*	PHD finger protein 21B
NM_024297	*PHF23*	PHD finger protein 23a
NM_015153	*PHF3*	PHD finger protein 3
NM_032335	*PHF6*	PHD finger protein 6
NM_016483	*PHF7*	PHD finger protein 7
NM_015107	*PHF8*	PHD finger protein 8
NM_017934	*PHIP*	pleckstrin homology domain interacting protein
NM_020901	*PHRF1*	PHD and ring finger domains 1
NM_001198	*PRDM1*	PRdomain zinc finger protein 1
NM_020228	*PRDM10*	PRDM zinc finger transcription factor
NM_021619	*PRDM12*	PRdomain containing protein 12

Table A.8: ShRNA gene target list as provided by PLACEBO - part III

RefSeq	Gene symbol	Preferred Gene Name
NM_021620	*PRDM13*	PRdomain containing protein 13
NM_024504	*PRDM14*	PRdomain zinc finger protein 14
NM_022115	*PRDM15*	zinc finger protein 298
NM_022114	*PRDM16*	PRdomain zinc finger protein 16
NM_012231	*PRDM2*	GATA3 binding protein G3B
NM_012406	*PRDM4*	PRdomain zincfinger protein PFM1
NM_018699	*PRDM5*	PRdomain zinc finger protein 5
NM_001136239	*PRDM6*	PRdomain zinc finger protein 6
NM_020226	*PRDM8*	PRdomain containing protein 8
NM_020227	*PRDM9*	PRdomain containing protein 9
NM_001536	*PRMT1*	HMT1 (hnRNP methyltransferase, S. cerevisiae)like 2
NM_001535	*PRMT2*	HMT1 (hnRNP methyltransferase, S. cerevisiae) like 1
NM_005788	*PRMT3*	HMT1 hnRNP methyltransferaselike 3
NM_006109	*PRMT5*	HMT1 hnRNP methyltransferaselike 5
NM_018137	*PRMT6*	HMT1 hnRNP methyltransferaselike 6
NM_019023	*PRMT7*	protein arginine Nmethyltransferase 7
NM_019854	*PRMT8*	HMT1 hnRNP methyltransferaselike 3
NM_015617	*PYGO1*	pygopus homolog 1
NM_138300	*PYGO2*	pygopus homolog 2
NM_030665	*RAI1*	retinoic acid induced 1
rfp	*RFP*	red fluorescent protein
NM_031277	*RNF17*	spermatogenesis associated 23|tudor domain containing 4
NM_016578	*RSF1*	HBV pX associated protein8|hepatitis B virus x associated protein
NM_003011	*SET*	HLADRassociated protein II|SET translocation (myeloid leukemiaassociated)
NM_014712	*SETD1A*	SET domain containing 1A
XM_001715003	*SETD1B*	SET domain containing 1B
NM_012271	*SETD2*	SET domaincontaining protein 2
NM_199123	*SETD3*	SET domaincontaining protein 3
NM_017438	*SETD4*	SET domaincontaining protein 4
NM_001080517	*SETD5*	SET domaincontaining protein 5
NM_024860	*SETD6*	SET domaincontaining protein 6
NM_030648	*SETD7*	H3K4HMTase|SET domaincontaining protein 7
NM_020382	*SETD8*	H4K20specific histone methyltransferase
NM_012432	*SETDB1*	ERGassociated protein with a SET domain
NM_031915	*SETDB2*	CLLL8 protein
NM_006515	*SETMAR*	SET domain and mariner transposase fusion
NM_173082	*SHPRH*	2610103K11Rik|OTTHUMP00000040140
NM_015477	*SIN3A*	SIN3 homolog A, transcriptional regulator
NM_015260	*SIN3B*	SIN3 homolog B, transcription regulator
NM_012238	*SIRT1*	sir2like 1|sirtuin 1
NM_012237	*SIRT2*	sir2related protein type 2|sirtuin 7
NM_012239	*SIRT3*	sir2like 3|sirtuin 3
NM_012240	*SIRT4*	sir2like 4|sirtuin 4
NM_012241	*SIRT5*	sir2like 5|sirtuin 5
NM_016539	*SIRT6*	sir2related protein type 6|sirtuin 6
NM_016538	*SIRT7*	sir2related protein type 7|sirtuin 7
NM_003069	*SMARCA1*	SWI/SNFrelated matrix associated actin dependent regulator of chromatin a1
NM_003070	*SMARCA2*	SWI/SNFrelated matrix associated actin dependent regulator of chromatin a2
NM_003072	*SMARCA4*	SWI/SNFrelated matrix associated actin dependent regulator of chromatin a4
NM_003601	*SMARCA5*	SWI/SNFrelated matrix associated actin dependent regulator of chromatin a5
NM_020159	*SMARCAD1*	WI/SNFrelated matrix associated actin dependent regulator of chromatin d1
NM_003073	*SMARCB1*	WI/SNFrelated matrix associated actin dependent regulator of chromatin b1
NM_003074	*SMARCC1*	SWI/SNFrelated matrix associated actin dependent regulator of chromatin c1
NM_003075	*SMARCC2*	SWI/SNFrelated matrix associated actin dependent regulator of chromatin c2
NM_003076	*SMARCD1*	SWI/SNFrelated matrix associated actin dependent regulator of chromatin d1
NM_003077	*SMARCD2*	SWI/SNFrelated matrix associated actin dependent regulator of chromatin d2
NM_003078	*SMARCD3*	SWI/SNF related matrix associated actin dependent regulator of chromatin d1
NM_006306	*SMC1A*	SMC1 structural maintenance of chromosomes 1like 1
NM_148674	*SMC1B*	SMC1 structural maintenance of chromosomes 1like 2
NM_006444	*SMC2*	SMC2 structural maintenance of chromosomes 2like 1
NM_005445	*SMC3*	chondroitin sulfate proteoglycan 6 (bamacan)
NM_005496	*SMC4*	SMC4 structural maintenance of chromosomes 4like 1
NM_000344	*SMN1*	gemin 1|spinal muscular atrophy
NM_017411	*SMN2*	gemin 1
NM_005871	*SMNDC1*	SMNrelated protein
NM_198274	*SMYD1*	CD8 beta opposite|zinc finger, MYND domain containing 18
NM_020197	*SMYD2*	zinc finger, MYND domain containing 14
NM_022743	*SMYD3*	zinc finger protein, subfamily 3A (MYND domain containing), 1
NM_052928	*SMYD4*	SET And MYND Domain Containing 4

Table A.9: ShRNA gene target list as provided by PLACEBO - part IV

RefSeq	Gene symbol	Preferred Gene Name
NM_006062	*SMYD5*	retinoic acid induced 15
NM_014390	*SND1*	EBNA2 coactivator p100
NM_003113	*SP100*	SP100HMG nuclear autoantigen
NM_007237	*SP140*	nuclear body protein Sp140
NM_138402	*SP140L*	hypothetical protein LOC93349
NM_032944	*STK31*	sugen kinase 396|tudor domain containing 8
NM_022491	*SUDS3*	Sin3 histone deacetylase corepressor complex component SDS3
XM_376044	*SUPT7L*	SPTFassociated factor 65 gamma
NM_003173	*SUV39H1*	Su(var)39 homolog 1|histone H3K9 methyltransferase 1
NM_024670	*SUV39H2*	suppressor of variegation 39 homolog 2
NM_017635	*SUV420H1*	suppressor of variegation 420 homolog 1
NM_032701	*SUV420H2*	suppressor of variegation 420 homolog 2
NM_015355	*SUZ12*	joined to JAZF1
NM_004606	*TAF1*	TBPassociated factor 1
XM_291729	*TAF3*	TAF3 RNA polymerase II, TATA box binding protein (TBP)associated factor
NM_138572	*TAF8*	TAF8 RNA polymerase II, TATA box binding protein (TBP)associated factor
NM_005650	*TCF20*	stromelysin 1 PDGFresponsive elementbinding protein
NM_198795	*TDRD1*	tudor domain containing protein 1
NM_030794	*TDRD3*	tudor domaincontaining protein 3
NM_173533	*TDRD5*	tudor domaincontaining protein 5
NM_001010870	*TDRD6*	tudor repeat 2
NM_014290	*TDRD7*	tudor repeat associator with PCTAIRE 2
NM_153046	*TDRD9*	hypoxiainducible HIG1
NM_006862	*TDRKH*	tudor and KH domaincontaining protein
NM_032271	*TRAF7*	ring finger and WD repeat domain 1
NM_003852	*TRIM24*	transcriptional intermediary factor 1 alpha
NM_005762	*TRIM28*	transcriptional intermediary factor 1beta
NM_015906	*TRIM33*	tripartite motifcontaining 33 protein
XM_001716253	*TRIM66*	transcriptional intermediary factor 1 delta
NM_003336	*UBE2A*	ubiquitinconjugating enzyme E2A
NM_003337	*UBE2B*	ubiquitinconjugating enzyme E2B
NM_003345	*UBE2I*	ubiquitinconjugating enzyme E2I (homologous to yeast UBC9)
NM_021988	*UBE2V1*	DNAbinding protein
NM_018108	*UBR7*	Ubiquitin Protein Ligase E3 Component N-Recognin 7
NM_013282	*UHRF1*	RING finger protein 106|nuclear zinc finger protein Np95
NM_152306	*UHRF2*	Np95like ring finger protein|nuclear zinc finger protein NP97
NM_007125	*UTY*	ubiquitous TPR motif protein UTY
NM_007331	*WHSC1*	WolfHirschhorn syndrome candidate 1 protein
NM_017778	*WHSC1L1*	WolfHirschhorn syndrome candidate 1like 1 protein
NM_006624	*ZMYND11*	BS69 variant 1
NM_183048	*ZMYND8*	zinc finger MYND domain containing protein 8

Table A.10: ShRNA gene target list as provided by PLACEBO - part V

A.6.2 Short list shRNA target genes

Gene	HairpinNr	Condition	Clone ID	% Remaining	POC Cell viability	POC ALP60
BRD4	1	+DEX	TRCN0000021425	44	92.1	35.1
BRD4	1	+DEX	TRCN0000021425	44	81.4	74.8
BRD4	1	OD	TRCN0000021425	44	178.7	112.1
BRD4	1	OD	TRCN0000021425	44	152.4	111.6
BRD4	1	+VitD3	TRCN0000021425	44	131.7	81.8
BRD4	1	+VitD3	TRCN0000021425	44	132.3	74.6
BRD4	1	+OSM	TRCN0000021425	44	110.7	55.8
BRD4	1	+OSM	TRCN0000021425	44	91.3	67.6
BRD4	5	+DEX	TRCN0000195245	137	109.9	47.7
BRD4	5	+DEX	TRCN0000195245	137	113.4	59.8
BRD4	5	OD	TRCN0000195245	137	143.3	126.8
BRD4	5	OD	TRCN0000195245	137	126.9	109.8
BRD4	5	+VitD3	TRCN0000195245	137	124.6	91.0
BRD4	5	+VitD3	TRCN0000195245	137	111.2	72.6
BRD4	5	+OSM	TRCN0000195245	137	100.8	72.8
BRD4	5	+OSM	TRCN0000195245	137	117.9	84.7
KDM1A	2	CM	TRCN0000046071	4	115.8	1059.3
KDM1A	2	CM	TRCN0000046071	4	104.3	629.2
KDM1A	2	OD	TRCN0000046071	4	116.8	2116.8
KDM1A	2	OD	TRCN0000046071	4	99.0	969.6
KDM1A	2	OD	TRCN0000046071	4	132.7	658.7
KDM1A	2	+DEX	TRCN0000046071	4	88.5	493.3
KDM1A	2	+DEX	TRCN0000046071	4	144.9	1807.1
KDM1A	2	+VitD3	TRCN0000046071	4	95.8	731.2
KDM1A	2	+VitD3	TRCN0000046071	4	112.6	782.6
KDM1A	2	+OSM	TRCN0000046071	4	92.3	540.4
KDM1A	2	+OSM	TRCN0000046071	4	110.0	700.1
KDM1A	3	CM	TRCN0000046070	34	125.1	267.1
KDM1A	3	CM	TRCN0000046070	34	127.4	202.3
KDM1A	3	OD	TRCN0000046070	34	135.0	344.5
KDM1A	3	OD	TRCN0000046070	34	118.4	225.8
KDM1A	3	OD	TRCN0000046070	34	127.4	234.7
KDM1A	3	+DEX	TRCN0000046070	34	125.8	316.8
KDM1A	3	+DEX	TRCN0000046070	34	164.8	306.6
KDM1A	3	+VitD3	TRCN0000046070	34	91.8	306.4
KDM1A	3	+VitD3	TRCN0000046070	34	100.1	278.8
KDM1A	3	+OSM	TRCN0000046070	34	102.5	168.4
KDM1A	3	+OSM	TRCN0000046070	34	104.0	217.8
KDM1A	4	CM	TRCN0000046068	5	105.7	150.4
KDM1A	4	CM	TRCN0000046068	5	102.2	216.0
KDM1A	4	OD	TRCN0000046068	5	109.6	296.3
KDM1A	4	OD	TRCN0000046068	5	106.0	235.5
KDM1A	4	OD	TRCN0000046068	5	125.5	209.8
KDM1A	4	+DEX	TRCN0000046068	5	133.4	293.5
KDM1A	4	+DEX	TRCN0000046068	5	135.9	226.8
KDM1A	4	+VitD3	TRCN0000046068	5	109.6	254.9
KDM1A	4	+VitD3	TRCN0000046068	5	94.2	216.3
KDM1A	4	+OSM	TRCN0000046068	5	99.6	148.4
KDM1A	4	+OSM	TRCN0000046068	5	124.2	184.1

Table A.11: ShRNA target genes - knockdown results *BRD4* and *KDM1A*

Gene	HairpinNr	Condition	Clone ID	% Remaining	POC Cell viability	POC ALP60
JMJD8	3	CM	TRCN0000166974	5	99.8	448.9
JMJD8	3	CM	TRCN0000166974	5	98.5	263.1
JMJD8	3	OD	TRCN0000166974	5	101.2	596.2
JMJD8	3	OD	TRCN0000166974	5	113.3	329.3
JMJD8	3	OD	TRCN0000166974	5	101.8	326.8
JMJD8	3	+DEX	TRCN0000166974	5	118.9	547.1
JMJD8	3	+DEX	TRCN0000166974	5	126.7	565.4
JMJD8	3	+VitD3	TRCN0000166974	5	88.1	325.6
JMJD8	3	+VitD3	TRCN0000166974	5	86.4	253.5
JMJD8	3	+OSM	TRCN0000166974	5	87.7	374.7
JMJD8	3	+OSM	TRCN0000166974	5	94.5	425.7
JMJD8	4	CM	TRCN0000167284	22	119.9	367.4
JMJD8	4	CM	TRCN0000167284	22	110.8	241.6
JMJD8	4	OD	TRCN0000167284	22	109.5	655.7
JMJD8	4	OD	TRCN0000167284	22	118.6	307.3
JMJD8	4	OD	TRCN0000167284	22	123.9	287.7
JMJD8	4	+DEX	TRCN0000167284	22	122.1	366.2
JMJD8	4	+DEX	TRCN0000167284	22	128.8	343.8
JMJD8	4	+VitD3	TRCN0000167284	22	79.2	364.8
JMJD8	4	+VitD3	TRCN0000167284	22	94.9	355.6
JMJD8	4	+OSM	TRCN0000167284	22	103.2	195.5
JMJD8	4	+OSM	TRCN0000167284	22	74.5	193.4
MORF4L1	3	CM	TRCN0000107583	12	121.1	184.7
MORF4L1	3	CM	TRCN0000107583	12	104.4	150.3
MORF4L1	3	OD	TRCN0000107583	12	99.6	809.6
MORF4L1	3	OD	TRCN0000107583	12	114.4	395.7
MORF4L1	3	OD	TRCN0000107583	12	99.6	174.7
MORF4L1	3	OD	TRCN0000107583	12	79.0	151.6
MORF4L1	3	+DEX	TRCN0000107583	12	130.1	350.8
MORF4L1	3	+DEX	TRCN0000107583	12	110.4	467.3
MORF4L1	3	+VitD3	TRCN0000107583	12	91.3	175.5
MORF4L1	3	+VitD3	TRCN0000107583	12	95.0	184.6
MORF4L1	3	+OSM	TRCN0000107583	12	77.1	183.8
MORF4L1	3	+OSM	TRCN0000107583	12	108.0	167.8
MORF4L1	4	CM	TRCN0000107581	3	105.7	195.9
MORF4L1	4	CM	TRCN0000107581	3	107.0	213.0
MORF4L1	4	OD	TRCN0000107581	3	114.8	468.8
MORF4L1	4	OD	TRCN0000107581	3	107.3	581.8
MORF4L1	4	OD	TRCN0000107581	3	122.0	378.9
MORF4L1	4	OD	TRCN0000107581	3	105.3	330.2
MORF4L1	4	+DEX	TRCN0000107581	3	117.7	404.4
MORF4L1	4	+DEX	TRCN0000107581	3	139.7	536.8
MORF4L1	4	+VitD3	TRCN0000107581	3	105.1	398.0
MORF4L1	4	+VitD3	TRCN0000107581	3	105.0	398.2
MORF4L1	4	+OSM	TRCN0000107581	3	104.7	251.1
MORF4L1	4	+OSM	TRCN0000107581	3	127.8	290.3

Table A.12: ShRNA target genes - knockdown results *JMJD8* and *MORF4L1*

Gene	HairpinNr	Condition	Clone ID	% Remaining	POC Cell viability	POC ALP60
PHIP	3	CM	TRCN0000130643	40	100.6	548.5
PHIP	3	CM	TRCN0000130643	40	72.0	710.2
PHIP	3	OD	TRCN0000130643	40	42.9	652.8
PHIP	3	OD	TRCN0000130643	40	88.5	1229.2
PHIP	3	OD	TRCN0000130643	40	92.7	531.5
PHIP	3	OD	TRCN0000130643	40	90.2	447.4
PHIP	3	+DEX	TRCN0000130643	40	102.9	1287.7
PHIP	3	+DEX	TRCN0000130643	40	110.6	1167.0
PHIP	3	+VitD3	TRCN0000130643	40	83.2	658.3
PHIP	3	+VitD3	TRCN0000130643	40	85.5	560.1
PHIP	3	+OSM	TRCN0000130643	40	67.7	329.4
PHIP	3	+OSM	TRCN0000130643	40	117.2	577.9
UBE2A	4	CM	TRCN0000004006	98	105.0	329.7
UBE2A	4	CM	TRCN0000004006	98	86.4	325.7
UBE2A	4	OD	TRCN0000004006	98	93.2	311.8
UBE2A	4	OD	TRCN0000004006	98	89.9	248.6
UBE2A	4	OD	TRCN0000004006	98	91.3	245.7
UBE2A	4	OD	TRCN0000004006	98	82.7	234.8
UBE2A	4	+DEX	TRCN0000004006	98	98.0	294.1
UBE2A	4	+DEX	TRCN0000004006	98	89.3	224.2
UBE2A	4	+VitD3	TRCN0000004006	98	98.9	319.6
UBE2A	4	+VitD3	TRCN0000004006	98	97.2	308.0
UBE2A	4	+OSM	TRCN0000004006	98	92.4	322.8
UBE2A	4	+OSM	TRCN0000004006	98	99.2	290.6
UBE2A	5	CM	TRCN0000004007	78	79.6	231.6
UBE2A	5	CM	TRCN0000004007	78	74.7	151.5
UBE2A	5	OD	TRCN0000004007	78	85.4	282.8
UBE2A	5	OD	TRCN0000004007	78	95.4	331.4
UBE2A	5	OD	TRCN0000004007	78	77.4	241.7
UBE2A	5	OD	TRCN0000004007	78	81.1	241.9
UBE2A	5	+DEX	TRCN0000004007	78	110.5	419.0
UBE2A	5	+DEX	TRCN0000004007	78	112.5	350.0
UBE2A	5	+VitD3	TRCN0000004007	78	85.4	348.9
UBE2A	5	+VitD3	TRCN0000004007	78	91.7	381.1
UBE2A	5	+OSM	TRCN0000004007	78	97.0	434.6
UBE2A	5	+OSM	TRCN0000004007	78	104.8	428.4

Table A.13: ShRNA target genes - knockdown results *PHIP* and *UBE2A*

A.7 Protein network analysis

Hits and interaction partners were mapped to known complexes, in order to determine which protein complexes are represented by the obtained targets. In tables A.14 to **??**, the complexes are listed according to their significance.

The criteria for the complexes are listed below:

Short explanation of titles:

cplx name —> complex name

cplx members —> complex members (Uniprot ID)

cplx size —> number of complex members

total hits —> hits that are part of this complex (target genes and interaction partners)

num hits —> number of hits (= total hits)

cplx cov —> complex coverage - percentage of how much of the complex is covered by the total hits

p-value —> how significant is this complex hit

hits —> how many "real hits" (from the target gene list)

interactors —> how many interactors (genes of this complex that are interacting with target genes)

corr_p —> corrected p-value (multivariate testing)

Filters:

num hits > 1

cplx size > 2

cplx cov > 0.75

Cplx name	Cplx members	Cplx size	Total Hits	Num Hits	Cplx cov	p-value	Hits	Interactors	corr_p
LARC complex (LCR-associated remodelling complex)	P60709, O96019, O14497, Q14839, Q92785, Q8WXI9, Q13547, Q92769, P07910, Q9UBB5, O95983, O94776, Q09028, P51532, Q12824, Q92922, Q8TAQ2, Q92925, Q969G3	19	['O94776', 'Q92769', 'Q12824', 'O14497', 'Q8WXI9', 'Q9UBB5', 'O95983', 'O96019', 'P51532', 'Q09028', 'Q13547', 'Q14839', 'Q8TAQ2', 'Q92922', 'Q969G3']	15	0.79	7.22E-24	4	11	3.45E-21
SIN3-ING1b complex II	O96019, O14497, Q4LE39, Q13547, Q92769, Q9UK53, Q09028, Q16576, O00422, O75446, Q96ST3, P51532, Q12824, Q92922, Q8TAQ2, Q96GM5	16	['Q92769', 'Q12824', 'O14497', 'Q96GM5', 'O96019', 'P51532', 'Q09028', 'Q13547', 'Q16576', 'Q8TAQ2', 'Q92922', 'Q96ST3', 'Q9UK53']	13	0.81	4.09E-21	3	10	9.75E-19
BRM-SIN3A complex	O96019, O14497, Q13547, Q92769, O14744, Q09028, Q96ST3, P51531, Q12824, Q92922, Q8TAQ2, Q96GM5, Q92925, Q6STE5, Q969G3	15	['Q92769', 'Q12824', 'O14497', 'Q96GM5', 'O96019', 'P51531', 'Q09028', 'Q13547', 'Q8TAQ2', 'Q92922', 'Q969G3', 'Q96ST3']	12	0.80	2.05E-19	3	9	1.63E-17
NuA4/Tip60 HAT complex	O96019, Q9H0E9, Q9HAF1, Q9NPF5, Q96L91, Q9H2F5, Q92993, Q9NXR8, Q9UBU8, Q15014, Q9NV56, Q9Y265, Q9Y230, Q9Y4A5, O95619	15	['Q92993', 'Q9UBU8', 'Q9H0E9', 'O95619', 'O96019', 'Q15014', 'Q9H2F5', 'Q9HAF1', 'Q9NPF5', 'Q9NV56', 'Q9NXR8', 'Q9Y4A5']	12	0.80	2.05E-19	3	9	1.95E-17
WINAC complex	O96019, O14497, Q9UIG0, Q13111, P51531, P51532, Q12824, Q92922, Q8TAQ2, Q96GM5, Q969G3, Q9Y5B9, Q02880, P11473	14	['Q12824', 'Q9UIG0', 'O14497', 'Q96GM5', 'O96019', 'P51531', 'P51532', 'Q02880', 'Q8TAQ2', 'Q92922', 'Q969G3']	11	0.79	1.01E-17	3	8	5.33E-16
BRG1-SIN3A complex	O96019, O14497, Q92769, O14744, Q09028, Q96ST3, P51532, Q12824, Q92922, Q8TAQ2, Q96GM5, Q92925, Q6STE5, Q969G3	14	['Q92769', 'Q12824', 'O14497', 'Q96GM5', 'O96019', 'P51532', 'Q09028', 'Q8TAQ2', 'Q92922', 'Q969G3', 'Q96ST3']	11	0.79	1.01E-17	3	8	5.99E-16

Table A.14: Protein complexes - Part I

Cplx name	Cplx members	Cplx size	Total Hits	Num Hits	Cplx cov	p-value	Hits	Interactors	corr_p
BRG1-SIN3A-HDAC containing SWI/SNF remodeling complex I	O96019, O14497, Q92769, O14744, Q96ST3, P51532, Q12824, Q92922, Q8TAQ2, Q96GM5, Q969G3	11	['Q92769', 'Q12824', 'O14497', 'Q96GM5', 'O96019', 'P51532', 'Q8TAQ2', 'Q92922', 'Q969G3', 'Q96ST3']	10	0.91	1.92E-17	3	7	9.15E-16
BRM-SIN3A-HDAC complex	O96019, O14497, Q92769, O14744, Q96ST3, P51531, Q12824, Q92922, Q8TAQ2, Q96GM5, Q92925, Q969G3	12	['Q92769', 'Q12824', 'O14497', 'Q96GM5', 'O96019', 'P51531', 'Q8TAQ2', 'Q92922', 'Q969G3', 'Q96ST3']	10	0.83	1.13E-16	3	7	3.18E-15
BAF complex	O96019, O14497, Q12824, Q92922, Q8TAQ2, Q96GM5, Q969G3, (P51531, P51532)	9	['Q12824', 'O14497', 'Q96GM5', 'O96019', 'P51531', 'P51532', 'Q8TAQ2', 'Q92922', 'Q969G3']	9	1.00	1.08E-16	2	7	3.21E-15
BAF complex	O96019, O14497, P51531, P51532, Q12824, Q92922, Q8TAQ2, Q96GM5, Q969G3	9	['Q12824', 'O14497', 'Q96GM5', 'O96019', 'P51531', 'P51532', 'Q8TAQ2', 'Q92922', 'Q969G3']	9	1.00	1.08E-16	2	7	3.43E-15
MTA2 complex	Q14839, Q13547, Q92769, O95983, O94776, Q09028, Q16576, (Q96ST3, O75182)	9	['O94776', 'Q92769', 'O75182', 'O95983', 'Q09028', 'Q13547', 'Q14839', 'Q16576', 'Q96ST3']	9	1.00	1.08E-16	3	6	3.67E-15
MeCP1 complex	Q14839, Q8WXI9, Q13547, Q92769, Q9UBB5, O95983, O94776, Q09028, Q16576	9	['O94776', 'Q92769', 'Q8WXI9', 'Q9UBB5', 'O95983', 'Q09028', 'Q13547', 'Q14839', 'Q16576']	9	1.00	1.08E-16	2	7	3.95E-15
BAF complex	O96019, O14497, Q12824, Q92922, Q8TAQ2, Q969G3, (P51531, P51532), (Q96GM5, Q92925, Q6STE5)	11	['Q12824', 'O14497', 'Q96GM5', 'O96019', 'P51531', 'P51532', 'Q8TAQ2', 'Q92922', 'Q969G3']	9	0.82	5.73E-15	2	7	1.44E-13
MeCP1 complex	Q14839, Q13547, Q92769, Q9UBB5, O95983, O94776, Q09028, Q16576	8	['O94776', 'Q92769', 'Q9UBB5', 'O95983', 'Q09028', 'Q13547', 'Q14839', 'Q16576']	8	1.00	6.52E-15	2	6	1.56E-13

Table A.15: Protein complexes - Part II

Cplx name	Cplx members	Cplx size	Total Hits	Num Hits	Cplx cov	p-value	Hits	Interactors	corr_p
BRG1-associated complex	O96019, O14497, O14744, P51532, Q12824, Q92922, Q8TAQ2, Q96GM5, Q969G3	9	['Q12824', 'O14497', 'Q96GM5', 'O96019', 'P51532', 'Q8TAQ2', 'Q92922', 'Q969G3']	8	0.89	5.77E-14	2	6	1.20E-12
BAF complex	O96019, O14497, P51532, Q12824, Q92922, Q8TAQ2, Q96GM5, Q92925, Q969G3	9	['Q12824', 'O14497', 'Q96GM5', 'O96019', 'P51532', 'Q8TAQ2', 'Q92922', 'Q969G3']	8	0.89	5.77E-14	2	6	1.25E-12
NuA4/Tip60 HAT complex	O96019, Q9H0E9, Q9NPF5, Q96L91, Q9H2F5, Q92993, Q9NXR8, Q9UBU8, Q9Y265, Q9Y4A5	10	['Q92993', 'Q9UBU8', 'Q9H0E9', 'O96019', 'Q9H2F5', 'Q9NPF5', 'Q9NXR8', 'Q9Y4A5']	8	0.80	2.84E-13	3	5	5.02E-12
BRM-associated complex	O96019, O14497, O14744, P51531, Q12824, Q92922, Q8TAQ2, Q96GM5, Q92925, Q969G3	10	['Q12824', 'O14497', 'Q96GM5', 'O96019', 'P51531', 'Q8TAQ2', 'Q92922', 'Q969G3']	8	0.80	2.84E-13	2	6	5.42E-12
Mi2/NuRD complex	Q14839, Q13547, Q92769, O95983, O94776, Q09028, Q16576	7	['O94776', 'Q92769', 'O95983', 'Q09028', 'Q13547', 'Q14839', 'Q16576']	7	1.00	3.93E-13	2	5	6.47E-12
DNMT3B complex	Q9UBC3, Q13547, O95239, Q96ST3, O60264, O95347, Q9NTJ3	7	['Q9UBC3', 'O95347', 'Q9NTJ3', 'O95239', 'O60264', 'Q13547', 'Q96ST3']	7	1.00	3.93E-13	3	4	6.70E-12
NuRD.1 complex	Q14839, Q6IT96, Q92769, O95983, Q13330, Q9BTC8, Q09028, Q16576	8	['Q92769', 'Q13330', 'Q9BTC8', 'O95983', 'Q09028', 'Q14839', 'Q16576']	7	0.88	3.09E-12	2	5	4.34E-11
PBAF complex (Polybromo- and BAF containing complex)	O96019, Q68CP9, Q86U86, P51532, Q12824, Q92922, Q8TAQ2, Q96GM5, Q969G3	9	['Q12824', 'Q96GM5', 'O96019', 'P51532', 'Q8TAQ2', 'Q92922', 'Q969G3']	7	0.78	1.37E-11	1	6	1.76E-10
HDAC1-associated protein complex	O60341, Q12873, Q13547, Q9UBB5, O95983, O94776, Q09028, Q16576, Q9UKL0	9	['O94776', 'O60341', 'Q9UBB5', 'O95983', 'Q09028', 'Q13547', 'Q16576']	7	0.78	1.37E-11	2	5	1.81E-10
PBAF complex (Polybromo- and BAF containing complex)	O96019, Q68CP9, Q86U86, P51532, Q12824, Q92922, Q8TAQ2, Q96GM5, Q969G3	9	['Q12824', 'Q96GM5', 'O96019', 'P51532', 'Q8TAQ2', 'Q92922', 'Q969G3']	7	0.78	1.37E-11	1	6	1.87E-10

Table A.16: Protein complexes - Part III

Cplx name	Cplx members	Cplx size	Total Hits	Num Hits	Cplx cov	p-value	Hits	Interactors	corr_p
NuRD	Q9UBB5, Q14839, Q16576, Q8WXI9, O94776, Q92769	6	['O94776', 'Q92769', 'Q8WXI9', 'Q9UBB5', 'Q14839', 'Q16576']	6	1.00	2.36E-11	2	4	2.96E-10
Brg1-associated complex II	O96019, O14497, O14744, P51532, Q12824, Q92922, Q8TAQ2	7	['Q12824', 'O14497', 'O96019', 'P51532', 'Q8TAQ2', 'Q92922']	6	0.86	1.62E-10	2	4	1.55E-09
NRD complex (Nucleosome remodeling and deacetylation complex)	O60341, Q12873, Q14839, Q13547, Q92769, Q13330, Q09028	7	['Q92769', 'O60341', 'Q13330', 'Q09028', 'Q13547', 'Q14839']	6	0.86	1.62E-10	3	3	1.58E-09
p300-CBP-p270-SWI/SNF complex	O14497, Q92793, Q09472, P51532, Q12824, Q92922, Q8TAQ2	7	['Q12824', 'O14497', 'P51532', 'Q09472', 'Q8TAQ2', 'Q92922']	6	0.86	1.62E-10	2	4	1.61E-09
mSin3A complex	Q13547, Q92769, Q09028, Q16576, Q96ST3	5	['Q92769', 'Q09028', 'Q13547', 'Q16576', 'Q96ST3']	5	1.00	1.41E-09	1	4	1.08E-08
PID complex	Q14839, Q13547, O95983, O94776, Q09028	5	['O94776', 'O95983', 'Q09028', 'Q13547', 'Q14839']	5	1.00	1.41E-09	1	4	1.10E-08
XFIM complex	O60341, P78347, Q13547, Q92769, Q14202	5	['Q92769', 'O60341', 'P78347', 'Q13547', 'Q14202']	5	1.00	1.41E-09	2	3	1.12E-08
Condensin I complex	Q15021, Q9BPX3, Q15003, O95347, Q9NTJ3	5	['O95347', 'Q9NTJ3', 'Q15003', 'Q15021', 'Q9BPX3']	5	1.00	1.41E-09	2	3	1.14E-08
13S condensin complex	Q15021, Q9BPX3, Q15003, O95347, Q9NTJ3	5	['O95347', 'Q9NTJ3', 'Q15003', 'Q15021', 'Q9BPX3']	5	1.00	1.41E-09	2	3	1.18E-08
MTA1 complex	Q6IT96, Q92769, O95983, Q13330, Q09028, Q16576	6	['Q92769', 'Q13330', 'O95983', 'Q09028', 'Q16576']	5	0.83	8.31E-09	2	3	6.00E-08
TIP5-DNMT-HDAC1 complex	Q9UIF9, P26358, Q9UBC3, Q13547	4	['Q9UBC3', 'Q9UIF9', 'P26358', 'Q13547']	4	1.00	8.37E-08	1	3	4.87E-07
Brg1-based SWI/SNF chromatin remodeling complex	O96019, Q12824, Q92922, Q8TAQ2	4	['Q12824', 'O96019', 'Q8TAQ2', 'Q92922']	4	1.00	8.37E-08	1	3	4.93E-07
DNMT1-RB1-HDAC1-E2F1 complex	P26358, Q01094, Q13547, P06400	4	['P06400', 'P26358', 'Q01094', 'Q13547']	4	1.00	8.37E-08	0	4	4.99E-07

Table A.17: Protein complexes - Part IV

Cplx name	Cplx members	Cplx size	Total Hits	Num Hits	Cplx cov	p-value	Hits	Interactors	corr_p
HuCHRAC complex	Q9NRL2, Q9NRG0, Q9NRF9, O60264	4	['Q9NRL2', 'Q9NRG0', 'Q9NRF9', 'O60264']	4	1.00	8.37E-08	2	2	5.05E-07
SWI/SNF chromatin-remodeling complex	Q13547, P51608, Q96ST3, P51531, Q969G3	5	['P51531', 'Q13547', 'Q969G3', 'Q96ST3']	4	0.80	4.12E-07	0	4	2.13E-06
MTA1-HDAC core complex	Q6IT96, Q92769, Q13330, Q09028, Q16576	5	['Q92769', 'Q13330', 'Q09028', 'Q16576']	4	0.80	4.12E-07	2	2	2.16E-06
Mi2/NuRD-BCL6-MTA3 complex	P41182, Q14839, Q13547, O95983, Q9BTC8	5	['Q9BTC8', 'O95983', 'Q13547', 'Q14839']	4	0.80	4.12E-07	0	4	2.18E-06
Mi-2/NuRD-MTA2 complex	P41182, Q13547, O95983, O94776, Q9BTC8	5	['O94776', 'Q9BTC8', 'O95983', 'Q13547']	4	0.80	4.12E-07	1	3	2.21E-06
NURF	Q12830, O60264, Q09028	3	['Q12830', 'O60264', 'Q09028']	3	1.00	4.95E-06	1	2	2.19E-05
Chromatin remodeling complex (TACC2, TACC3, PCAF)	Q92831, O95359, Q9Y6A5	3	['Q92831', 'O95359', 'Q9Y6A5']	3	1.00	4.95E-06	1	2	2.21E-05
RB1-HDAC1-BRG1 complex	Q13547, P06400, P51532	3	['P06400', 'P51532', 'Q13547']	3	1.00	4.95E-06	0	3	2.23E-05
mSin3A-HDAC1-HDAC2 complex	Q13547, Q92769, Q96ST3	3	['Q92769', 'Q13547', 'Q96ST3']	3	1.00	4.95E-06	1	2	2.25E-05
TIF1gamma-SMAD2-SMAD3 complex	Q15796, P84022, Q9UPN9	3	['Q9UPN9', 'P84022', 'Q15796']	3	1.00	4.95E-06	1	2	2.27E-05
ING1-p300-PCNA complex	Q09472, Q9UK53, P12004	3	['P12004', 'Q09472', 'Q9UK53']	3	1.00	4.95E-06	0	3	2.29E-05
DNMT1-G9a-PCNA complex	P26358, Q96KQ7, P12004	3	['Q96KQ7', 'P12004', 'P26358']	3	1.00	4.95E-06	0	3	2.32E-05

Table A.18: Protein complexes - Part V

A.8 Assay method small molecule inhibitor screen

Human bone marrow-derived MSCs (Lonza, Basel, Switzerland) of passage 4 to 5 were cultured in mesenchymal stem cell medium (MesenPro-RS™, Invitrogen/Life Technologies, California, USA) and plated onto 384-well, flat bottom plates (Corning, NY, USA) at 1000 cells in 50µl of medium per well. The following day, medium was changed to mesenchymal stem cell medium or osteogenic medium plus compounds at a concentration of 1µM in 0.1% DMSO unless otherwise specified. Medium was changed on day 5 of culture and compounds were refreshed. After 7 days of culture, cell viability assays were performed as previously described. After incubation for 30 minutes at 37°C fluorescence was measured (544nm excitation, 590nm emission) using a fluorescence plate reader (FLUOStar OPTIMA, BMG Labtechnologies). Relative units of fluorescence intensity from the reduction of resazurin to red fluorescent resorufin in the presence of metabolically active cells were used as indication for cell viability. Cells were then washed three times with PBS and lysed in the wells with 10µl of CelLytic M™ (Sigma, St. Louis, MO, USA) containing 2% protease inhibitor. After 15 minutes incubation at room temperature cells were transferred to a plate shaker and shaken for 30 sec at 10 Hertz, followed by the addition of 4-Methylumbelliferyl phosphate (4-MUP) as previously described. Plates were measured using a fluorescence plate reader (360nm excitation, 460nm emission) immediately after substrate addition (ALP_0) and were then read every 30 minutes for 1 hour (ALP_{30} and ALP_{60}) to determine ALP activity.

A.9 Dose-response experiments of hits derived from small molecule inhibitor screen

A.9.1 DOT1L

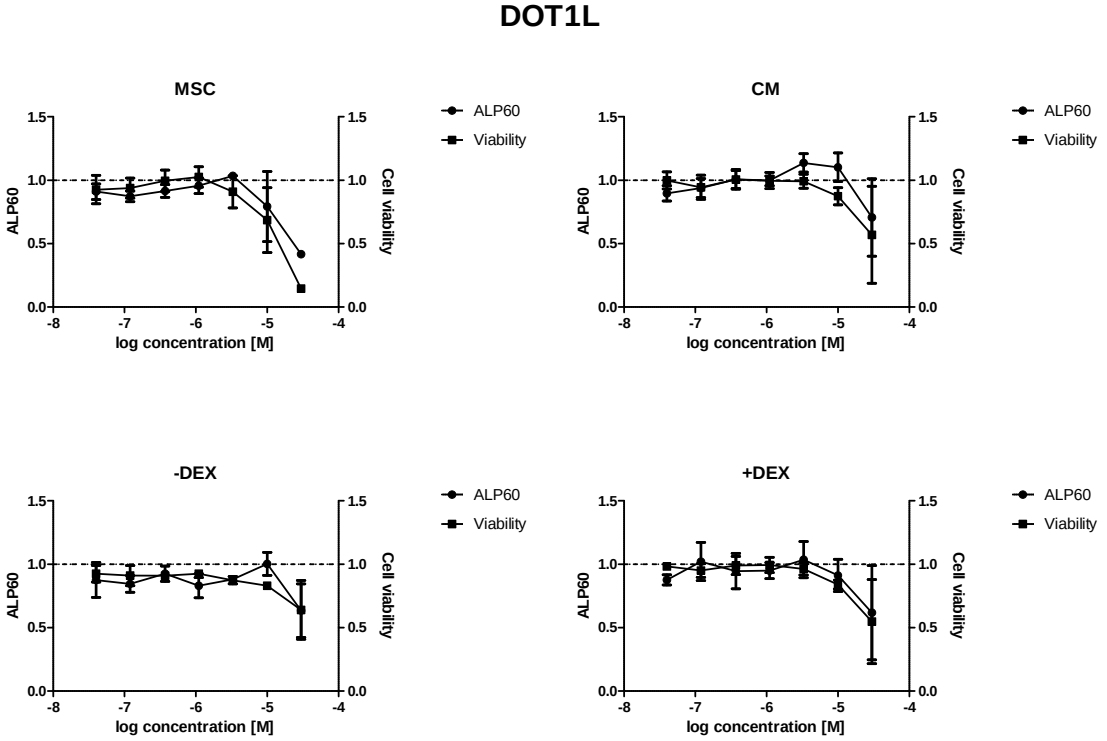

Figure A.9: Dose response curves under DOT1L inhibitor treatment. The x-axis shows applied concentrations in log [M], left y-axis shows level of alkaline phosphatase activity compared to the control (=1), right y-axis shows level of cell viability compared to the control (=1). 1 indicates 100% (of the control). Doses ranged from 0.04µM to 30µM in 0.1% DMSO. Medium was changed on day 5 of culture and compounds were replenished. After 7 days of culture, both cell viability and alkaline phosphatase activity were assessed.

A.9.2 SAHA

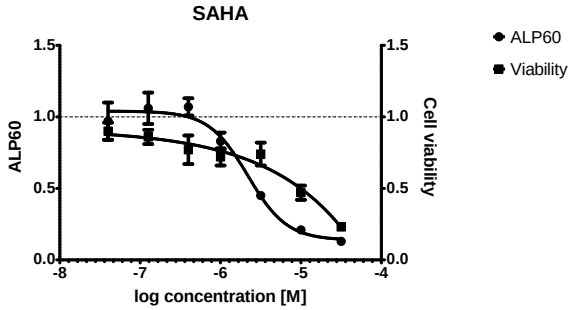

Figure A.10: Dose response curves under SAHA treatment. The x-axis shows applied concentrations in log [M], left y-axis shows level of alkaline phosphatase activity compared to the control (=1), right y-axis shows level of cell viability compared to the control (=1). 1 indicates 100% (of the control). Doses ranged from 0.04µM to 30µM in 0.1% DMSO. Medium was changed on day 5 of culture and compounds were replenished. After 7 days of culture, both cell viability and alkaline phosphatase activity were assessed.

A.9.3 Valproic acid

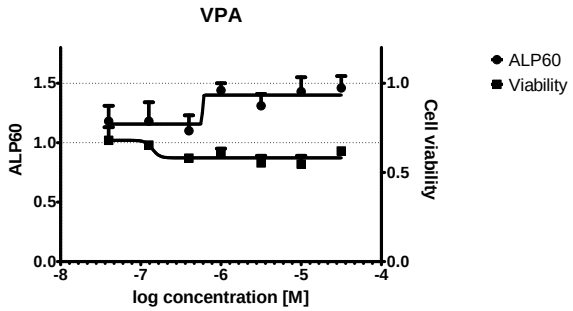

Figure A.11: Dose response curves under valproic acid treatment. The x-axis shows applied concentrations in log [M], left y-axis shows level of alkaline phosphatase activity compared to the control (=1), right y-axis shows level of cell viability compared to the control (=1). 1 indicates 100% (of the control). Doses ranged from 0.04µM to 30µM in 0.1% DMSO. Medium was changed on day 5 of culture and compounds were replenished. After 7 days of culture, both cell viability and alkaline phosphatase activity were assessed.

A.9.4 (-)-JQ1

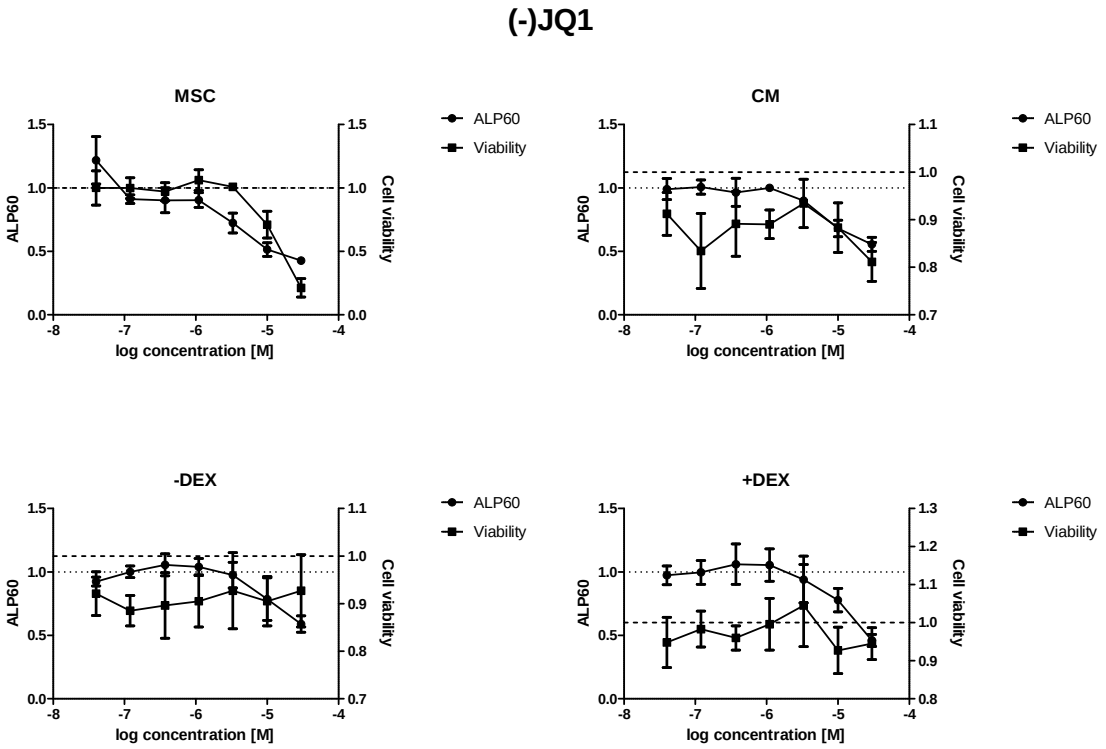

Figure A.12: Dose response curves under (-)-JQ1 treatment. The x-axis shows applied concentrations in log [M], left y-axis shows level of alkaline phosphatase activity compared to the control (=1), right y-axis shows level of cell viability compared to the control (=1). 1 indicates 100% (of the control). Doses ranged from 0.04µM to 30µM in 0.1% DMSO. Medium was changed on day 5 of culture and compounds were replenished. After 7 days of culture, both cell viability and alkaline phosphatase activity were assessed.

A.10 (+)-JQ1 treatment - microarray data

The gene expression data of MSCs undergoing dexamethasone-induced differentiation (+/- (+)-JQ1 treatment) obtained from microarray studies as described in chapter 4 will be deposited and an accession number is available on request.